Technische Universität München
Wissenschaftszentrum Weihenstephan
für Ernährung, Landnutzung und Umwelt

Lehrstuhl für Proteomik und Bioanalytik

Generation of a spatiotemporally inducible reporter mouse model for *in vivo* imaging of pancreatic cancer therapy

Andreas Arbeiter

Vollständiger Abdruck der von der Fakultät Wissenschaftszentrum Weihenstephan für Ernährung, Landnutzung und Umwelt der Technischen Universität München zur Erlangung des akademischen Grades eines

Doktors der Naturwissenschaften

genehmigten Dissertation.

Vorsitzender:		Univ.-Prof. Dr. Michael Schemann
Prüfer der Dissertation:	1.	Univ.-Prof. Dr. Bernhard Küster
	2.	apl. Prof. Dr. Dieter K. M. Saur

Die Dissertation wurde am 17.07.2014 bei der Technischen Universität München eingereicht und durch die Fakultät Wissenschaftszentrum Weihenstephan für Ernährung, Landnutzung und Umwelt am 29.09.2014 angenommen.

Table of Contents

Table of Abbreviations

%	per cent
°C	degree celsius
µF	microfarad
µg	microgram
µl	microliter
Ad-Cre	adenovirus expressing the Cre recombinase
AFN	atipamezole, flumazenil, naloxone
Akt	protein kinase B (PKB)
Amp	ampicillin
approx.	approximately
Arf	alternative reading frame
ATP	adenosine triphosphate
att site	attachment site
BGH	bovine growth hormone
bidest.	double distilled water
BLI	bioluminescence imaging
bp	base pairs
BRCA2	breast cancer 2, early onset
BrdU	5-Bromo-2´-deoxyuridine
BSA	bovine serum albumin
CAG	synthetic promoter
CCD	charge coupled device

ccdB	bacterial „suicide gene“, gyrase (topoisomerase) inhibitor
CCW	counter clockwise
CDK	cyclin-dependent kinase
CDKN2A	cyclin-dependent kinase inhibitor 2 A
CHYSEL	cis-acting hydrolase element
cm	centimeter
CmR	chloramphenicol resistance gene
CMV	cytomegalovirus
CO_2	carbondioxid
Cre	causes recombination (recombinase)
ctrl	control
DAB	3,3'-diaminobenzidine tetrahydrochloride
DMEM	Dulbecco`s Modified Eagle Medium
DMSO	dimethylsulfoxid
DNA	desoxyribonucleic acid
dNTP	desoxyribonucleotide triphosphate
DsRed	*Discosoma species* Red
DTA	diphteria toxin
d-Tomato	dimer tomato
E.coli	Escherichia coli
EBFP	enhanced blue fluorescent protein
Ecadh	E-cadherin
ECFP	enhanced cyan fluorescent protein
EDTA	ethylendiamintetraacetic acid
EGF	epidermal growth factor
EGFP	enhanced green fluorescent protein
EGFR	epidermal growth factor receptor
EP	electroporation
ER^{T2}	mutated form of the ligand binding domain of the human estrogen receptor
ES cell	embryonic stem cell
EtOH	ethanol
EYFP	enhanced yellow fluorescent protein
FCS	fetal calf serum
Flp	flippase (recombinase)
fLuc	firefly luciferase
fmol	femtomol
FRT	Flp recombinase target
FSF	FRT-STOP-FRT cassette
Fsp1	fibroblast specific protein 1
g	gram
G (cell cycle)	gap
G418	geneticine
GEMM	genetically engineered mouse model
GFP	green fluorescent protein
Gly	glycin
h	hour

H&E	Haematoxilin-Eosin
H_2O	water
H_2O_2	hydrogen peroxid
HCl	hydrogen chloride
hrLuc	humanized renilla luciferase
i.p.	intraperitoneal
Ink4A	inhibiting cyclin-dependent kinase 4 A
IRES	internal ribosomal entry site
Kan	kanamycin
kb	kilobase
KCl	potassium chloride
KCM	KCl, $CaCl_2$ and $MgCl_2$
kDa	kilo Dalton
kg	kilogram
KPC	Kras, p53 and Cre (mouse model)
Kras	V-Kirsten rat sarcoma 2 viral oncogene homolog
l	liter
lacZ	β-galactosidase
LB	lysogeny broth
LIF	leukemia inhibitory factor
loxP	locus of crossover in bacteriophage P1
LSL	loxP-STOP-loxP cassette
M	molar
M (cell cycle)	mitosis
MARCKS	myristoylated alanine-rich C-kinase substrate
mCherry	monomeric cherry
MCS	multiple cloning site
MEF	mouse embryonic fibroblast
mem-td-Tomato	membrane-tandem-dimer-Tomato
mg	milligram
min	minute
ml	milliliter
mM	millimolar
mm	millimeter
MMF	midazolam, medetomidine, fentanyl
mRFP1	monomeric red fluorescent protein 1
msec	millisecond
mTFP1	monomeric teal fluorescent protein 1
mTOR	murine target of rapamycin
mTORC1	mammalian target of rapamycin complex 1
mut	mutated
n.a.	not available
n.s.	not significant
NaAc	sodium acetat
Nab-paclitaxel	nano-albumin bound paclitaxel
NaCl	sodium chloride

NADH	nicotine amide adenine dinucleotide
NEAA	non-essential amino acids
neo^R	neomycin resistance gene
nm	nanometer
NMP	N-methyl-pyrrolidon
OD600	optical density at 600 nm wavelength
p	protein or plasmid (context-dependent)
pA	polyadenylation signal
PanIN	pancreatic intraepithelial neoplasia
PBS	phosphate buffered saline
PCNA	proliferating cell nuclear antigen
PCR	polymerase chain reaction
PDAC	pancreatic ductal adenocarcinoma
Pdx1	pancreas duodenum homeobox 1
PEG	polyethylenglycol
PFA	paraformaldehyde
pgk	phosphoglycerat kinase
PI3K	phosphoinositol-3-kinase
PLB	passive lysis buffer
pos	positive
Ptf1a	pancreas transcription factor 1 α-subunit
R26	Rosa26
RAS	rat sarcoma
RFP	red fluorescent protein
RLU	relative light units
rLuc	renilla luciferase
RNA	ribonucleic acid
ROI	region of interest
rpm	revolutions per minute
S (cell cycle)	synthesis
s.c.	subcutaneous
SA	splice acceptor
SDS	sodium dodecyl sulfate
sec	seconds
SEM	standard error of the mean
Ser	serin
shRNA	short hairpin RNA
Smad4	mothers against decapentaplegic homolog 4 (homolog of the *Drosophila melanogaster* protein MAD and the *Caenorhabditis elegans* protein SMA)
sp.	species
SV-40	simian virus 40
T	temperature
t	time
TAE	Tris, acetat, EDTA buffer
td-Tomato	tandem dimer Tomato
TP53	tumor protein 53 (human)

Trp53	transformation-related protein 53 (murine)
Tyr	tyrosin
U	units
UV	ultra violet
V	Volt
w/o	without
WT	wildtype

List of Figures

List of Tables

A. Introduction

1. *In vivo* imaging

In vivo imaging of small animals like mice is increasingly applied within preclinical research approaches. Mainly in the field of oncology and cancer therapy it has become an important translational tool supporting the development of novel anti-cancer drugs. This can easily be achieved by monitoring the treatment response in real time and investigating the chemotherapeutic efficiency. In conventional mouse models of disease the usual analysis strategy is based on end point assays, revealing only a snapshot of the biological processes at a specific time point. For investigating mouse models of cancer, the only possibility in monitoring tumor growth *in vivo* is to measure the volume of palpable sub-surface tumors by caliper measurements (Weissleder, 2002). This seems to be insufficient regarding the highly complex and dynamic nature of most biological systems like cancer. Using *in vivo* imaging techniques instead opens a new world for the real time monitoring of tumor initiation and progression and thus also deep-seated tumors can be detected and investigated non-invasively (Weissleder, 2002; Weissleder and Ntziachristos, 2003). If conventional and *in vivo* imaging mouse models are compared directly, the advantages of a non-invasive research strategy become obvious. In a given experiment where 6 animals are analyzed at 4 different time points, the conventional researcher would need to sacrifice 24 animals within this *ex vivo* approach. Performing the same experiment using the *in vivo* imaging technology, only 6 instead of 24 animals would need to be sacrificed. When applying this technique, all animals can be monitored dynamically in real time for any desired time point. Beside the massive reduction in animals needed, the results of the experiment will produce better data containing less biological variability since each animal serves as its own control. Additionally, real time imaging enables to visualize a dynamic biological process more accurate compared to the snapshot approach used conventionally. Furthermore there is no restriction in the number of time points which can be analyzed. Compared to the conventional research, *in vivo* imaging is additionally much cheaper and faster (Weissleder, 2002; Weissleder and Ntziachristos, 2003; Sadikot and Blackwell, 2005).

There are numerous application possibilities for *in vivo* imaging described within the literature. Amongst others, this technology can be used to track tumor cells, stem cells, immune cells or bacteria. In addition, gene expression, protein-protein interaction, protein phosphorylation, gene therapy, tumor formation and most important tumor therapy can be visualized (Contag and Bachmann, 2002; Weissleder, 2002; Weissleder and Ntziachristos, 2003; Sato et al., 2004; Doyle et al., 2004; Sadikot and Blackwell, 2005). Visualization of the pharmacological inhibition of tumor growth will be one focus of the present study.

A broad range of different high-resolution *in vivo* imaging systems for non-invasively investigating mouse models are available (reviewed in Weissleder, 2002). Within this thesis the main focus will lie on optical imaging modalities, in detail fluorescence and bioluminescence imaging (BLI).

1.1. Bioluminescence imaging (BLI)

BLI is based on a biochemical reaction which is producing light. This photon emitting reaction is catalyzed by photoproteins called luciferases which can be isolated and subsequently cloned from many different non-mammalian organisms like prokaryotes, marine organisms and insects. Amongst others, luciferases from firefly (*Photinus*), jellyfish (*Aequorea*), sea pansy (*Renilla*), corals (*Tenilla*), click beetle (*Pyrophorus plagiophthalamus*), and different bacterial species (*Vibrio fischeri, Vibrio harveyi*) have already been successfully cloned (Hastings, 1996). From an evolutionary point of view, different selection pressures emerged yielding in the generation and maintenance of bioluminescent reactions within these species. Light production can result in having advantages in locating food, identifying mates and reducing oxidative stress by using these reactions as an electron dump. Independent evolution finally resulted in a variety of different luciferases using different substrates and emitting light of variable colors (Hastings, 1996). These luciferases have been widely used within transgenic mouse models as reporter genes. At the beginning, the luciferase activity could only be detected *ex vivo* using homogenized tissue and a luminometer since no *in vivo* BLI systems were available (Nguyen et al., 1988). After implementation of the first BLI systems, this technology became wide-spread since it represents a non-invasive, convenient and cheap alternative to other imaging modalities (Weissleder, 2002; Hong et al., 2011). Most important, BLI is extremely sensitive since this light-producing reaction does not occur intrinsically within mammalian tissues. Consequently there is no background signal in contrast to the autofluorescence observed using fluorescence imaging modalities (Hong et al., 2011). Due to the absence of intrinsic bioluminescence, images with extremely high signal-to-noise ratios can be produced (Sadikot and Blackwell, 2005). It was already shown that as few as 1,000 luciferase expressing tumor cells can be detected within the peritoneal cavity (Contag et al., 2000).

Today there are mainly two different luciferases used in animal models of disease, namely the firefly (fLuc) and the renilla (rLuc) luciferase. The fLuc was isolated and cloned from male North American firefly *Photinus pyralis*, who are generating bioluminescent flashes within their abdomen in order to find mating partners (de Wet et al., 1985). In the presence of oxygen, ATP and magnesium, the benzothiazoyl–thiazole D-luciferin is oxidized to oxyluciferin coupled to the generation of light. Photon emission is broad-band (530–640 nm) with a peak at 562 nm (yellow-green color; Rice et al., 2001). Due to the temperature dependency of the luciferase emission, the wavelength peak is shifted from 562 nm at 22°C to 612 nm at 37°C which lies within a favourable tissue transmission window (Zhao et al., 2005; Contag, 2007). Consequently this emission wavelength enables an optimal tissue penetration (see chapter 1.2 below). The fLuc is seen as the luciferase imaging system with the highest efficiency (Branchini et al., 2005).

Beside the fLuc there is another luciferase isolated from the sea pansy *Renilla reniformis* which is also increasingly applied in different mouse models, namely the renilla luciferase (rLuc; Bhaumik and Gambhir, 2002). Light production in the sea pansy is triggered by mechanical stimulation. This enzyme has been firstly cloned and sequenced in 1991 (Lorenz,

1991). Yet this luciferase differs from the fLuc in several aspects. As a substrate, rLuc uses coelenterazine instead of luciferin. Additionally the oxidation reaction catalyzed by this enzyme requires no co-factors since it is magnesium and ATP independent. The rLuc produces a blue-green light at a wavelength of 482 nm (Bhaumik and Gambhir, 2002).

Comparing both luciferases directly reveals some biochemical difficulties in using the rLuc *in vivo*. Besides being much smaller (36 compared to 61 kDa), the rLuc shows different light kinetics containing a faster light production with shorter duration (flash light kinetics). In contrast to this, the fLuc produces a stronger signal that persists much longer within the cell. Compared to D-luciferin less amount of coelenterazine has to be injected when using rLuc. However, coelenterazine is unstable in plasma and oxidation leads to a higher background compared to the fLuc signal. In addition, the target site delivery (biodistribution) of coelenterazine is less efficient due to serum protein binding of this substrate. Regarding the *ex vivo* luciferase assay, rLuc might be superior to fLuc due to its fast light kinetics and no co-factor requirement (Bhaumik and Gambhir, 2002; Sato et al., 2004).

In addition to the native rLuc there exists another synthetic version of this reporter gene already expressed in living mice. This so-called hrLuc (humanized rLuc) is also used within the present study and represents a mammalian codon-optimized variant of the native gene. It has already been shown *in vitro* as well as in living animals that coelenterazine and hrLuc produce a stronger signal than D-luciferin and fLuc (Bhaumik et al., 2004; Hong et al., 2011).

1.2 Tissue transmission of light – optical properties of mammalian tissues

The light produced by luciferases must travel through tissue in order to be detectable. By doing so it is scattered as well as absorbed (Cheong et al., 1990; Rice et al., 2001; Tuchin, 2007). Photons are absorbed by tissue (amongst others by hemoglobins, lipids and water) in a wavelength-dependent manner. In the shorter wavelength region there is a high tissue absorbance as well as a peak in tissue autofluorescence detectable. In contrast to this, tissue absorbance and autofluorescence significantly decrease in the longer wavelength region of the spectrum, whereas photon scattering increases. Consequently optimal light transmission through tissue requires wavelengths above 600 nm (tissue transmission window). This is the reason for developing novel luciferases showing a more red-shifted emission spectrum to provide best signal intensities even within deep tissues (Weissleder and Ntziachristos, 2003). Due to the blue-shifted emission spectrum of the rLuc, the tissue transmission of the photons is worse than for the red-shifted emission spectrum of the fLuc. The light produced by luciferases is able to penetrate mouse tissue for several millimeters to centimeters with a 10-fold decrease in photon intensity for each centimeter of tissue depth (Contag et al., 1995). In addition, the presence of black fur is attenuating the photon intensity by photon scattering drastically. It was already shown that photon absorption by pigmentation (melanin) as well as photon scattering by the presence of fur can lead to a 90% decrease in bioluminescence signal intensity (Curtis et al., 2010). Consequently a highly sensitive bioluminescence detection system must be applied.

1.3 BLI instrumentation

The detectors of such a system are able to measure the amount of photon emission per unit of area. Light of 400 nm – 1000 nm wavelength can be detected by low-light, photon counting charge coupled device cameras (CCD) which convert the incoming photons hitting silicon wafers into electrons (Spibey et al., 2001). The CCD camera converts the spatial distribution of incoming photons and their respective intensity into an electrical charge pattern which in the end is converted into a 2-dimensional image. The intensity of the produced light (number of emitted photons striking the silicon detector at a specific point) is represented by a pseudo-color image generated by the software. This visual interpretation allows comparison of signal intensities by quantification of specific regions of interests (ROI) (Rice et al., 2001). The use of cooled, back-thinned and integrating CCDs is optimal for highly sensitive *in vivo* BLI applications, where the expected light signal might be extremely weak and originating from deep tissues (reviewed by Rice et al., 2001). These cameras show a high quantum efficiency of 90% at wavelengths above 600 nm (percentage of incoming photons which are transformed into electrons). Since they are cooled down to -70°C, the dark current is kept extremely low. Beside a low read noise and high resolution, these systems provide integration times of 0.5 sec up to 10 min which is also suitable in case of very weak signal intensities.

1.4 Distinction from fluorescence imaging

The great benefit of using BLI instead of fluorescence reporter genes for *in vivo* imaging applications lies in the significantly better signal-to-noise ratio, since mammalian tissue shows autofluorescence within the wavelength region used to excite fluorescent proteins (mainly within the blue region of the spectrum; Weissleder and Ntziachristos, 2003). Endogenous chromophores like elastin, collagen, tryptophan, NADH, porphyrins and flavins show an intrinsic fluorescence leading to an increased background signal (Troy et al., 2004). In contrast to this, there is no autoluminescence detectable within tissue as already mentioned before. In addition, the maturation of luciferases is much faster due to the lack of posttranslational modifications and a faster protein folding compared to fluorescence proteins (fluorescence proteins usually consist of a complex quaternary structure containing many subunits due to posttranslational oligomerization; Thompson, 1991; Corish and Tyler-Smith, 1999; Baird et al., 2000; Campbell et al., 2002; Shaner et al., 2004; Gross and Piwnica-Worms, 2005; Zinn et al., 2008). Furthermore, taking a look at the turnover rate, the biological half-life of luciferases within the cell usually is 3-5 hours compared to almost one day for fluorescence reporters. Thus BLI is much more suitable for visualization of gene expression or highly sensitive kinetic experiments (Thompson, 1991; Corish and Tyler-Smith, 1999; Lipshutz et al., 2001).

Summing up all these different aspects of BLI, the following disadvantages/advantages can be worked out. First of all a reporter gene (luciferase) is required, meaning to either stably transfect a cell line or to generate a transgenic mouse model as done within the present thesis. Since light production is based on a biochemical reaction, the substrate (D-luciferin

and coelenterazine, respectively) has to be injected which is not necessary when using fluorescent imaging reporters. In case of using fLuc on one hand, magnesium, oxygen and ATP are required co-factors. When imaging tumors with high hypoxia this can be a crucial problem since ATP and the substrate must be available in excess. If using rLuc on the other hand, no additional co-factors are necessary. Yet this enzyme shows a higher background signal, flash light kinetics and impaired biodistribution of its substrate coelenterazine. Furthermore, the emission spectrum of the luciferases is not optimal since their peaks lie outside of the tissue transmission window. The fLuc shows a better tissue penetration due to its more red-shifted emission spectrum compared to the rLuc. Finally there is no absolute quantification of the bioluminescence possible due to the unknown amount of photon absorption and scattering during tissue transmission. Thus luciferase signals can only be compared relative to one another using the region of interest function.

Turning to the advantages of BLI, the most important fact is the extremely high sensitivity of this technology due to the absence of intrinsic autoluminescence within mammalian tissues. This background-free imaging is not possible using fluorescence reporters. These proteins usually show high background and low signal-to-noise ratios due to tissue autofluorescence. Compared to fluorescence imaging, in BLI there is no need for an excitation since light production is conducted biochemically. Photons produced by luciferases show a quite good tissue penetration of up to 2 cm. Since the fLuc is oxygen and ATP dependent, it can ideally be employed for imaging exclusively living and metabolically active cells. The rLuc on the other hand can be used to visualize extracellular compartments due to the lack of co-factors needed to drive the light producing reaction. Moreover, less amount of coelenterazine is needed in contrast to D-luciferin. Especially when applying the humanized variant hrLuc *in vivo*, the signal was already reported to be stronger than by using fLuc.

2. *Ex vivo* imaging – fluorescent reporter proteins and distinction from BLI

Next to applying fluorescent proteins for *in vivo* optical imaging approaches using highly sensitive CCD cameras similar to BLI (e.g. Yang et al., 2000; Hoffman and Yang, 2006), there is also the option for *ex vivo* imaging of histological tissue sections. Fluorescence is substrate independent and only requires light excitation and a fluorescence microscope for emission detection. After preparation and fixation of the organs, the tissue of interest can be analyzed by histological sections. These sections can further be excited with light of a specific wavelength which will be absorbed by the fluorophore of the specific fluorescent protein. Upon absorption, the fluorophore will emit light of lower energy (longer wavelengths) which can easily be detected via fluorescence microscopy (Troy et al., 2004). Within this experimental setting, the big advantage over *in vivo* BLI is that the cells which are expressing the reporter gene can exactly be quantified by counting. Hence although being more laborious, an absolute quantification is now possible. In contrast to this, BLI is not used for imaging fixed tissue sections, since it requires different substrates only available within living and metabolically active cells but not within fixed tissues (ATP and oxygen). Furthermore, the biological half-life of luciferases is much shorter compared to fluorescent proteins.

Consequently *ex vivo* BLI is possible on the organ level but not feasible within fixed tissue sections of an organ. For *in vitro* applications on the other hand, BLI can be used to specifically measure luciferase activity with high sensitivity using homogenized cells or tissue samples for further luminometer analysis (Nguyen et al., 1988).

2.1 Enhanced green fluorescent protein (EGFP) as a fluorescent reporter protein

One of the first reporter genes used to visualize gene expression has been *lacZ* (β-galactosidase; sequenced by Kalnins et al., 1983) which was initially used in *E.coli*. The major drawback of *LacZ* staining is that it requires a substrate in order to generate the blue dye since it is based on an enzymatic reaction. The next generation of reporter genes started with the successful cloning of the green fluorescent protein (GFP; Prasher et al., 1992) 30 years after it was discovered in the jellyfish *Aequorea victoria* (Shimomura et al., 1962). Also GFP was firstly applied in different bacterial species (Chalfie et al., 1994). In 1997 finally the first transgenic mouse model was generated expressing GFP (the green mouse; Okabe et al., 1997). This green mouse expresses enhanced GFP (EGFP) under the control of a *CAG* promoter ubiquitously in the whole body, which demonstrates that this fluorescent reporter is not toxic *in vivo*. EGFP is a mutant containing optimized codon usage of highly expressed human proteins and chromophore mutations leading to higher expression levels and improved fluorescence intensity compared to the WT GFP protein (Yang et al., 1996; Tsien, 1998). The fluorophore of EGFP is mainly composed of the tripeptide Ser65, Tyr66, and Gly67, which is responsible for the generation of green fluorescence in the presence of photon excitation independent of additional enzymes or co-factors (Heim et al., 1994; Cubitt et al., 1995; Ormo et al., 1996; Reid and Flynn, 1997). EGFP has two distinct maximal excitation wavelengths at 400 nm and 470-490 nm (blue light). Like all fluorescent proteins, after absorption of the photons the fluorophore is excited to a higher energy state. Afterwards it emits photons of a longer wavelength at 480-520 nm which is visible as green light (Verkhusha and Lukyanov, 2004; Troy et al., 2004). In 2008 the discovery and development of GFP was awarded with the Nobel Prize in chemistry. After EGFP became widely used for monitoring sub-cellular protein localizations and gene expressions (e.g. Heim and Tsien, 1996; Jakobs et al., 2000), there were other spectral variants of this protein generated, e.g. enhanced blue fluorescent protein (EBFP), enhanced yellow fluorescent protein (EYFP) and enhanced cyan fluorescent protein (ECFP). Also these variants were successfully used in living mice (Tsien, 1998; Hadjantonakis and Nagy, 2000; Srinivas et al., 2001). Since the emission spectra of these EGFP-derived reporters are extremely close, it is not possible to distinguish between them and thus they cannot be combined within one mouse model (Feng et al., 2000). Consequently spectral distinct colors for reporter proteins were intensively sought afterwards in order to avoid an emission overlapping.

2.2 Red fluorescent proteins (RFPs) and the development of tandem-dimer-Tomato (td-Tomato)

The first red fluorescent protein was DsRed (*Discosoma sp.* Red) which has been isolated in 1999 from the tropical coral *Discosoma sp*. (Matz et al., 1999; Baird et al., 2000). Shortly afterwards, a group tried to generate a transgenic mouse line expressing this reporter protein but failed (Hadjantonakis et al., 2002). As it is known today, the problem of using red fluorescent proteins is the long maturation time of the chromophore, inefficient protein folding, poor solubility and additionally oligomerization to tetramers leading to cytotoxic effects (Baird et al., 2000; Campbell et al., 2002; Shaner et al., 2004). There was a lot of effort being made in developing more suitable red fluorescent proteins. DsRed2 and DsRedT3 are both modified versions of the original protein generated by random mutagenesis and showing faster maturation (Verkhusha et al., 2001; Bevis & Glick, 2002; transgenic mouse models using DsRed variants are reviewed in Hong et al., 2011). A transgenic mouse model expressing DsRedT3 has been successfully established, but still there were problems in generating DsRed fusion proteins due to the multimer formation (Vintersten et al., 2004). After further stepwise advancement of DsRed to a dimer and then finally to a monomer, the first true monomeric RFP could be generated, designated mRFP1 (monomeric red fluorescent protein 1; Campbell et al., 2002). Ultimately a transgenic mouse model could be established where mRFP1 is expressed under the control of the *CAG* promoter (Long et al., 2005). Further on this protein has successfully been used in its native form, but also as a fusion with other proteins *in vivo*. Today there is a broad variety of different monomeric RFPs derived from DsRed and other RFPs applied in transgenic mouse models (Chudakov et al., 2010). Amongst others, mCherry (monomeric Cherry) is an improved monomeric RFP which is brighter, shows a higher photostability and faster maturation compared to mRFP1. In addition, termini derived from GFP result in a higher tolerance for fusions with other proteins and it also has been codon-optimized (Shaner et al., 2004). mCherry has already been used in many different mouse models. However, in some of these transgenic models it has been reported that the mice get infertile which might be due to some toxicity of the protein (Larina et al., 2009; Poche et al., 2009; Sunmonu et al., 2009; Armstrong et al., 2010; Fink et al., 2010).

Beside generation of a true monomeric RFP, another alternative strategy has been followed to improve DsRed. During the directed evolution strategy applied by the authors, a dimeric version of DsRed was generated, named dimer2. This protein was further improved by some additional random mutations leading to generation of dimer-Tomato (d-Tomato), showing improved maturation kinetics and a small emission red-shift, amongst others. Similar to mCherry, d-Tomato contains termini derived from GFP which facilitates C-and N terminal fusions of the reporter due to a higher tolerance (Campbell et al., 2002; Shaner et al., 2004). In order to establish a non-aggregating RFP, a tandem dimer was further on produced by fusing two copies of the *dimer-tomato* gene with a polypeptide linker. This fusion covers the critical dimer interaction sites by enabling intramolecular contacts between both partners of the tandem which are encoded as a single polypeptide. Hence an artificial monomeric RFP

could have been established showing a faster and complete maturation (one hour compared to ten hours for DsRed), facilitated C-and N terminal fusion possibilities, extreme brightness and less cytotoxicity. In addition, it was demonstrated to be 10-fold more photostable than mRFP1. This RFP was designated tandem-dimer-Tomato (td-Tomato; Campbell et al., 2002; Shaner et al., 2004).

In the present study mem-td-Tomato (membrane-td-Tomato) is used as a fluorescent reporter protein. This td-Tomato protein has an additional membrane tag which will target it towards the plasma membrane of the cell after expression. The membrane tag consists of eight amino acids derived from the MARCKS protein, which are fused to the N-terminus of the full-length td-Tomato allowing membrane anchorage (Muzumdar et al., 2007). This membrane-bound reporter protein has already been used in a genetically engineered mouse model (GEMM) and it could be demonstrated that the membrane localization allows *ex vivo* imaging of cellular morphology and visualization of membrane structures (Muzumdar et al., 2007). The excitation maximum of td-Tomato is 554 nm. Its emission maximum is around 581 nm (Shaner et al., 2004). Since the excitation as well as emission spectra of EGFP and td-Tomato are distinct, they can be simultaneously imaged and it is possible to apply both reporters within one mouse model (Muzumdar et al., 2007; Hong et al., 2011). In comparison to EGFP, the emission wavelength of td-Tomato is more red-shifted which is also beneficial for *in vivo* imaging applications due to an increased tissue penetration at longer wavelengths (lower tissue absorption in the red-shifted region of the spectrum, see Weissleder and Ntziachristos, 2003). Since intrinsic tissue autofluorescence is mainly restricted to shorter wavelengths, td-Tomato will be less affected and hence showing less background signal than EGFP (Weissleder and Ntziachristos, 2003; Troy et al., 2004).

3. Pancreatic cancer as an application for *in* and *ex vivo* imaging

3.1 Human pancreatic ductal adenocarcinoma (PDAC)

Since *in vivo* imaging is extremely useful in detecting deep seated tumors, this technology can ideally be applied for monitoring of pancreatic cancer. Pancreatic ductal adenocarcinoma (PDAC) is one of the deadliest types of cancers existing, with estimated 227,000 deaths per year worldwide and an extremely high mortality rate of almost 100% (Raimondi et al., 2009; Vincent et al., 2011; Muniraj et al., 2013). The main risk factors that might lead to development of this devastating disease are cigarette smoking, alcohol abuse, a familiar background of chronic pancreatitis and genetic predisposition, advanced age and male sex (Klein et al., 2004). Beside this, there are many other potential risk factors known today. Amongst others obesity, non-O blood group, exposure to chlorinated hydrocarbon solvents and nickel, African-American ethnic background, high-fat diet or diets with high meat and low vegetables and folate as well as probably *Helicobacter pylori* infection (Ojajärvi et al., 2000; Raimondi et al., 2009; Amundadottir et al., 2009; Wolpin et al., 2009; Vincent et al., 2011).

Taking a look at the pathophysiology of this cancer, it usually develops through a cascade of non-invasive precursor lesions known as pancreatic intraepithelial neoplasias (PanINs).

These lesions have defined morphological structures which can be investigated on a histological level and are based upon typical genetic as well as epigenetic alterations (Hruban et al., 2000; Hruban et al., 2001). The usual genetic alterations found in PDAC are an activating oncogenic *KRAS* mutation, inactivating mutations of tumor-suppressor genes like *CDKN2A*, *TP53*, *SMAD4* and *BRCA2*, chromosomal losses, several gene amplifications and telomere shortening resulting in chromosomal instability (Rozenblum et al., 1997; van Heek et al., 2002; Jones et al., 2008). The oncogenic *KRAS* mutation resembles the earliest event within the advancing cascade of precursor lesions, as found already in low-grade PanINs. In the course of progression to higher grade PanINs, additional inactivation and loss of heterozygosity of crucial tumor suppressor genes like *TP53* and the *CDKN2A* locus occur, resulting in the establishment of highly invasive and metastatic PDAC (Vincent et al., 2011). Beside the mentioned PDAC driver genes, changes on an epigenetic level contain alterations in DNA methylation and histone modifications as well as false regulation of non-coding RNAs. The *CDKN2A* locus which is encoding the two tumor suppressor genes $p16^{INK4A}$ and $p19^{ARF}$ is known to be promoter hypermethylated and silenced in PDAC. The epigenetic silencing occurs in tumors showing no inactivation of this locus (Schutte et al., 1997).

The major obstacle of PDAC therapy is the role of the tumor microenvironment. Pancreatic cancer shows an extremely strong fibrotic reaction of the stromal compartment, resulting in formation of an extremely solid tumor showing only poor vascularization. This desmoplasia constitutes an obstruction for therapeutic interventions, since it acts like a barrier preventing the penetration of chemotherapeutics towards the malignant cancer cells within the epithelium of the organ (Hezel et al., 2006; Ghaneh et al., 2007). It has already been shown that if crucial signaling pathways like the hedgehog signaling cascade involved in the tumor-stroma communication are inhibited, therapeutic efficiency is increasing. In a murine PDAC model a combination of the standard chemotherapeutic gemcitabine and an inhibitor of the hedgehog pathway led to prolonged survival of the mice compared to the monotherapy (Olive et al., 2009).

In addition to the fibrosis, the absence of early detection possibilities, the retroperitoneal location of the pancreas as well as the absence of symptoms until late stages of the disease, it is often impossible to cure PDAC. Usually only palliative treatment remains. Most of the human PDAC arise within the head of the pancreas leading quite early to a symptomatic biliary obstruction. Beside this, also pancreatic cancer arising from the body or the tail of the pancreas are observed, showing almost no symptoms at all. Due to the late clinical presentation of the patients, the cancer is usually highly progressed and lymph node, liver as well as lung metastases have already formed. In these late stages of the disease surgical resection of the cancer is impossible. The standard chemo- as well as radiotherapies applied are not able to heal the patient, since only 4% of patients will survive longer than 5 years upon diagnosis. (Kelsen et al., 1997; Pelaez-Luna et al., 2007; Vincent et al., 2011; Muniraj et al., 2013).

Recently there have been several clinical studies evaluating new chemotherapeutics for specifically treating highly advanced and metastatic PDAC. Folfirinox, which is a combination

of different chemotherapeutics, showed modest increase in survival time of around 4 months compared to standard gemcitabine therapy (Conroy et al., 2011; Muniraj et al., 2013). Nab-paclitaxel (nano-albumin-bound paclitaxel), which is thought to improve the drug delivery hence overcoming the mentioned problem of the poor vascularization within the desmoplastic pancreatic cancer, is another novel chemotherapeutic. Clinical trials showed also slightly increased survival times for patients receiving a combination of Nab-paclitaxel and gemcitabine compared to a gemcitabine monotherapy (Komar et al., 2009; Von Hoff et al., 2011; Von Hoff et al., 2013; Muniraj et al., 2013).

Contributing to this poor prognosis is also the molecular evolution of the tumor during the course of carcinogenesis. If the primary tumor and distant metastasis are compared directly, it was reported that besides showing the same genetic alterations within the major tumor driver genes, there is also a genetic heterogeneity arising. Since the genetic instability continues after dissemination of the cancer, it makes therapeutic intervention even more complex. Because single metastasis will remain chemo-resistant due to a different mutational signature compared to the original primary tumor or other metastasis, therapeutic success is strongly impaired (Campbell et al., 2010).

In conclusion, it becomes obvious that future therapy of PDAC must consider the genetic signature of the tumor in order to tailor a patient specific therapeutic approach. As has already been applied with the novel chemotherapeutics, there should always be a combination of different drugs used to block different molecular targets known to be altered within the specific tumor. Inhibition of one pathway leading to upregulation of another redundant pathway due to a compensation effect represents another critical fact for consideration. In addition, more attention should be paid for inhibiting the tumor-stroma interaction in order to prevent fibrosis. This could lead to more efficient drug delivery and in combination with a variety of other molecular targeting drugs could show better outcome and enhanced survival.

3.2 Mouse models of human PDAC

In order to monitor pancreatic cancer *in vivo* as well as for therapeutic intervention studies, a preclinical murine model has been used within the present study. The great benefit of applying this mouse model is that it is able to histopathologically and genetically resemble the human disease in many aspects (Hingorani et al., 2003; Hruban et al., 2006). Within this mouse model, oncogenic $Kras^{G12D}$ (*Kras* containing the point mutation G12D) is used to initiate carcinogenesis, since it is known that this mutation leads to constitutively activated RAS signaling (Jackson et al., 2001). In order to generate a conditional knock in mouse model, a loxP site flanked stop cassette (LSL) has been placed upstream of the oncogenic *Kras* allele. Thus only in the presence of a Cre recombinase, oncogenic *Kras* will be expressed. For targeting expression towards the precursor cells of the pancreas, these mice have to be bred with *Pdx1-Cre* or $Ptf1a\ (p48)^{Cre}$ mice. The latter express the Cre recombinase under the control of the *Pdx1* or the *Ptf1a* promoter, respectively, which drive expression of transcription factors involved in pancreatic development. Most important, both

transcription factors are active in progenitor cells which give rise to all cells of the adult pancreas. In case of the *Pdx1* transgene originating mice, Cre is expressed stochastically within the pancreas, whereas it is consistently expressed in the whole pancreas when applying the *Ptf1a* knock in mice (Kawaguchi et al., 2002; Hingorani et al., 2003). After Cre mediated recombination, oncogenic *Kras* will be expressed at endogenous levels from the targeted allele (one WT *Kras* allele remains; complete *Kras* silencing is embryonic lethal). This expression was shown to result in the full histological PanIN progression also seen in human PDAC and leads to the establishment of invasive and metastatic PDAC after a long time (around 14 months). In order to find out the requirements for establishing invasive PDAC within the murine system, the same group generated an accelerated version of the standard oncogenic *Kras* model two years later. In this new model, a conditional mutated *Trp53* allele is included. The $Trp53^{R172H}$ gene carries a hot-spot point mutation often seen in human PDAC (equals the human $TP53^{R175H}$ point mutation observed in Li Fraumeni syndrome; Srivastava et al., 1990). The expression of this mutated tumor suppressor gene has been silenced by an upstream LSL cassette. Consequently upon Cre recombination the stop cassette will be deleted and the mutated form of the tumor suppressor will be expressed. After crossing this allele into the standard $Ptf1a^{Cre}$, $Kras^{G12D}$ mouse model, the mutated *Trp53* gene expression will be targeted to the pancreas. Development of invasive and metastatic PDAC is highly accelerated using this model (around 5 months) while maintaining the resemblance with the human disease (Hingorani et al., 2005). Consequently this so called KPC model (Kras, p53 and Cre) is widely used and represents the gold standard for modeling human PDAC in mice.

Beside this, there were numerous other mouse models generated trying to resemble human PDAC (reviewed in Hruban et al., 2006). Another conditional, Cre-loxP based approach was established by Aguirre who crossed the *Pdx1-Cre,* $Kras^{G12D}$ mice with conditional *Ink4a/Arf* null mice (Aguirre et al., 2003; Bardeesy et al., 2006). In this model, exon 2 and 3 of the endogenous *Cdkn2a* locus are flanked by loxP sites. Upon Cre mediated recombination, deletion of both exons leads to elimination of both tumor suppressor genes $p16^{INK4A}$ and $p19^{ARF}$, since they are sharing same exons in alternative reading frames. Consequently, in addition to oncogenic *Kras* signaling, two important tumor suppressor genes are deleted within the same cells. Similar to the KPC mouse model, the additional alteration of tumor suppressor genes leads to an accelerated progression to invasive and metastatic disease (Bardeesy et al., 2006). Furthermore, this model resembles human PDAC equally to the KPC model since deletion of these two tumor suppressors are also often found in human PDAC (Aguirre et al., 2003; Vincent et al., 2011).

3.3 Proliferating cell nuclear antigen (Pcna) as proliferation marker suitable for BLI of murine PDAC

In order to image proliferation of murine PDAC *in vivo*, a suitable marker gene is needed. For this purpose the *proliferating cell nuclear antigen* (*Pcna*) gene has been selected. The resulting protein is a homotrimer which is wrapped around the DNA generating the so called

sliding clamp (Krishna et al., 1994; Schurtenberger et al., 1998; Biasio and Blanco, 2013). Its main function lies in recruiting all proteins necessary to build the eukaryotic chromosomal DNA replisome, amongst others the DNA polymerase δ (Kelman and O'Donnell, 1995; Wyman and Botchan, 1995). Since Pcna is encircling the DNA, it also prevents the replicative polymerase from falling off the template strand during replication of the genome (Kelman and O'Donnell, 1995). Pcna binds to many different proteins involved in the cell cycle regulation. Amongst others, it can directly interact with cyclin-cyclin-dependent kinase (Cdk) complexes for cell cycle progression as well as the Cdk inhibitor p21 for cell cycle arrest (Xiong et al., 1992; Gulbis et al., 1996; Knibiehler et al., 1996). In case of DNA damage, senescence or differentiation, p21 expression is triggered resulting in inhibition of G1 to S phase cell cycle transition. This cell cycle arrest is achieved by binding of p21 to Cdks using its N-terminus and by simultaneously binding to Pcna using its C-terminus (Chen et al., 1995; Luo et al., 1995; Chen et al., 1996; Moskowitz et al., 1996).

Pcna expression is cell cycle dependent. It has been demonstrated that during late G1 and especially within S phase there is a significant increase in Pcna expression levels compared to G0-G1 phase, where almost no expression could be detected. In G2-M phase, the Pcna expression level strongly decreases again, yet it is elevated relative to G0-G1 phase (Kurki et al., 1986). In conclusion, Pcna integrates and transduces positive as well as negative signals depending on the highly complex interactions with many different proteins. When binding to Cdk-cyclin-complexes it can lead to cell cycle progression whereas the competitive binding of p21 can lead to destruction of the latter complexes and thus sudden cell cycle arrest (Maga and Hübscher et al., 2003). The strong connection with cell cycle regulating proteins and especially its requirement for the successful G1 to S phase transition make Pcna the perfect marker that is specifically expressed in replicating cells. Since Pcna expression levels are strongly coupled to cell cycle phases, its promoter activity can consequently be used as a direct read out for the proliferation state of a cell.

4. Aims of this study

In order to establish a PDAC model suitable for BLI and therapeutic intervention studies, a new knock in mouse line has been generated in our lab. In this model, the *fLuc* is knocked into the ATG start codon of the endogenous *Pcna* locus, thereby destroying one *Pcna* allele. Expression of the knock in allele is silenced by an LSL cassette in order to generate a tissue-specific, conditional allele. After crossing the allele into the above mentioned murine PDAC model, the luciferase expression can be selectively targeted to the pancreas (due to use of the *Ptf1a*^{Cre} allele). Since the fLuc will only be expressed in cells which show *Pcna* promoter activity, exclusively proliferating cells within the tumor entity can be visualized by BLI.

Applying this *LSL-Pcna*$^{ATG\text{-}fLuc/+}$ mouse model, first of all a characterization of the murine PDAC model will be conducted by non-invasive real time *in* and *ex vivo* BLI of proliferation. Furthermore, the next aim of this study is to use this reporter mouse model as an *in vivo* drug evaluation platform, applying novel chemotherapeutics showing the most promising impacts within previous preclinical *in vitro* assays. In order to evaluate novel anti cancer drugs, it is of

great importance to use an *in vivo* experimental approach which is able to incorporate all aspects of the human disease as accurate as possible in its natural context. Therefore, the effect of the dual PI3K and mTOR inhibitor NVP-BEZ235 on the proliferation activity of murine PDAC within the endogenous *LSL-Pcna*$^{ATG\text{-}fLuc/+}$ mouse model will be evaluated.

Since this reporter mouse model is based upon the classic KPC approach, there are several disadvantages arising. Within the KPC mouse model all genetic alterations like oncogene activations and tumor suppressor gene inactivations occur simultanously upon tissue-specific, Cre-mediated recombination. As the human PDAC shows a progressing cascade of genetic events, this model is not able to mimic the true nature of the cancer. In order to resemble the sequential, step-wise cascade of genetic alterations occurring to drive the PanIN progression towards invasive PDAC, a new mouse model is needed. Such a model has also been established within our lab and is based upon the combination of two recombination systems (Cre-loxP and Flp-FRT). Due to using two different recombinases and additionally inducible alleles, it is now possible to spatiotemporally activate/inactivate the desired PDAC driver genes. This means the sequential nature of carcinogenesis can now faithfully be recapitulated by turning genes on/off at any time point in the tissue of interest. Consequently, the role of single proteins within the many different oncogenic signaling cascades can be better elucidated, since not all mutations occur synchronized such as in the KPC mouse model.

There is the need to establish a new reporter mouse line which is able to visualize all the possibilities arising when applying the dual recombination system based PDAC mouse model. For that reason, the main goal of the present thesis is the generation of a new, spatiotemporally inducible reporter mouse model for *in vivo* as well as *ex vivo* imaging of murine PDAC. Two distinct reporter gene cassettes will be constructed in order to allow reporting of Cre as well as of Flp mediated recombination events. Furthermore, each reporter cassette will consist of a pair of reporter genes, one for bioluminescence-based *in vivo* imaging using luciferases and one for fluorescence-based *ex vivo* imaging using fluorescent proteins. Both reporter genes of each cassette will be connected via viral 2A sites to achieve high simultaneous expression levels.

B. Materials and Methods

1. Materials

1.1 Chemicals

Compound	Source of supply
1kb DNA Extension Ladder (Invitrogen™)	Life Technologies GmbH, Darmstadt
2-Log DNA Ladder	New England Biolabs GmbH, Frankfurt am Main
2-Mercaptoethanol	Sigma-Aldrich Chemie GmbH, Steinheim
5-Bromo-2´-deoxyuridine (BrdU)	Sigma-Aldrich Chemie GmbH, Steinheim
6x DNA Loading Dye	Fermentas GmbH, St. Leon-Rot,
Agarose	PEQLAB Biotechnologie GmbH, Erlangen
Ampicillin sodium salt	Carl Roth GmbH & Co. KG, Karlsruhe
Bovine serum albumin (BSA) for Bradford assay	Bio-Rad Laboratories GmbH, München
Bradford reagent	Bio-Rad Laboratories GmbH, München
BSA (Bovine Serum Albumin) for cloning	New England Biolabs GmbH, Frankfurt am Main
Calciumchloride ($CaCl_2$)	Sigma-Aldrich Chemie GmbH, Steinheim
Chloramphenicol	Applichem, Darmstadt
Deoxyribonucleoside triphosphate (dNTP)	Fermentas GmbH, St. Leon-Rot
dH_2O (Ecotainer® Aqua B. Braun)	B. Braun Melsungen AG, Melsungen
Dimethylsulfoxid (DMSO)	Sigma-Aldrich Chemie GmbH, Steinheim
D-luciferin-sodium	Synchem, Felsberg/Altenburg
DMEM (+ 4.5 g/l D-Glucose)	Gibco, Life Technologies GmbH, Darmstadt
EDTA (1% in PBS)	Biochrom AG, Berlin
EDTA	Sigma-Aldrich Chemie GmbH, Steinheim
ESGRO® (Murine Leukemia Inhibitory Factor, LIF)	Merck KGaA, Darmstadt, Millipore (Chemicon)
Ethanol absolute	Merck KGaA, Darmstadt
Ethidiumbromide	Carl Roth GmbH, Karlsruhe
Fetal calf serum (FCS)	Biochrom AG, Berlin
Fetal calf serum for embryonic stem cell culture (ES-FCS)	Gibco, Life Technologies, Darmstadt
G418-BC (Geneticin)	Biochrom AG, Berlin
Gelatin	Invitrogen, Karlsruhe
GeneRuler™ 100bp Plus DNA Ladder	Fermentas GmbH, St. Leon-Rot
Glycerol	Sigma-Aldrich Chemie GmbH, Steinheim
Hydrochloric acid (HCl)	Carl Roth GmbH & Co. KG, Karlsruhe
Hydroxypropyl-Methylcellulose	Sigma-Aldrich Chemie GmbH, Steinheim
Isofluran Forene	Abbott GmbH, Wiesbaden
Isopropanol	Carl Roth GmbH, Karlsruhe
Kanamycin-sulfate	Carl Roth GmbH & Co. KG, Karlsruhe
LB-Agar (Luria/Miller)	Carl Roth GmbH & Co. KG, Karlsruhe
LB-Broth (Luria/Miller)	Carl Roth GmbH & Co. KG, Karlsruhe

Compound	Source of supply
L-glutamine	Life Technologies GmbH, Darmstadt
Magnesium chloride ($MgCl_2$)	Sigma-Aldrich Chemie GmbH, Steinheim
N-Methyl-Pyrrolidon (NMP)	Sigma-Aldrich Chemie GmbH, Steinheim
Non-essential amino acids (NEAA)	Life Technologies GmbH, Darmstadt
NVP-BEZ235 hydrochloride	Chemdea, Ridgewood, NJ, USA
Penicillin-Streptomycin	Life Technologies GmbH, Darmstadt
Phosphate buffered saline (PBS 1x)	Gibco, Life Technologies, Darmstadt
Polyethylenglycol (PEG-300)	Sigma-Aldrich Chemie GmbH, Steinheim
Potassium chloride (KCl)	Sigma-Aldrich Chemie GmbH, Steinheim
Roti® Phenol/Chloroform/Isoamylalcohol	Carl Roth GmbH, Karlsruhe
Roti®-Histofix 4 % Paraformaldehyde solution (PFA)	Carl Roth GmbH & Co. KG, Karlsruhe
S.O.C. Medium (Invitrogen™)	Life Technologies GmbH, Darmstadt
Sodium acetate	Sigma-Aldrich Chemie GmbH, Steinheim
Sodium chloride (NaCl)	Carl Roth GmbH & Co. KG, Karlsruhe
Sodium dodecyl sulphate (SDS)	Carl Roth GmbH & Co. KG, Karlsruhe
Tris-HCl	Carl Roth GmbH & Co. KG, Karlsruhe
TritonX-100	Sigma-Aldrich Chemie GmbH, Steinheim
Trypsin-EDTA	Life Technologies GmbH, Darmstadt
Tween-80	Carl Roth GmbH, Karlsruhe

1.2 Enzymes

Compound	Source of supply
Gateway® LR Clonase® II Enzyme Mix	Invitrogen, Life Technologies GmbH, Darmstadt
HotStarTaq DNA Polymerase	Qiagen GmbH, Hilden
Platinum® Blue PCR SuperMix	Life Technologies GmbH, Darmstadt
Proteinase K	Roche Diagnostics Deutschland GmbH, Mannheim
Quick Ligation Kit Ligase	New England Biolabs GmbH, Frankfurt am Main
rAPid Alkaline Phosphatase	Roche Diagnostics Deutschland GmbH, Mannheim
REDTaq® ReadyMix™ PCR Reaction Mix	Sigma-Aldrich Chemie GmbH, Steinheim
Restriction endonucleases (cloning)	New England Biolabs GmbH, Frankfurt a.M.
RNAse A	Fermentas GmbH, St. Leon-Rot
T4 DNA Ligase	Invitrogen, Life Technologies GmbH, Darmstadt

1.3 Buffers and solutions

All solutions were prepared with bidest. H_2O.

Solution	Ingredients
50x TAE-buffer pH 8.5	2 M Tris 100 mM EDTA 5.71% acetic acid (glacial)

Solution	Ingredients
Agarose solution (e.g. 2%)	2g agarose 100ml 1xTAE
ES cell lysis buffer	100 mM Tris pH 8.5 5 mM EDTA 0.8 mM HCl 2% SDS 200 mM NaCl 0.1 mg/mL proteinase K (add prior to use)
Gitschier's buffer (10x)	670 mM Tris pH 8.8 166 mM $(NH_4)_2SO_4$ 67 mM $MgCl_2$
KCM buffer (transformation of competent bacteria)	500 mM KCl 150 mM $CaCl_2$ 250 mM MgC_{l2}
Loading buffer orange G (6x)	60% glycerol 60 mM EDTA 0.24% orange G 0.12% SDS
Mouse tail lysis buffer (soriano buffer)	0.5% Triton X-100 1% β-mercaptoethanol 10% 10x Gitschier's buffer 400 µg/ml proteinase K (add prior to use)
Paraffin lysis buffer (for subsequent DNA extraction)	10 mM TrisHCl 1 mM EDTA 1% SDS 20 mg/mL proteinase K (add prior to use)

1.4 Bacterial strains and cell lines

Bacterial strain or cell line	Source of supply
MIA PaCa-2 (human pancreatic cancer cell line)	American Type Culture Collection, Manassas, VA, USA
NovaBlue Competent Cells	Merck KGaA, Darmstadt, Millipore
One Shot® Stbl3™ chemically competent *E.coli*	Life Technologies GmbH, Darmstadt,
One Shot® TOP10 chemically competent *E.coli*	Life Technologies GmbH, Darmstadt,
W4/129S6 ES Cells	Taconic Farms Inc., Hudson, NY, USA

1.5 Cell culture medium

Medium	Ingredients
Mediums for culturing the MIA PaCa-2 cell line and murine PDAC cell lines	
Standard culture medium	DMEM (high glucose) 10% FCS 1% Penicillin-Streptomycin

Medium	Ingredients
Freezing medium (cryopreservation)	DMEM (high glucose) 20% FCS 10% DMSO
Mediums for ES cell culture	
MEF culture medium	DMEM (high glucose; w/o L-glutamine) 10% FCS 1% Penicillin-Streptomycin 1% L-glutamine
ES cell culture medium	DMEM (high glucose; w/o L-glutamine) 15% ES-FCS 1% Penicillin-Streptomycin 1% L-Glutamine 1% sodium pyruvate 1% non-essential amino acids 0.1% 10^{-1}M β-mercaptoethanol 1000 U/mL LIF
ES cell freezing medium (cryopreservation)	ES cell culture medium 10% DMSO

1.6 Disposables

Disposable	Source of supply
100 Sterican gauge-needle, Gr. 20	B. Braun Melsungen AG, Melsungen
27-gauge needles	BD Bioscience, Franklin Lakes, NJ, USA
BioPur® combitips	Eppendorf AG, Hamburg
Cell culture disposables (petri dishes, flasks, other plastics)	BD Bioscience, Franklin Lakes, NJ, USA TPP Tissue Culture Labware, Trasadingen, CH and Cell Star, Greiner Bio One, Greiner Bio-One GmbH, Frickenhausen
Cell culture scrapers	TPP Tissue Culture Labware, Trasadingen, CH
Cover glass	Menzel-Gläser, Braunschweig
CryoPure tubes	Sarstedt AG&Co., Nümbrecht
Cryotubes™	Nunc™ Brand Products, Napeville, IL, USA
Cuvettes	Greiner Bio-One GmbH, Frickenhausen
Filter tips for pipets	Nerbe Plus GmbH, Winsen (Luhe)
GelStar™ Nucleic Acid Gel Stain	BioWhittaker Molecular Applications, Rockland, ME, USA
Gene pulser/Micropulser cuvettes (0.2 cm gap)	Bio-Rad Laboratories GmbH, München
Microtome blade	Feather Safety Razor Co, Ltd., Osaka, Japan
Omnifix®-F syringe	B. Braun Melsungen AG, Melsungen
Parafilm M	Brand GmbH & Co KG, Wertheim
Pasteur Pipets (cell culture)	Hirschmann Laborgeräte GmbH & Co. KG, Eberstadt

Disposable	Source of supply
PCR reaction tubes (0.2 ml)	Eppendorf AG, Hamburg Sarstedt AG&Co., Nümbrecht
PCR reaction tubes 8 strips	Brand GmbH + Co KG, Wertheim
Plastic embedding device	Bio Optica Milano S.p.A., Milan, Italy
Plating scoop	Sarstedt, Nümbrecht
Reaction tubes 0.5 ml, 1,5 ml and 2 ml	Eppendorf AG, Hamburg
Safe-lock reaction tubes 1,5 ml and 2 ml BioPur®	Eppendorf AG, Hamburg
Scalpel	Feather Safety Razor Co., Ltd, Osaka, Japan
Semper Care Gloves latex and nitril	Semperit Technische Produkte GmbH, Segment Sempermed, Wien, Austria
Serological pipettes (cell culture)	BD Bioscience, Franklin Lakes, NJ, USA
Single use syringe	CODAN Medizinische Geräte GmbH, Lensahn
Sterile inoculation loop	Greiner Bio-One GmbH, Frickenausen
Sterile pipette tips	Biozym Scientific GmbH, Hessisch Oldendorf
Superfrost® Plus glass slides	Menzel Gläser, Braunschweig

1.7 Kits

Kit	Source of supply
AxyPrep Plasmid Miniprep Kit	Axygen, Corning Gilbert Inc., Arizona, USA
Dual-Luciferase® reporter Assay System	Promega GmbH, Mannheim
Effectene Transfection reagent	Qiagen GmbH, Hilden
MinElute PCR purification kit	Qiagen GmbH, Hilden
Nachweis von Mykoplasmen in Zellkulturen mittels PCR (AM029)	Bund/Länder Arbeitsgemeinschaft Gentechnik; www.lag-gentechnik.de
QIAamp DNA Mini Kit	Qiagen GmbH, Hilden
QIAEx 2 Gel Extraction Kit	Qiagen GmbH, Hilden
Qiagen EndoFree Plasmid Maxi Kit (plasmid isolation for ES cell culture gene targeting)	Qiagen GmbH, Hilden
Qiagen Endofree Plasmid Midi kit (plasmid isolation for MIA PaCa-2 transfections)	Qiagen GmbH, Hilden
Qiagen Min Elute Gel Extraction Kit	Qiagen GmbH, Hilden
Qiagen Plasmid Midi Kit	Qiagen GmbH, Hilden
QIAPREP Spin Miniprep Kit	Qiagen GmbH, Hilden
QIAquick PCR Purification Kit	Qiagen GmbH, Hilden
Quick Blunting Kit	New England Biolabs GmbH, Frankfurt am Main
Quick Ligation Kit	New England Biolabs GmbH, Frankfurt am Main

1.8 Antibodies

Antibody	Source of supply
Anti-BrdU (rat) (# MCA2060)	AbD Serotec, Düsseldorf
Biotinylated Anti-Rat IgG (goat) (# BA-9400)	Vector Laboratories, Burlingame, CA, USA

1.9 Reagents for histochemistry

Reagent	Source of supply
Acetic acid (glacial)	Merck KgaA, Darmstadt
Antigen unmasking solution (citric acid based)	Vector Laboratories, Burlingame, CA, USA
Avidin/Biotin blocking kit	Vector Laboratories, Burlingame, CA, USA
DAB peroxidase substrate kit	Vector Laboratories, Burlingame, CA, USA
Eosin	Waldeck GmbH, Münster
Goat serum (# G9023)	Sigma-Aldrich Chemie GmbH, Steinheim
H_2O_2	Merck KgaA, Darmstadt
Haematoxylin	Merck KgaA, Darmstadt
Pertex mounting medium	Medite GmbH, Burgdorf
Roti® Histofix (4% formalin)	Carl Roth GmbH, Karlsruhe
Roti® Histol	Carl Roth GmbH, Karlsruhe
VECTASTAIN® Elite ABC solution	Vector Laboratories, Burlingame, CA, USA

1.10 Initial cloning vectors and linkers

Vector/linker name	Source of supply
Acc65-1-loxP-Xho1-linker	Eurofins MWG Operon, Ebersberg
pBlue-FsaSF-minPGK	AG Saur, Klinikum rechts der Isar, München, modified containing pBluescript backbone
pcDNA3.1	AG Saur, Klinikum rechts der Isar, München
pCHMWS-EGFP-P2A-fLuc-T2A-HSV1-sr39tk	AG Saur, Klinikum rechts der Isar, München
pCHMWS-EGFP-T2A-fLuc	AG Saur, Klinikum rechts der Isar, München (firefly luciferase derived from pSP-luc+NF, Promega, Wisconsin, USA)
pC-S2-TAG-mem-td-Tomato-T2A-H2B-EGFP-pA	Order ID: 26772; Addgene, Massachusetts, USA
pEntr-CAG-saFSF-CreER^{T2}-pA	AG Saur, Klinikum rechts der Isar, München, modified containing pEntr backbone (*CAG* promoter with SA derived from pTriEx™ neo2; Novagen, Darmstadt)
pEntr-sa-FSF-MCS-pA	AG Saur, Klinikum rechts der Isar, München, modified containing pEntr backbone
pEntryBlue	AG Saur, Klinikum rechts der Isar, München
phrG-B-Ecadh-hrLuc-pA	AG Saur, Klinikum rechts der Isar, München, modified containing phrG-B-backbone

Vector/linker name	Source of supply
pRosa-RFA	Rosa26 gene targeting vector; AG Saur, Klinikum rechts der Isar, München
Xho1-EcoR1-Bgl2-2nt-Nco1 linker	Eurofins MWG Operon, Ebersberg
Xho1-Xma1-Avr2-Pml1-loxP-1nt-BamH1-linker	Eurofins MWG Operon, Ebersberg

1.11 Additional plasmids used for co-transfection as well as co-transformation experiments

Vector Name	Source of supply
CMV-EGFP-pA (EGFP expression vector, positive ctrl)	AG Saur, Klinikum rechts der Isar, München
Mammalian Cre expression plasmid	AG Saur, Klinikum rechts der Isar, München
pFlpo (bacterial Flp expression plasmid)	Order ID: 13792; Addgene, Massachusetts, USA
pPGK-Flpo-bpA (mammalian Flp expression plasmid)	Order ID: 13793; Addgene, Massachusetts, USA

1.12 Oligonucleotides for screening-PCRs and sequencing (cloning primers)

Screening primers for the *Dual Reporter* construct designed by using Primer Express® Software v2.0 (Applied Biosystems; Life Technologies GmbH, Darmstadt). All primers were ordered at Eurofins MWG Operon in Ebersberg, if not stated otherwise.

Table 1: Cloning primer sequences

Primer name	Sequence 5` to 3`
BrpA-LP	TAAAATACAGCATAGCAAAACTTTAACCTCCAAATC
BrpA-UP	CTAGAAGCTCGCTTTCTTGCTGTCCAATTTCT
CAGGS-sc-LP	GTACTTGGCATATGATACACTTGATGTAC
CAGGS-sc-UP4	GTTCGGCTTCTGGCGTGTGTGT
CAGGS-sc-UP5	CGTGCTGGTTATTGTGCTGTCTCATCATT
CAGGS-sc-UP6	CATTTTGGCAAAGAATTGGATCGGAC
CMV-forward	CGCAAATGGGCGGTAGGCGTG
EGFP-GT-LP	CGGACTGGGTGCTCAGGTAGT
EGFP-GT-UP	GGGCACAAGCTGGAGTACAACT
EGFP-sc-neu-LP1	GTCCTTGAAGAAGATGGTGCGCTC
Entr65-UP	GACGTTGTAAAACGACGGCCAGTCT
fLuci-UP1	CGGAGGAGTTGTGTTTGTGGA
FsaSF-neo-sc-LP-1	GTCAAGAAGGCGATAGAAGGCGATG
FsaSF-neo-sc-LP-2	ATTGCATCAGCCATGATGGATACTTTCT
FSF-neo-Nco-LP	GCATCGCCATGGGTCACGACGA
loxP-linker-LP	CTCGAGATAACTTCGTATAATGTATGCTATACGAAGTTATGGTACC
loxP-linker-LP (pBC)	GGATCCTATAACTTCGTATAATGTATGCTATACGAAGTTATCACGTGCCTAGGCCCGGGCTCGAG
loxP-linker-UP	GGTACCATAACTTCGTATAGCATACATTATACGAAGTTATCTCGAG

Primer name	Sequence 5` to 3`
loxP-linker-UP (pBC)	CTCGAGCCCGGGCCTAGGCACGTGATAACTTCGTATAGCAT ACATTATACGAAGTTATAGGATCC
M13-FP (derived from GATC Biotech AG, Konstanz)	TGTAAAACGACGGCCAGT
M13-RP (derived from GATC Biotech AG, Konstanz)	CAGGAAACAGCTATGACC
mBlue-LP	ACACAGGAAACAGCTATGACCATGA
mBlue-UP	GTTGTAAAACGACGGCCAGTGA
neo-TM-LP1	GTGCCCAGTCATAGCCGAAT
neo-TM-UP1	TGGATTGCACGCAGGTTCT
oIMR0872-UP (EGFP)	AAGTTCATCTGCACCACCG
oIMR1416-LP (EGFP)	TCCTTGAAGAAGATGGTGCG
pBroad-pA-5038-UP	CGCTTTCTTGCTGTCCAATTTCTAT
pBroad-pA-5219-UP	GGTCAGTGCATTTAAAACATAAAGAAATG
pBroad-pA-5268-LP	CCAAGGTTTGAACTAGCTCTTCATTT
pEntr-sc-LP	GCTGCCAGGAAACAGCTATGAC
pEntr-sc-UP	GTTGTAAAACGACGGCCAGTCTT
Pgl3-pA-Pause-UP	TGAATAGTTAATTGGAGCGGCCGCAATA
pgl3-UP(RV3)	CTAGCAAAATAGGCTGTCCC
phrgb-RP	GCCACGGGCTCGATGTGAGG
R26-lA-LP1	CATTCTCAGTGGCTCAACAACACT
R26-td-Emut-LP	TCAATGGGCGGGGGTCGTT
R26-Tva-GT-UP	AAAGTCGCTCTGAGTTGTTAT
R26-Tva-GT-SA-mut-LP	GCGAAGAGTTTGTCCTCAACC
R26-Tva-GT-wt-LP	GGAGCGGGAGAAATGGATATG
Reni-LP	GAAGCTCTTGATGTACTTACCCATTTC
Reni-UP	CTCATATCGCCTCCTGGATCACT
Ros-ES-LP1	GGAGCCTGCTTTTTTGTACAAACTTGTGA
Ros-ES-LP2	ACCTCGAGGGTACCCGGTGAAGG
Ros-ES-UP1	GCTTGGTGCGTTTGCGGGGATG
Ros-ES-UP2	GCTCCTCAGAGAGCCTCGGCTAGGTAG
Td-Tom-sc-LP4	TCGGAGCGCTCGTACTGTTCCA
Tomato-LP2	AGGTTGTCCTTGCGCTTGCTCTTGAT
Tom-LP1	ATACATTATACGAAGTTATAGGATCCACTAGAGC
Vtd-Tom-sc-LP3	TCACCATGGAGGCGACCGGT

1.13 Oligonucleotides for genotyping of the transgenic mouse lines

Template DNA for all genotyping PCRs was genomic DNA extracted from a mouse tail tip biopsy. All genotyping primers were synthesized by Eurofins MWG Operon in Ebersberg.

Table 2: Genotyping primers

Name of transgenic mouse line	Primer name	Sequence 5` to 3`
Pdx1-Cre	Cre-neu-UP	CCTGGAAAATGCTTCTGTCCG
	Cre-neu-LP	CAGGGTGTTATAAGCAATCCC
	Gabra1-UP	AACACACACTGGAGGACTGGCTAGG
	Gabra1-LP	CAATGGTAGGCTCACTCTGGGAGATGATA
Ptf1a^{Cre} (*p48*^{Cre})	p48-Cre-GT-wt-UP	CCACGGATCACTCACAAAGCGT
	p48-Cre-GT-mut-UP-neu	GCCACCAGCCAGCTATCAA
	p48-Cre-GT-LP-URP	CCTCGAAGGCGTCGTTGATGGACTGCA
LSL-Kras^{G12D}	Kras-wt-UP1	CACCAGCTTCGGCTTCCTATT
	Kras-URP-LP1	AGCTAATGGCTCTCAAAGGAATGTA
	Kras^{G12D} mut-UP	CCATGGCTTGAGTAAGTCTGC
LSL-Trp53^{R172H}	Trp53^{R172H}-WT-UP2	AGCCTTAGACATAACACACGAACT
	Trp53^{R172H}-URP-LP	CTTGGAGACATAGCCACACTG
	Trp53^{R172H}-mut UP4	GCCACCATGGCTTGAGTAA
LSL-Trp53^{R172H} (screen for presence of the LSL stop cassette)	Trp53^{R172H}-lox-UP	AGCCTGCCTAGCTTCCTCAGG
	Trp53^{R172H}-lox-LP	CTTGGAGACATAGCCACACTG
Cdkn2a^{lox} (*p16*^{Ink4A} /*p19*^{Arf} floxed)	Ink4A-UP	CCAAGTGTGCAAACCCAGGCTCC
	Ink4A-LP	TTGTTGGCCCAGGATGCCGACATC
LSL-Pcna$^{ATG\text{-}fLuc/+}$	Pcna-ATG-UUP	GCACAGCTCGATTTGCCTG
	Pcna-ATG-Mut-LP	TACGAACGGTAATTAACAATTCGATATCAAG
	Pcna-ATG-WT-LP	CCCGACACCATAGACCAATCAG
LSL-Pcna$^{ATG\text{-}fLuc/+}$ (screen for presence of the LSL stop cassette)	pGL3-pA-pause-4645-UP	TGAATAGTTAATTGGAGCGGCCGCAATA
	pGL-3LP	CTTTATGTTTTTGGCGTCTTCC
Rosa26 locus genotyping (different reporter gene knock ins)	R26-Tva-GT-UP	AAAGTCGCTCTGAGTTGTTAT
	R26-Tva-GT-WT-LP	GGAGCGGGAGAAATGGATATG
	R26-Tva-GT-SA-mut-LP	GCGAAGAGTTTGTCCTCAACC

Name of transgenic mouse line	Primer name	Sequence 5` to 3`
Rosa26 locus genotyping (screen for presence of the LSL stop cassette)	R26-Tva-GT-UP	AAAGTCGCTCTGAGTTGTTAT
	Tva-LP-353	CATCTCACCAGCTCACAGCAA

1.14 Sequencing

All sequence analyses were performed by the company GATC Biotech AG in Konstanz.

1.15 Equipment

Equipment	Source of supply
ASP300 Automated Vaccuum Tissue Processor	Leica Mikrosysteme Vertrieb GmbH, Wetzlar
Avanti® J25 centrifuge	Beckman Coulter Inc., Brea, CA, USA
AxioCam MRc	Carl Zeiss AG, Oberkochen
Bacterial incubator (agar plates)	Heraeus Holding GmbH, Hanau
Bacterial thermoshaker (liquid cultures)	C. Gerhardt, Königswinter
Balance Kern AGB	Gottlieb Kern & Sohn GmbH, Balingen-Frommern
Biometra WT 18 Shaker	Biometra, Analytik Jena AG, Jena
Biorad Power Pack 1.000/200 power supplies	Biorad Laboratories GmbH, München
Centrifuge 5417R	Eppendorf AG, Hamburg
Centrifuge Mikro 220R	Hettich Zentrifugen, Andreas Hettich GmbH & Co.KG, Tuttlingen
Centrifuge Z323K	HERMLE Labortechnik GmbH, Wehingen
CO_2 incubator HERAcell®	Heraeus Instruments GmbH, Osterode
Compact L/XL electrophoresis chambers and gel casting apparatus containing gel trays and combs	Biometra, Analytik Jena AG, Jena
Cryo 1°C Freezing Container (Nalgene Cryocontainer)	Thermo Fisher Scientific, Langenselbold
Dewar Carrying Flask, type B	KGW-Isotherm, Karlsruhe
Digital CCD camera ORCA II-ER-1394	Hamamatsu, Herrsching
Easy Pet	Eppendorf, Hamburg
Electrophoresis-power supply Power Pac 200	Bio-Rad Laboratories GmbH, München
Elisa Plate reader Anthos 2001	Anthos Mikrosysteme GmbH, Krefeld
Eppendorf 5432 mixer	Eppendorf AG, Hamburg
Eppendorf Pipets Research	Eppendorf AG, Hamburg
Flex Cycler Thermocycler	Analytik Jena AG, Jena
Flu-O-Blu (blue light transmission table for preparative gels stained with GelStar™ Nucleic Acid Gel Stain)	Biozym Scientific GmbH, Hessisch Oldenburg

Equipment	Source of Supply
Galaxy Mini (PCR reaction tube centrifuge)	Merck Eurolab GmbH, Ismaning
GalaxyMini single reaction tubes table centrifuge	VWR International GmbH, Ismaning
Gel doc XR+ documentation system	Bio-Rad Laboratories GmbH, München
Gene Pulser II	Bio-Rad Laboratories GmbH, München
Genequant Pro	Biochrom Ltd., Cambrige, UK
Hemocytometer (Neubauer improved)	LO-Laboroptik GmbH, Bad Homburg
Hera Safe biological safety cabinet	Thermo Fisher Scientific Inc.Waltham, MA, USA
Hera Safe laminar flow cell culture hood (for ES cell culture)	Heraeus Instruments, Heraeus Holding GmbH, Hanau
Histosette®	Sigma-Aldrich Chemie GmbH, Steinheim
Horizontal gel electrophoresis system	Biozym Scientific GmbH, Hessisch Oldenburg
Incubator (for genomic DNA extraction of transgenic ES cells)	MELAG Medizintechnik, Berlin
Leica EG 1150 H embedding system	Leica Mikrosysteme Vertrieb GmbH, Wetzlar
Luminometer Lumat LB 9501	Berthold Technologies GmbH, Bad Wildbad
Magnetic stirrer COMBIMAG	IKA-Werke GmbH, Staufen
Magnetic stirrer MR3000	Heidolph Elektro GmbH & Co. KG, Kelheim
Microscope Axiovert 25	Carl Zeiss AG, Oberkochen
Microscope DM LB	Leica Mikrosysteme Vertrieb GmbH, Wetzlar
Microtome Microm HM355S	Thermo Scientific, Walldorf
Microwave	Siemens, München
Millifuge	Merck-Millipore, Merck KgaA, Darmstadt
Multi-channel Transferpette® S -8	Brand GmbH & Co KG, Wertheim
Multipette® stream	Eppendorf AG, Hamburg
Paraffin tissue floating bath Microm SB80	Thermo Fisher Scientific Inc., Waltham, MA, USA
PCR-Thermocycler T-1	Biometra, Analytik Jena AG, Jena
pH-meter	WTW GmbH, Weilheim
Photometer gene quant pro RNA/DNA calculator (OD600 measurement of bacterial cultures)	Gemini BV, DG Apeldoorn, Netherlands
Pipetus®	Hirschmann Laborgeräte GmbH und Co. KG, Eberstadt
Polymax 1040 shaker (for luciferase cell harvesting)	Heidolph Instruments GmbH, Schwabach
Power supply	Consort, Turnhout, Belgium
Precision balance Kern FTB	Gottlieb Kern & Sohn GmbH, Balingen-Frommerns
PrimoStar microscope	Carl Zeiss AG, Oberkochen
PTC-200 DNA Engine (for cloning)	MJ Research, GMI Inc., Minnesota, USA

Equipment	Source of supply
Rotina 46R and Universal 320R centrifuges	Hettich Zentrifugen, Andreas Hettich GmbH & Co.KG, Tuttlingen
Schott Duran® glass ware	Schott UK Ltd, Stafford, UK
Special accuracy balance	Sartorius AG, Göttingen
Spectrophotometer Nanodrop ND-1000	PEQLAB Biotechnologie GmbH, Erlangen
Sunrise™ electrophoresis apparatus	Gibco, Life Technologies GmbH, Regensburg
Table centrifuge 5415D (used for cloning)	Eppendorf AG, Göttingen
T-Gradient Thermocycler	Biometra, Analytik Jena AG, Jena
Thermo Stat plus shaker	Eppendorf AG, Hamburg
Thermomixer compact	Eppendorf AG, Hamburg
Thermomixer S436	Eppendorf AG, Hamburg
Thermoshake	Gerhardt GmbH, Königswinter
UV Solo TS Imaging System	Analytik Jena AG, Jena
VacuGene pump	GE Healthcare Europe GmbH, Freiburg
VacuGene XL	GE Healthcare Europe GmbH, Freiburg
Vortex Genie 2	Scientific Industries Inc., Bohemia, New York, USA
Vortex Reax 2000	Heidolph Instruments GmbH, Schwabach
Vortex VF2	IKA-Werke GmbH, Staufen
Water bath (for FCS inactivation)	Memmert GmbH u. Co. KG, Schwabach
Water bath (for ES cell culture)	Dinkelberg Analytics GmbH, Gablingen
Water bath 1003 (for primary cell culture)	GFL Gesellschaft für Labortechnik GmbH, Burgwedel
Water bath GFL-1083 (for MIA PaCa-2 cell culture)	hilab.de C/O Nanolytik Baghini, Düsseldorf
Zeiss and Schott KL 1500 LCD/ KL200 illumination for stereo microscopy	Carl Zeiss AG, Oberkochen and Schott UK Ltd, Stafford, UK
Zeiss LSM 510	Carl Zeiss AG, Oberkochen
Zeiss Stemi SV-11 stereo microscope	Carl Zeiss AG, Oberkochen

2. Methods

2.1 Mouse breeding and experiments

In order to characterize the *LSL-Pcna*$^{ATG\text{-}fLuc/+}$ mouse model *in vivo* for BLI of PDAC proliferation and for chemotherapeutic intervention experiments, tumor mice were generated. Based on the conditional Cre-loxP system, *Pdx1-Cre* and *Ptf1a*^{Cre} mice were interbred with *LSL-Kras*^{G12D} and *LSL-Trp53*^{R172H} as well as *p16/p19*^{lox} mice in order to generate mice that develop PDAC with 100% penetrance. To further accelerate PDAC formation, the *LSL-Trp53*^{R172H} and *p16/p19*^{lox} alleles were further interbred to reach homozygosity. The *LSL-Pcna*$^{ATG\text{-}fLuc/+}$ allele was crossed into this mouse model in order to targed the fLuc expression towards the proliferating cell population of the developing PDAC.

Tumor mice were supervised routinely by the animal keepers as well as the researcher and housed within specific pathogen free (SPF) facilities. In case of bad health condition or high tumor burden, mice were sacrificed using isofluran inhalation and cervical dislocation and

further analyzed. All GEMM BLI experiments as well as therapeutic intervention studies were approved by respective authorities.

2.1.1 Genotyping

At the age of three weeks mice were genotyped using a tail tip biopsy. One week later, female and male offsprings were separated. For determination of the genotype an approx. 1 mm tail tip was lysed in mouse tail lysis buffer (soriano buffer) and proteinase K (2% proteinase K addition just prior to use) at 55°C for 90 min. After 15 min proteinase K denaturation at 95°C, lysed tail tips were thoroughly vortexed (10 sec) and centrifuged at 14,000 rpm and 4°C for 10 min. Approx. 1.5 µl of the clear supernatant was used as template genomic DNA for a 25 µl genotyping PCR (40 cycles). Primer sets are designed to allow a discrimination between a WT, heterozygous and homozygous state of an allele. In order to confirm correct Cre-loxP recombination of the respective allele (deletion of the LSL stop cassettes or deletion of floxed genes), tissue or isolated PDAC cell lines were used to extract template genomic DNA. PCR product was applied on a 1.5 % agarose gel if not stated otherwise. Electrophoresis was running approx. 1.5-2 hours at 110 V depending on the expected band sizes until a clear separation of the bands (WT and mutated allele) was visible. Electrophoresis running buffer was 1x TAE (also used to prepare the agarose gel). Gels (stained with ethidiumbromide) were photographed using an UV gel documentation system for further genotype evaluation.

Table 3: PCR conditions for genotyping

Genotyping PCR	Denaturation	Annealing	Extension	Expected size of bands (% agarose gel)
Pdx1-Cre	95 °C 45 sec	58 °C 1 min	72 °C 1.5 min	290 bp (internal control) 390 bp (Pdx1-Cre) (2%)
Ptf1a^{Cre}	95 °C 45 sec	60 °C 1 min	72 °C 1.5 min	600 bp (WT) 400 bp (Ptf1a^{Cre})
Kras^{G12D}	95 °C 45 sec	55 °C 1 min	72 °C 1.5 min	270 bp (WT) 170 bp (LSL-Kras^{G12D}) 300 bp (LSL stop cassette deleted after recombination)
Trp53^{R172H}	95 °C 45 sec	60 °C 1 min	72 °C 1.5 min	570 bp (WT) 270 bp (LSL-Trp53^{R172H})
LSL-Trp53^{R172H} (screen for deleted LSL stop cassette)	95 °C 45 sec	55 °C 1 min	72 °C 1.5 min	290 bp (WT) 330 bp (LSL stop cassette deleted after recombination) (2-3%)
p16/p19^{lox}	95 °C 45 sec	58 °C 1 min	72 °C 1.5 min	140 bp (WT) 180 bp (p16/p19^{lox}) (2-3%)
Pcna$^{ATG\text{-}fLuc/+}$	95 °C 45 sec	60 °C 1 min	72 °C 1.5 min	780 bp (WT) 490 bp (Pcna$^{ATG\text{-}fLuc/+}$)

Genotyping PCR	Denaturation	Annealing	Extension	Expected size of bands
LSL-Pcna$^{ATG\text{-}fLuc/+}$ (screen for deleted LSL stop cassette)	95 °C 45 sec	64 °C 1 min	72 °C 1.5 min	330 bp (LSL stop cassette present)
Rosa26 locus	95 °C 45 sec	62 °C 1 min	72 °C 1.5 min	600 bp (WT) 310 bp (mutated R26 locus containing a knock in)
Rosa26 locus (screen for deleted LSL stop cassette)	95 °C 45 sec	53 °C 1 min	72 °C 1.5 min	900 bp (LSL stop cassette deleted after recombination)

2.1.2 Section and preparation of *LSL-Pcna$^{ATG\text{-}fLuc/+}$* tumor mice

LSL-Pcna$^{ATG\text{-}fLuc/+}$ tumor mice were treated with 50 mg/kg bromodeoxyuridine (BrdU) 2 h prior to sacrificing using isofluran inhalation and cervical dislocation. After sterilization with ethanol mice were sectioned and organs were washed in 1xPBS. Tissue samples from tail tip as well as from the pancreatic cancer and metastasis were taken for DNA isolation and regenotyping/checking of successful recombination of all involved alleles. After photo documentation of the tumor, organs were fixed in 4% PFA solution for 24 h at 4°C. Following washing in 1xPBS, organs were dehydrated and embedded in paraffin for further histological and immunohistochemical analyses.

2.1.3 Histological PDAC analyses - stainings

2.1.3.1. Paraffin tissue sections

PFA fixed organs were dehydrated using ASP300 Tissue Processor (Leica) and further on embedded in paraffin. Histological sections were performed using a microtom. Serial sections (10-20 sections per series) of approx. 3.5 µm thickness were produced. In order to get a full cross-section of the organ, thicker sections were produced to separate the different series.

2.1.3.2 Haematoxylin-Eosin staining (H&E staining)

For further histological analyses H&E stainings were generated. Several representative cross-sections of the respective organ were selected. After removal of paraffin by treating the tissue sections with Roti® Histol (Histoclear) for 10 min, a downward ethanol series was applied for rehydration of the tissue (2x99.9%, 2x96%, and 2x80% for 3 min each). After 1 min in bidest. water the sections were stained with haematoxylin for 5 sec before immediately washing them in cold and running tap water for 10 min. Further on the slides were stained with eosin for approx. 25 sec. After washing with bidest. water, the slides were dehydrated using an upward ethanol series (2x80%, 2x96% and 2x99.9% for 3 min each) followed by approx. 10 min of Roti® Histol treatment before mounting in Pertex and covering with a cover slip. Slides were stored in dark boxes for further microscopical analyses.

2.1.3.3 Immunohistochemistry – BrdU staining

Slides with tissue sections were prepared for paraffin removal and rehydrated as described in 2.1.3.2. Afterwards slides were boiled in antigen unmasking solution in the microwave for 9 min. When slides were cooled down (at least 20 min) and washed with bidest. water, treatment with 3% H_2O_2 for 10 min was used to block endogenous peroxidase activity. Following washing steps with bidest. water (1x) and 1xPBS (2x), slides were incubated with 5% goat serum for 1 h in order to inhibit unspecific antibody binding. After washing with 1x PBS, primary anti-BrdU antibody was diluted 1:250 in 1xPBS containing 5% goat serum and incubated in a wet chamber overnight at 4°C. Avidin/Biotin blocking kit was used according to the manufacturer's protocol. The next day primary antibody was removed by washing 3x with 1x PBS. Afterwards the biotinylated secondary antibody was diluted 1:200 in 1x PBS containing 3% goat serum and incubated for 1 h at room temperature. After another round of 1x PBS washing, the VECTASTAIN® Elite ABC solution was applied according to the manufacturer`s protocol followed by incubation with 3,3'-diaminobenzidine tetrahydrochloride (DAB) until the slides showed a brownish staining (approx. 1.5-2 min). Washing with 1xPBS (3x) and bidest. water (1x) stopped the staining reaction in order to prevent unspecific overstaining. After counterstaining the nuclei with haematoxylin, the slides were dehydrated and mounted in Pertex as already described in 2.1.3.2. Slides were stored in dark boxes for further microscopic analyses.

For the correlation of *in vivo* luciferase signal intensities to the number of BrdU positive cells in a cohort of differential progressed *LSL-Pcna*$^{ATG\text{-}fLuc/+}$ tumor mice, stained cells of 15 microscopic visual fields were counted per mouse (100x magnification).

2.1.4 DNA extraction from paraffin embedded tissues

In order to confirm the correct genotype as well as successful recombination of the respective alleles, DNA was isolated from paraffin embedded tissue sections of the tumor. For this, several 10 µm thick sections were generated, dewaxed and rehydrated as described in 2.1.3.2. Afterwards the pancreatic tissue was scraped and transferred into a reaction tube for further overnight incubation at 52°C in paraffin lysis buffer. Genomic DNA was isolated by phenol-chloroform-isoamylalcohol extraction and subsequent isopropanol precipitation. Pellet was dissolved in bidest. water and 50-100 ng of genomic DNA (DNA concentration determined by nanodrop spectrophotometer measurement) were applied for further genotyping PCRs.

2.1.5 Bioluminescence imaging

In order to measure the luciferase signal intensity of the *LSL-Pcna*$^{ATG\text{-}fLuc/+}$ tumor mice *in vivo*, mice were first of all anesthetized with MMF (5 mg/kg midazolam, 500 µg/kg medetomidine, 50 µg/kg fentanyl) via i.p. injection. Afterwards the mouse received eye creme to prevent drying-out and the fur was shaved at the position of expected signal emission. D-luciferin (225 mg/kg body weight) was i.p. injected afterwards and approx. 15 min later the luciferase

signal was measured. For this reason a cooled, back-thinned and integrating CCD camera containing an image intensifier unit (ORCA II-ER-1394, Hamamatsu) was applied (see also Saur et al., 2005; von Burstin et al., 2008). In the first step a grey-scale bright field photo was taken. Later on BLI measurements were launched, starting with maximum gain and low exposure times of 10 sec up to 10 min maximum, depending on the signal intensity. After finishing measurements, a pseudocolor image of the original bioluminescence photo was generated by the software and subsequently overlapped with the bright field image (SimplePCI software, Hamamatsu). In order to compare different measurements, the exposure times were strictly kept constant for each mouse within an experiment. In addition, quantifications of the luciferase signal were conducted using the region of interest (ROI) function of the software. The size of the ROI was kept constant for each mouse. After finishing the experiment, MMF anesthesia was antagonized by applying AFN (750 µg/kg atipamezole, 500 µg/kg flumazenil and 1.2 mg/kg naloxone) via subcutaneous injection (s.c.). Mice were kept in a warm chamber during the waking up phase. Alternatively mice were sacrificed and analysed as described in 2.1.2. For the *ex vivo* BLI, after section of the mice was completed tumor as well as other organs were put into a 1xPBS filled petri dish and BLI measurements were performed as described above.

2.1.6 Chemotherapeutic intervention with NVP-BEZ235

NVP-BEZ235 (40 mg/kg body weight) was pre-dissolved and vortexed in N-methyl-pyrrolidon (NMP). After the solution became clear, polyethylenglycol (PEG-300) was added in a 1:9 ratio (10% NMP and 90% PEG-300) and vortexed again. A total maximum volume of 10 ml/kg body weight was administered by oral administration. Alternatively a suspension instead of a solution can be used. Therefor 0.5% hydroxypropyl-methylcellulose (dissolved in bidest. water over night at 4°C) and 0.2% Tween-80 were mixed and vortexed thoroughly. NVP-BEZ235 was added and vortexed to generate the suspension for oral administration. All NVP-BEZ235 applications were prepared freshly just prior to chemotherapeutic intervention (maximum of 2 h before use). Initial luciferase signal intensity was measured prior to the single dose NVP-BEZ235 treatment and changes in luciferase signal intensity due to drug application were monitored as indicated. The control cohort was treated with a single dose of isotonic 0.9% NaCl solution via oral application and luciferase signal intensity was monitored as indicated.

2.2 Generation of the *R26 Dual Reporter* mouse line

2.2.1 Cloning

All restriction endonuclease digestions (enzymes from New England Biolabs), plasmid purifications (Qiagen PCR Purification Kit and MinElute PCR Purification Kit) as well as blunting reactions (Quick Blunting Kit from New England Biolabs) were performed according to the manufacturer's protocols. Prior to each ligation reaction, the acceptor plasmid was dephosphorylated using the rAPid alkaline phosphatase kit (Roche) according to the

manufacturer`s protocol in order to prevent religation. For a standard ligation reaction with high efficiency, 90 fmol of insert and 30 fmol of acceptor plasmid were applied. If necessary, this relation was up- or downscaled accordingly. For the graphical depictions of the respective cloning steps the software Serial Cloner version 2.6.1 (Franck Perez, SerialBasics) was used.

2.2.1.1 Purification of plasmid DNA

Plasmid DNA was basically purified in two different ways during the cloning procedure. If the respective buffer, additives, enzymes or small plasmid fragments of up to 100 bp had to be removed for downstream cloning applications, the PCR purification kits (Qiagen) were applied according to the manufacturer`s protocols. In contrast to this, if bigger plasmid fragments like vector backbones had to be removed, a preparative gel electrophoresis with subsequent gel extraction was applied. If the donor as well as the acceptor plasmid contained the same antibiotic resistance gene, this technology is crucial in order to separate the insert from the vector backbone from which it is derived, hence preventing a false positive religation of the donor plasmid. The preparative gel was usually 0.7% agarose without addition of ethidiumbromide. For staining of DNA, GelStar™ Nucleic Acid Gel Stain was used. The stock solution was first diluted 1:100 with DMSO. After dilution, 120 µl of digested plasmid (up to 30 µg of DNA), 20 µl of 6x loading dye and 15 µl of the gel star solution were mixed and loaded into a broad gel slot generated by a special broad comb. After running for several hours (depending on the separation of the bands) at 70-80 V, the desired band was extracted using a sterile scalpel and the Flu-O-Blu illumination table (Biozym; gel star is illuminated with blue light instead of UV light). Extracted plasmid fragments were purified using the gel extraction kits (Qiagen) according to the manufacturer`s protocols.

2.2.1.2 Transformation

For transformation of competent bacteria two different methods were applied. In case of One Shot® TOP10 chemically competent *E.coli* as well as NovaBlue competent bacteria, the heat shock transformation technique was used. Therefor 1 µl of ligated plasmid was added to 50 µl of competent bacteria suspension and incubated on ice for 5 min. After heat shock for 30 sec at 42°C, bacteria suspension was put on ice for 2 min. Subsequently 250 µl of room-temperatured S.O.C. medium (Invitrogen™) were added and mixed. After shaking incubation at 37°C for approx. 1.5-2 h, transformed bacteria were plated onto the respective antibiotic containing agar plate in different concentrations. 50 µl on one plate, 50 µl of a 1:10 dilution with LB broth on the second plate and 50 µl with centrifuged (1,000 rpm for 1 min) and redissolved pellet of the remaining bacteria on the third plate.

In case of One Shot® Stbl3™ competent *E.coli*, the KCM method was applied (transformation by high salt concentration). For this, 5 µl of the ligation reaction were added to 20 µl of KCM and 75 µl of bidest. water. After adding 100 µl of competent bacteria, the suspension was incubated at 4°C for 20 min followed by another 10 min incubation at room

temperature. Afterwards, 800 µl of room-temperatured S.O.C. medium were added and the bacteria were incubated in a shaker for 1.5-2 h at 25°C. After incubation the bacteria were plated on the respective agar plates as described above. Ampicillin (100 µg/ml), kanamycin (50 µg/ml) and chloramphenicol (30 µg/ml) agar plates were produced by adding the respective antibiotic prior to casting.

2.2.1.3 Screening PCRs, plasmid preparations and diagnostic digestions

If resistant colonies reached a sufficient size, several clones (number depending on amount of growing colonies and complexity of the respective cloning step) were picked using a sterile toothpick and further analysed by screening PCRs in order to reduce the amount of clones used for diagnostic digestions. Usually internal as well as external screens (directed screens) were performed for detection of the correct orientation of the insert. After picking a clone, one part was streaked onto a fresh back-up agar plate (further incubated and finally stored at 4°C with parafilm sealing). The second part was streaked into a PCR reaction tube filled with approx. 50 µl of bidest. water. In case of very few growing clones, a third part of each colony was directly used to inoculate LB medium in order to grow the clone in liquid culture for plasmid extraction and subsequent diagnostic digestions. The dissolved colonies for the screening PCRs were heat denatured at 95°C for 5 min. Afterwards 5 µl of the solution were applied as template DNA for the different screening PCRs (50 µl total reaction volume; RedTaq ReadyMix based).

After selection of correct ligated clones based on the PCR results, diagnostic digestions were performed. Therefor selected clones from the back-up plate were inoculated in LB medium containing the respective antibiotic resistance and incubated with agitation at 25°C (One Shot® Stbl3™ bacteria) respectively 37°C (One Shot® TOP10 and Novablue bacteria). If the medium reached an OD600 of around 1-1.3, bacteria were harvested and either pellets were stored at -20°C or directly used for further plasmid extraction. In order to generate bacterial permanent cultures, 500 µl of the suspension were added to 400 µl of glycerol and mixed thoroughly. These long term glycerol stocks were then immediately frozen at -80°C. According to the amount of plasmid DNA needed for further digestions or other downstream cloning applications, the Mini or Midi Plasmid extraction kits were applied according to the manufacturer`s protocol (Qiagen). The concentration of the isolated plasmid DNA was measured using the nanodrop spectrophotometer (Peqlab). For further diagnostic digestions, different internal as well as external restriction sites were chosen to check correct orientation of the insert. In addition, destruction or restoration of restriction sites due to ligation was surveyed and multiple insert integrations could be excluded by evaluation of the respective band pattern. Depending on the expected fragment sizes 0.7% up to 2% agarose gels were used for analysis.

2.2.1.4 Preparation of the final gene targeting plasmid

After the *Dual Reporter* cassette has successfully been cloned, the Gateway Cloning Technology (Gateway® LR Clonase® II Enzyme Mix, Invitrogen™) has been used in order to

transfer the *Dual Reporter* into the Rosa26 targeting plasmid. This vector contains both homologous arms flanking the *Dual Reporter* insert, which are needed to allow integration into the murine *Rosa26* locus of the ES cells via homologous recombination. For the gene targeting experiment, an endotoxin free plasmid maxi prep kit was used (Qiagen Endo-free Plasmid Maxi Kit). The glycerol stock of the final gene targeting vector was inoculated in fresh antibiotic containing LB medium using a sterile toothpick and grown until reaching an OD600 of approx. 1.2 (two independent inoculations in different flasks have been generated in order to have some back up DNA in case of a plasmid breakdown during bacterial growth phase/replication). Bacteria were harvested and plasmid was extracted according to the manufacturer`s protocol. After elution of the plasmid from the QIA filter cartridge, an isopropanol precipitation of the plasmid has been performed. The pellet was redissolved in sterile and endotoxin free 1x TE buffer at room temperature. Afterwards a small portion of the plasmid (approx. 30 µl) was separated and both portions were ethanol and sodium-acetat precipitated at -20°C overnight (10% NaAc and 2.5 volumes of EtOH). Plasmid of the small portion was extracted first in order to perform diagnostic digestions. At first a Pac1 linearization was performed to check if this restriction site is intact (needed for linearization prior to gene targeting). In addition, the presence of any other smaller fragments was evaluated in order to exclude a potential plasmid breakdown during the growth phase. In the next step other restriction endonucleases have been used to fragmentate the huge targeting vector and to check for the correct full length. Finally the bigger portion of the precipitated plasmid was further on centrifuged and washed several times with ice cold, endotoxin free 70% ethanol. The pellet was dried under a sterile hood for approx. 20 min and then carefully dissolved in sterile and endotoxin free 1x TE buffer at 4°C over night.

2.2.1.5 Generation of the Flp recombined *Dual Reporter* construct by co-transformation of competent *E.coli*

For further cell culture expression experiments, the final *Dual Reporter* construct was Flp recombined in order to delete the FSF stop cassette and allow expression of EGFP and fLuc. To achive this, a co-transformation has been performed. The final *Dual Reporter* construct together with a bacteria specific Flp expression vector were simultaneously transformed into competent *E.coli* as described in 2.2.1.2. After transformation, bacteria were grown in liquid culture (LB-medium) containing two different antibiotics, ampicillin and kanamycin, respectively. Since the *Dual Reporter* construct and the Flp expression plasmid are expressing the corresponding antibiotic resistances, it is possible to generate the respective selection pressure needed for maintenance of both plasmids within one bacterial cell. After harvesting of resistant bacteria, both plasmids were isolated as described in 2.2.1.3. Since probably not all *Dual Reporter* plasmids have successfully been Flp recombined, the isolated plasmids were digested with different restriction endonucleases which are exclusively cutting within the FSF cassette. Consequently all non-recombined *Dual Reporter* plasmids will be destroyed as well as the Flp expression plasmid which is also unspecifically digested by these enzymes. After selection of Flp recombined plasmids by applying these digestions, the

plasmids were transformed into competent bacteria again; this time using only one antibiotic for selection of the Flp recombined *Dual Reporter* vector. After picking colonies, several diagnostic digestions as well as internal and external screening PCRs were performed as described in 2.2.1.3. Results revealed one positive clone which was sent for sequencing to confirm the correct Flp mediated recombination of the *Dual Reporter* plasmid. This plasmid was further used for the different *in vitro* characterization studies transfecting MIA PaCa-2 cells.

2.2.2 Embryonic Stem cell (ES cell) culture – *Rosa26* knock in and *R26* "short arm" screening

All cell culture plastics were pretreated with 0.1% gelatin from porcine skin for at least 30 min at room temperature and completely dried after removal. Since the murine ES cells are growing on a monolayer of mitotically inactivated mouse embryonic fibroblasts (MEFs), neomycin-resistant and irradiated primary MEFs were seeded on a 10 cm cell culture dish to produce 100% confluency. The next day murine ES cells (W4/129S6 ES cells, Taconic) were seeded on top of the MEF layer and grown for approx. 4 days until ES cell colonies were big and tall enough for the gene targeting experiment (medium changed once per day; colonies did not touch each other in order to stay undifferentiated). For the knock in experiment, $1x10^7$ ES cells were used. Just prior to the gene targeting experiment the *Rosa26* targeting plasmid was Pac1 digested for linearization. 25 µg of freshly linearized targeting vector were added to the ES cells, mixed and put into the electroporation cuvette in ice cold 1xPBS (total volume of 800 µl). Electroporation (EP) was performed at 268 V and 500 µF for 7.5 msec. The rest of the Pac1 digested plasmid was loaded on agarose gel for verification of successful linearization of the targeting vector.

After EP the cells were splitted onto five 10 cm dishes. Beside this, a small portion of unelectroporated WT ES cells were seeded on gelatin-coated 6-well plates without MEFs for further harvesting of WT genomic DNA as negative control. 18 h later, 200 µg/ml geneticine were added to the ES cell medium for selection. After approx. one week of selection (medium changed 1-2 times per day and washed with pure DMEM to remove dead cells), single ES cell colonies were picked onto 24-well plates for further expansion of the respective clone as well as in parallel on 96-well plates (only gelatin-coated, no MEF layer) for the initial screening PCR (usually two days picking colonies). Approx. 2-3 days after the first picking, genomic DNA was isolated in order to perform the initial PCR screen (96-wells were not 100% confluent since at least 100 ES cells are enough for the PCR screening). Therefor medium of the 96-well plate was removed completely and 20 µl of mouse tail lysis buffer (soriano buffer) containing 1% freshly added proteinase K were added per well. After incubation at 55°C for at least 1 h in a wet chamber, the lysed ES cells were transferred into a new tube and proteinase K was heat denatured at 95°C for 10 min. 2 µl of pre-sheared genomic DNA was used in a 50 µl PCR. In order to screen for clones which show homologous recombination within the *Rosa26* locus, a screening PCR strategy was applied. Primers are binding outside of the homologous *R26* arm within the genomic sequence and

within the 5` end of the *Dual Reporter* construct, respectively. Consequently integration into the correct genomic locus of the ES cells could be verified.

Table 4: PCR conditions *R26* "short arm" ES cell screening

***Rosa26* "short arm" ES cell screen**	Ros-ES-UP2 (Ros-ES-UP1) Ros-ES-LP2 (Ros-ES-LP1) 5x Q-solution 10x PCR buffer dNTP bidest. water HotStar Taq DNA Polymerase Template genomic DNA Total volume	2 µl 2 µl 11 µl 5 µl 2 µl 25,65 µl 0.35 µl 2 µl 50 µl
PCR conditions	95°C 95°C 62°C 65°C 65°C 25°C	16 min 40 sec 45 sec 4 min 10 min pause

45x

Δdt +3 sec/cycle

PCR product (primers Ros-ES-UP2 and Ros-ES-LP2) was mixed with 6x orange G loading buffer and loaded onto 0.8% agarose gel. For the nested PCR strategy applied, 1 µl of PCR product was added to a new PCR reaction containing primers Ros-ES-UP1 and Ros-ES-LP1, respectively. Positive clones were immediately further subcultured from the 24-well plate into 6-well plates, if colonies were huge enough. A small portion of each positive clone was further splitted onto additional gelatin-coated 6-well plates without MEFs for harvesting of additional genomic DNA for further screening PCRs. Negative clones as well as clones already showing signs of differentiation were discarded. Positive clones were further splitted from the 6-well plates onto the 6 cm cell culture dish. In parallel, a portion of the splitted cells were already frozen to generate back up, low passage permanent cultures (two aliquots per clone). As freezing medium standard ES cell medium containing 10% DMSO was used. ES cells from the 6 cm dish were frozen (three aliquots per clone) and a small portion was seeded onto gelatin-coated 24-well plates without MEFs and cultured for at least two weeks in ES cell medium containing no antibiotics. Medium was changed every day in order to remove the antibiotics completely. After two weeks supernatant of 1-2 days old medium was taken for further mycoplasma detection according to the manufacturer`s protocol (Nachweis von Mykoplasmen in Zellkulturen mittels PCR (AM029); www.lag-gentechnik.de). For generating permanent cultures of positive ES cell clones, aliquoted cryo vials were put into refrigerator pre-cooled Cryo 1°C Freezing Container (Nalgene Cryocontainer) containing isopropanol according to the manufacturer`s protocol. After one day storage at -80°C cryo vials were transferred into liquid nitrogen for long term storage.

2.2.2.1 Genomic DNA extraction from transgenic ES cell clones

In order to characterize ES cells with the *R26 Dual Reporter* knock in on the DNA level and hence check for full length integration of the construct, several additional screening PCRs were performed. Therefor each positive ES cell clone was further cultured on MEF-free 6-well plates until reaching confluency. After complete medium removal, 2 ml of freshly prepared ES cell lysis buffer were added and plates were incubated at 55°C over night in a wet chamber. The next day 4 ml of 99.9% ethanol were carefully added to precipitate the genomic DNA of the ES cells. After another over night incubation at room temperature the plate was carefully turned in order to remove the buffer. Each well was washed three times with 2 ml of 70% ethanol with caution and incubated at room temperature for at least 15 min up to several hours for each washing step. After the last washing step the alcohol was removed and the plate was dried until the DNA pellet became slightly white. Genomic DNA pellet was dissolved in approx. 300 µl of bidest. water and sheared thoroughly by pipetting in order to fragmentate genomic DNA for use as PCR template. Concentration of the isolated DNA was measured using nanodrop spectrophotometer and approx. 50-100 ng of genomic DNA were used as screening PCR template if not stated otherwise.

2.2.2.2 Internal screening PCRs and genotyping

For checking the homologous recombination integration lengths of the different ES cell clones, an internal screening strategy was developed covering the whole *Dual Reporter* cassette. PCRs were performed using the Platinum® Blue PCR SuperMix from Invitrogen™ and 50 µl reaction volumes according to the manufacturer`s protocol. For the standard genotyping PCR of the *R26 Dual Reporter* mouse line, a 25 µl reaction volume containing RedTaq ReadyMix from Sigma-Aldrich was used. Screening PCRs were running for 40 cycles. PCR products were loaded on respective agarose gels depending on the expected product lengths for evaluation.

Table 5: PCR conditions internal screens and genotyping of the *R26 Dual Reporter* mouse

Screening PCR primers	Denaturation	Annealing	Extension	Expected band size
Caggs-UP6 + FsaSF-neo-sc-LP2	95°C, 2min (initial) 95°C, 45 sec	62°C, 1 min	72°C, 1.5 min	505 bp
pgl3-pA-pause-UP + EGFP-sc-neu-LP1	95°C, 2min (initial) 95°C, 45 sec	62°C, 1 min	72°C, 1.5 min	590 bp
fLuci-UP1 + tomato-LP1	95°C, 2min (initial) 95°C, 45 sec	60°C, 1 min	72°C, 1.5 min	438 bp
Reni-UP1 + R26-Tva-GT-LP	95°C, 2min (initial) 95°C, 45 sec	60°C, 1 min	68°C; 2 min	1551 bp
Caggs-UP6 + EGFP-sc-neu-LP1	95°C, 2min (initial) 95°C, 45 sec	62°C, 1 min	72°C, 1.5 min	No product (2850 bp product too large -> intact FSF cassette)

				450 bp (FSF cassette deleted/lost)
Dual Reporter genotyping PCR (RedTaq ReadyMix based) R26-td-Emut-LP + R26-Tva-GT-UP + R26-Tva-GT-wt-LP	95°C, 3 min (initial) 95°C, 45 sec	62°C, 1 min	72°C, 1.5 min	650 bp WT 450 bp mut (*Dual Reporter* knock in)

2.2.2.3 *R26* "long arm" screening

In order to detect the 3` end of the *R26 Dual Reporter* knock in another screening PCR was applied. Primers pBroad-pA-5219-UP and R26-lA-LP1 are binding outside of the 3` *R26* homologous "long arm" within the genomic sequence and the *R26 Dual Reporter* sequence, respectively, to confirm the correct locus of integration.

Table 6: PCR conditions *R26* "long arm" screen standard

***Rosa26* " long arm" ES cell screen**	pBroad-pA-5219-UP R26-lA-LP1 10x PCR buffer dNTP bidest. water HotStar Taq DNA Polymerase Template genomic DNA (100-200 ng) Total volume	2 µl 2 µl 5 µl 2 µl 25,65 µl 0.35 µl 2 µl 50 µl
PCR conditions	95°C 95°C 62°C 65°C 65°C 25°C	16 min 40 sec 45 sec 4 min 10 min pause

45x

Δdt +3 sec/cycle

Since this PCR is extremely difficult due to the length of the product (4638 bp), an alternative "touch down" PCR program for screening the *R26* "long arm" has been developed. For this PCR exactly 90 ng of genomic template DNA was applied per clone.

Table 7: PCR conditions *R26* "long arm" screen "touch-down"

"touch-down" PCR conditions	95°C	20 min
	95°C	35 sec
	65°C (9x ΔdT -1°C/cycle)	1 min
	65°C	10 min
	95°C	35 sec
	55°C (39x)	45 sec
	65°C (Δdt +5 sec/cycle)	10 min
	65°C	20 min
	25°C	pause

2.2.3 Generation of chimeric *R26 Dual Reporter* mice

In order to establish the *R26 Dual Reporter* mouse line, selected ES cell clones were chosen which showed positive results in all screening PCRs as well as ideal phenotypic characteristics. Two clones were sent to the Institute of Stem Cell Research at the Helmholtz Center in Neuherberg. Chimeric mice were generated using the morula aggregation technology (Wood et al., 1993; Eakin and Hadjantonakis, 2006).

2.2.4 Checking for the germline transmission of the *R26 Dual Reporter* allele within the chimeric mice

Mice showing the highest degree of chimerism were further interbred with C57Bl6/J mice. 1 mm tail tips of the offsprings were used to check for the germline transmission of the *R26 Dual Reporter* allele. Genomic DNA from the tail tips was isolated using the QIAamp DNA Mini Kit (Qiagen) according to the manufacturer`s protocol. Approx. 50 ng of genomic DNA was used as template for further internal as well as external screening PCRs as described in 2.2.2. and 2.2.2.2.

2.3 Cell culture

2.3.1 Basic principles

As a standard cell culture medium DMEM (high glucose 1x DMEM) with 10% FCS (heat-inactivated) and 1% Penicillin/Streptomycin was used. MIA PaCa-2 cells, murine PDAC cell lines isolated from tumor mice as well as the murine embryonic stem cells were cultured at 37°C in steam-saturated incubators containing 5% CO_2. For a standard expansion of a cell line, cells were firstly seeded in 5 cm^2 cell culture flasks after thawing. Medium was changed the next day in order to remove DMSO from the freezing medium. When confluent cells were

washed with 1x PBS, trypsinated at 37°C for 5 min and resuspended in fresh DMEM in order to split them into 75 cm^2 flasks. For freezing and generating permanent cultures, cells were further splitted into 175 cm^2 flasks. When confluent, five aliquots of permanent cultures were generated. Therefor cells were washed with 1xPBS, trypsinated and resuspended in standard medium. After centrifugation at 1,000 rpm for 5 min, medium was removed and cell pellet was resuspended in ice cold freezing medium (DMEM containing 20% FCS and 10% DMSO). After generating 1 ml aliquots in cryo vials, cells were immediately stored at -80°C for several days. Afterwards permanent cultures were transferred into liquid nitrogen for long term storage.

2.3.2 Transient MIA PaCa-2 transfection experiments – Effectene

For the initial characterization experiments of the *Dual Reporter* modules during cloning as well as for the co-transfection experiments of the finished *Dual Reporter* construct with Flp- and Cre-expression plasmids within MIA PaCa-2 cells, the Effectene transfection kit (Qiagen) has been used according to the manufacturer`s protocol. The protocol was scaled down to 12-well cell culture plates. $0.5x10^5$ cells were seeded per 12-well one day prior to the transfection experiments. Culture conditions and handling are described in 2.3.1. All transfection experiments were performed in triplicates. Detection of EGFP and mem-td-Tomato expression by fluorescence imaging was performed using the Axiovert 25 microscope (Zeiss), the Axio Vision software (Zeiss) and an UV-lamp with respective filters for the correct excitation wavelengths.

2.3.3 Transduction of transgenic ES cells by Ad-Cre infection

In order to evaluate correct mem-td-Tomato and hrLuc expression of the *Dual Reporter* construct within the genomic context of the *Rosa26* locus in gene targeted ES cells, Cre expressing adenovirus has been applied (Anton and Graham, 1995). Ad-Cre infection experiments were performed in triplicates. Therefor three different amounts of the targeted ES cells were seeded on gelatin-coated 24-well plates without MEFs ($6x10^4$, $1x10^4$ and $0.5x10^4$ cells per 24-well, respectively). The next day medium of the 24-well plates was removed. Afterwards, 150 µl of a 1:100 dilution of Ad-Cre virus (Ad-Cre virus containing cell culture supernatant diluted 1:100 with fresh ES-DMEM) was pipetted on each 24-well. Plates were incubated at 37°C for 1 h and every 10 min carefully shaken in order to distribute the virus over the whole well surface. Subsequently each virus-containing well was filled up to 2 ml total volume with fresh ES-DMEM and further incubated at 37°C. The next day medium was removed and exchanged by fresh ES-DMEM. Approx. two days after infection, photos were taken to document successful Cre mediated recombination and consequent expression of mem-td-Tomato.

2.3.4. Electroporation of transgenic ES cells with mammalian Flp expression plasmid

In the next step correct EGFP and fLuc expression of the *Dual Reporter* construct within the genomic context of the *Rosa26* locus in gene targeted ES cells was evaluated. Therefor the transgenic ES cells were electroporated a second time (first time *Dual Reporter* EP) with a mammalian Flp expression plasmid for a transient Flp expression and consequent deletion of the FSF stop cassette. Culture, handling and EP of the targeted ES cells were conducted as described in 2.2.2. Since EP should lead to a transient expression of the Flp recombinase within the ES cells, no additional selection pressure was applied in contrast to geneticine selection during the first EP. When double-electroporated ES cell colonies were huge enough, several EGFP positive colonies were picked and further cultured as described in 2.2.2. In contrast to the first EP, ES cells were cultured on gelatin-coated dishes without MEFs after picking. Finally, picked EGFP positive ES cell colonies were further seeded on gelatin-coated 24-well plates without MEFs for evaluation of the molecular switch from first to second reporter cassette expression via Ad-Cre virus infections as described in 2.3.3.

2.4 Protein isolation of MIA PaCa-2 cells and transgenic ES cells for *in vitro* measurement of luciferase activity

Cells were grown to approx. 80% confluency and then washed 2-3 times with 1xPBS in order to remove residual medium completely. Afterwards, 1x passive lysis buffer (1xPLB) was added according to the manufacturer`s protocol (Dual-Luciferase® Reporter Assay System, Promega) and cells were incubated at room temperature for 10 min on a shaker for agitation. Subsequently cells were scraped from the cell culture dishes using a cell scraper, pipetted several times and centrifuged at 14,000 rpm and 4°C for 15 min in order to remove cellular debris. Finally the protein samples were immediately transferred to -20°C or -80°C for long term storage, respectively.

2.5 Bradford Assay

In order to correlate the luciferase activity of the transgenic ES cells to the protein content of the respective sample for a quantitative analysis, the Bradford assay (Biorad) was used to determine protein concentrations. Samples and standard were diluted in 0.2xPLB before using in the Bradford assay (for decreasing background signal generated by PLB). Each sample (including the BSA standard curve) was measured in triplicates.

2.6 *In vitro* luciferase assay

All luciferase assays were performed using the Dual-Luciferase® Reporter Assay System (Promega). In contrast to the manufacturer`s protocol, 15 µl of sample were added to 50 µl of Luciferase Assay Reagent II (LAR II) in order to measure firefly luciferase activity. Afterwards 100 µl of Stop & Glo® Reagent were added to quench firefly luciferase activity and

simultaneously quantify the renilla luciferase activity within the same sample. All samples were measured in triplicates.

2.7 Statistical analysis

Statistical analysis was done using the GraphPad Prism5 software (La Jolla, USA). Depicted bars represent the arithmetic mean of the respective experiment performed in a triplicate. The standard error of the mean (+/- SEM) is shown. Statistical significance was calculated using the two-sided unpaired student`s t-test. Error probability p is depicted ($p<0.05$ is defined as statistically significant). Correlation coefficient (r) was calculated using the Spearman correlation and the Spearman`s permutation test (p).

C. Results

1. The *LSL-Pcna*$^{ATG\text{-}fLuc/+}$ mouse model

For *in vivo* and *ex vivo* imaging of PDAC proliferation, an LSL-cassette (loxP-pgk-neo^{R}-4xpA-RNA-pol-pause-loxP) followed by the coding sequence of the firefly luciferase with downstream placed pA signal has been knocked into the ATG start codon of the murine *Pcna* locus as already mentioned before (schematic representation of the gene targeting construct see PhD thesis of Baumann, 2011). This mouse model was generated in our lab and has been firstly characterized within the PhD thesis of Sandra Baumann (Baumann, 2011). It could be shown that the heterozygous knock in of the targeting construct has no phenotype compared to *Pcna* wild-type animals, whereas the homozygous knock in leads to embryonic lethality. Furthermore, this mouse model gives the possibility to image cell proliferation *in vivo* as well as *ex vivo* in real time. In the context of pancreatic cancer, tumor cell lines isolated from these *LSL-Pcna*$^{ATG\text{-}fLuc/+}$ knock in mice were further characterized *in vitro* by Sandra Baumann. As one of the major conclusions of her thesis, it could be shown that this *in vitro* model represents a high-throughput drug screening platform for the evaluation of the efficacy of novel cancer therapeutics. The most promising drug candidates which show the highest overall response in all cancer cell lines tested *in vitro* can consequently be validated *in vivo* using an orthotopic transplantation model or the endogenous *LSL-Pcna*$^{ATG\text{-}fLuc/+}$ mouse model. This might be the most important step concerning the translation of novel drugs for the human disease. In order to give consideration to this important aspect, the endogenous *LSL-Pcna*$^{ATG\text{-}fLuc/+}$ tumor mouse model has been applied for the validation of *in vitro* drug screening assays using the dual PI3K and mTOR inhibitor NVP-BEZ235 as an example.

1.1 *In vivo* and *ex vivo* imaging of PDAC proliferation

The *LSL-Pcna*$^{ATG\text{-}fLuc/+}$ knock in mouse model was crossed into the above mentioned, genetically defined PDAC mouse model containing the floxed *Cdkn2a* locus for acceleration of tumor progression (I previously established and characterized this PDAC mouse model in our lab, see Eser et al., 2013 and data not shown). Fig. 1A depicts an *LSL-Pcna*$^{ATG\text{-}fLuc/+}$ tumor mouse with already established PDAC showing a strong luciferase signal *in vivo* (left foto). After preparation of the organs the pancreatic cancer still shows a strong proliferation signal. The liver and the lungs of this mouse didn`t show any luciferase activity revealing that the tumor has not metastasized yet (right foto, positive signal on the spleen derived from contamination with tumor tissue).

A

Ptf1a$^{Cre/+}$;*LSL-Kras*$^{G12D/+}$;*Ink4a/Arf* ^{lox};*LSL-Pcna*$^{fLuc/+}$

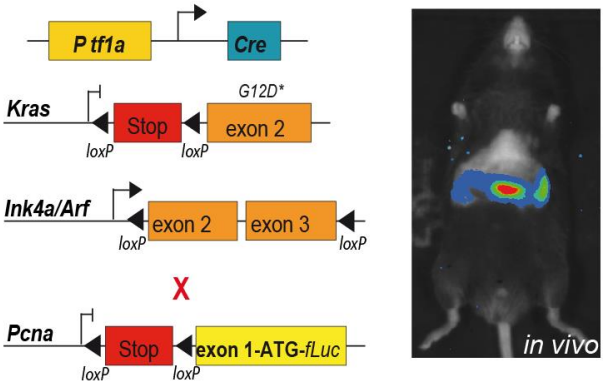

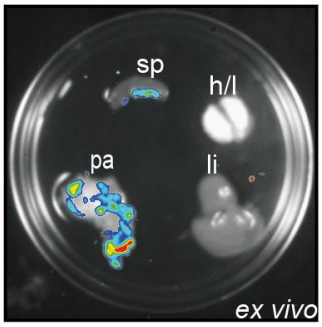

B

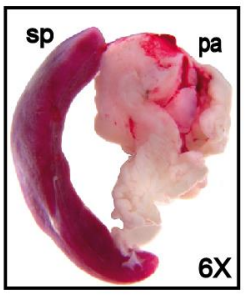

C

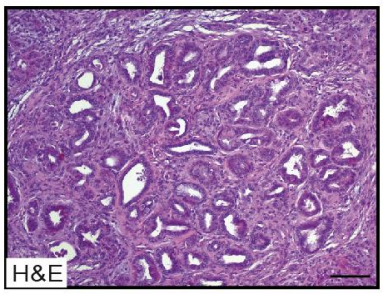

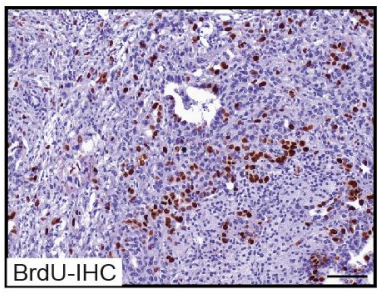

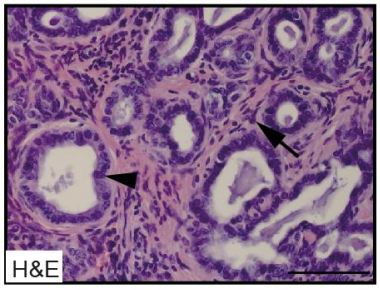

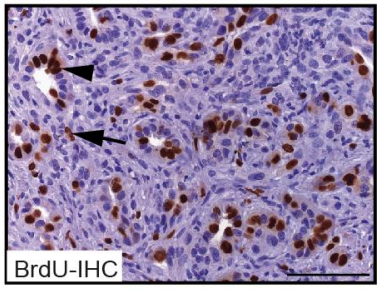

D

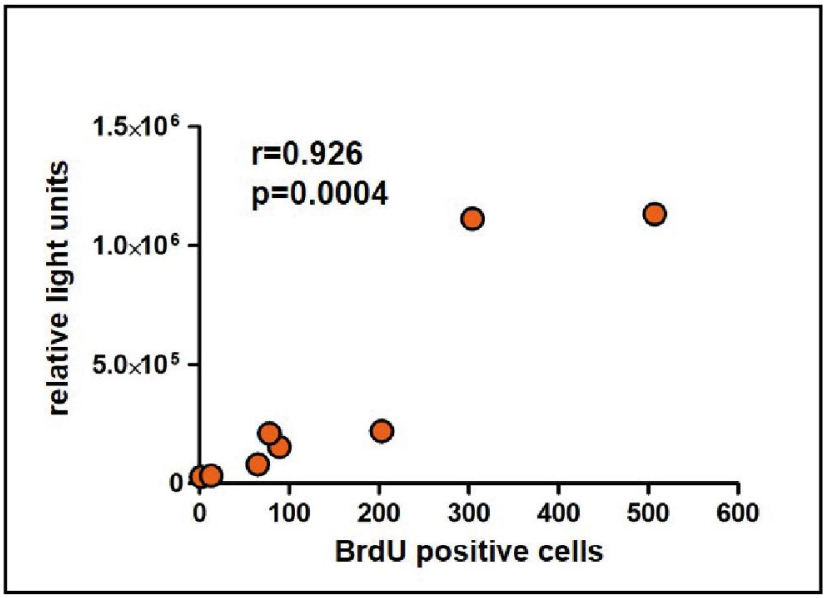

Figure 1: Pcna as a proliferation marker - *in vivo* and *ex vivo* imaging of PDAC proliferation: (A) Genetic scheme of *LSL-Pcna*$^{ATG\text{-}fLuc/+}$ mice crossed into the standard PDAC tumor mouse model (left). Tumor mouse with established PDAC shows strong proliferation signal in the pancreas (pa) *in vivo* (middle) and *ex vivo* (right). No luciferase signal could be detected on other organs. Spleen (sp), liver (li), heart and lungs (h/l). (B) Macroscopic image of the spleen (sp) and the pancreas (pa) with 6x magnification. (C) H&E staining of paraffin sections of the tumor (left side) and immunohistochemistry with anti-BrdU antibody counterstained with haematoxylin (right side). Arrow head shows epithelial cancer cell; arrow shows stromal fibroblast. Scale bars equal 100 µm. (D**)** Correlation between luciferase signal (relative light units) and number of BrdU positive PDAC cells. The luciferase signal has been quantified and BrdU positive PDAC cells from representative histological sections were counted (15 microscopic visual fields at 100x magnification per mouse). Each dot represents one mouse. n=8. Correlation coefficient r (Spearman correlation) and statistical significance p (Spearman`s permutation test) are depicted.

On a macroscopic level, the pancreas shows several solid tumors (Fig. 1B). Further histological analysis of the tumor reflects a well-differentiated PDAC containing many ductal structures surrounded by stromal cells. Proliferation of the cancer cells (arrowhead, Fig. 1C) as well as of the fibroblasts (arrow, Fig. 1C) could be confirmed by BrdU incorporation. In order to demonstrate the correlation between the luciferase signal due to an activated *Pcna* promoter and the replication activity of a cell measured by BrdU uptake, a cohort (n=8) of *LSL-Pcna*$^{ATG\text{-}fLuc/+}$ tumor mice containing different progression stages of PDAC have been analyzed and the number of BrdU positive PDAC cells was plotted against the *in vivo* luciferase signal intensity (Fig. 1D).

1.2 The *LSL-Pcna*$^{ATG\text{-}fLuc/+}$ mouse model as *in vivo* drug validation platform – NVP-BEZ235 chemotherapy

After generating a cohort of *LSL-Pcna*$^{ATG\text{-}fLuc/+}$ tumor mice, chemotherapeutic intervention studies were conducted. For the *in vivo* validation of drug candidates a kinetic experiment was performed. A cohort of *LSL-Pcna*$^{ATG\text{-}fLuc/+}$ tumor mice were mock treated and the luciferase signal of the tumor was quantified at different time points post-treatment (0, 16 and 24 h; Fig. 2A and B). This experiment revealed that the luciferase signal is increasing over time and no decrease in proliferation activity could be detected in the absence of a therapeutic intervention.

Furthermore another cohort of *LSL-Pcna*$^{ATG\text{-}fLuc/+}$ tumor mice were treated with the dual PI3K and mTOR inhibitor NVP-BEZ235. Eight hours after single-dose treatment of *LSL-Pcna*$^{ATG\text{-}fLuc/+}$ tumor mice with NVP-BEZ235, the proliferation signal was already decreasing. 16 hours after the treatment the signal disappeared completely and 24 hours after therapy the luciferase signal reappeared. Quantification of the signal showed a significant reduction of proliferation activity of the PDAC 16 hours after NVP-BEZ235 therapeutic intervention (Fig. 2 C and D).

Summarizing the data, it could be shown that the *LSL-Pcna*$^{ATG\text{-}fLuc/+}$ model is a powerful tool for *in vivo* imaging of cell proliferation in real time. In addition, it could be demonstrated that this model can be used as a drug screening platform for the validation of potent drug candidates *in vivo* which have been chosen in previous *in vitro* drug screening assays.

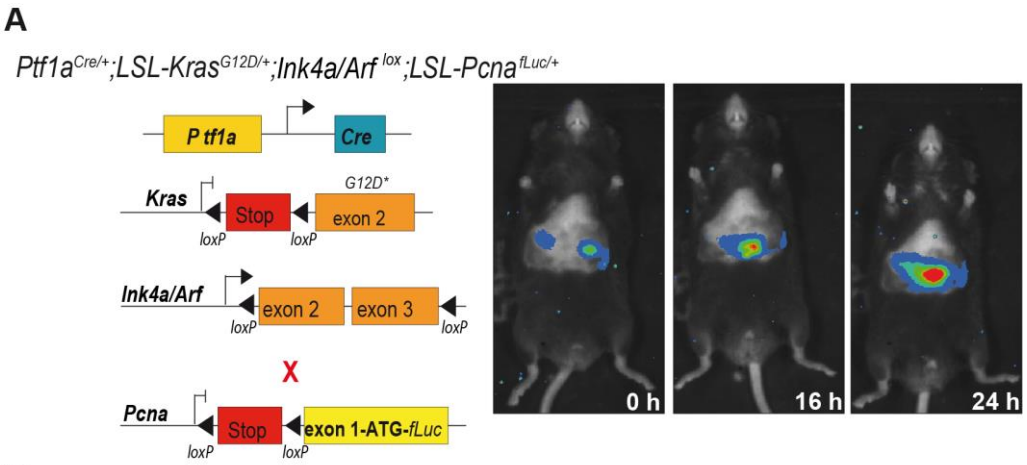
A
Ptf1a^Cre/+;LSL-Kras^G12D/+;Ink4a/Arf^lox;LSL-Pcna^fLuc/+
Ptf1a
Cre
Kras
Stop
G12D*
exon 2
loxP
loxP
Ink4a/Arf
exon 2
exon 3
loxP
loxP
X
Pcna
Stop
exon 1-ATG-fLuc
loxP
loxP
0 h
16 h
24 h

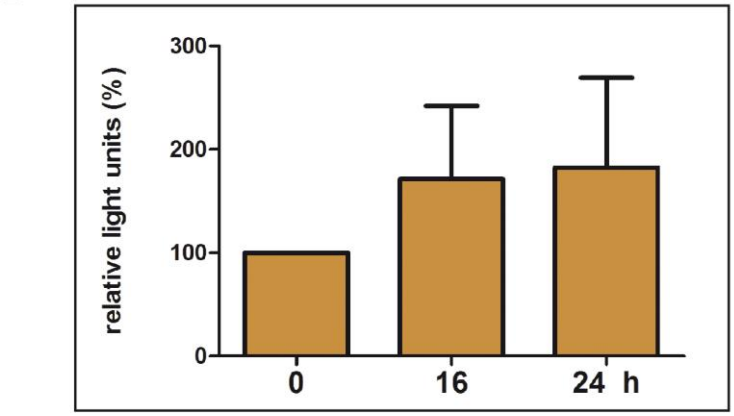
B
relative light units (%)
300
200
100
0
0
16
24 h

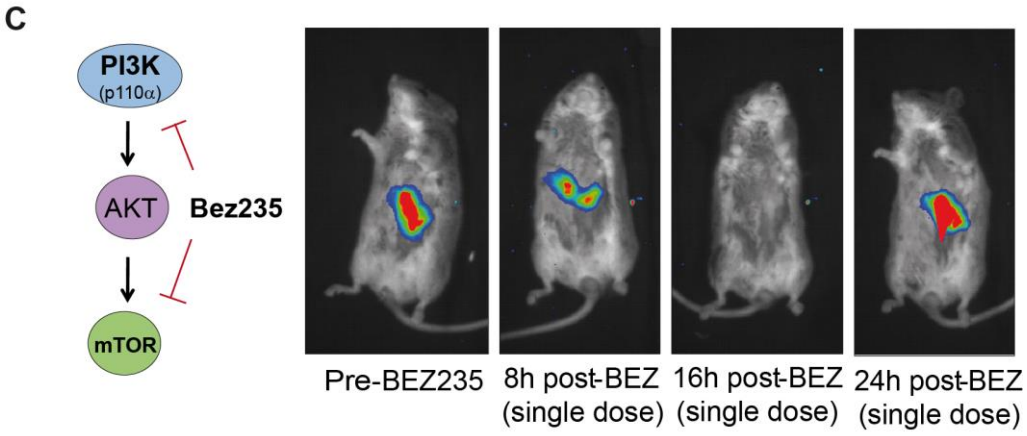
C
PI3K
(p110α)
AKT
Bez235
mTOR
Pre-BEZ235
8h post-BEZ
(single dose)
16h post-BEZ
(single dose)
24h post-BEZ
(single dose)

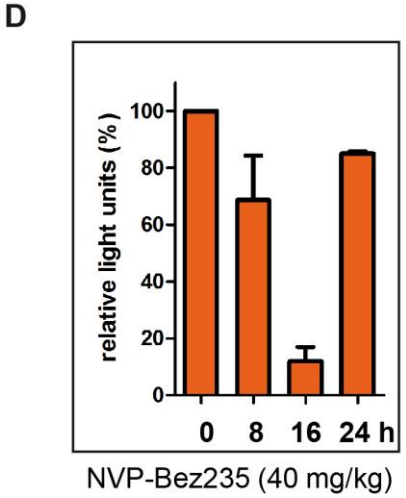
D
relative light units (%)
100
80
60
40
20
0
0
8
16
24 h
NVP-Bez235 (40 mg/kg)

Figure 2: The *LSL-Pcna*$^{ATG\text{-}fLucl+}$ mouse model as *in vivo* drug validation platform – chemotherapy with dual PI3K and mTOR inhibitor NVP-BEZ235: (A) A cohort of *LSL-Pcna*$^{ATG\text{-}fLucl+}$ tumor mice (n=3) were orally treated with single dose of vehicle (0.9% NaCl solution) at time point 0 h and the luciferase signal of the tumor was measured at time points 0, 16 and 24 h after treatment. (B) Depicted is the mean + SEM of the relative light units for each time point. (C) A cohort of *LSL-Pcna*$^{ATG\text{-}fLucl+}$ tumor mice (n=3) were treated with dual inhibitor NVP-BEZ235 (40 mg/kg orally as a single dose) at time point 0 h and the luciferase signal was measured at time points 0, 8, 16 and 24 h after therapeutic intervention. (D) Depicted is the mean + SEM of the relative light units for each time point.

2. The dual recombination system

In order to overcome limitations of the standard KPC mouse model, a new tumor mouse model has been developed by our lab. It is based on the combination of the Cre-loxP and Flp-FRT recombination systems (dual recombination system) which recapitulates the step by step wise progression of mutations and hence is able to resemble the human nature of PDAC more accurately.

To generate this model, a transgenic *Pdx1-Flp* mouse line was established. In this mouse, the Flp recombinase is under the control of the *Pdx1* promoter which permits targeting the Flp expression towards the pancreas. As a second step, the *FSF-Kras*^{G12D} mouse line was generated. Similar to the well-known *LSL-Kras*^{G12D} mouse, in this new mouse line the expression of an oncogenic *Kras* allele is silenced by an upstream FRT site flanked stop cassette (FRT-Stop-FRT; FSF). Upon Flp mediated recombination, the FSF stop cassette will be deleted and a single FRT site remains. Oncogenic *Kras* expression is consequently targeted to the pancreas and induces PanIN and PDAC formation shown for the standard Cre-loxP based *Pdx1-Cre; LSL-Kras*^{G12D} tumor mouse model (Fig. 3). For acceleration of tumor development, an FRT site flanked *Trp53* allele *(Trp53*^{FRT}*)* (Lee et al., 2012) can be crossed into this mouse line (KFP model) which leads to deletion of this tumor suppressor gene upon Flp mediated recombination. Median tumor specific survival time is comparable to the standard KPC tumor mouse model (data not shown). In order to conduct a sequential activation/inactivation of additional oncogenes and tumor suppressor genes, a new allele is needed which was also generated in our lab. The *FSF-R26*$^{CAG\text{-}CreERT2}$ mouse line carries a knock in at the ubiquitous and constitutively expressed *Rosa26* locus. The knock in consists of the *CreER*^{T2} gene, which represents a fusion of the Cre recombinase and a mutated form of the ligand binding domain of the human estrogen receptor (Feil et al., 1997; Indra et al., 1999). The construct is driven by the strong *CAG* promoter and expression is silenced by an upstream placed FSF stop cassette. Upon Pdx1-Flp mediated recombination, CreER^{T2} will be expressed specifically in the pancreas but remains inactive in the cytoplasm of the cell due to fusion with the ligand binding domain of the estrogen receptor. Upon tamoxifen treatment and binding to the ER^{T2} domain, Cre is able to translocate into the nucleus and perform recombination. Consequently in the context of a Flp recombined *Kras*^{G12D} driven PDAC it is now possible to sequentially activate and/or inactivate additional genes of interest (containing loxP sites) at desired time points by treating the animals with tamoxifen (Cre recombination of all Flp^{+} cells, Fig. 3).

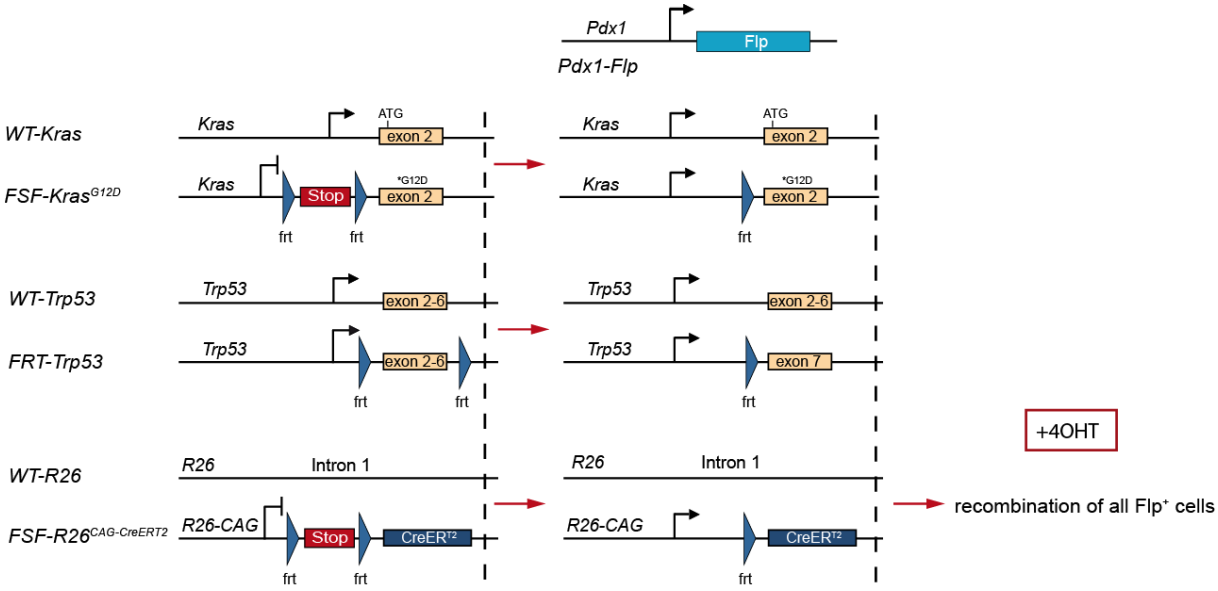

Figure 3: The dual recombination system-based PDAC mouse model – an improved spatiotemporally inducible, conditional tumor mouse model: Schematic illustration of the different alleles of the new mouse model and principle of Flp and Cre mediated recombination. 4-OHT = 4-hydroxy-tamoxifen.

As a proof of principle when using an LSL stop cassette silenced *LacZ* reporter gene, it could be shown that upon tamoxifen treatment PanINs as well as the tumor cells in established PDAC are Cre recombined (data not shown). Beside this temporally inducible, conditional mouse model it is also possible to target different compartments of an organ (e.g. epithelium and stroma) depending on the promoters of the Cre recombinase used. Thus the establishment of a spatiotemporally inducible, conditional mouse model becomes feasible.

3. Generation of the *R26 Dual Reporter* mouse line

With the establishment of this improved tumor mouse model in our lab, there is a need for the generation of a new reporter mouse model fitting the possibilities originating from the use of the dual recombination system (Fig. 4).

For the generation of a new reporter mouse line the ubiquitously expressed *Rosa26* locus was chosen since it is known to be accessible for gene targeting by homologous recombination (Soriano, 1999). To achieve a high expression level of the reporter genes, the *CAG* promoter was used (Miyazaki et al., 1989; Niwa et al., 1991; Okabe et al., 1997 and Alexopoulou et al., 2008). The whole construct consists of two different reporter gene cassettes. Each reporter cassette is composed of a fluorescence reporter gene followed by a bioluminescence reporter gene. Both genes are connected via viral 2A sites allowing high level transgene expression. The construct is silenced by an FSF stop cassette and the first reporter cassette together with the FSF cassette are additionally flanked by loxP sites; this allows monitoring of Flp and Cre induced recombination events.

In detail, the *CAG* promoter is followed by the first loxP site. The downstream placed FSF cassette silences expression of EGFP and firefly luciferase (fLuc) which are connected via a P2A site. A BGH-pA signal stops expression after the first reporter cassette and a 3´ second

loxP site allows excision of the EGFP-fLuc cassette by Cre recombinase. The second reporter cassette consists of *mem-td-Tomato* and *humanized renilla Luciferase* (*hrLuc*) fused via a T2A site. At the end of the construct a β-globin pA signal was chosen to stop expression of the second reporter cassette.

After crossing this mouse line into the Pdx1-Flp driven tumor mouse model, the FSF cassette will be deleted and EGFP/fLuc will be expressed in all Flp recombined cells. Upon tamoxifen treatment at desired time points, the Cre recombinase of the *FSF-R26*$^{CAG\text{-}CreERT2}$ allele can be activated and Cre mediated recombination leads to deletion of the floxed first reporter cassette. This results in molecular switching from the first to the second reporter cassette expression. All Flp^{+} cells will switch to mem-td-Tomato/hrLuc expression (Fig. 4).

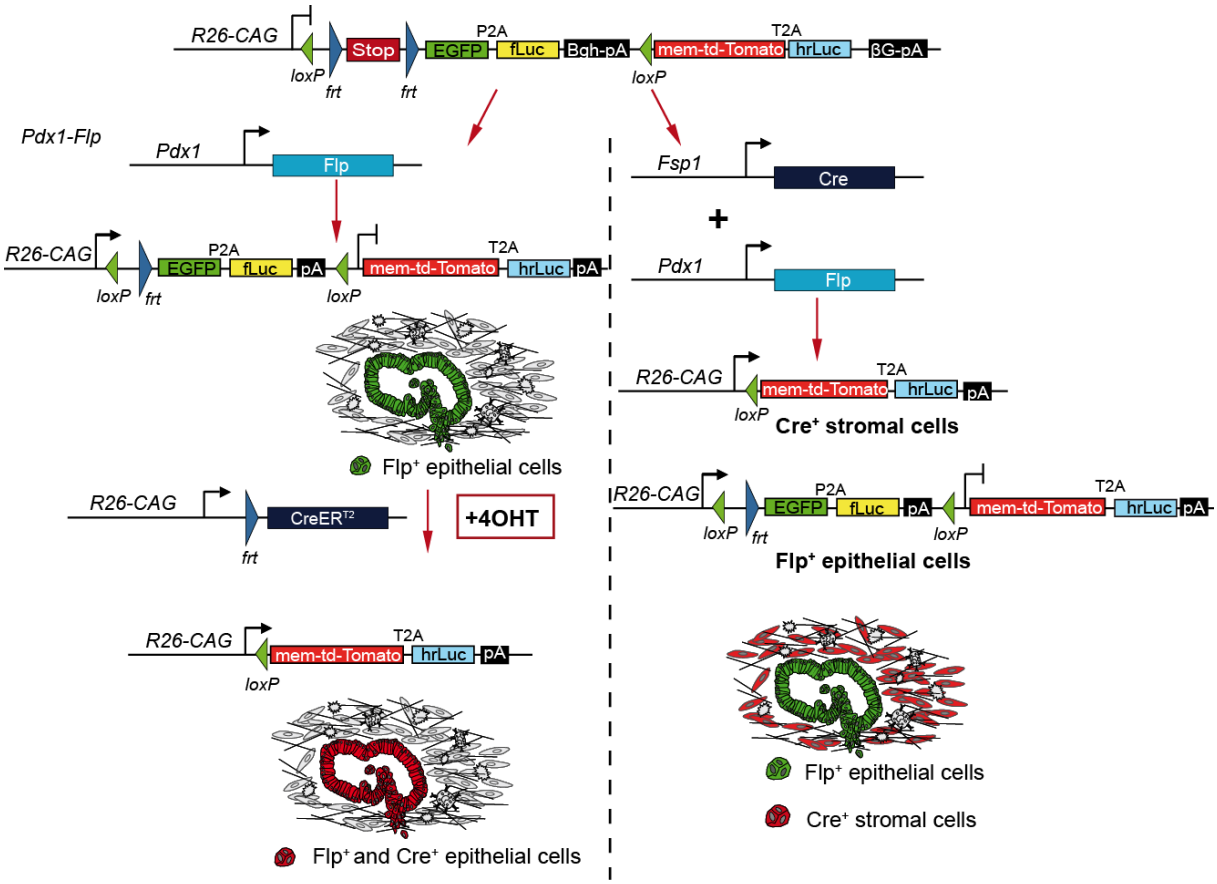

Figure 4: Schematic representation of the *Dual Reporter* construct and function: Shown is the DNA construct for generating the *R26 Dual Reporter* mouse. Left side demonstrates Pdx1-Flp mediated recombination of the construct followed by a temporally induction of Cre recombination by tamoxifen treatment. The draft shows a PDAC lesion which is switching from first to second reporter cassette expression upon Cre recombination. Right side shows Flp and Cre recombination of the construct using a Pdx1-Flp and a stroma specific Cre recombinase (Fsp1-Cre). The draft shows a PDAC lesion with first reporter cassette expression (upon Pdx1-Flp mediated recombination) surrounded by stromal fibroblasts expressing the second reporter cassette (upon Fsp1-Cre mediated recombination). 4OHT = 4-hydroxy-tamoxifen. Fsp1-Cre = fibroblast specific protein 1-Cre.

Beside this temporally inducible system which will allow reporting the sequential manipulation of genes during PDAC development, the spatial separated activation of the reporter gene cassettes is also possible. In this case, the *R26 Dual Reporter* mouse is again crossed into the Pdx1-Flp driven tumor mouse model. Now the resulting mouse will specifically express

EGFP/fLuc in all Flp$^+$ cancer cells in the epithelium of the pancreas. Expression of Cre under the control of a stroma specific promoter instead of using the CreER^{T2} system activates mem-td-Tomato/hrLuc expression of all Cre$^+$ cells of the stroma of the pancreas. Based on this compartment specific system it will be possible to target and analyze tumor-stroma interactions. The resulting reporter mouse model will consequently allow for a spatiotemporally imaging approach (Fig. 4).

3.1 Cloning strategy for the *Dual Reporter* gene targeting construct

Due to the complexity of the DNA construct, cloning was divided into four major modules which were connected in the end to achieve the final gene targeting vector.

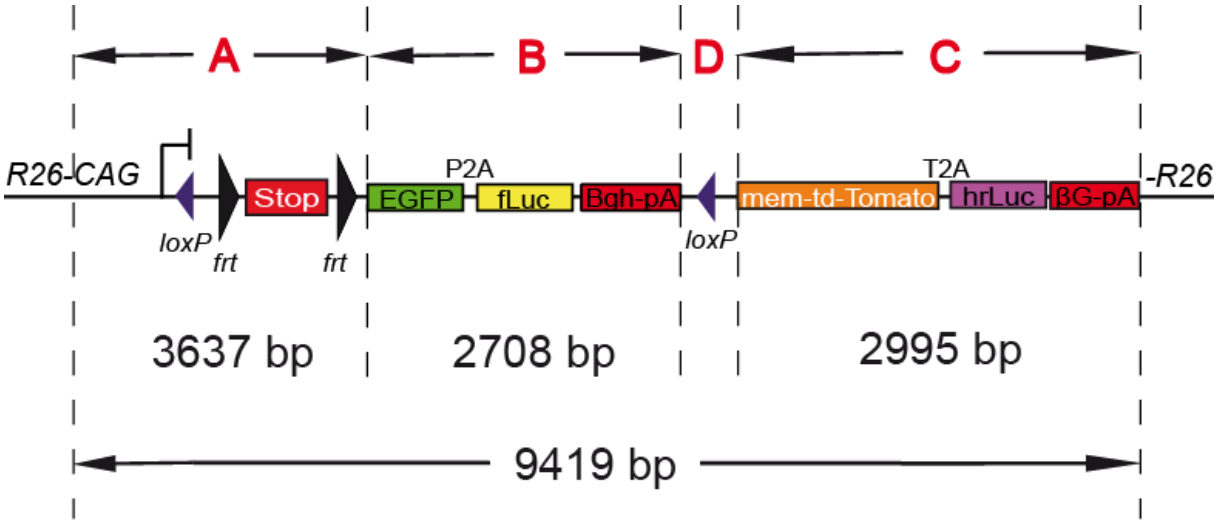

Figure 5: Schematic representation of the cloning strategy for the *Dual Reporter* construct: The *Dual Reporter* gene targeting construct was divided into four different modules which in the end will be connected to generate the final construct for homologous recombination in embryonic stem cells. Module A consists of the *CAG* promoter, the first loxP site and the FSF stop cassette. Module B consists of the first reporter cassette with *EGFP* and *fLuc* connected via a P2A site and followed by the BGH-pA signal. Module C represents the second reporter cassette and consists of *mem-td-Tomato* and *hrLuc* connected via a T2A site and followed by a β-globin pA signal. Module D represents the cloning of the second loxP site 5` to the second reporter cassette.

The first module (A in Fig. 5) contains the *CAG* promoter, the first loxP site and the FSF stop cassette. The second module (B in Fig. 5) represents the first reporter cassette containing *EGFP* and *fLuc* connected via a P2A site and followed by the BGH-pA signal. The third module (C in Fig. 5) represents the second reporter cassette with *mem-td-Tomato* and *hrLuc* connected via a T2A site and followed by the β-globin pA signal. Finally the fourth module (D in Fig. 5) represents the second loxP site which will be connected with the second reporter cassette.

3.1.1 Cloning of module A

Table 8: Cloning steps of module A

Cloning step #	Name of plasmid (abbreviation)	Modifications	Name of insert (abbreviation)	Modifications	Purpose of cloning
1	pEntr-sa-FSF-MCS-pA (atg-1)	Xho1 and Nco1 digestion and gel elution	pBlue-FsaSF-minPGK (axz-2)	Xho1 and Nco1 digestion and gel elution	Removal of the *pgk* promoter 5` to the *neomycine* resistance gene in the pEntr vector
2	pEntr-FsaSF-minPGK-MCS-pA (bca-3)	Acc1 and EcoR1 digestion, blunting and religation	n.a.	n.a.	Removal of the splice acceptor site 5` to the promoterless *neomycin* resistance gene
3	pEntr-CAG-saFSF-CreER^{T2}-pA (ayg-23)	Cla1 digestion and religation	n.a.	n.a.	Preparation of the *CAG* promoter donor plasmid for a facilitated excision of the promoter afterwards – removal of the multiple Cla1 restriction sites
4	pEntr-FSF-minPGK-MCS-pA (bcb-1)	Acc65I digestion and blunting	pEntr-CAG-saFSF-CreER^{T2}-pA-Cla1-religand (bcc-1)	Cla1 and Sal1 digestion, gel elution and blunting	Subcloning the *CAG* promoter 5` to the FSF cassette
5	pEntr-CAG-FSF-minPGK-MCS-pA (bcd-7)	Acc65I and Xho1 digestion	Acc65I-loxP-Xho1 linker	n.a.	Integration of the first loxP site 5` to the first FRT site

All steps for generating module A are summarized in table 8. Starting the cloning of the *Dual Reporter* construct first of all the FSF cassette was prepared. The FSF stop cassette (containing 4xpA from SV-40 virus and an RNA-polymerase-pause-sequence; Seidler et al., 2008) has been generated previously in our lab and two vectors containing different kinds of

this cassette (Fig. 6, pEntr and pBlue) were available to start cloning. Since the whole construct will be driven by the *CAG* promoter, there is no need for a splice acceptor site upstream of the FSF cassette although the construct will be knocked into an intron. In addition, there is also no need for a splice acceptor site downstream of the first FRT site prior to the *neomycin* resistance gene. Since the gene trap technique will not be used, the *neomycin* resistance gene will be directly transcribed by the *CAG* promoter. Due to this fact there is also no need for an additional *Pgk* promoter to drive the *neomycin* resistance gene transcription.

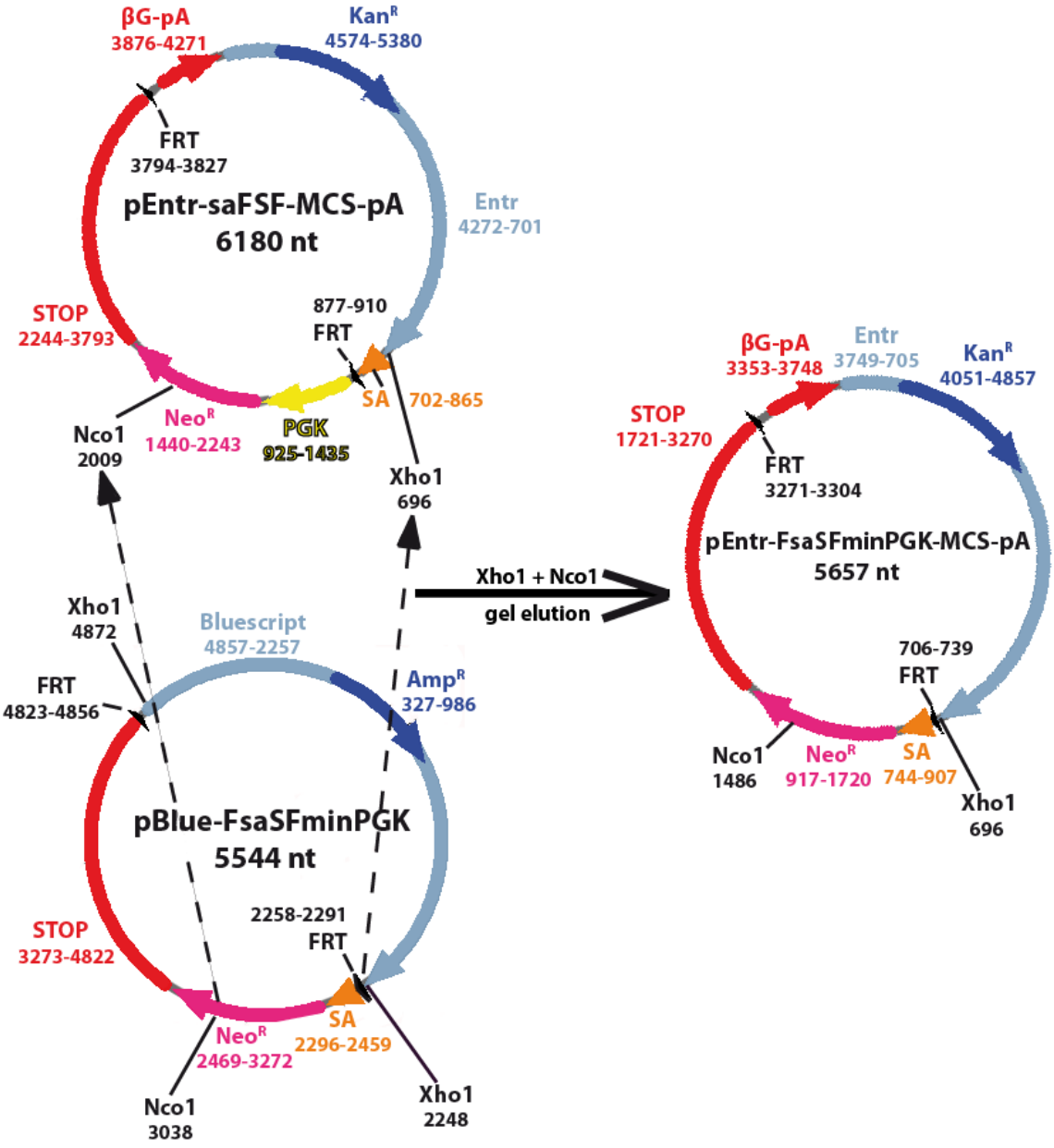

Figure 6: Module A – 1. Removal of the *Pgk* promoter 5` to the *neomycine* resistance gene in the pEntr vector

To achieve all of these goals, a fragment ranging from the first FRT site (Xho1) to a unique Nco1 restriction site within the *neoR* cassette of the pEntr vector was exchanged by the

similar fragment of the pBlue vector. Consequently the *Pgk* promoter upstream of the *neoR* cassette was removed (Fig. 6).

In the next step the SA upstream of the *neoR* cassette was removed. To do this, the pEntr vector was digested with EcoR1 and Acc1. Afterwards the incompatible sticky ends were blunted and the vector backbone was religated leading to the restoration of the EcoR1 restriction site (Fig. 7).

Having generated the correct FSF stop cassette the next step was to clone the *CAG* promoter upstream of the FSF cassette into the pEntr vector.

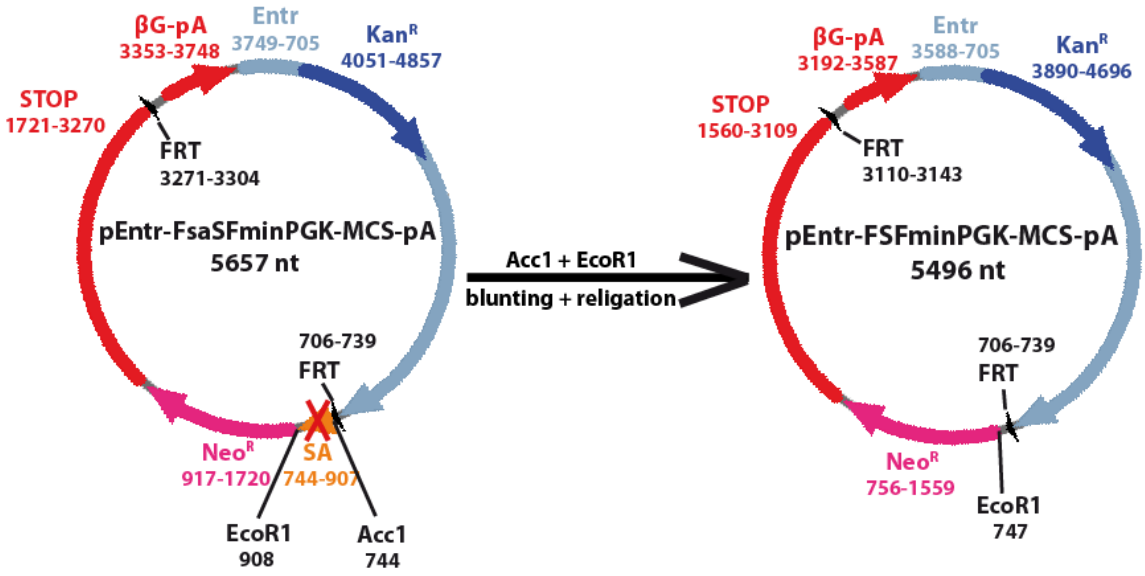

Figure 7: Module A – 2. Removal of the splice acceptor site 5` to the promoterless *neomycin* resistance gene

Therefore, another pEntr vector existing in our lab was used which contains the *CAG* promoter (Fig. 8). For a facilitated excision of the *CAG* promoter, the donor plasmid was digested with Cla1 which cuts multiple times. After sticky end religation of the donor vector backbone, only one Cla1 restriction site remains which now can be used together with the Sal1 restriction site for excision of the *CAG* promoter. A gel elution was used to separate the excised promoter from the donor vector (Fig. 9). The pEntr acceptor plasmid was opened with Acc65I cutting upstream of the first FRT site. After blunting of the gel-eluted promoter as well as of the opened acceptor plasmid, ligation was performed.

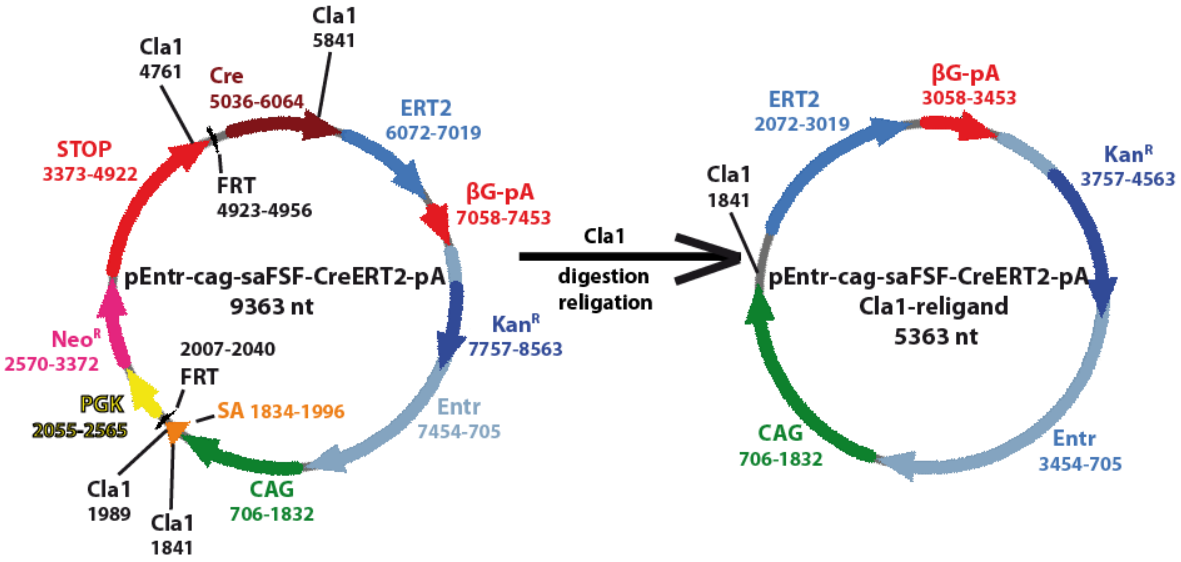

Figure 8: Module A – 3. Preparation of the *CAG* promoter donor plasmid for a facilitated excision of the promoter afterwards

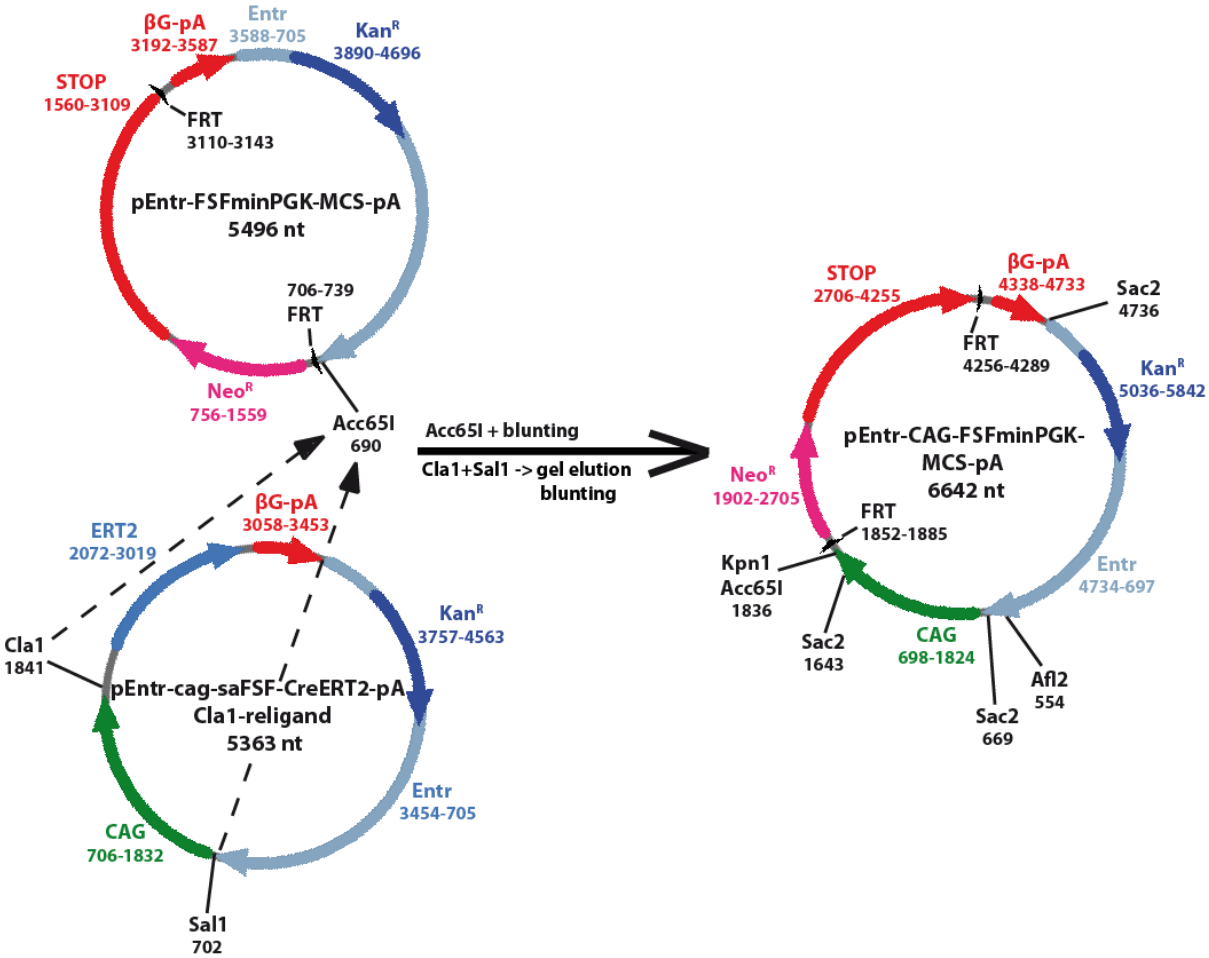

Figure 9: Module A – 4. Subcloning the *CAG* promoter 5` to the FSF cassette

Successful insertion of the *CAG* promoter was confirmed by directed diagnostic digestion since the blunted insert can integrate in both directions (enzymes are depicted in Fig. 9).

As the final cloning step finishing module A the first loxP site was inserted between the *CAG* promoter and the first FRT site. For a directed sticky end ligation of the loxP site, Acc65I and Xho1 restriction sites were chosen. The loxP site was designed as an oligonucleotide linker with Acc65I and Xho1 compatible sticky ends (Fig. 10).

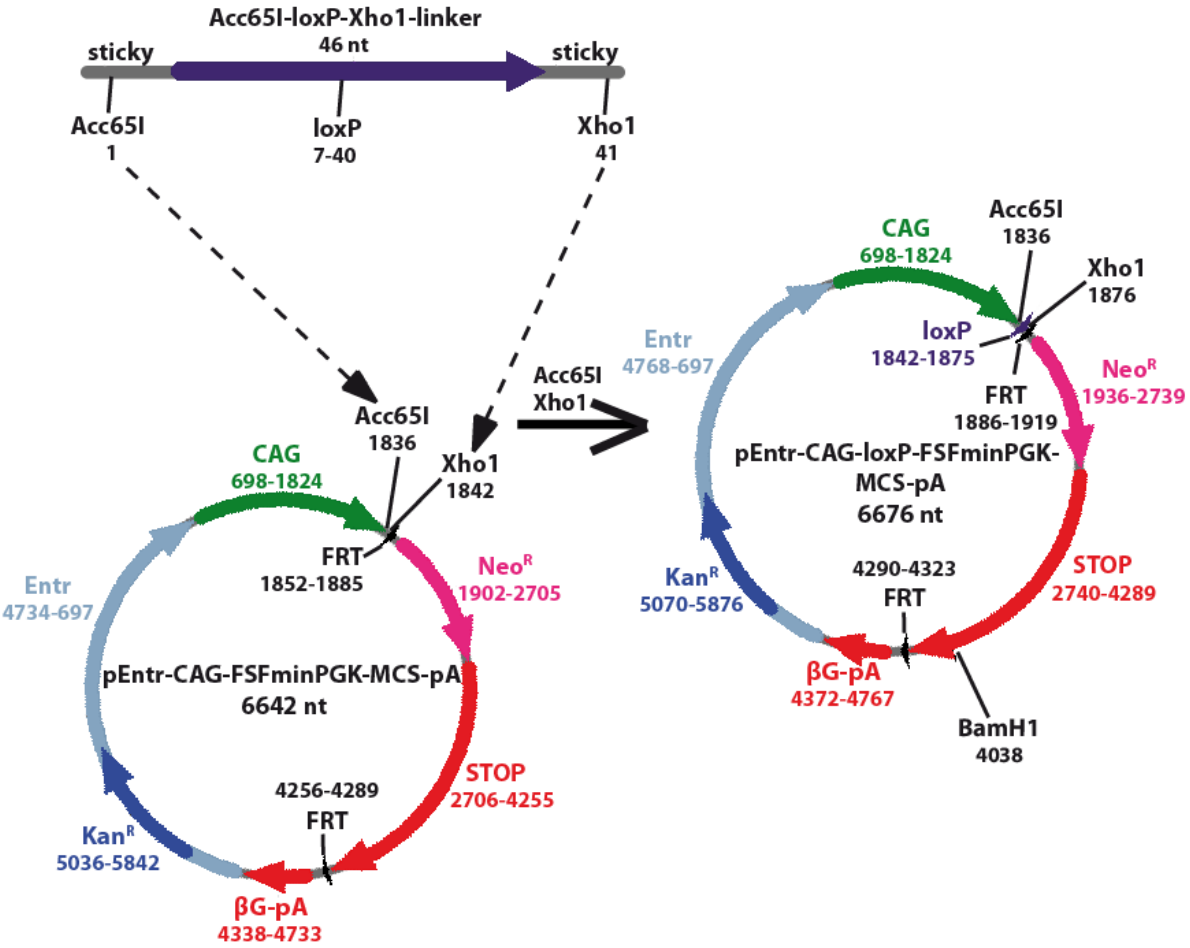

Figure 10: Module A – 5. Integration of the first loxP site 5` to the first FRT site.

3.1.2 Cloning of module B

Table 9: Cloning steps of module B

Cloning step #	Name of plasmid (abbreviation)	Modifications	Name of insert (abbreviation)	Modifications	Purpose of cloning
1	pEntry-Blue (amm-8)	Xba1 and BamH1 digestion	pCHMWS-EGFP-P2A-fLuc-T2A-HSV1-sr39tk (bea-2)	Xba1 and BamH1 digestion	Subcloning of the *EGFP*-P2A fragment into the pEntry vector
2	pEntry-Blue-EGFP-P2A (bef-8)	BamH1 and Xma1 digestion	pCHMWS-EGFP-T2A-fLuc (beb-2)	BamH1 and Xma1 digestion	Subcloning the *fLuc-stop* fragment in frame to the *EGFP*-P2A open reading frame
3	pcDNA3.1	Pme1 digestion	pEntry-Blue-EGFP-P2A-fLuc-stop (bei-1)	Sma1 and Eco53kI digestion and gel elution	Subcloning the first reporter cassette into the pcDNA3.1 expression vector

Module B consists of the first reporter cassette with *EGFP* and *fLuc* connected via a P2A site and followed by the BGH-pA signal. The different cloning steps are summarized in table 9. As a first step, a plasmid existing in our lab was used which contains the *EGFP* open reading frame (ORF) without a stop codon followed by the P2A site and the *fLuc* ORF also without a stop codon. The *EGFP*-P2A fragment was subcloned into the pEntry multiple cloning site using the Xba1 and BamH1 restriction sites (Fig. 11).

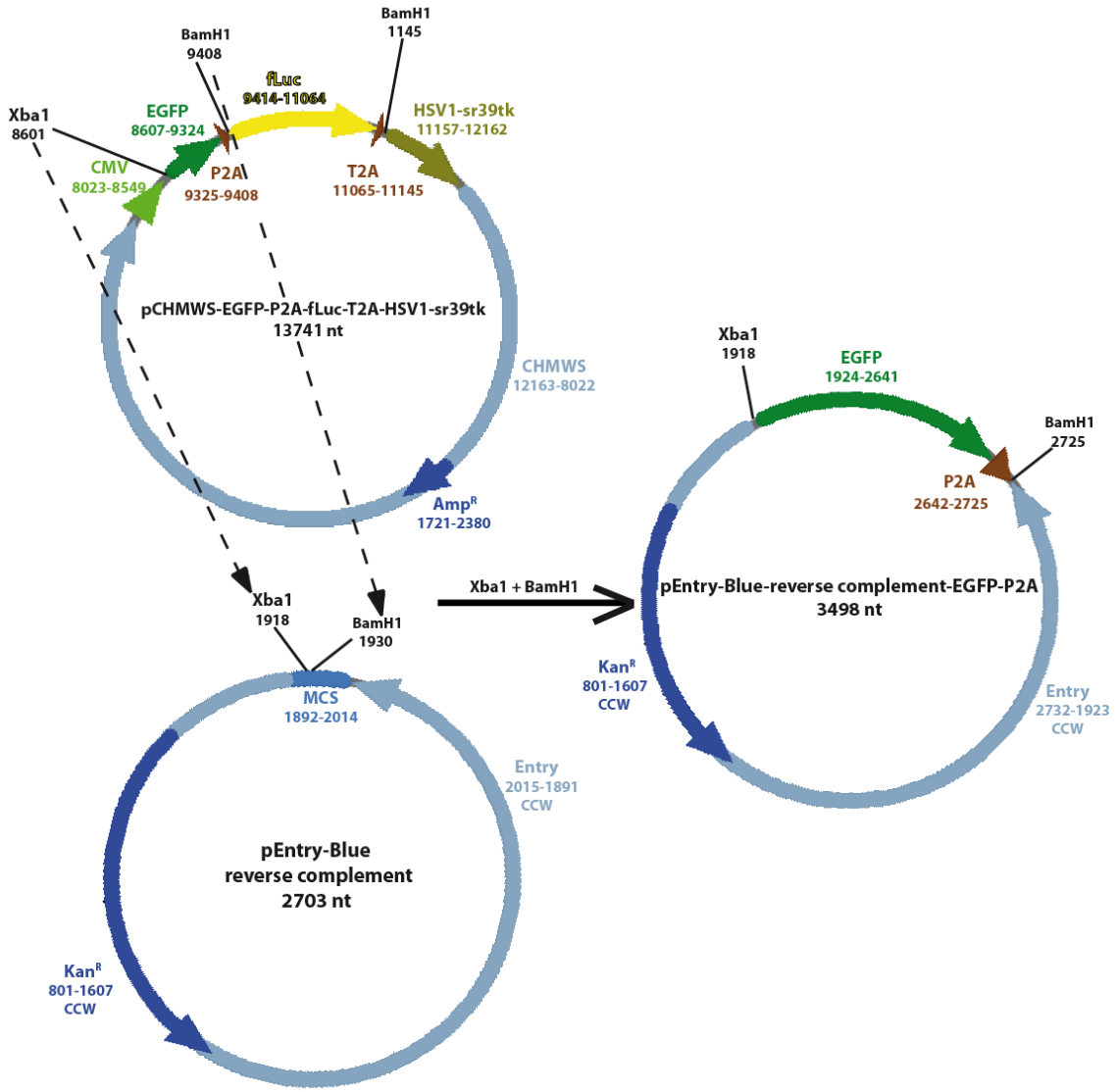

Figure 11: Module B – 1. Subcloning of the *EGFP*-P2A fragment. Note: The following plasmid maps of pEntry-Blue show the reverse complementary sequence.

Since *fLuc* of the initial donor plasmid has no stop codon, we used the *fLuc* ORF from vector pCHMWS-*EGFP*-T2A-*fLuc* to generate the EGFP-P2A-fLuc cassette (Fig. 12).

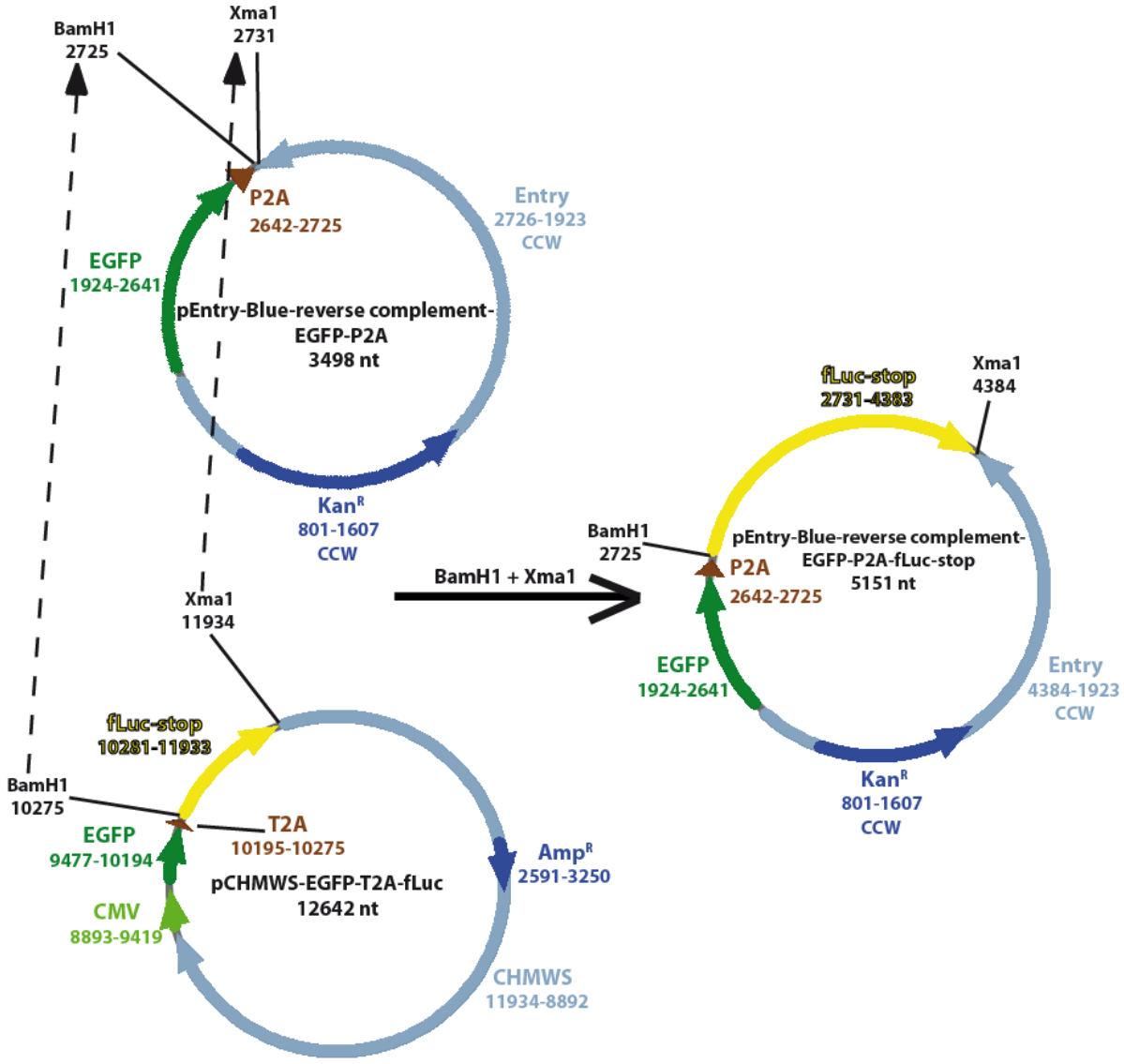

Figure 12: Module B – 2. Subcloning the *fLuc-stop* fragment in frame to the *EGFP*-P2A open reading frame

In the following step, the *fLuc-stop* fragment from pCHMWS-*EGFP*-T2A-*fLuc* was subcloned in frame to the P2A site of the pEntry vector using the BamH1 and Xma1 restricition sites (Fig. 12). Summing it up, the stop codon-containing *fLuc* is now placed into the correct reading frame downstream of the stop codon-less *EGFP* ORF and the P2A site. Consequently the *EGFP-fLuc* fusion gene can be correctly transcribed and expressed.

For finishing the construction of module B, the BGH-pA site is still missing in order to stop the transcription of the first reporter cassette. For this last cloning step the *EGFP*-P2A-*fLuc* reporter cassette was excised with Eco53kI and Sma1 (both blunt end cutters) and inserted into the Pme1 (blunt end cutter) digested pcDNA3.1 expression vector which contains the BGH-pA signal downstream to the Pme1 restriction site. In addition, the strong *CMV* promoter of this expression vector can be used to check for the functionality of this first

reporter cassette on protein level. For a facilitated cloning the insert was gel eluted and afterwards blunt end ligated into pcDNA3.1 (Fig. 13).

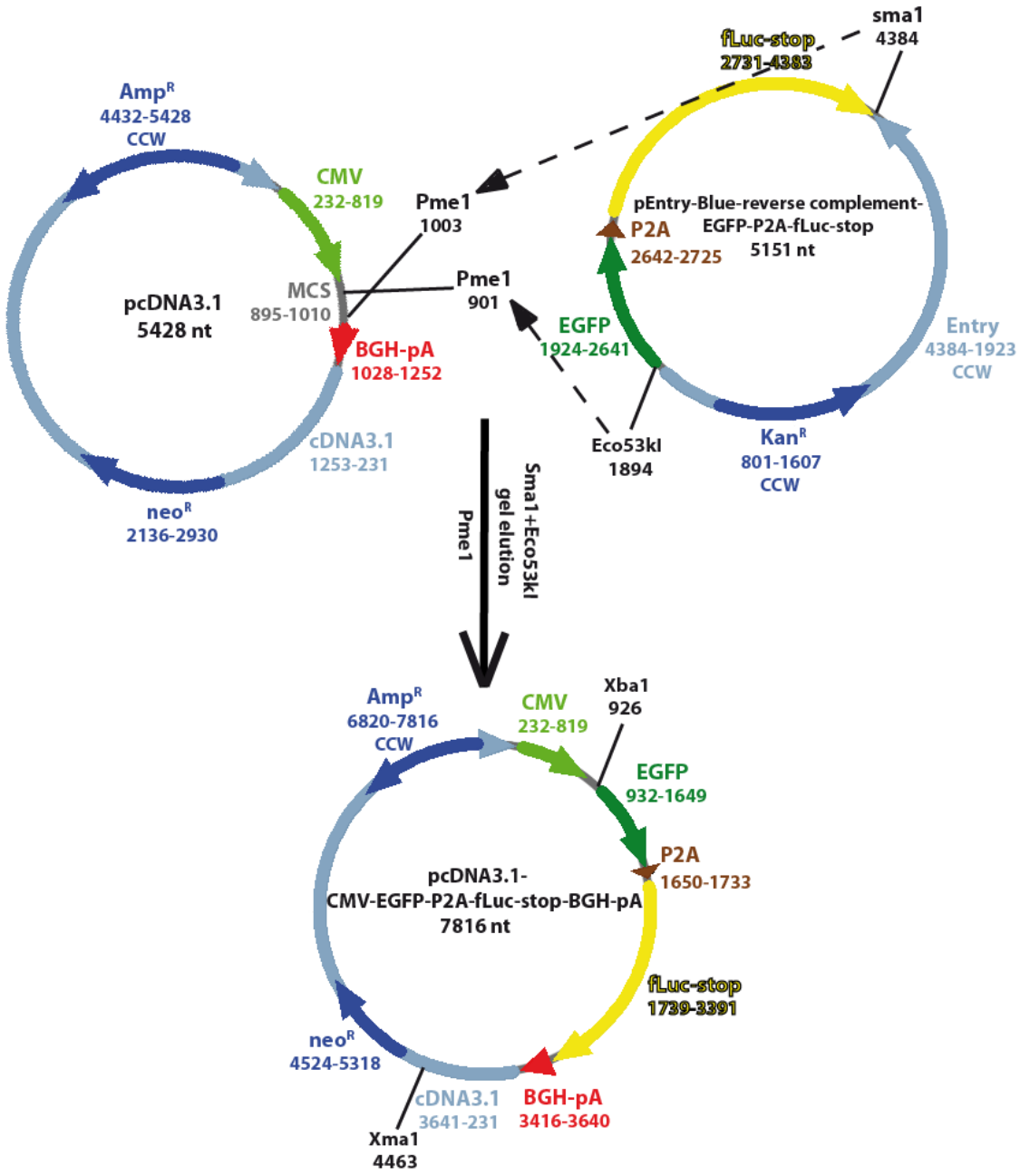

Figure 13: Module B – 3. Subcloning the first reporter cassette into the pcDNA3.1 expression vector to add a 3´BGH-pA sequence.

In order to check for the functionality of the finished first reporter cassette on the protein level, the *CMV* promoter driven expression vector was tranfected into MIA PaCa-2 pancreatic cancer cells. Afterwards *in vitro* assays to confirm the correct expression of EGFP as well as fLuc were performed (see chapter 3.2.1).

3.1.3 Cloning of module C

Table 10: Cloning steps of module C

Cloning step #	Name of plasmid (abbreviation)	Modifications	Name of insert (abbreviation)	Modifications	Purpose of cloning
1	phrG-B-Ecadh-hrLuc-pA (akb-1)	Xho1 and Nco1 digestion	Xho1-EcoR1-Bgl2-2 nt-Nco1-linker	Xho1 and Nco1 sticky ends	Insertion of a linker 5` to the *hrLuc*
2	phrG-B-Ecadh-linker-hrLuc-pA (bed-19)	Xho1 and Bgl2 digestion	pC-S2-TAG-mem-td-Tomato-T2A-H2B-EGFP-pA	Xho1 and Bgl2 digestion and gel elution	Insertion of *mem-td-Tomato*-T2A 5` to *hrLuc*

Continuing the construction of the *Dual Reporter*, the second reporter cassette was prepared in the following cloning steps (table 10). This cassette consists of the *mem-td-Tomato* and the *hrLuc* reporter gene connected via a T2A site. For this purpose, the phrG-B expression vector was available in our lab which contains the *hrLuc* and in addition the *Ecadh* promoter that allows for further expression analyses.

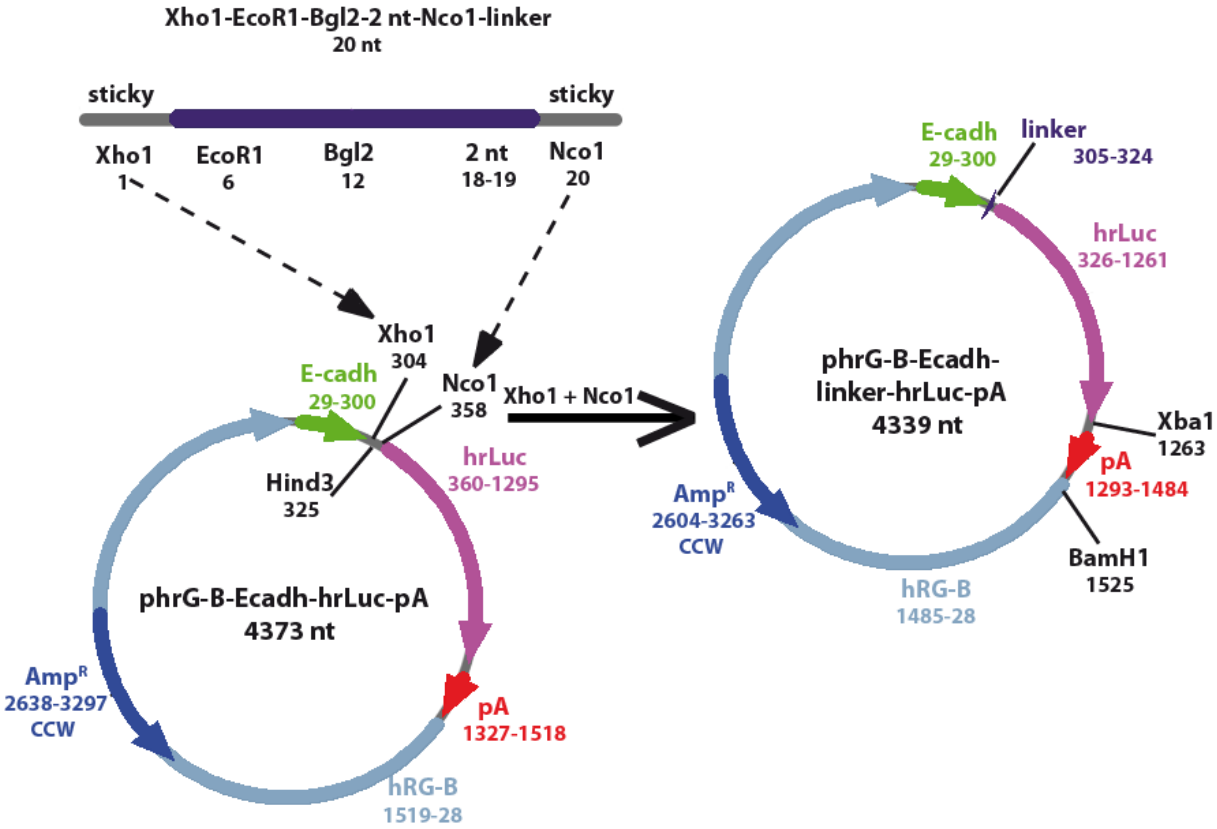

Figure 14: Module C – 1. Insertion of a linker containing 2 restriction sites 5` to the *hrLuc*

In the first step a sticky end oligonucleotide linker was inserted into the Xho1 and Nco1 restriction sites upstream of the *hrLuc* ORF. This linker contains Xho1 and Bgl2 restriction

sites for the insertion of the *mem-td-Tomato* gene together with a 3´ T2A sequence in the next step. In addition an EcoR1 restriction site is inserted between Xho1 and Bgl2 for diagnostic digestion. To keep the *hrluc* ORF in the correct reading frame relative to the *mem-td-Tomato* gene, two nucleotides prior to an Nco1 restriction site were inserted in order to avoid frame shifting (Fig. 14).

In the following step the *mem-td-Tomato* coding sequence connected to the T2A site was subcloned upstream of the linker. For this purpose, a plasmid which contains the *mem-td-Tomato* ORF without a stop codon followed by the T2A site was used (pC-S2-TAG plasmid, Fig. 15). This fragment was excised with Xho1 at the 5` site and Bgl2 at the 3` site. After gel elution this fragment was ligated into the corresponding sticky end restriction sites of the acceptor plasmid (Fig. 15).

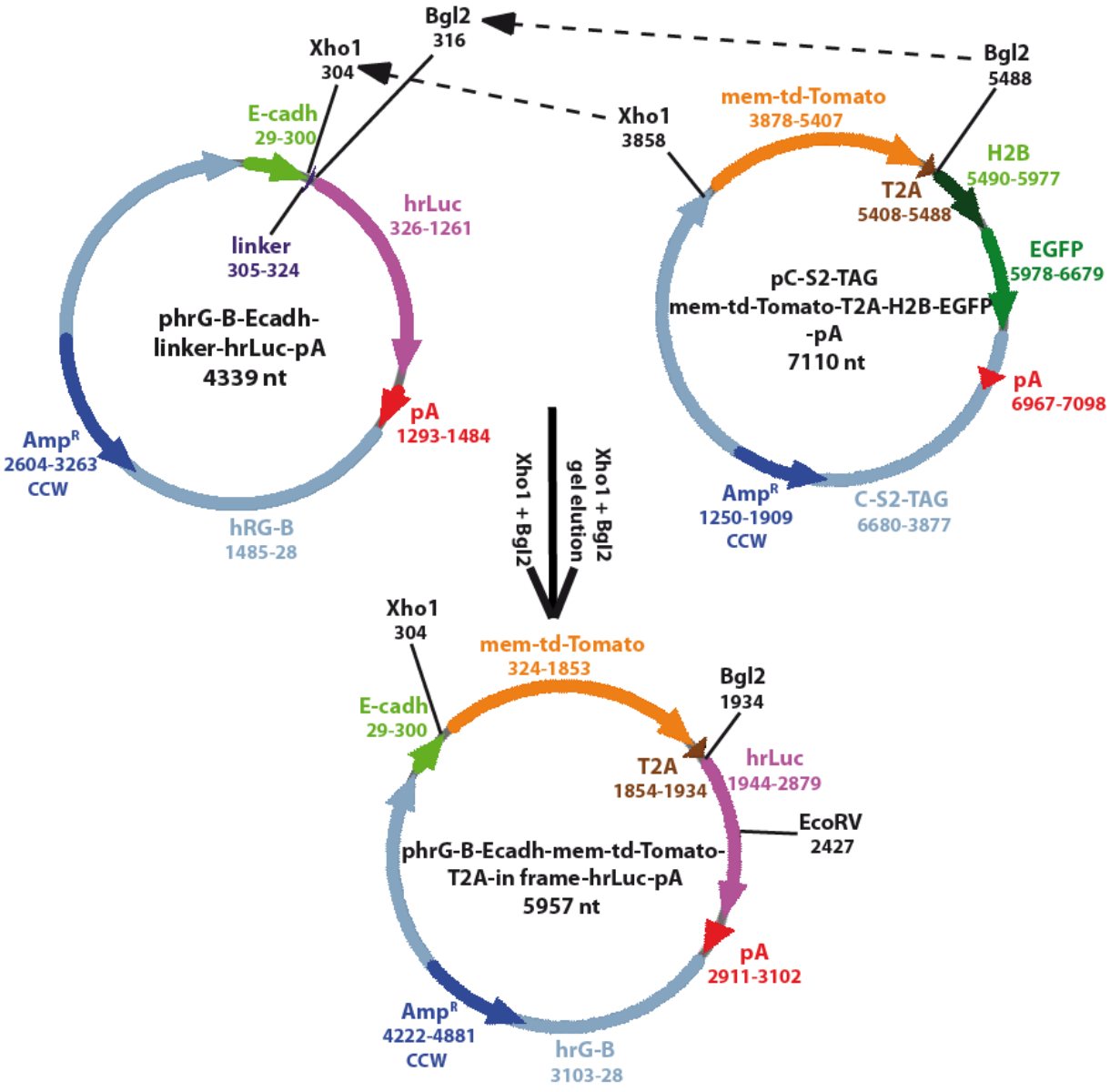

Figure 15: Module C – 2. Insertion of *mem-td-Tomato*-T2A 5` to the hrLuc ORF

Consequently the *mem-td-Tomato* ORF is now placed in the correct reading frame relative to the *hrLuc*.

In order to check for the functionality of the finished second reporter cassette on the protein level, the *E-cadh* promoter driven expression vector was tranfected into MIA PaCa-2 cells. Afterwards *in vitro* assays were performed to confirm the correct expression of mem-td-Tomato as well as hrLuc (see chapter 3.2.1).

3.1.4 Cloning of module D

Table 11: Cloning steps of module D and the final gene targeting vector

Cloning step #	Name of plasmid (abbreviation)	Modifications	Name of insert (abbreviation)	Modifications	Purpose of cloning
1	pEntry-Blue (amm-8)	Xho1 and BamH1 digestion	Xho1-Xma1-Avr2-Pml1-loxP-1 nt-BamH1-linker	Xho1 and BamH1 sticky ends	Subcloning the loxP linker into the pEntry-Blue vector
2	pEntry-Blue-loxP linker (beo-1)	Spe1 and Xba1 digestion	phrG-B-Ecadh-mem-td-Tomato-T2A-in frame-hrLuc-pA (beg-2)	Xba1 digestion	Insertion of the second reporter cassette downstream of the loxP linker
3	pEntr-CAG-loxP-FSF-minPGK-pA-MCS (beh-11)	Xma1 and Avr2 digestion	pEntry-Blue-loxP-linker-mem-td-Tomato-T2A-hrLuc (beq-22)	Xma1 and Xba1 and ApaL1 digestion and gel elution	Subcloning the second reporter cassette into the CAG-loxP-FSF-βG-pA plasmid
4	pEntr-CAG-loxP-FSFminPGK-loxP-mem-td-Tomato-T2A-hrLuc-βG-pA (bet-2)	Avr2 and Pml2 digestion	pcDNA3.1-CMV-EGFP-P2A-fLuc-stop-BGH-pA (bes-11)	Xba1, Pvu2 and ApaL1 digestion and gel elution	Subcloning the first reporter cassette and the BGH-pA signal 5` to the second reporter cassette
5	pRosa-RFA (aqt-1)	5´ and 3´ att sites	pEntr-5´ att-Dual Reporter-3´ att (bfabc-6)	5´ and 3´ att sites	Gateway clonase reaction: Subcloning the *Dual Reporter* construct into

					the *R26* gene targeting vector
	pRosa-RFA-Dual Reporter (bfo-1)	n.a.	n.a.	n.a.	final gene targeting vector

Cloning steps of module D as well as the generation of the final gene targeting vector are summarized in table 11. In this last module the second loxP site has to be placed upstream of the second reporter cassette.

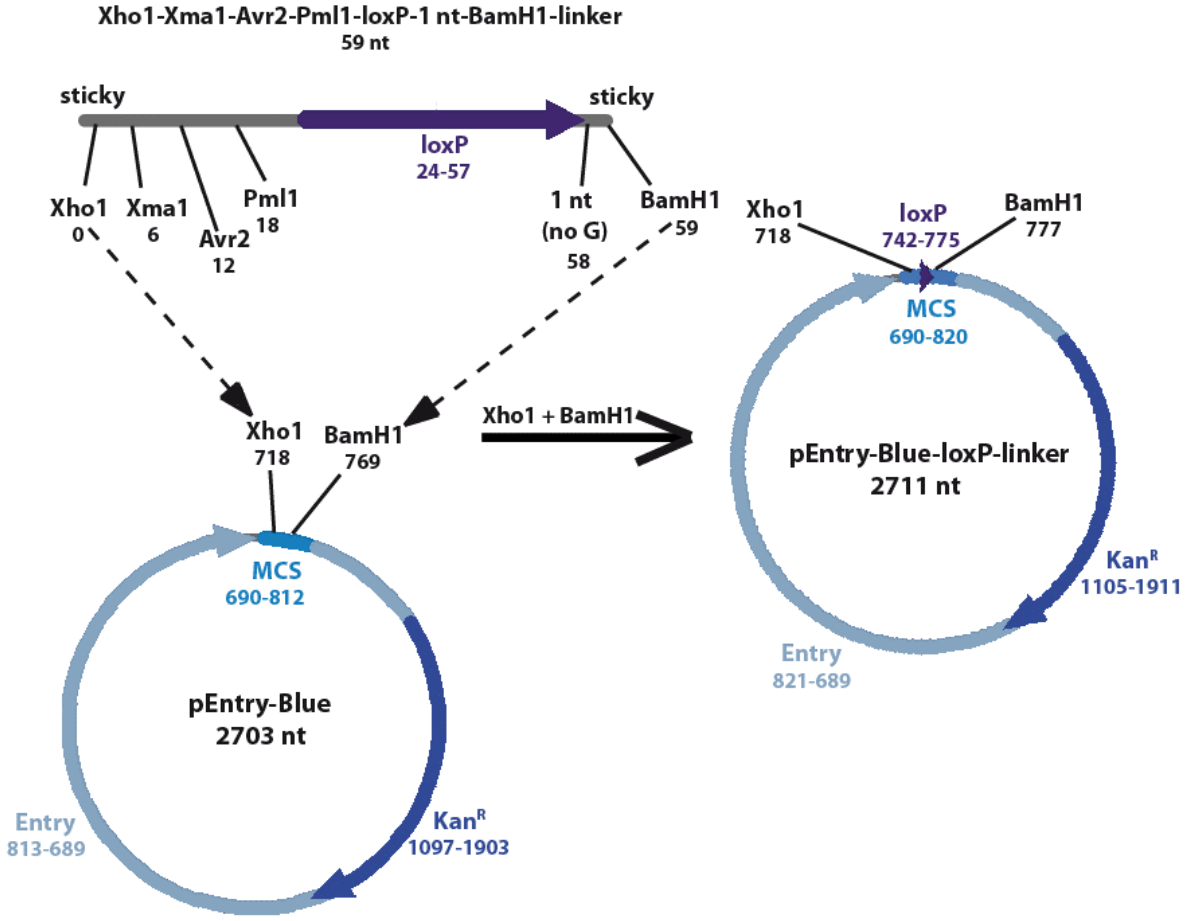

Figure 16: Module D – 1. Subcloning the loxP linker into the pEntry-Blue vector

In order to achieve this, a loxP site containing linker was designed which contains unique restriction sites for later cloning steps (Xma1, Avr2 and Pml1) and which is flanked by two sticky ends for insertion into the acceptor plasmid (Xho1 and BamH1). Since the loxP site ends with the two bases A and T and the following BamH1 site starts with a G, there was a need to put one additional nucleotide between both elements in order to avoid generation of an unwanted start codon. The loxP linker was inserted into the multiple cloning site of the pEntry-Blue cloning vector by Xho1 and BamH1 sticky end ligation (Fig. 16).

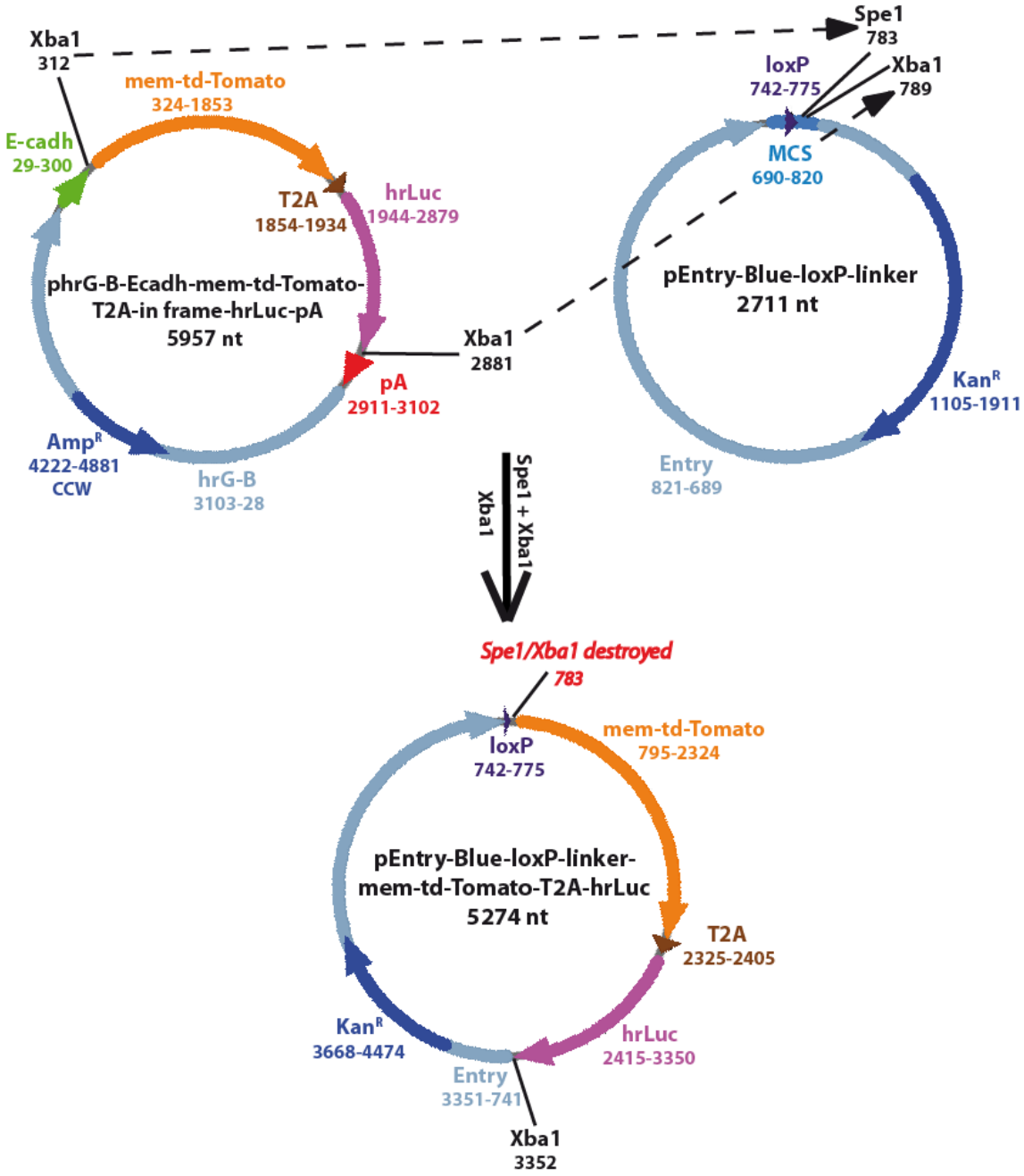

Figure 17: Module D – 2. Insertion of the second reporter cassette (module C) downstream of the loxP linker

In the next step the *mem-td-Tomato*-T2A-*hrLuc* fragment was excised of the phrG-B expression vector using the flanking Xba1 restriction sites. Afterwards this reporter cassette was inserted downstream of the loxP linker in the pEntry-Blue vector via sticky end ligation with a Spe1 and Xba1 restriction site respectively, thereby leading to destruction of the 5` Spe1 site and restoration of the Xba1 site (Fig. 17).

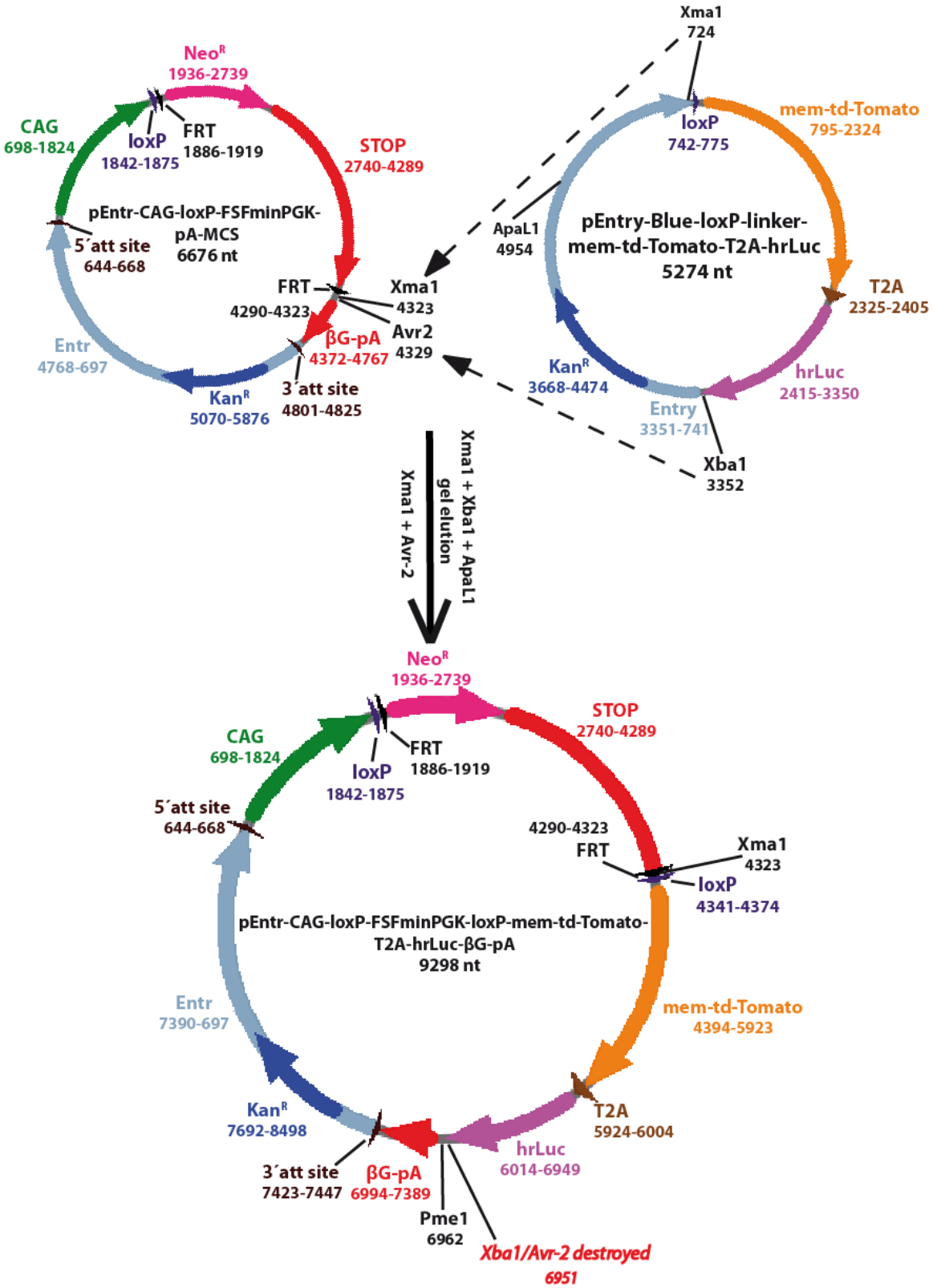

Figure 18: Generation of the final gene targeting construct – 1. Subcloning the second reporter cassette into the CAG-loxP-FSF-βG-pA plasmid

3.1.5 Generation of the final gene targeting construct

After having generated the single modules of the final construct, all the fragments were connected and furthermore subcloned into the gene targeting destination plasmid which contains the *Rosa26* homologous arms. In the first step the second reporter cassette (module C) will be inserted into the pEntr vector constructed in module A. The second reporter cassette is excised via the Xma1 restriction site of the loxP linker and the Xba1 restriction site at the end of the reporter cassette. Since the cassette is purified by gel elution, ApaL1 was chosen as an additional restriction site in the vector backbone for a facilitated separation of the fragments in the gel. The destination vector was opened with Xma1 and Avr2 restriction sites directly 3´ of the FSF cassette. After directed sticky end ligation, the 5` Xma1 site remains whereas the 3` Avr2 and Xba1 sites will be destroyed (Fig. 18).

For finishing the *Dual Reporter* construct, the first reporter cassette and the BGH-pA signal (module B) have to be inserted between the FSF cassette and the following second reporter cassette. The first reporter and the BGH-pA signal are excised out of the pcDNA3.1 expression vector using the Xba1 and Pvu2 restriction sites. ApaL1 is used as additional restriction site in the vector backbone for a facilitated gel elution of the Xba1-Pvu2 fragment. The destination vector is opened between the second FRT and loxP site using Avr2 and Pml1 restriction sites (both derived from the loxP linker). Consequently the insert will be ligated half sticky end (destruction of the 5´ Xba1 and Avr2 restriction sites) and half blunt end (destruction of the 3` blunt end restriction sites Pvu2 and Pml1; Fig. 19).

In order to complete the final gene targeting plasmid, the *Dual Reporter* construct has to be flanked by the *Rosa26* homologous arms on both sides. These arms will allow the homologous recombination event to take place within the embryonic stem cells afterwards, thus targeting the *Dual Reporter* construct into the endogenous *R26* locus. To achieve this, the Gateway cloning technique from Invitrogen™ was used. The *Dual Reporter* construct which was assembled in a pEntr vector, which contains *attL* (attachment) sites flanking the the *Dual Reporter* cassette is transferred into the existing *R26* targeting plasmid, which was constructed by our lab to contain *attR* sites. Thereby, it is possible to transfer the conditional *Dual Reporter* cassette into the *R26* targeting vector by recombination mediated cassette exchange. The sequence between the *att* sites of the *R26* destination vector contains a suicide gene (*ccdB*) for selection of correctly exchanged clones harboring the *Dual Reporter* insert. Beside this, both *R26* homologous arms as well as a *Pgk* promoter driven *diphtheria toxin A* (*DTA*) gene are present in the *R26* destination vector backbone. This *DTA* gene is later used for negative selection during the gene targeting experiment in case of non-homologous full integration of the whole plasmid into the embryonic stem cell genome. For linearization of the final gene targeting plasmid, a unique Pac1 restriction site is placed 5´ to the *R26* homologous short arm of the vector (Fig. 20).

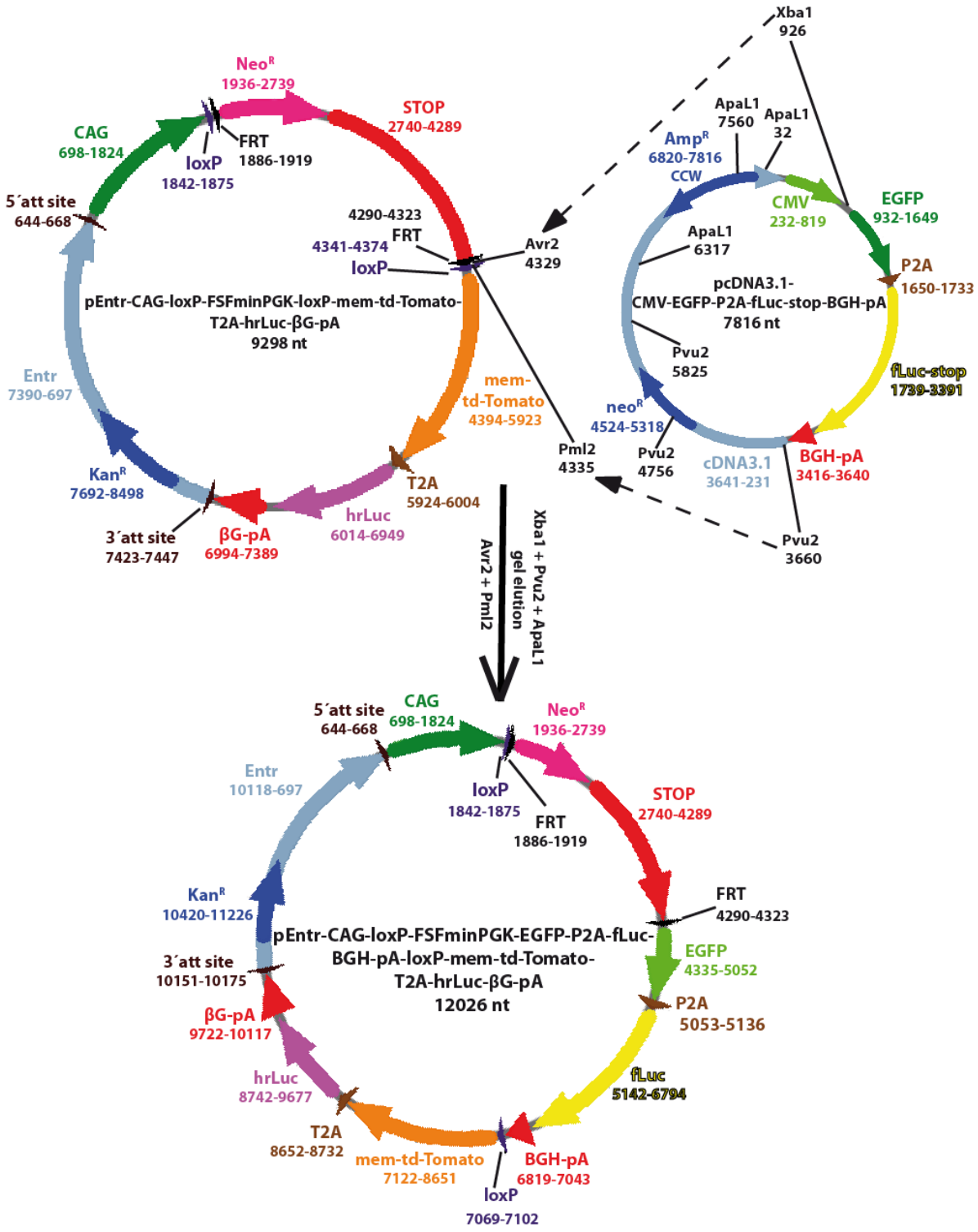

Figure 19: Generation of the final gene targeting construct – 2. Subcloning the first reporter cassette and the BGH-pA signal (module B) 5` to the second reporter cassette

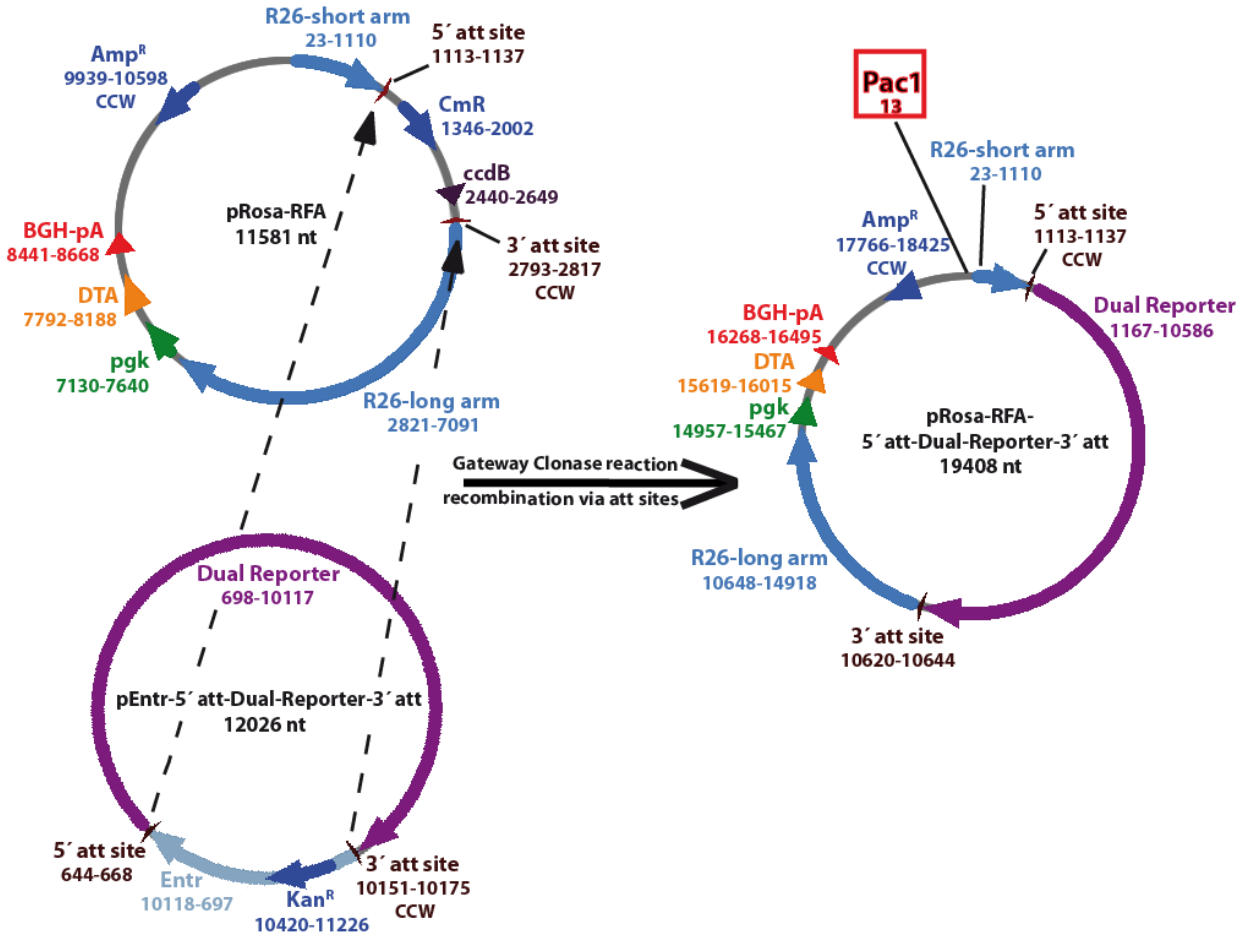

Figure 20: Generation of the final gene targeting construct – 3. Gateway clonase reaction: Subcloning the *Dual Reporter* construct into the *R26* gene targeting vector by recombination mediated cassette exchange.

3.2 *In vitro* characterization of reporter gene expression

3.2.1 Transient MIA PaCa-2 transfections with individual reporter cassette expression vectors

In order to evaluate the correct expression of the two reporter cassettes constructed (module B and module C, see 3.1.2 and 3.1.3), the established human pancreatic cancer cell line MIA PaCa-2 was used for further transient transfection experiments.

Starting with the EGFP-P2A-fLuc reporter cassette, first of all a mock plasmid (negative control) was transfected into the MIA PaCa-2 cells which resulted in no EGFP expression as shown by fluorescence microscopy (Fig. 21 A). As a positive control these cells were transfected with a *CMV* promoter driven EGFP expression vector which led to EGFP detection (Fig. 21 B). In the third experiment, the pcDNA3.1 expression vector was transfected which contains the first reporter cassette under the control of the *CMV* promoter, confirming the EGFP expression (Fig. 21 C).

For testing the second reporter cassette, a mock transfection was conducted which revealed no mem-td-Tomato expression of the cells (Fig. 22 A). In the next step the expression vector

containing the second reporter cassette under the control of the *E-cadh* promoter was transfected. Here it could be shown that the mem-td-Tomato expression is detectable (Fig. 22 B).

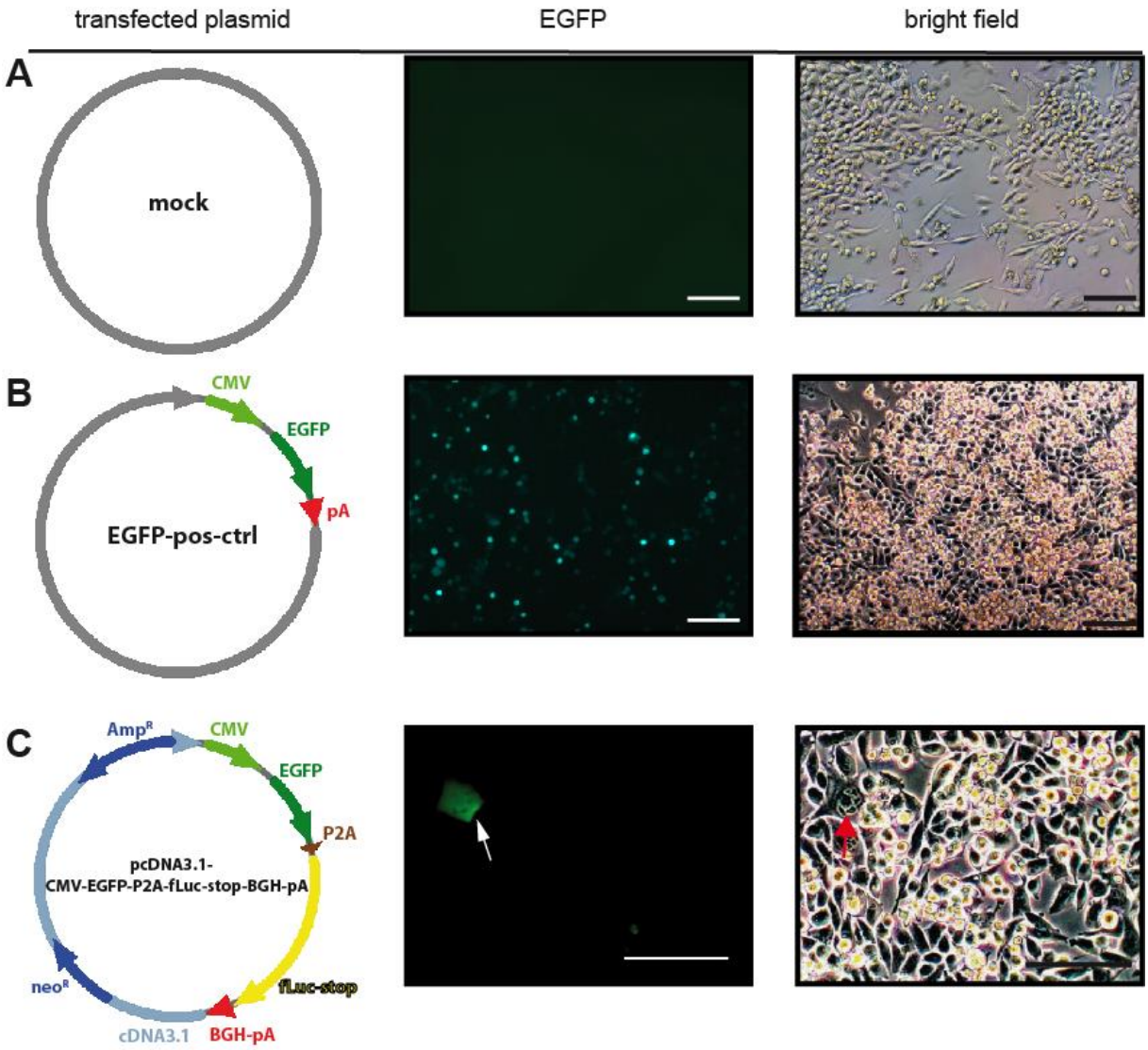

Figure 21: *In vitro* characterization of EGFP expression: (A) MIA PaCa-2 cells transfected with mock plasmid as negative control show no EGFP expression. (B) MIA PaCa-2 cells transfected with EGFP expression vector as positive control reveals EGFP expression. (C) MIA PaCa-2 cells transfected with pcDNA3.1 expression vector containing the first reporter cassette (EGFP-P2A-fLuc) show correct EGFP expression. Arrow shows a single cell with strong EGFP expression. Scale bars equal 100 µm. Photos were taken approx. 36 h after transient transfection. All transfection experiments were performed in triplicates (n=3). Representative photos are depicted.

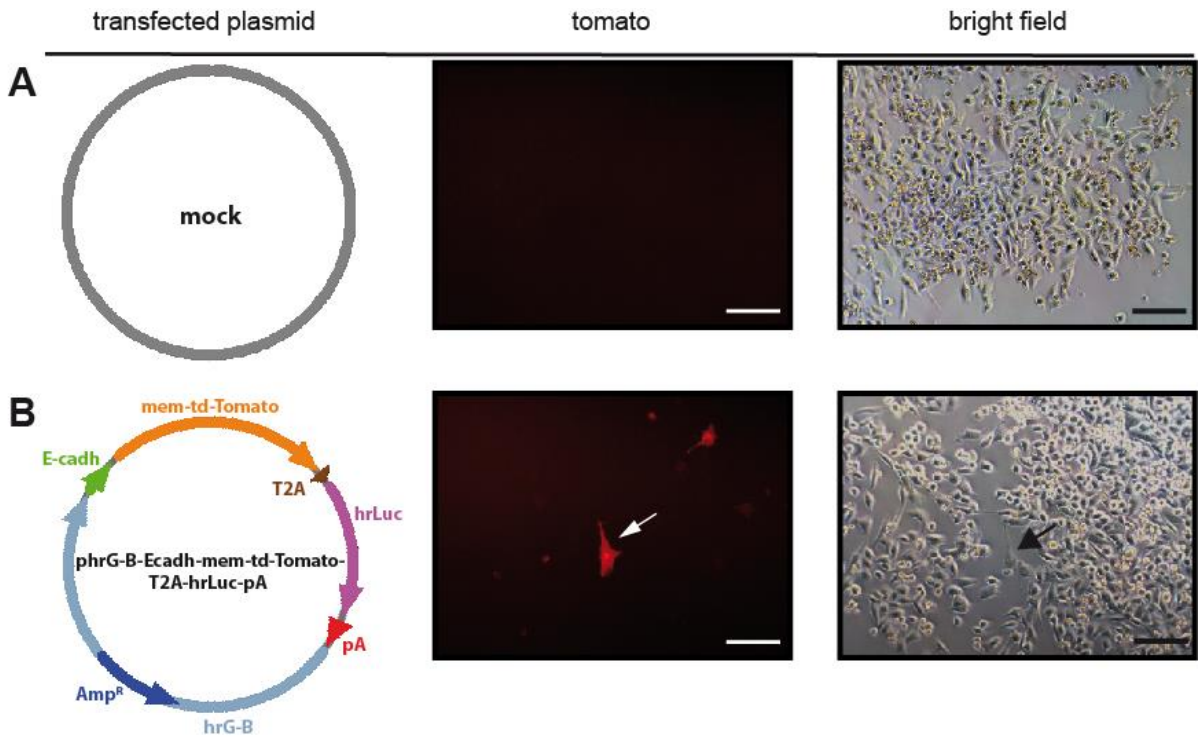

Figure 22: *In vitro* characterization of mem-td-Tomato expression: (A) MIA PaCa-2 cells transfected with mock plasmid show no mem-td-Tomato expression (negative control). (B) MIA PaCa-2 cells transfected with the phrG-B expression vector containing the second reporter cassette (mem-td-Tomato-T2A-hrLuc) reveal correct expression of mem-td-Tomato. Arrow shows a single cell with strong mem-td-Tomato expression. Scale bars equal 100 µm. Photos were taken approx. 36 h after transient transfection. All transfection experiments were performed in triplicates (n=3). Representative photos are shown.

After validating the correct expression of the fluorescence reporter genes in both cassettes *in vitro*, luciferase assays were performed in order to confirm the correct expression of both luciferases. This is another important validation step since it will show the correct in frame cloning of the different *2A* sites used in both reporter cassettes.

Luciferase assays revealed a strong activity of firefly and renilla luciferase of both reporter cassettes in transfected MIA PaCa-2 cells compared to the background signal of the mock transfected cells, respectively (Fig. 23).

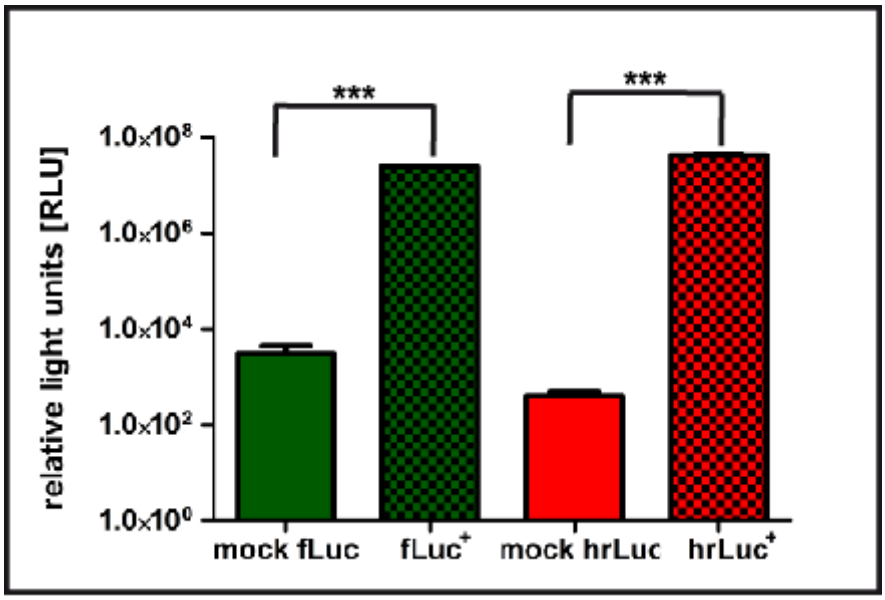

Figure 23: *In vitro* characterization of fLuc and hrLuc expression: Mock (promoterless mock fLuc and mock hrLuc plasmids), first reporter cassette (EGFP-P2A-fLuc, fLuc$^+$) and second reporter cassette (mem-td-Tomato-T2A-hrLuc, hrLuc$^+$) plasmids were transfected into MIA PaCa-2 cells and cells were harvested 48 h after transient transfection. Total protein was extracted and firefly and renilla luciferase activitiy were measured. Cells were harvested at approx. 80% confluency. Luciferase assays were performed in triplicates (n=3) and mean values + SEM are depicted (***p<0.0001; two-sided unpaired student`s t-test).

3.2.2 Transient MIA PaCa-2 co-transfections with the *Dual Reporter* construct – functional characterization of genetic elements

After having finished all cloning steps for the *Dual Reporter* gene targeting construct, another *in vitro* analysis of the final construct was executed before starting the embryonic stem cell culture for the knock in experiment. This is another crucial step since it will test the different genetic elements of the construct (Cre- and Flp mediated recombination and expression of the respective reporters of the final construct).

The characterization of the first reporter cassette (EGFP-P2A-fLuc) was launched and MIA PaCa-2 cells were co-transfected with the final *Dual Reporter* expression plasmid (Fig. 19; pEntr-CAG) and a mock plasmid. As expected there was no EGFP expression detectable (Fig. 24 A). In the next step a *CMV* promoter driven EGFP expression vector and a mock plasmid were co-transfected into the cells as positive control. This resulted in a strong EGFP expression (Fig. 24 B). In order to check the functionality of the first reporter cassette, the cells were co-transfected with the final *Dual Reporter* plasmid and a Flp expression plasmid. Two days after transfection, a strong EGFP signal but no mem-td-Tomato expression (second reporter cassette) could be detected (Fig. 24 C). Testing the second reporter cassette, the cells were co-transfected with the final *Dual Reporter* plasmid and a Cre expression vector. This resulted in a strong mem-td-Tomato expression of the cells due to Cre-mediated deletion of the floxed first reporter cassette (Fig. 24 D).

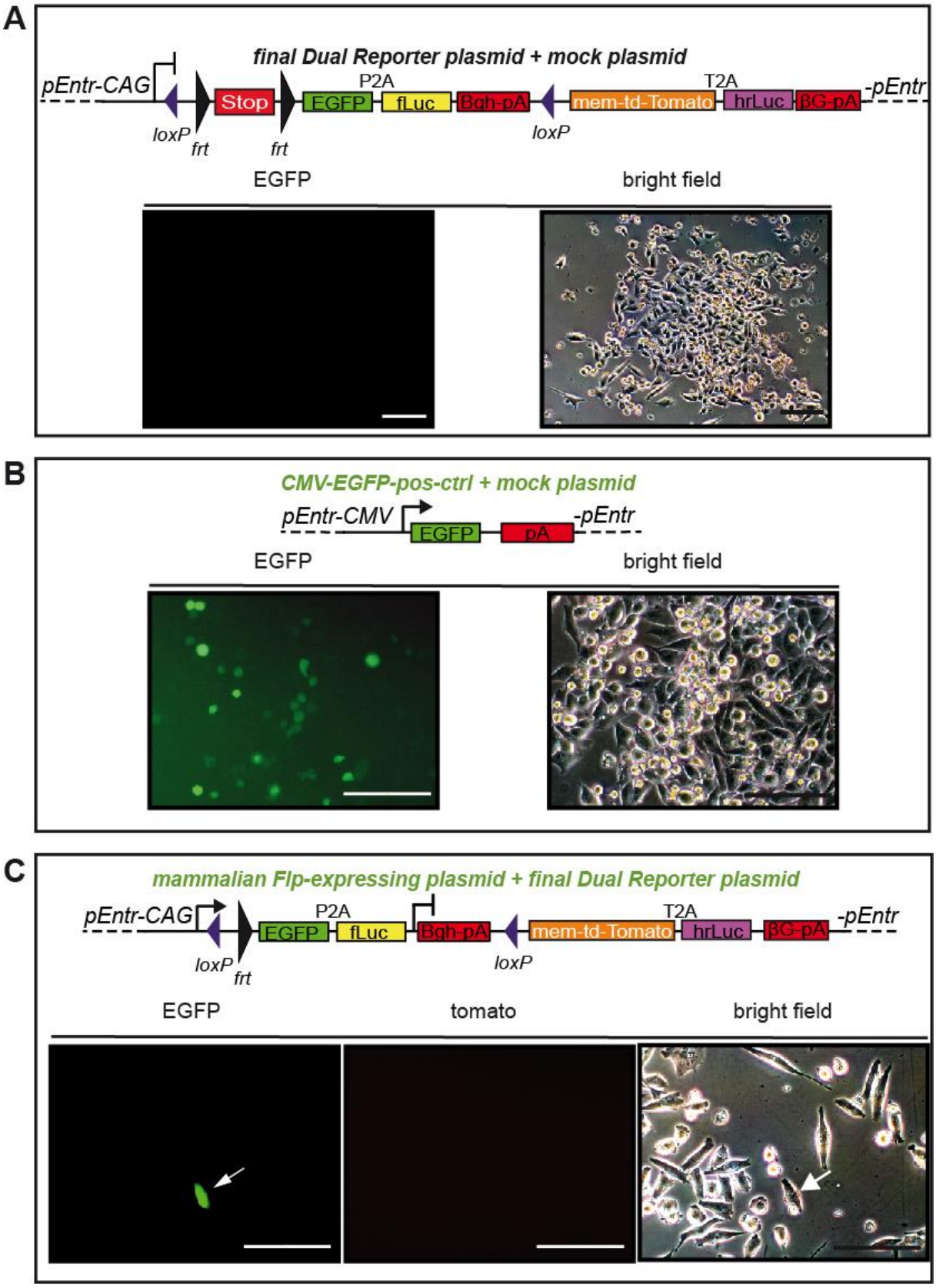
A
final Dual Reporter plasmid + mock plasmid
pEntr-CAG
Stop
P2A
EGFP
fLuc
Bgh-pA
T2A
mem-td-Tomato
hrLuc
βG-pA
-pEntr
loxP
frt
frt
loxP
EGFP
bright field
B
CMV-EGFP-pos-ctrl + mock plasmid
pEntr-CMV
EGFP
pA
-pEntr
EGFP
bright field
C
mammalian Flp-expressing plasmid + final Dual Reporter plasmid
pEntr-CAG
P2A
EGFP
fLuc
Bgh-pA
T2A
mem-td-Tomato
hrLuc
βG-pA
-pEntr
loxP
frt
loxP
EGFP
tomato
bright field

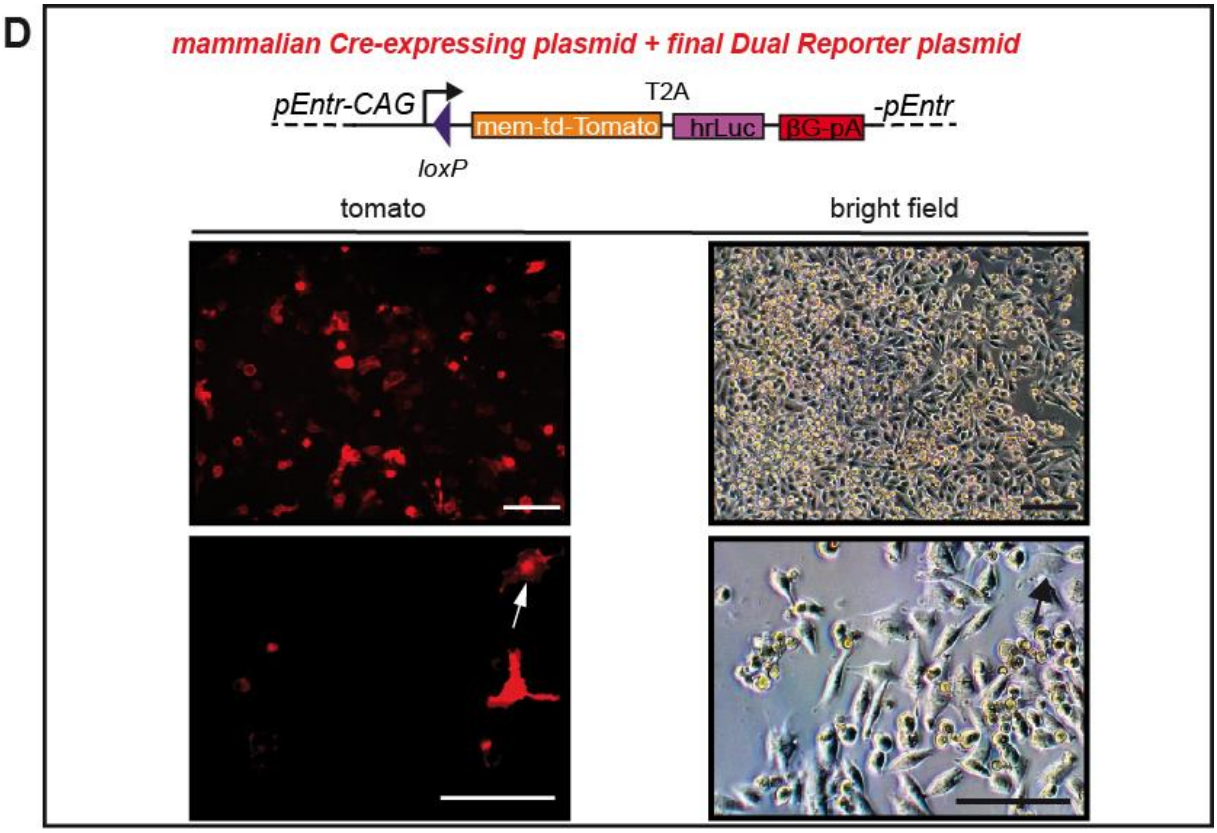

Figure 24: *In vitro* characterization of the final *Dual Reporter* construct by transient co-transfections of MIA PaCa-2 cells – functional characterization of genetic elements: (A) Co-transfection of *Dual Reporter* plasmid and mock plasmid as negative control shows no EGFP expression. (B) Co-tranfection of EGFP expression vector and mock plasmid shows strong EGFP signal. (C) Co-transfection of a Flp expression vector and the *Dual Reporter* vector shows strong EGFP expression due to Flp mediated deletion of the FSF cassette. Arrow depicts a single EGFP positive cell. (D) Co-transfection of a Cre expression vector and the *Dual Reporter* vector shows strong mem-td-Tomato expression due to Cre-mediated deletion of the floxed first reporter cassette. Arrow depicts a single mem-td-Tomato positive cell. Scale bars equal 100 µm. Photos were taken approx. 48h after co-transfections. All co-transfection experiments were performed in triplicates (n=3) and representative photos are shown.

In another experiment the molecular switching from the first to the second reporter cassette expression was imitated, as it will be used in the *R26 Dual Reporter* mouse line when inducing a Cre recombinase in an already Flp recombined genetic background. Therefore the Flp recombined *Dual Reporter* construct was generated, which could be achieved by a co-transformation of competent *E.coli* bacteria with the *Dual Reporter* plasmid and a bacterial-specific Flp expression plasmid. Flp mediated deletion of the FSF cassette was confirmed by screening PCR analyses and in addition the recombined *Dual Reporter* construct was sequenced. Afterwards, the plasmid was co-transfected into MIA PaCa-2 cells with a mock plasmid. EGFP, but no mem-td-Tomato expression could be detected (Fig. 25 A).

In the following step these cells were co-transfected with a Cre-expression vector and a mock plasmid. Two days after co-transfection there were still some EGFP positive cells visible, but most of the cells have already switched to mem-td-Tomato expression due to Cre recombination (Fig. 25 B).

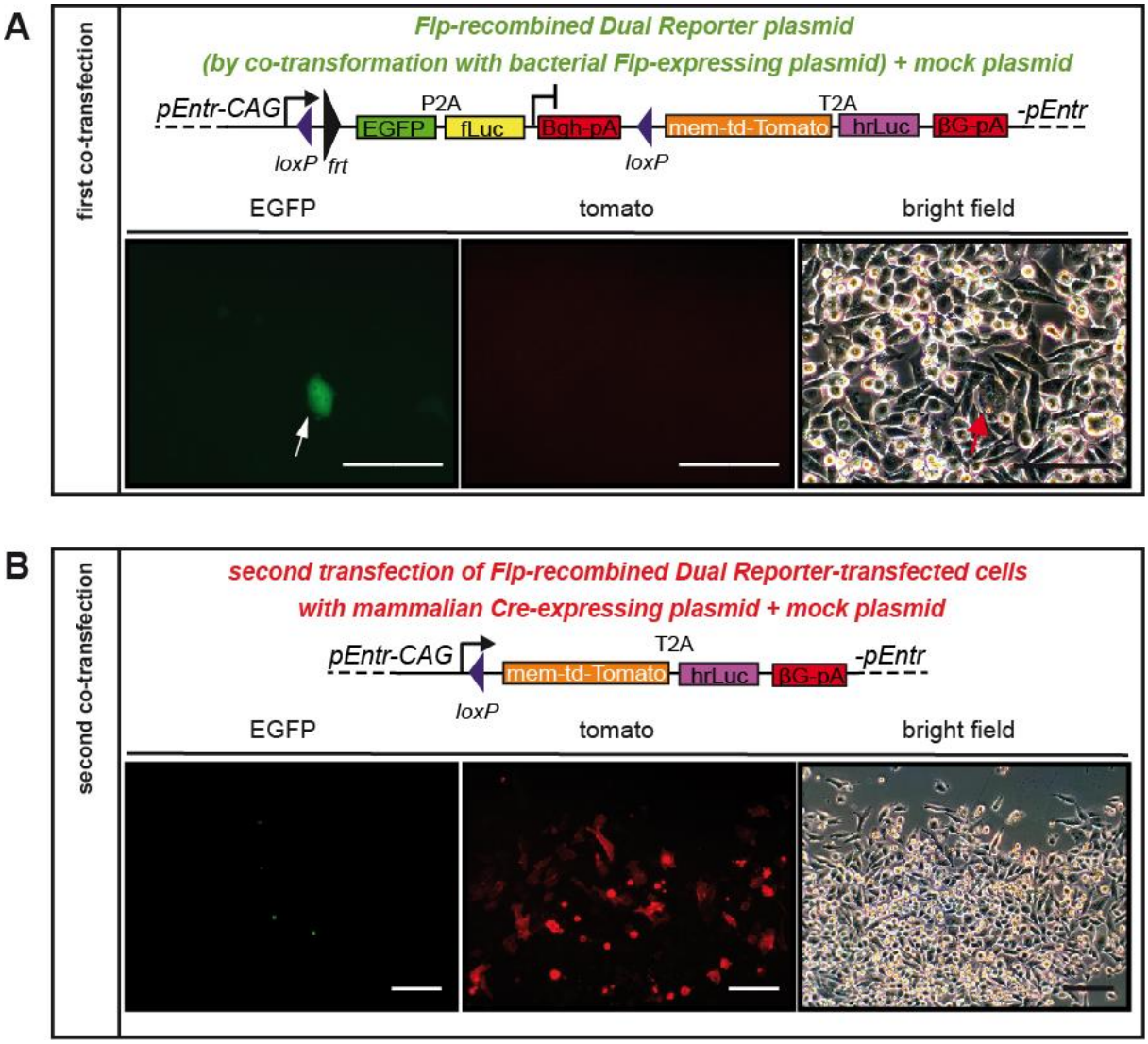

Figure 25: *In vitro* characterization of the final *Dual Reporter* construct by transient co-transfections of MIA PaCa-2 cells – molecular switching from first to second reporter cassette expression: (A) Competent *E.coli* bacteria were co-transformed with the *Dual Reporter* plasmid and a bacterial-specific Flp expression vector. Flp mediated deletion of the FSF cassette was confirmed by screening PCR and sequence analysis. The recombined construct was co-transfected into MIA PaCa-2 cells with a mock plasmid and EGFP expression could be detected. Arrow shows a single cell with strong EGFP expression. (B) Upon co-transfection of EGFP-positive cells with a mammalian-specific Cre-expression plasmid and a mock plasmid, only few cells still show EGFP expression. The bulk of the cells have switched to mem-td-Tomato expression due to Cre-mediated deletion of the floxed first reporter cassette. Scale bars equal 100 µm. Photos were taken approx. 48h after co-transfections. All co-transfection experiments were performed in triplicates (n=3) and representative photos are depicted.

3.3 Embryonic stem cell culture: Gene targeting – *Rosa26* knock in

3.3.1 The *Dual Reporter* knock in

A

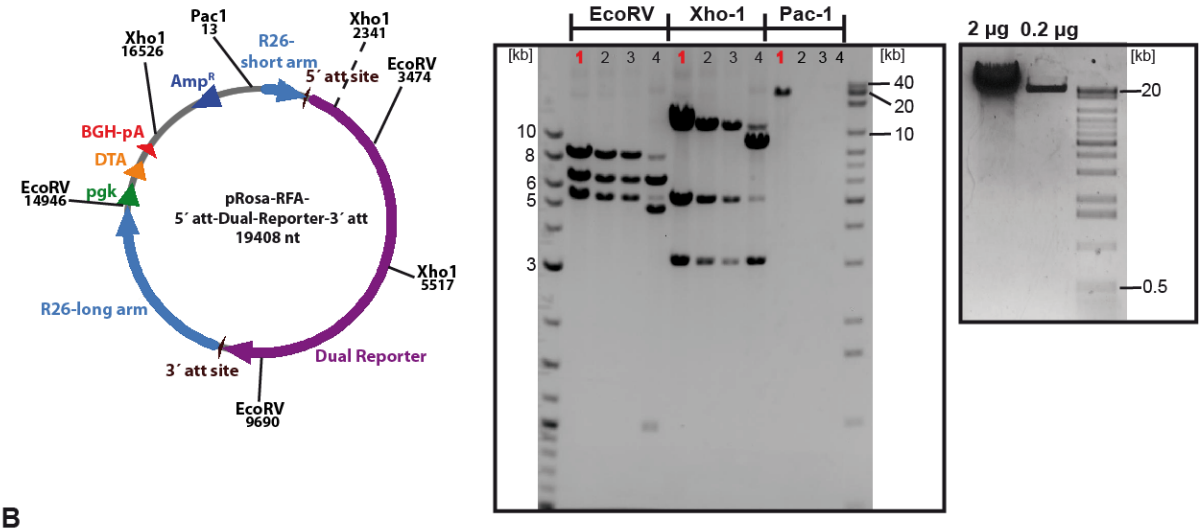

B

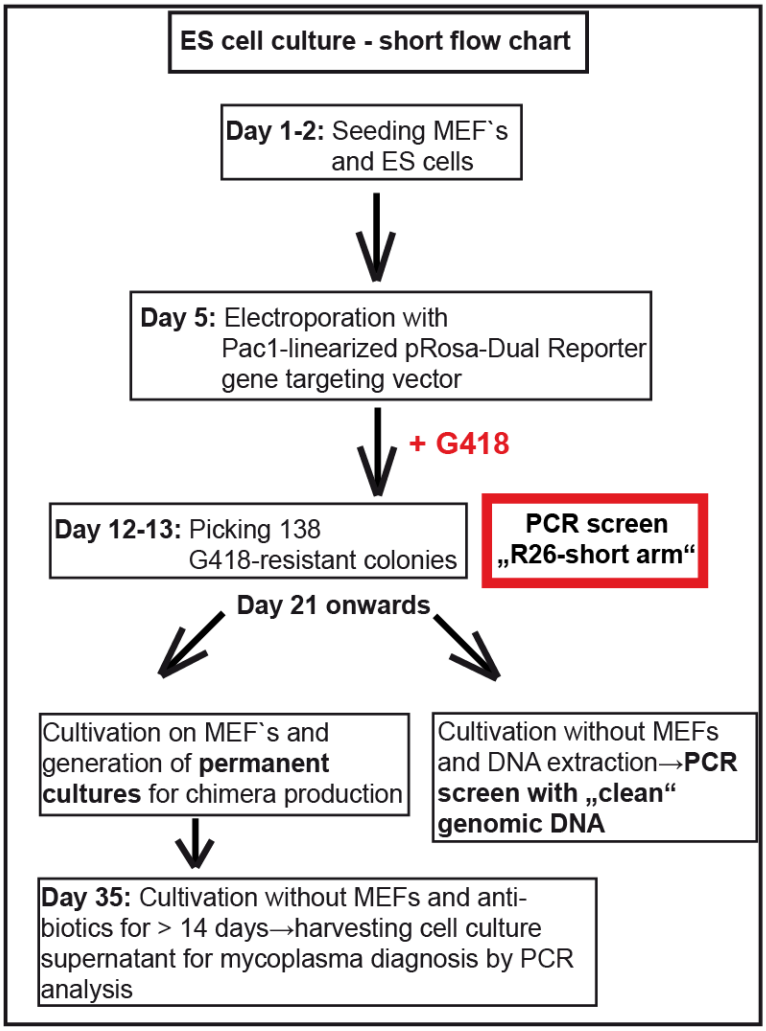

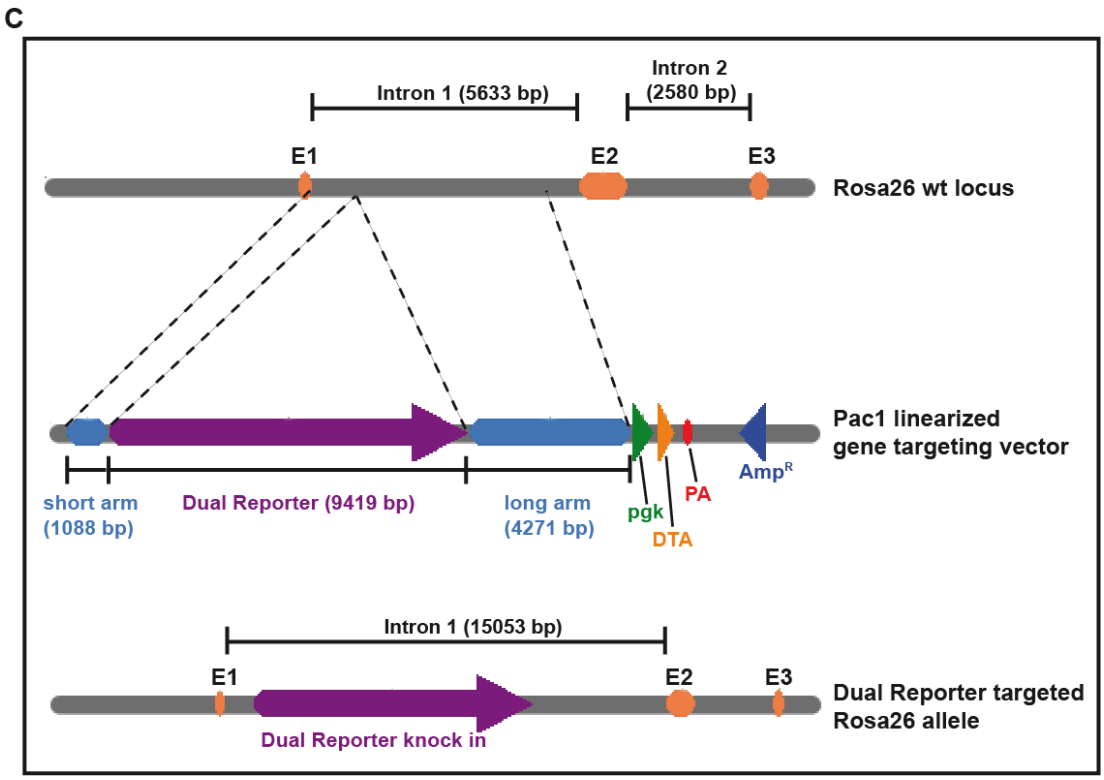

Figure 26: Embryonic stem cell culture – *Rosa26 Dual Reporter* knock in: (A) Diagnostic digestions of the final *R26 Dual Reporter* gene targeting plasmid were performed from four different clones. Clone #1 shows the correct restriction pattern in all digestions and was chosen for the gene targeting procedure. Gel photo on the right side shows Pac1 linearization of clone #1 before electroporation. Even when loading 2 µg of digested *R26 Dual Reporter* plasmid on the gel, no smaller fragments are visible confirming successful digestion containing no incomplete digested plasmid. (B) Overview of the most important steps during the embryonic stem cell culture. (C) Schematic representation of the *R26* targeting. E = exon.

Summing up the data so far, the functionality of the *Dual Reporter* construct could be demonstrated *in vitro* on the protein level. Flp- and Cre-mediated recombination events with expression of the corresponding reporter cassettes could successfully be demonstrated.

In order to generate the *R26 Dual Reporter* knock in mouse line, ES cell culture was applied in the following step. Initially check digestions of the final *R26 Dual Reporter* gene targeting plasmid were performed to confirm the successful clonase reaction (Fig. 26 A). After choosing the correct clone, the construct was linearized using the unique Pac1 restriction site in the vector backbone (Fig. 26 A). W4/129S6 ES cells were electroporated with the linearized targeting vector and cells were treated with G418 for a positive selection of recombined ES cell clones (*neomycin* resistance gene contained within the FSF cassette for positive selection and *DTA* gene contained in the vector backbone in case of a random, non-homologous integration event for negative selection) (Fig. 26 B). After successful homologous recombination, the *Dual Reporter* construct is integrated into intron 1 of the endogenous *Rosa26* locus (Fig. 26 C).

A

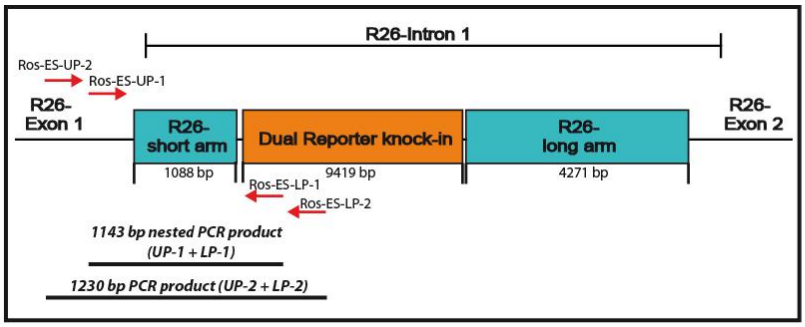
R26-Intron 1
Ros-ES-UP-2
Ros-ES-UP-1
R26-
Exon 1
R26-
short arm
Dual Reporter knock-in
R26-
long arm
R26-
Exon 2
1088 bp
9419 bp
4271 bp
Ros-ES-LP-1
Ros-ES-LP-2
1143 bp nested PCR product
(UP-1 + LP-1)
1230 bp PCR product (UP-2 + LP-2)

B

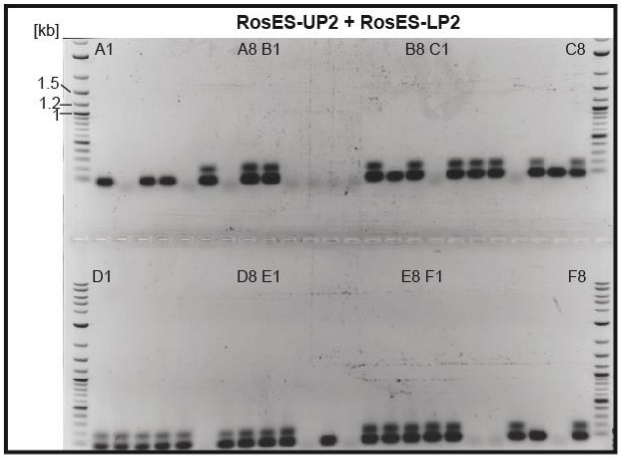
RosES-UP2 + RosES-LP2
[kb]
A1
A8 B1
B8 C1
C8
1.5
1.2
1
D1
D8 E1
E8 F1
F8

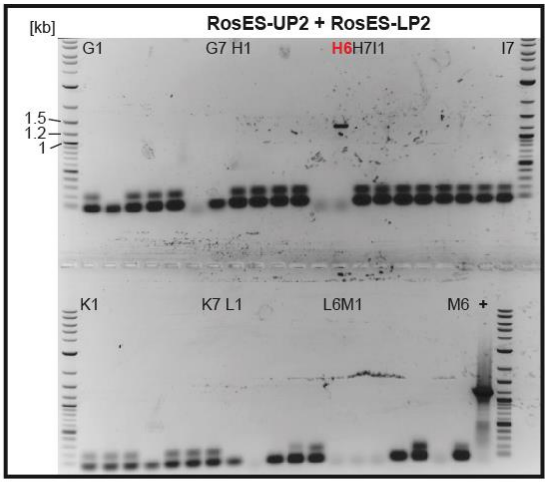
RosES-UP2 + RosES-LP2
[kb]
G1
G7 H1
H6H7I1
I7
1.5
1.2
1
K1
K7 L1
L6M1
M6 +

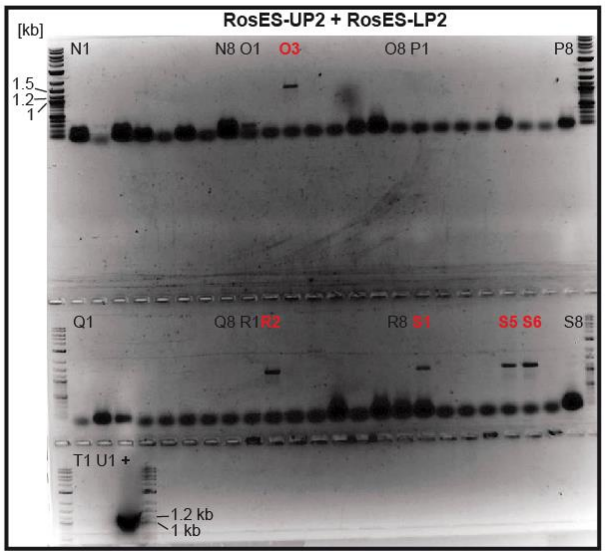
RosES-UP2 + RosES-LP2
[kb]
N1
N8 O1
O3
O8 P1
P8
1.5
1.2
1
Q1
Q8 R1
R2
R8 S1
S5 S6
S8
T1 U1 +
1.2 kb
1 kb

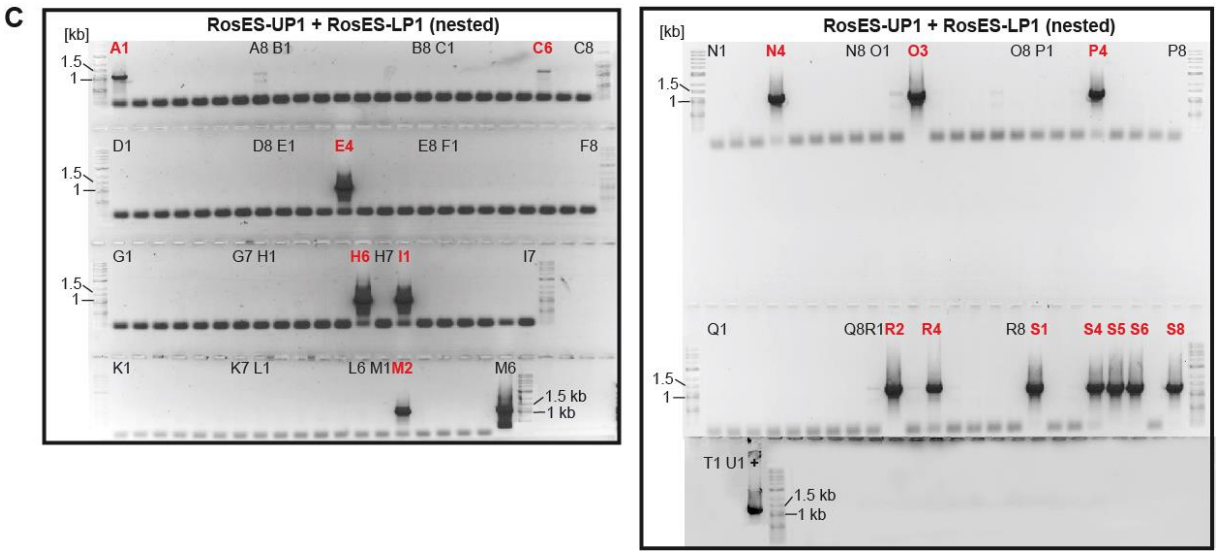

Figure 27: PCR screening strategy for identification of homologous recombined ES cell clones: (A) Nested PCR screening strategy for the detection of the 5´ end of the *R26 Dual Reporter* construct. Primer combinations and PCR product lengths are depicted. (B) Agarose gels from all screening PCRs with the primer pair Ros-ES-UP2 and Ros-ES-LP2 are shown. (C) Agarose gels from all nested screening PCRs using the primer pair Ros-ES-UP1 and Ros-ES-LP1 are shown. Positive clones are marked in red. "+" represents the positive control which is genomic DNA isolated from a mouse containing a *Rosa26* knock in. The correct band size for correctly targeted ES cell clones is 1230 bp for B and 1143 bp for C.

For identifying correctly recombined ES cell clones after the positive-negative selection procedure, 138 colonies were picked and a screening PCR was performed which is detecting the 5´ end of the *R26 Dual Reporter* knock in. The primers are binding outside of the *R26* homologous "short arm" within the genomic sequence as well as within the construct sequence, to make sure that only the homologous recombined colonies will get a positive PCR result (Fig. 27 A). Out of the 138 picked colonies, 6 colonies show positive PCR results (Fig. 27 B; positive clones are marked in red).

To confirm results of the first PCR and perform a second amplification step to detect positive ES cell colonies with low DNA content, a nested PCR was performed. Therefore, another primer pair was used binding within the amplified product of the first PCR (Fig. 27 A). The nested PCR revealed 10 more positive colonies. Consequently 16 out of 138 picked colonies show a successful homologous recombination event (Fig. 27 C; positive clones marked in red).

12 out of these 16 positive clones were chosen for further cultivation (depending on the phenotype of the colony, e.g. growth behavior, differentiation status, amount of cells etc.). For further characterization of the knock in it is important to screen for the complete integration of the *Dual Reporter* construct.

3.3.2. PCR screening strategy to check for completed recombination

In order to span the whole knock in, a PCR screening strategy was developed consisting of four different internal PCRs ranging from the 5´ end to the 3´ end of the *Dual Reporter* construct (Fig. 28 A). PCR results showed different lengths of integration for the positive ES

cell clones (Fig. 28 B). 6 out of the 12 tested clones showed integration of all important parts of the construct, the other 6 clones lacked specific fragments of the *R26 Dual Reporter* cassette, most likely due to deletion during homologous recombination (Fig. 28 B).

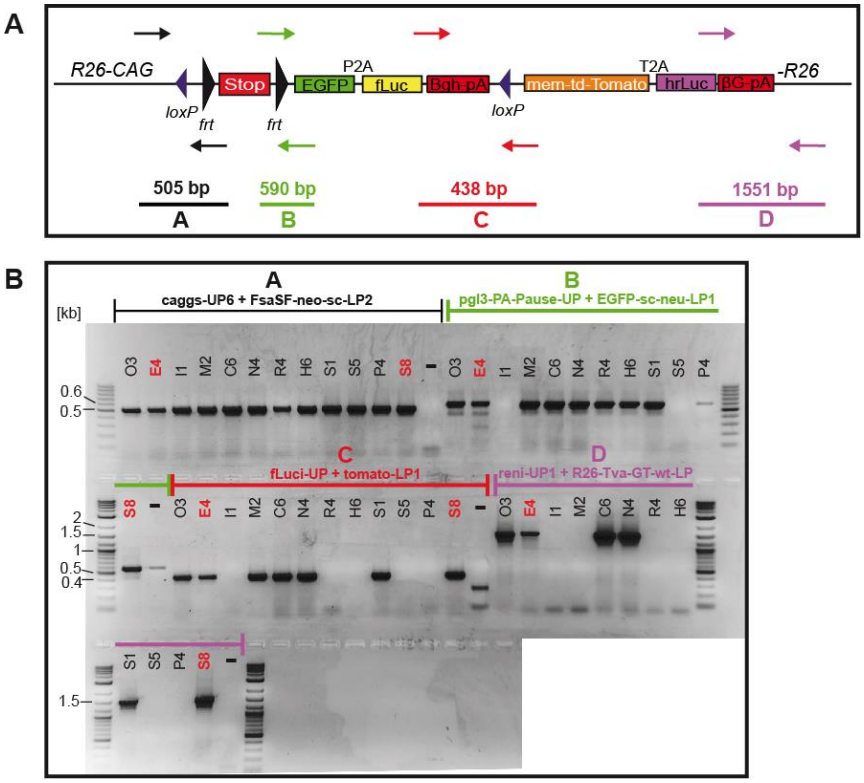

Figure 28: Internal screening PCR strategy: (A) Schematic representation of the *R26 Dual Reporter* knock in allele and all internal screening primer binding sites. Lengths of respective PCR products are depicted for each PCR (A, B, C and D). (B) Agarose gel of all internal screening PCRs. Clone E4 and S8 are highlighted since both clones were later selected for the generation of the *R26 Dual Reporter* mouse line. "–" represents the negative control which contains equal amount of template genomic DNA from WT 129S6 ES cells.

To complete the characterization of the *R26 Dual Reporter* knock in on the DNA level, the 3´ end of the construct has to be confirmed. The *R26* homologous "long arm" on the 3´ site of the construct is more than 4 kb large and the screening PCR primers have to bind outside of the homologous arm in order to confirm integration into the correct genomic locus (Fig. 29 A). In order to detect this region, a "standard" PCR was performed with 6 positive ES cell clones. 3 clones showed the expected PCR product (Fig. 29 B; left photo). Since one of the clones, E4 did not show any PCR product, a "touch-down" PCR strategy was performed additionally and the PCR was repeated with clone E4 using different template amounts and clone O3 as a positive control. This PCR could finally validate the full length integration of the *Dual Reporter* construct also for clone E4 (Fig. 29 B; right photo).

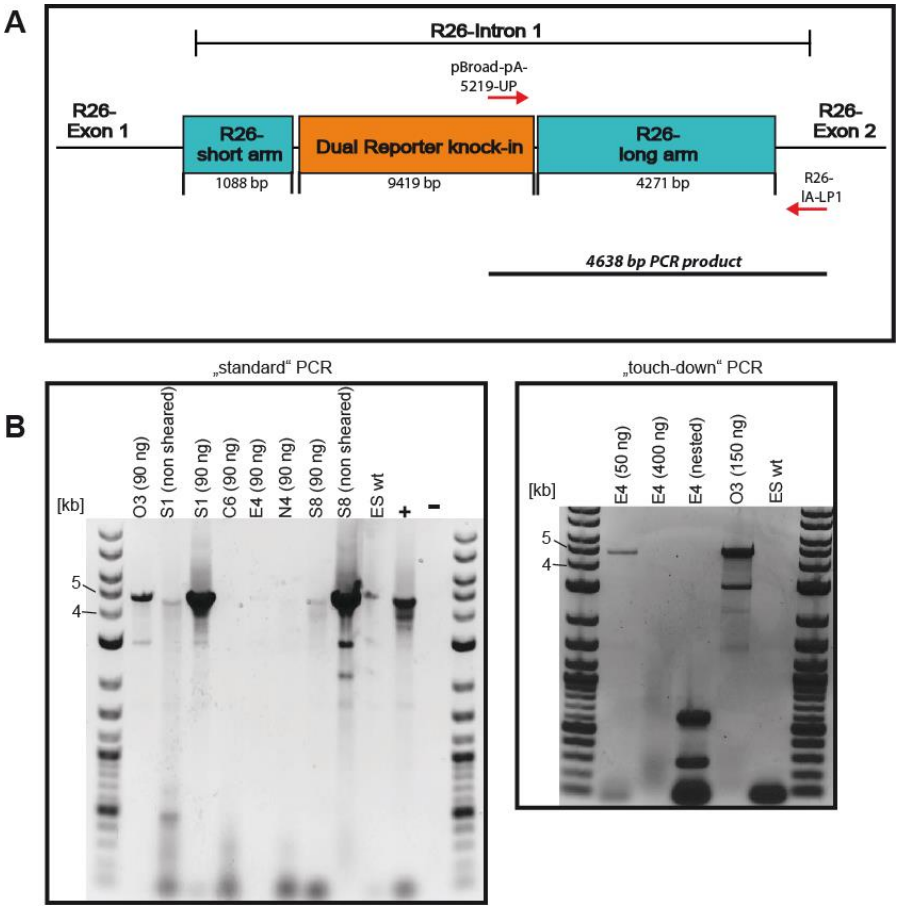

Figure 29: Screening the 3´ end of the *R26 Dual Reporter* knock in - *R26* "long arm" screen: (A) Schematic representation of the *R26 Dual Reporter* knock in and primer binding sites for the detection of the 3´ end of the construct are shown. Length of the PCR product is depicted. (B) Agarose gels of the 3´ end screening PCR ("standard" PCR left photo and "touch-down" PCR right photo"). Amount of template DNA used is depicted. "non sheared" means template genomic DNA from respective ES cell clone has not been sheared before use. In all other cases, template genomic DNA from the ES cell clones has been sheared. "ES wt" represents genomic DNA from WT 129S6 ES cells (= negative control). "+" is genomic DNA from a mouse carrying a *R26* knock in (= positive control). "–" depicts negative control without template DNA.

Summing up the data, homolougous recombination and targeting of the *R26* locus with the *R26 Dual Reporter* cassette could be verified on the DNA level (Fig. 30). Out of the initial 12 positive ES cell clones showing recombination of the *R26* "short arm", 5 clones showed positive PCR results for both external (*R26* "short arm" and *R26* "long arm") and the internal screening PCRs (Fig. 30 A). All other ES cell clones lost specific parts of the construct (Fig. 30 B).

A

ES cell clone #	growth behavior	5´ external PCR screen "R26-short arm"	5´ external PCR screen "R26-short arm" *nested*	internal PCR screen A (*CAG*-promoter, first loxP and frt sites and *neo*^{R} casette)	internal PCR screen B (stop casette, second frt site and *EGFP*)	internal PCR screen C (*fLuc*, BGH-pA, second loxP site and *mem-td-Tomato*)	internal PCR screen D (*hrLuc* and βG-pA)	3´ external PCR screen "R26-long arm"
H6	"++"	"++"	"+++"	"+++"	"++"	"-"	"-"	n.a.
O3	"++"	"+"	"+++"	"++"	"++"	"++"	"+++"	"+"
S1	"++"	"+"	"+++"	"+++"	"++"	"+++"	"++"	"+++"
S5	"++"	"+"	"+++"	"+++"	"-"	"-"	"-"	n.a.
C6	"+++"	"-"	"+"	"+++"	"++"	"+++"	"+++"	"-"
E4	"+++"	"-"	"+++"	"++"	"++"	"++"	"++"	"+"
I1	"+"	"-"	"+++"	"+++"	"-"	"-"	"-"	n.a.
M2	"++"	"-"	"+++"	"+++"	"+++"	"+++"	"-"	n.a.
N4	"++"	"-"	"+++"	"+++"	"+++"	"+++"	"+++"	"+/-"
P4	"+"	"-"	"+++"	"+++"	"+/-"	"-"	"-"	n.a.
R4	"+"	"-"	"++"	"++"	"+++"	"-"	"-"	n.a.
S8	"++"	"-"	"++"	"+++"	"++"	"+++"	"+++"	"+++"

B

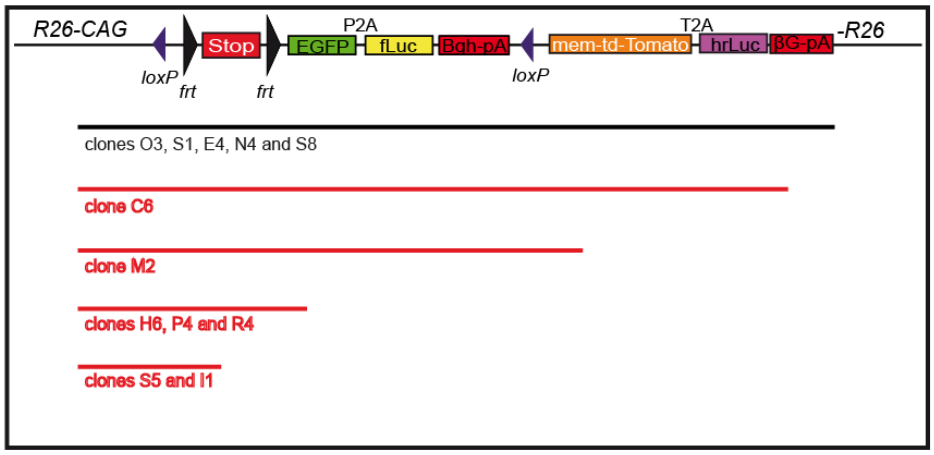

Figure 30: Summary of genotyping PCRs of recombined ES cell clones: (A) Table shows the summary of all genotyping PCRs for the external (*R26* "short arm" and "long arm") and the internal PCRs for the 12 initially positive ES cell clones. In addition, the *in vitro* growth behavior of all clones is depicted. The 5 clones which are positive in all genotyping PCRs are marked in green and yellow, respectively. The 2 clones E4 and S8 marked in yellow were later chosen for the generation of the *R26 Dual Reporter* knock in mouse line. All depicted data are ranked from "-" to "+++". "-" represents slow growth behavior of the respective clone or no visible PCR product on the agarose gel, respectively. "+++" depicts fast growth behavior of the respective clone or a prominent PCR product, respectively. (B) Schematic representation of the recombined ES cell clones. Shown are the different integration lengths of the 12 initially positive ES cell clones according to the results of the genotyping PCR characterization. The black line represents the full length integration whereas the red lines show only partial integration due to interruption of the homologous recombination event.

3.3.3. Functional characterization of positive ES cell clones on the protein level

3.3.3.1. Validation of the fluorescence reporter gene expression

Another important step on the way to the generation of the *R26 Dual Reporter* knock in mouse line is the validation of the functionality of the construct within the ES cells. Since the construct is no longer transiently expressed as a plasmid (in case of the MIA PaCa-2 cell transfection experiments), it is crucial to check for the correct expression within the genomic context of the murine *Rosa26* locus. At first the positive ES cell clones were checked for EGFP and mem-td-Tomato expression, respectively. As expected, no fluorescence could be

detected (Fig. 31 A). In order to delete the FSF cassette and allow for the expression of the first reporter cassette, another electroporation was performed using the already gene targeted, positive ES cell clones. This second electroporation leads to a transient expression of a mammalian Flp expression plasmid. Approx. three days after electroporation, the EGFP, but not a mem-td-Tomato signal could be detected (Fig. 31 B). One week after electroporation, several ES cell colonies with the strongest EGFP expression were picked and cultured (Fig. 31 C). In order to check for the second reporter cassette expression, the established and well-known Adeno-Cre virus approach was used (Anton and Graham, 1995). In this experiment, an adenovirus which is expressing Cre recombinase infects the unrecombined *R26 Dual Reporter* ES cells. After successful infection, the Cre recombinase is expressed and the floxed first reporter cassette will be deleted together with the FSF cassette. Subsequentely, the second reporter cassette is expressed under the control of the *CAG* promoter. Two days after virus infection, a strong mem-td-Tomato expression could be detected (Fig. 31 D).

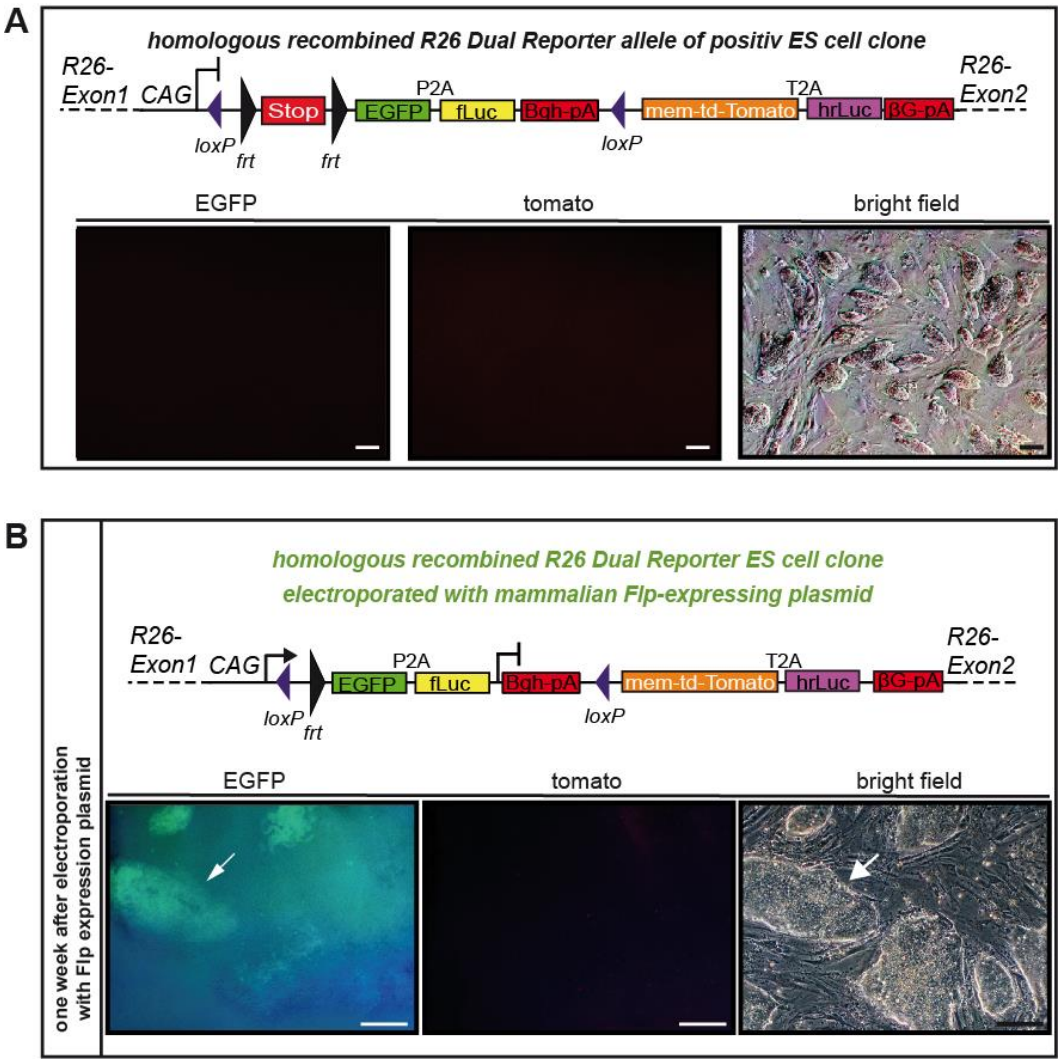

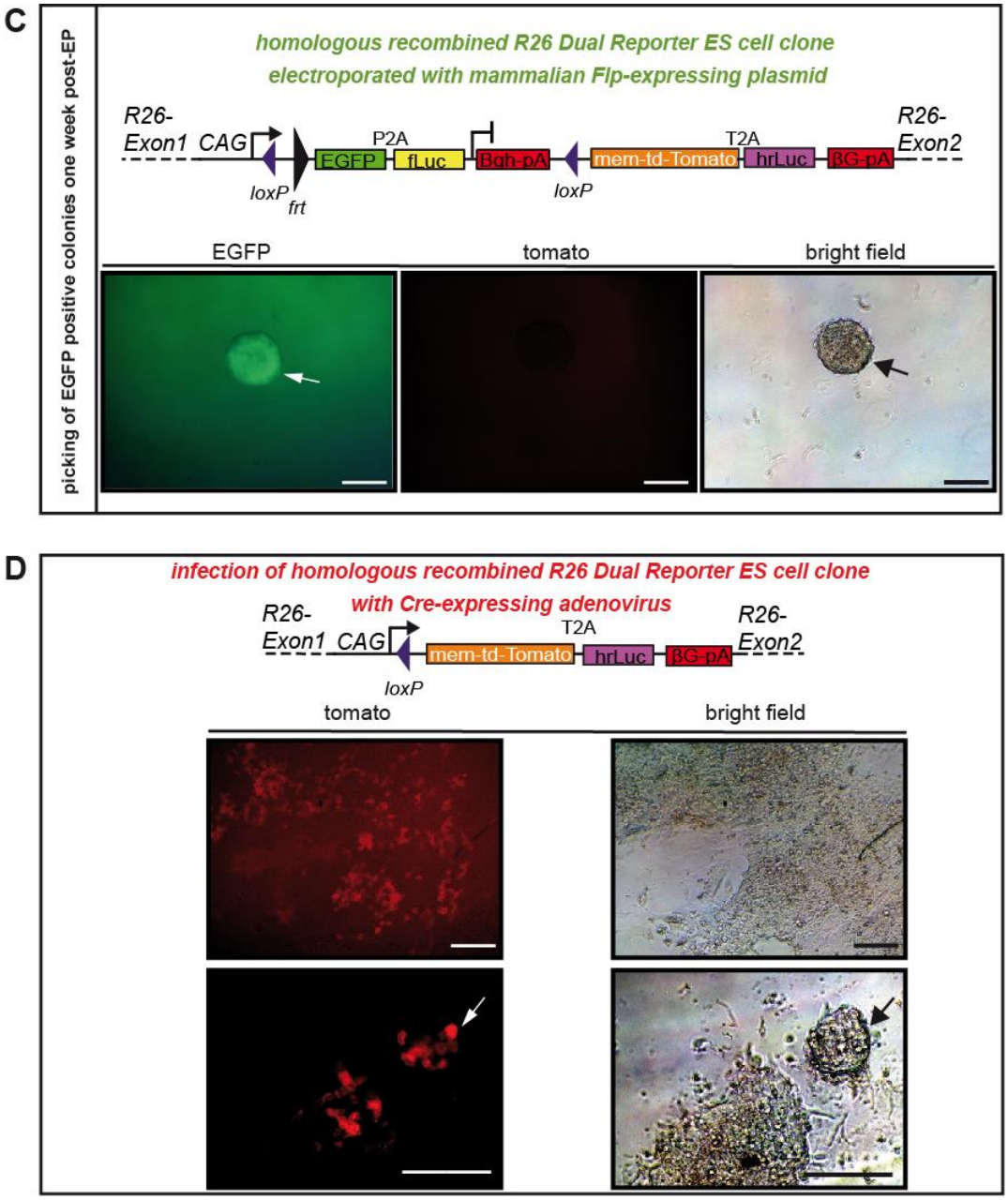

Figure 31: Functional characterization of positive homologous recombined *R26 Dual Reporter* ES cell clones: (A) Positive *R26 Dual Reporter* ES cell clones do not show EGFP or mem-td-Tomato expression, respectively. (B) After ectroporation of *R26 Dual Reporter* ES cell clones with a mammalian Flp expression vector, EGFP expression but no mem-td-Tomato expression could be detected within the ES cell colonies. Arrow shows a prominent ES cell colony with strong EGFP expression. Images were taken approx. one week after electroporation. (C) One week after electroporation, ES cell colonies were picked and further cultured. These cells show strong EGFP expression, but no mem-td-Tomato expression. Arrow shows a picked, EGFP positive ES cell colony. (D) Positive unrecombined *R26 Dual Reporter* ES cell clones were infected with a Cre recombinase expressing adenovirus. Two days after the virus infection, a strong mem-td-Tomato expression could be detected within the ES cells. Arrow shows an ES cell colony with several ES cells demonstrating a strong mem-td-Tomato expression. Scale bars equal 100 µm. All electroporation and adenovirus infection experiments have been performed in triplicates (n=3). Representative photos are shown.

In addition, the molecular switch from expression of the first to the second reporter cassette within the positive ES cell clones was proofed. ES cell colonies which showed a strong

EGFP expression upon electroporation with the Flp expression plasmid were chosen. After picking and further cultivation, the colonies were infected with Cre-expressing adenovirus. Two days after virus infection, some ES cells on the surface of the colony have switched from EGFP to mem-td-Tomato expression upon Cre mediated recombination while the large part of the colony remained EGFP positive (Fig. 32).

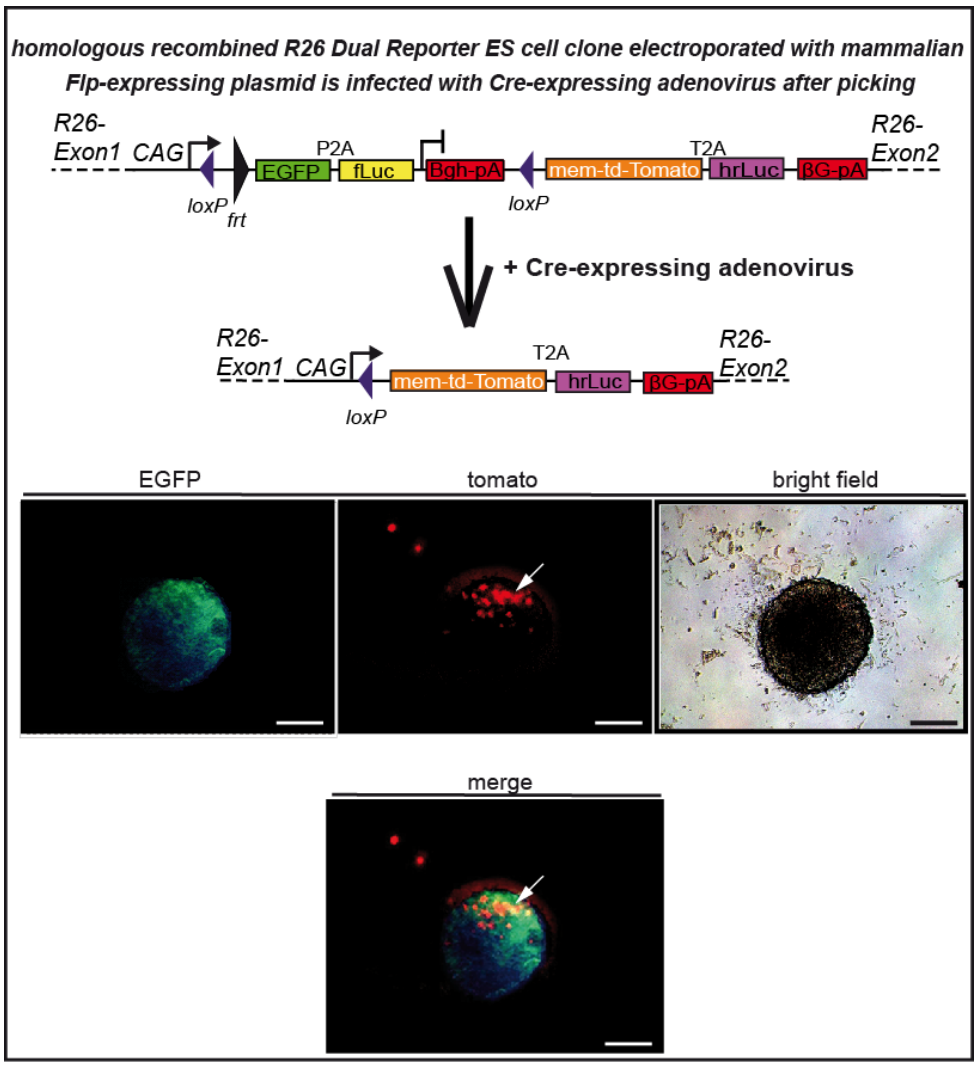

Figure 32: Functional characterization of positive homologous recombined *R26 Dual Reporter* ES cell clones – molecular switch from expression of the first to the second reporter cassette: Schematic representation of the *R26 Dual Reporter* construct is shown after Flp mediated recombination. Upon treatment with Cre-expressing adenovirus, reporter cassette expression is switched from EGFP to mem-td-Tomato expression. Photos show a single EGFP positive *R26 Dual Reporter* ES cell colony after picking (electroporated with a mammalian Flp expression plasmid) and infection with Cre-expressing adenovirus. The large part of this colony is still expressing EGFP. Some cells at the top of the colony have switched to mem-td-Tomato expression due to Cre recombination. Arrow shows some ES cells on the surface of the colony which have switched to mem-td-Tomato expression. Photos were taken two days after adenovirus infection. Scale bars equal 100 µm. All electroporation and adenovirus infection experiments have been performed in triplicates (n=3). Representative photos are shown.

3.3.3.2. Validation of the luciferase reporter gene expression

For the final characterization step before generating the new *R26 Dual Reporter* mouse model, the luciferase reporter gene expression levels normalized to the protein concentration of the positive *R26 Dual Reporter* ES cell clones were validated. Compared to the ES cell clones without Flp expression, the firefly luciferase (fLuc) expression is significantly increased within the Flp recombined ES cell clones. In contrast, renilla luciferase (hrLuc) expression in both ES cell clone populations shows no significant difference (Fig. 33 A). In the ES cell population infected with Cre expressing adenovirus, renilla luciferase expression is significantly increased, whereas firefly luciferase expression levels are not significantly changed (Fig. 33 B). Finally, the ES cell population which was transfected with Flp expression plasmid and infected with Cre expressing adenovirus shows a significant increased expression of both firefly and renilla luciferase compared to the ES cells without additional Flp and Cre expression (Fig. 33 C).

Summarizing the data, the *R26 Dual Reporter* construct has been successfully knocked into the *Rosa26* locus of the murine ES cells. Furthermore, the integrity as well as the functionality of the knock in could be demonstrated by full characterization of the *Dual Reporter* construct on the DNA as well as on the protein level in the gene targeted ES cells. Expression of all reporter genes involved could be proofed. In addition, functionality of the Flp and Cre mediated recombination correlated with the molecular switch from expression of the first to the second reporter cassette could be demonstrated. In the following steps the new *R26 Dual Reporter* knock in mouse line was generated.

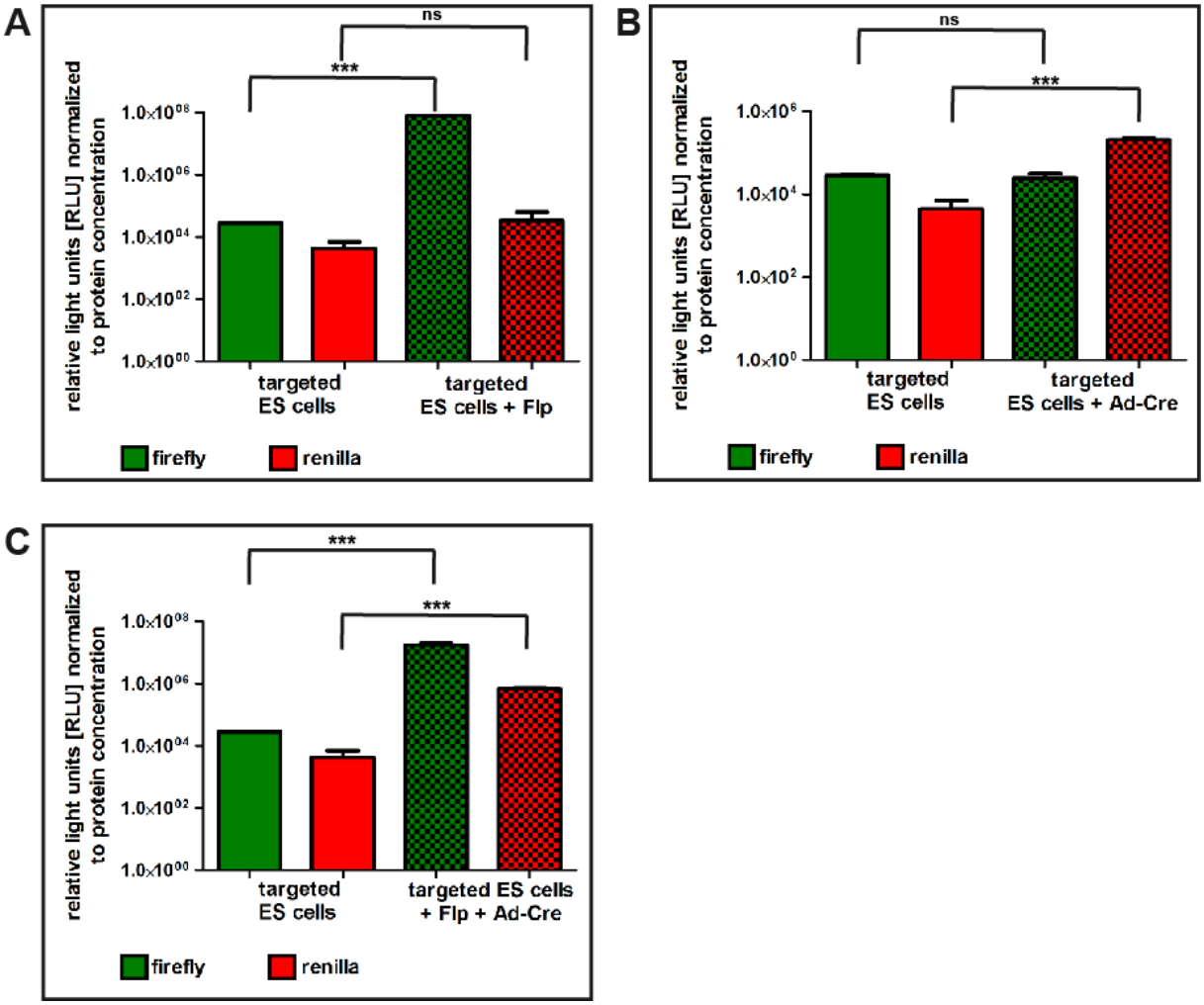

Figure 33: Luciferase reporter gene expression in gene targeted *R26 Dual Reporter* ES cells. (A) *R26 Dual Reporter* targeted ES cells transfected with Flp expression plasmid show significant increase in firefly luciferase expression compared to the *R26 Dual Reporter* targeted ES cells without additional Flp expression. Renilla luciferase expression shows no significant difference. (B) *R26 Dual Reporter* targeted ES cells infected with Cre expressing adenovirus show significant increase in renilla luciferase expression compared to the *R26 Dual Reporter* targeted ES cells without additional Cre expression. Firefly luciferase expression shows no significant difference in both ES cell pools. (C) *R26 Dual Reporter* targeted ES cells transfected with Flp expression plasmid and additionally infected with Cre expressing adenovirus afterwards show significant increase in both firefly and renilla luciferase expression compared to the *R26 Dual Reporter* targeted ES cells without additional Flp and Cre expression. Depicted is the mean of the relative light units (RLU) + SEM. RLU have been normalized to the respective protein concentration of each ES cell sample measured (determined by Bradford assay) to allow an exact quantification and comparison of the luciferase expression levels. All experiments were performed in triplicates (n=3) and statistical significance according to two-sided unpaired students t-test is depicted. *** $p<0.0001$. n.s. $p>0.05$.

3.4. Generation of chimeric *R26 Dual Reporter* mice

3.4.1 Establishing the *R26 Dual Reporter* mouse line

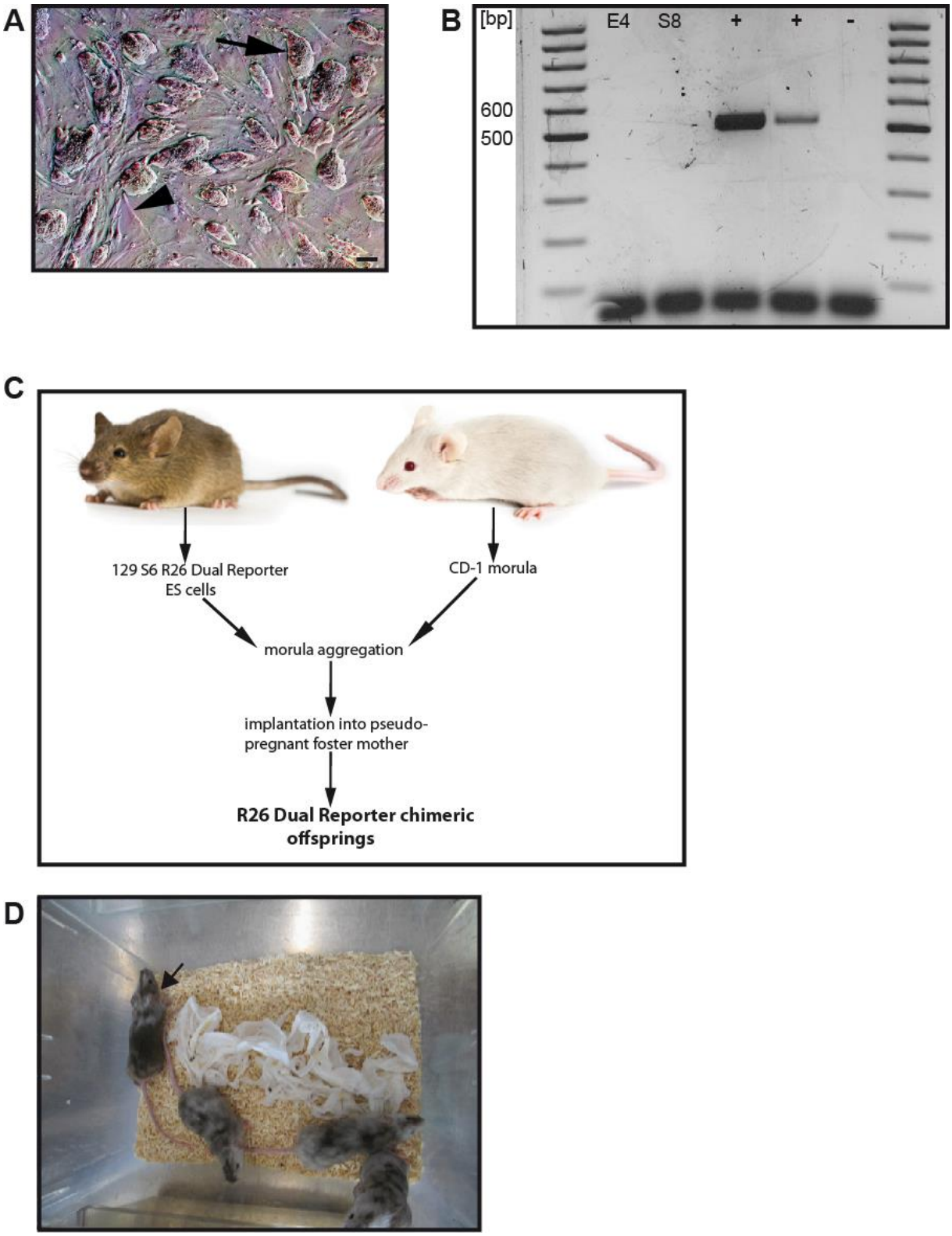

Figure 34: Generation of the *R26 Dual Reporter* mouse line – chimera production. (A) Microscopic photo of ES cell clone S8 which gave rise to the *R26 Dual Reporter* mouse line. ES cell colonies (arrow) can be seen on

top of the MEF layer (arrowhead). Scale bar equals 100 µm. (B) Agarose gel showing the results of the mycoplasma detection PCR. ES cell clones E4 and S8 are mycoplasma-free since they don`t show a positive band. (+) depicts positive controls. (-) represents negative control (water instead of cell culture supernatant). Positive band is 510 bp. (C) Schematic representation of the production of chimeric *R26 Dual Reporter* mice by morula aggregation. Photo of mouse with albino fur derived from B6SJL-Tg(SOD1*G93A)1Gur/J mouse strain; stock number: 002726 (Jackson Laboratories). Photo of mouse with brown fur derived from 129S1/SvImJ mouse strain; stock number: 002448 (Jackson Laboratories). Images © The Jackson Laboratory 2014 used with permission. (D) Foto of the four chimeric mice produced by morula aggregation of clone S8. Arrow shows chimeric mouse with highest (>90%) chimerism.

For the generation of the *R26 Dual Reporter* mouse line, clones S8 and E4 were chosen since both showed a robust phenotype and growth behavior *in vitro* besides being positive for all characterization steps on the DNA and expression level (Fig. 34 A and not shown). Before using the clones for the chimera production, a potential mycoplasma infection of the cells must be excluded by PCR analysis. Here it could be demonstrated that both clones are mycoplasma-free and therefore suitable for the generation of the chimeras (Fig. 34 B). Both clones were sent to the Institute of Stem Cell Research of the Helmholtz Center in Neuherberg for the generation of chimeras via morula aggregation.

Briefly, the targeted ES cell clones which are derived from a 129S6 genetic background (brown coat color) are fused with the morula of a CD-1 genetic background (albino coat color) and implanted into the uterus of a pseudo-pregnant foster mother. This mouse gives birth to the chimeric offsprings derived from a mixture of the targeted *R26 Dual Reporter* ES cells and the WT morula cells as seen by the brown and white spotted coat color (Fig. 34 C). After successful morula aggregation of clone S8, four chimeric mice with high (> 90%) chimerism were born (Fig. 34 D).

3.4.2 Characterization of the *R26 Dual Reporter* mice

After breeding the four chimeras with WT mice on a C57Bl6/J genetic background, the successful germline transmission of the *R26 Dual Reporter* construct was investigated by tail tip genotyping of the offsprings. This crucial step is necessary in order to be sure that the targeted ES cells rather than the WT morula cells have colonized the germline of the chimeras. Therefore, the *R26 Dual Reporter* allele of the chimera offsprings was characterized on the DNA level to demonstrate the successful establishment of this new mouse line. In the first step, the four internal genotyping PCRs previously applied in the characterization of the targeted ES cell clones were performed. 6 out of the 12 offsprings showed positive results for all four internal screens, demonstrating germline transmission of the *R26 Dual Reporter* allele (Fig. 35 A). In the next step, an internal-external genotyping PCR strategy was developed which allows not only the detection of the *R26 Dual Reporter* knock in but in addition the discrimination between the *Rosa26* WT and *R26 Dual Reporter* targeted mutated allele.

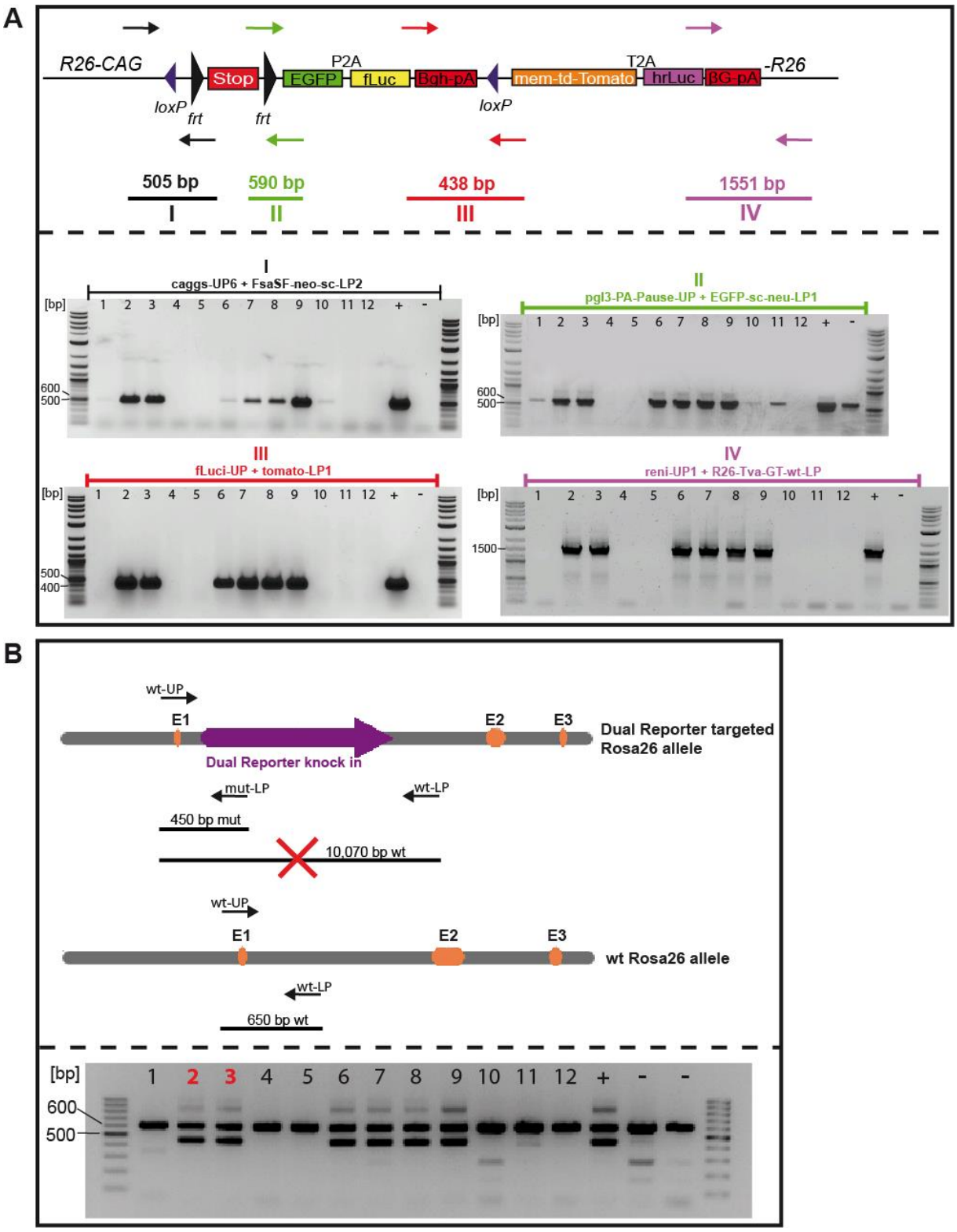
A
R26-CAG
Stop
EGFP
P2A
fLuc
Bgh-pA
loxP
frt
frt
loxP
mem-td-Tomato
T2A
hrLuc
BG-pA
-R26
505 bp
590 bp
438 bp
1551 bp
I
II
III
IV
I
caggs-UP6 + FsaSF-neo-sc-LP2
II
pgl3-PA-Pause-UP + EGFP-sc-neu-LP1
III
fLuci-UP + tomato-LP1
IV
reni-UP1 + R26-Tva-GT-wt-LP
[bp]
1 2 3 4 5 6 7 8 9 10 11 12 + -
600
500
400
1500
B
wt-UP
E1
E2
E3
Dual Reporter knock in
Dual Reporter targeted Rosa26 allele
mut-LP
wt-LP
450 bp mut
10,070 bp wt
wt-UP
E1
E2
E3
wt Rosa26 allele
wt-LP
650 bp wt
[bp]
1 2 3 4 5 6 7 8 9 10 11 12 + - -
600
500

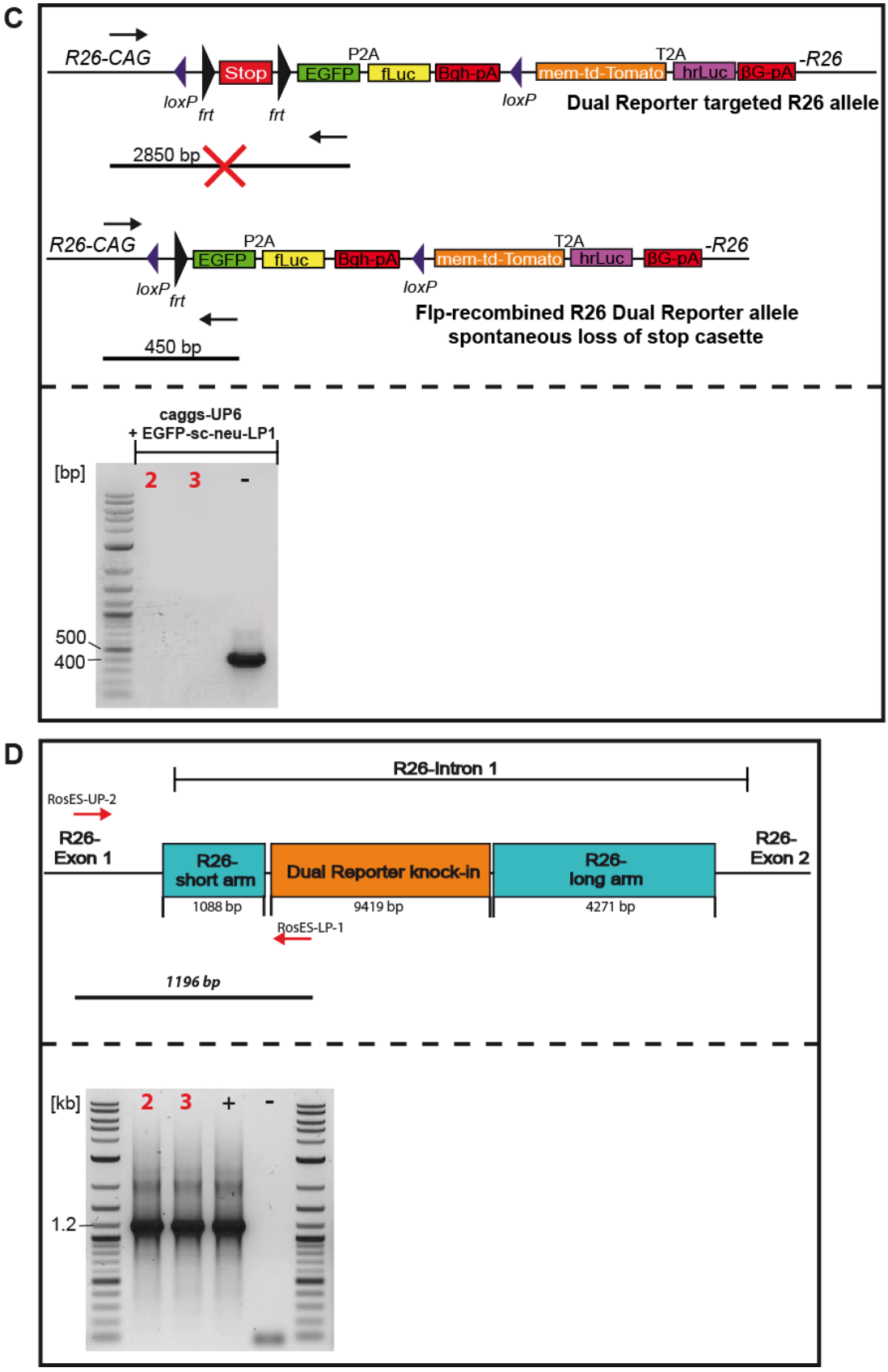

Figure 35: Characterization of the *R26 Dual Reporter* mouse line: (A) Internal genotyping PCR strategy. Schematic representation of the four different internal PCRs. Primer binding sites and PCR product lengths are depicted. Agarose gel showing the results of all PCRs. (B) External-internal genotyping PCR for the *R26 Dual*

Reporter allele. Schematic representation of the genotyping PCR is shown. Primer binding sites for both primers detecting the WT allele as well as for the primer detecting the mutated knock in allele with respective PCR product sizes are depicted. Agarose gel shows results of the genotyping PCR. E = exon. (C) Presence of the FSF stop cassette. Schematic representation of the genotyping PCR to detect a potential loss of the FSF stop cassette. Primer binding sites and PCR product length are depicted. Agarose gel showing the results of the PCR. (D) PCR screening for the *Rosa26* homologous "short" arm. Primer binding sites and PCR product length are shown. Agarose gel showing PCR results. Samples 1-12 represent offsprings of the *R26 Dual Reporter* chimeras. "+" depicts *R26 Dual Reporter* positive ES cell genomic DNA as PCR template (positive control). "–" represents WT ES cell genomic DNA as PCR template (negative control).

In line with the results of the internal genotyping PCRs, 6 out of the 12 offsprings were heterozygous for the *R26 Dual Reporter* allele and showed the *Rosa26* WT as well as the mutated band. All other offsprings lacked the mutated band since they had two *Rosa26* WT alleles (Fig. 35 B).

Another crucial point is the presence of the FSF stop cassette within the *R26 Dual Reporter* allele. In order to validate correct function of the *R26 Dual Reporter* allele, we tested for deletion of the FSF cassette (Fig. 35 C). PCR results for the heterozygous *R26 Dual Reporter* offsprings 2 and 3 showed no band that indicates deletion of the FSF cassette. As a positive control, a FSF deleted *R26 Dual Reporter* plasmid was used (Fig. 35 C).

In the final step the correct integration of the *R26 Dual Reporter* knock in at the *Rosa26* locus was confirmed by screening for the *Rosa26* "short" homologous arm. Again, this PCR verified the integration of the *R26 Dual Reporter* cassette into the genomic *Rosa26* locus (Fig. 35 D).

Summarizing the data, germline transmission of the *R26 Dual Reporter* allele and consequently successful generation of the *R26 Dual Reporter* mouse line could be confirmed.

D. Discussion

1. The *LSL-Pcna*$^{ATG\text{-}fLuc/+}$ mouse model

1.1 Non-invasive real time imaging of PDAC proliferation *in vivo*

Bioluminescence imaging represents a very useful tool in basic cancer research since it helps to overcome the limited insight given by the traditional use of end point analyses. Employing luciferases as light producing enzymes has opened new gates and enables a closer look at the complex and dynamic nature of tumor initiation, progression and most important, therapeutic response (Contag et al., 1995; Contag et al., 2000, Contag et al., 2006; Dothager et al., 2009, Kocher and Piwnica-Worms et al., 2013). There have been numerous studies applying luciferase transfected tumor cell lines expressing the reporter gene under the control of a constitutively active promoter. After tail vein injection, subcutaneous or orthotopic transplantation of these cell lines into recipient mice, it is possible to monitor the growth of the tumor *in vivo* in real time (Edinger et al., 1999; Jenkins et al., 2003; Jenkins et al., 2005; Miretti et al., 2008; Kim et al., 2010). As a crucial drawback of mouse allograft as well as of human xenograft preclinical cancer models, it is not possible to reflect the human nature of cancer initiation and progression since there is no sporadic transformation of normal cells occurring. In addition to the lack of mimicking all steps of tumorigenesis, the microenvironment and especially the role of the immune system is completely excluded when using immune suppressed recipient mice (Johnson et al., 2001; Voskoglou-Nomikos et al., 2003; Sausville et al., 2006).

To overcome all of these crucial modeling problems, the use of genetically defined reporter mouse models has become indispensable (Becher and Holland, 2006; Olive and Tuveson, 2006; Sharpless and Depinho, 2006; Heyer et al., 2010; Cheon and Orsulic, 2011). There have several studies been done applying transgenic reporter mouse models to image tumor development *in vivo* (Vooijs et al., 2002; Lyons et al., 2003; Safran et al., 2003; Uhrbom et al., 2004; Woolfenden et al., 2009; Buschow et al., 2010). In one of those models the fLuc expression is controlled by the *E2F1* promoter which is coupled to the cell cycle regulation, specifically the G1 to S phase transition. Consequently bioluminescence could be correlated with cell proliferation using the *E2F1* promoter activity as a proliferation marker (Uhrbom et al., 2004). Since this mouse model is lacking a conditional regulation of the luciferase expression, the background signal is high.

In our lab a new conditional Cre-loxP based reporter mouse model for tissue-specific bioluminescence imaging of cell proliferation has been established. In this mouse model, the fLuc expression is controlled by the endogenous *Pcna* promoter as a proliferation marker and silenced by an LSL stop cassette. After crossing this model into the standard, conditional Cre-loxP based pancreatic tumor mouse model (Cre is expressed under the control of the *Ptf1a* or *Pdx1* promoter, respectively), the luciferase expression is restricted to proliferating cells within the developing pancreatic cancer. Beside non-invasive real time monitoring of

tumor development, it is now possible to longitudinal image the effect of a therapeutic intervention on the proliferation state within the pancreatic cancer. Visualization of the cancer cell proliferation seems to be of great importance, since inhibition of proliferation is the first step in order to stop tumor development, progression and metastasis formation.

In the present thesis it could be demonstrated that the *LSL-Pcna*$^{ATG\text{-}fLuc/+}$ mouse model is a powerful tool to monitor pancreatic tumor cell proliferation in real time *in vivo* as well as *ex vivo*. The luciferase signal intensity of the *LSL-Pcna*$^{ATG\text{-}fLuc/+}$ mouse model correlates well with the volume of the pancreatic cancer *in vivo* using a subcutaneous transplantation model (Baumann, 2011). The present study demonstrates a direct correlation between the luciferase signal intensity measured *in vivo* and the number of BrdU positive proliferating cells measured by further *ex vivo* immunohistochemical analysis. This shows as a proof of principle the reliability of the *LSL-Pcna*$^{ATG\text{-}fLuc/+}$ mouse model in terms of specifically visualizing proliferating cells within a tumor *in vivo*.

1.2 Establishment of an *in vivo* drug validation platform

A platform for the validation of potent drug candidates *in vivo* is an important requirement for preclinical drug development and target validation. Especially in the context of PDAC, this step is crucial for investigating the *in vivo* efficacy of a chemotherapy of this poorly vascularized and perfused cancer type. The desmoplastic stromal compartment present in human as well as murine pancreatic cancer acts like a barrier. This prevents the ability of therapeutic agents to reach the cancer cells within the pancreatic epithelium (therapeutic resistance due to tumor-stroma interaction; see Olive et al., 2009). Consequently the *in vivo* validation of *in vitro* data concerning the response of pancreatic cancer cells towards different drugs or drug combination is a crucial evaluation step.

Molecular profiling showed impressively that human cancers are extremely heterogenous (Paez et al., 2004; Sotiriou and Piccart, 2007). Patients suffering from the same kind of cancer might show completely different genetic as well as phenotypic signatures and consequently different therapeutic responses (Brindle et al., 2008). In order to achieve an individualized cancer therapy, it is of great importance to use imaging systems for preclinical testing the response and efficiency of novel anti-cancer drugs *in vivo* in a fast and easy manner.

There have been numerous studies using transplantation models coupled to BLI in order to monitor the growth and regression dynamics of specific types of established cancers upon targeted therapy. Sweeney et al. describe a xenograft model where labeled human HeLa cells are engrafted into immunodeficient mice and tumor response towards a number of different chemotherapeutics like cisplatin, 5′-fluorouracil, cyclophosphamide as well as immunotherapeutics was evaluated (Sweeney et al., 1999). In another study luciferase expressing A549 cancer cells were injected into the mediastinum of athymic nude mice to establish a model of advanced human lung cancer. Paclitaxel chemotherapy or irradiation were used to analyze the effects of therapeutic intervention by BLI (Li et al., 2011). A further

interesting study focused on squamous cell carcinoma. UMSCC1 tumor cells were transfected with a multidomain chimeric reporter and xenografted. The reporter represents the phosphorylated substrate of EGFR which reconstitutes a luciferase activity in the unphosphorylated state. This enabled quantitative and dynamic monitoring of EGFR activation. This model can be used for the evaluation of drug availability and cancer cell targeting (Khan et al., 2011). In a recent study, colorectal cancer growth and metastasis were imaged by applying a novel bicistronic IRES construct expressing fLuc and MACC1 (gene involved in metastasis formation, motility and proliferation). This construct was transfected into colorectal cancer cells with low endogenous MACC1 expression levels. The cells were xenotransplanted intrasplenically in order to monitor tumor growth and proliferation which could be inhibited by applying *MACC1* specific shRNA (Pichorner et al., 2012). Bornmann et al. used an orthotopic model of pancreatic cancer by implanting luciferase transfected MIA PaCa-2 cells into nude mice and imaged the response of established PDAC towards a novel lipid formulation of the well-known standard pancreatic cancer drug gemcitabine (Bornmann et al., 2008).

All of these transplantation models as well as *in vitro* based systems are not able to recapitulate human cancer. Consequently, genetically engineered tumor mouse models connected with BLI have been studied in terms of therapeutic intervention (Becher and Holland, 2006). One work was focusing on the early detection of tumor formation in an endogenous mouse model of retinoblastoma-dependent sporadic cancers (Vooijs et al., 2002). In another study numerous treatment regimens were investigated in a RAS-driven, Ink4a/Arf deficient melanoma GEMM as well as in different subtypes of breast cancer GEMM (Roberts et al., 2012). As a chemotherapeutic intervention strategy the authors were using a combination therapy of a MEK inhibitor and the dual PI3K and mTOR inhibitor NVP-BEZ-235, since the tumors were refractory to the standard single agent chemotherapies. In contrast to the latter, applying the combined treatment regimen which is blocking two crucial signaling pathways responsible for proliferation and survival, yields significant tumor regression and enhanced survival in a broad spectrum of malignancies.

Within the present thesis the dual PI3K and mTOR inhibitor NVP-BEZ-235 was used as an example to evaluate novel anti-cancer drugs. This drug was reported to be an efficient inhibitor of the PI3K/AKT/mTOR signaling pathway with good tolerance and little cross-reactivity towards other kinases (Maira et al., 2008). As an imidazo[4,5-c]quinoline derivative, NVP-BEZ-235 binds to the ATP binding cleft of PI3K and mTOR, thereby competitively inhibiting the kinase activity of both enzymes and consequently inducing G1 cell cycle arrest. This drug has successfully been tested in different cellular settings as well as in *in vivo* models of human cancers (Schnell et. al, 2008; Serra et al., 2008; Eichhorn et al., 2008; Engelman et al., 2008; Brachmann et al., 2009; Konstantinidou et al., 2009; Liu et al., 2009; Chiarini et al., 2010). The great benefit of dual PI3K and mTOR inhibitors lies in the effective blocking of AKT activation, since they prevent the feedback activation of PI3K signaling usually found when using mTORC1 specific inhibitors like rapamycin (Mukherjee et al., 2012). NVP-BEZ235 has already been investigated in phase 1/2 clinical trials for therapeutic

intervention in a broad spectrum of different advanced solid tumors (reviewed in Garcia-Echeverria and Sellers, 2008).

Treatment of *LSL-Pcna*$^{ATG\text{-}fLuc/+}$ pancreatic cancer mice with the dual PI3K-mTOR inhibitor NVP-BEZ235 showed a significant decrease in tumor cell proliferation *in vivo* followed by a full restoration of proliferation after metabolic degradation of the drug. This shows that PI3K-mTOR inhibition blocks cell proliferation, but does not induce apoptosis or cell death.

In conclusion it could be demonstrated that the *LSL-Pcna*$^{ATG\text{-}fLuc/+}$ tumor mouse model can be utilized as an easy to use and fast drug validation platform. Besides non-invasive real time monitoring of tumor development and progression over an optional time scale, it is possible to image the drug action on proliferation of the cancer cells in real time *in vivo*. Furthermore the perfusion and diffusion of the drug into the cancer cells can be investigated *in vivo*, which is a crucial aspect regarding cancer types showing a strong fibrotic reaction and thus potential impaired drug delivery (Olive et al., 2009). Another interesting aspect is the possibility to distinguish between a cytostatic and a cytotoxic effect of a treatment regimen. If the drug application leads to growth arrest of the cancer cells, the luciferase signal will reappear after degradation of the drug since proliferation inhibition is abrogated. Consequently the biological half-life of drugs can be easily calculated. In case of a cytotoxic drug effect, the proliferating cancer cell mass and consequently the luciferase signal of the tumor would decrease and remain at a lower level even if the drug is already degraded.

In future steps, larger cohorts of mice as well as different drugs and drug combinations which were previously chosen in *in vitro* drug screening assays (see Baumann, 2011) can be rapidly validated using this *in vivo* drug validation platform. Investigating therapeutic response over a longer time scale will additionally help to elucidate the long-time efficiency as well as potential adverse effects of a specific treatment regimen.

2. The *R26 Dual Reporter* mouse generation

The dual recombination system enables spatio-temporal control of gene expression during pancreatic cancer formation as well as progression. To monitor Flp and Cre mediated recombination events in this system, there is an urgent need for a dual reporter mouse line, which enables visualization of recombination events *in vitro* and *in vivo*. To generate such a model, we constructed a gene targeting construct, which consits of a Flp activatable EGFP-firefly luciferase gene expression cassette and a Cre activatable td-Tomato-renilla luciferase cassette.

2.1. Cloning of the gene targeting construct

Due to the complexity of the *Dual Reporter* construct, it was divided into four different modules. The big advantage of dividing the cloning procedure into different modules is the possibility of validating functionality of the different modules. In order to achieve this, expression vectors were chosen which contained a strong promoter to drive expression of the insert *in vitro* in a mammalian cell line.

2.2 Genetic elements used for the *R26 Dual Reporter* construct assembly

For the knock in of the *R26 Dual Reporter* construct the ubiquitously and constitutively expressed *Rosa26* locus was chosen, since the chromatin structure of this locus is known to be easily accessible for gene targeting experiments. In addition, the *Rosa26* gene product is an untranslated RNA and knock in of gene expression cassettes into intron 1 of *R26* has no phenotype (Soriano, 1999; Hohenstein et al., 2008). In order to achieve maximum expression levels of all reporter genes, the strong *CAG* promoter was chosen to drive the *Dual Reporter* expression. This synthetic promoter consists of a fusion of the cytomegalovirus immediate early enhancer element (C), the chicken β-actin promoter (A) and the splice acceptor of the rabbit β-globin gene (G). In addition, a highly conserved enhancer element in intron 1 of the chicken β-actin gene is also included (Miyazaki et al., 1989; Niwa et al., 1991; Okabe et al., 1997 and Alexopoulou et al., 2008). The whole construct is silenced by an FRT site flanked stop cassette. Upon Flp mediated recombination the first reporter cassette containing EGFP and fLuc will be expressed. Following Cre mediated recombination, the floxed first reporter cassette (with or without the FSF cassette) will be deleted and the second reporter is expressed under the control of the *CAG* promoter, leading to mem-td-Tomato and hrLuc expression.

The fluorescence reporter genes *EGFP* and *mem-td-Tomato* were selected. EGFP is known to be a bright and photostable reporter protein for many years and has already been expressed *in vivo* under the control of a *CAG* promoter as a knock in at the *Rosa26* locus (Cormack et al., 1996; Thastrup et al., 2001; Zong et al., 2005, Muzumdar et al., 2007). A single copy cytoplasmic EGFP expression was also shown to be sufficient in order to visualize individual cells (Zong et al., 2005). The second fluorescent reporter gene is *membrane-tandem-dimer-Tomato*, a *dsRed* variant (Shaner et al., 2004). This red fluorescence reporter contains an N-terminal tag that allows membrane anchorage (Muzumdar et al., 2007). Its brightness and photostability is higher compared to EGFP*;* td-Tomato shows a 3-fold increased brightness in solution (Shaner et al., 2004). Mem-td-Tomato could already be used in a genetically engineered mouse model *in vivo* (Muzumdar et al., 2007). There is a very small overlapping in the excitation and emission spectrums of both fluorescence proteins reported in the literature. Yet this leads to almost no cross-reacting background emission which enables the use of both reporter proteins within the same mouse model (Shaner et al., 2004; Muzumdar et al., 2007).

For the *in vivo* bioluminescence reporter genes, *fLuc* and *hrLuc* were chosen. Both luciferases can be used together since their substrates as well as their emission wavelengths are different (Bhaumik and Gambhir 2002; Close et al., 2011). In contrast to the fluorescence reporter proteins used in this study which have long half-lifes of around 12-26 hours, the luciferases show very short half-lifes within 2-5 hours only and are thermo-unstable. In addition, the read out of kinetic processes is more robust applying luciferase reporters, since their folding and posttranslational function is much more rapid compared to fluorescence reporters (Thompson 1991; Corish and Tyler-Smith 1999; Gross and Piwnica-Worms, 2005; Zinn et al., 2008; Kocher and Piwnica-Worms 2013).

As already described in the discussion of the *LSL-Pcna*$^{ATG\text{-}fLuc/+}$ mouse model, there have been numerous studies using the fLuc *in vivo* for non-invasive real time monitoring of tumor progression and response to therapeutic intervention (see for additional references also Rehemtulla et al., 2000; Negrin et al., 2002; Hashizume et al., 2009; Buschow et al., 2010; Lee et al., 2010; Mezzanotte et al., 2010). Also rLuc has already been successfully used as a reporter gene for *in vivo* imaging approaches, amongst others in terms of non-invasive imaging of tumor development (e.g. Massoud and Gambhir, 2003; Gross and Piwnica-Worms, 2005; Shah et al., 2005; Venisnik et al., 2006; Deroose et al., 2007).

Since each reporter cassette of the *Dual Reporter* construct consists of a fluorescence and a bioluminescence reporter gene, there exist different options in connecting them. One option is to clone a fusion gene in order to express a fusion protein containing both reporters. Such a strategy has the disadvantage of reduced activities of both proteins due to impaired posttranslational folding or decreased expression levels (Amersham Pharmacia Biotech, 2000).

Another option to achieve a multicistronic expression of several transgenes under the control of a single promoter is the use of *IRES* sequences, which has been the gold standard in GEMM (Jang et al., 1988; Trichas et al., 2008). Several open reading frames derived from a single transcript can be translated into multiple proteins in a 5´cap-independent manner, since the *IRES* sequence separating the different ORFs is directly recognized by the ribosomes triggering translation. Yet there are many known disadvantages reported using *IRES* sequences. The expression of the second cistron usually depends on its position downstream of the *IRES* site; normally it is much lower than that of the first cistron. In addition, the *IRES* site is very large (around 600 bp) and no equivalent expression of all genes separated by *IRES* sites can be achieved (Trichas et al., 2008; Chan et al., 2011).

A further technology of expressing multicistronic constructs represents *2A* sites. Similar to the *IRES* sequence, the *2A* sites have also been found in picornaviruses, yet in different subgroups, amongst others the well-known Foot and Mouth disease virus (Robertson et al, 1985; Donnelly et al., 2001). These sites are around 20 bp long and lead to a co-translational cleavage of two proteins separated by a *2A* site. In detail, these sites prevent the formation of a peptide bond between the glycine and the last proline, leading to ribosomal skipping to the following codon (Donnelly et al., 2001). Consequently upon cleavage of the nascent peptide, the *2A* peptide remains fused to the C-terminus of the upstream protein, whereas the proline remains fused to the N-terminus of the downstream protein. Because of their reaction mode the *2A* peptides are also called cis-acting hydrolase element (CHYSEL) (de Felipe and Ryan, 2004; Trichas et al., 2008).

One group compared the usage of *IRES* and *F2A* sites for multicistronic expression in GEMMs. They found out that using *EGFP* as a reporter gene in a bicistronic construct, the ribosomal skipping can be inefficient and also some fusion proteins are generated (Chan et al., 2011). The advantages of using these *2A* sites instead of *IRES* on the other hand lies in the exact stoichiometric co-expression pattern of reporter genes separated by these sites

(Szymczak et al., 2004; for a review about the advantages of *2A* sites see also de Felipe et al., 2006). Beside the efficient and equimolar expression as well as co-translational cleavage of multiple proteins separated by *2A* sites, it also has already been demonstrated that these peptides can be used in transgenic mice. These sites have no toxic effect in any tissues or at any stage of the murine development (Ryan and Drew, 1994; Trichas et al., 2008). Since *2A* sites are more reliable and superior to *IRES*, the reporter genes in both cassettes of the presented *R26 Dual Reporter* construct were separated by a *P2A* and a *T2A* site, respectively. These *2A* sites are derived from different viral species. This is a crucial consideration point in establishing a transgenic mouse line, because homologous sequences should be avoided in gene targeting constructs, since they are prone to unspecific recombination events during cloning and also gene targeting (Barascu et al, 2013).

2.3 Functional characterization of the *Dual Reporter* construct *in vitro*

Before targeting the *Dual Reporter* construct to the murine *Rosa26* locus, the different reporter cassettes have already been checked during the cloning procedure. In this first characterization approach, the expression of both fluorescence reporter genes could be successfully demonstrated by transfecting MIA PaCa-2 cells with the respective expression vectors. For testing the correct cloning of both *2A* sites, the expression of both luciferases was also tested by subsequent *in vitro* luciferase assays revealing robust luciferase expression. After finishing cloning of the final *R26 Dual Reporter* construct by combining the different modules, another characterization of the whole reporter construct was performed by co-transfection experiments using MIA PaCa-2 cells. In the course of these studies, the functionality of the *CAG* promoter to drive the expression of both reporter cassettes as well as of the upstream FSF cassette in silencing the expression could be demonstrated. In the next step, the correct Cre and Flp mediated recombination was evaluated *in vitro* by using Flp as well as Cre expression plasmids. The results of these experiments nicely demonstrated the correct function of all genetic elements involved. Flp mediated recombination induced EGFP expression without detectable mem-td-Tomato expression, showing no leacky mem-td-Tomato expression and blockade of transcriptional readthrough by the first pA signal. Upon Cre mediated deletion of the floxed first reporter cassette, EGFP expression switched to mem-td-Tomato expression. Comparing the expression levels of both reporter cassettes revealed a much stronger fluorescence intensity of mem-td-Tomato in contrast to EGFP. td-Tomato is known to show a brighter fluorescence signal and the membrane anchorage of the mem-td-Tomato protein promotes an even stronger signal compared to the cytoplasmatic localization of the EGFP (Shaner et al., 2004; Muzumdar et al., 2007).

2.4 ES cell gene targeting – *Rosa26* knock in and screening strategies

After the functional *in vitro* characterization of the *R26 Dual Reporter* construct was completed, the murine embryonic stem cell culture was applied for the gene targeting experiment. The *R26 Dual Reporter* was successfully knocked into the murine *Rosa26* locus

via homologous recombination using the positive-negative selection gene targeting technology (McCarrick III et al., 1993; Donoho et al., 1998). In order to confirm the successful integration of the *R26 Dual Reporter* construct into the *Rosa26* locus, a PCR screening strategy was developed. Out of 138 picked ES cell clones, 16 colonies showed initial positive results for the screening of the correct integration site within the murine genome. This equals a homologous recombination efficiency of around 12%. In the literature, a homologous recombination frequency of around 25% is reported for the *Rosa26* locus (Soriano, 1999; Hohenstein et al., 2008). However, this frequency is highly dependent on the length of the transgene inserted into the locus. In the current study, the insert size was around 9.5 kb and consequently significantly larger than in the study done by Soriano.

After full characterization of the ES cell clones on the DNA level, only 5 out of 12 positive clones (12 out of the 16 initial positive clones were further cultured and characterized) showed a full integration of the *R26 Dual Reporter* construct. All other clones showed only partial integration. As reported in the literature, it is believed that the crossover junctions for the homologous recombination event are formed at the ends of the linearized targeting vector, suggesting two independent recombination events, one for each homologous arm (Deng et al., 1993; LePage and Conlon, 2006). The larger the knock in construct is, the higher the probability that the homologous recombination event will stop before full length integration has completed. Since the *R26 Dual Reporter* construct ranges around 9.5 kb, it might explain the observed low frequency of full length integration (around 42%).

2.5 *In vitro* functional characterization of successfully targeted ES cells

Before generating the new mouse line another functional characterization of selected ES cell clones was launched. Since the *R26 Dual Reporter* construct is integrated into the murine *Rosa26* locus on chromosome 6, it is of interest to investigate the functionality of the construct within this genomic context. As could be demonstrated by electroporation with a Flp expression plasmid, the ES cell colonies started to express EGFP in contrast to the untransfected colonies, validating the function of the FSF cassette. Again no mem-td-Tomato expression could be detected. Some EGFP positive ES cell colonies were picked with strong EGFP expression for further *in vitro* characterization. Ad-Cre infection of these cells induced strong mem-td-Tomato expression due to Cre mediated deletion of the floxed first reporter cassette.

For validating the expression of both luciferases, ES cells from all experiments were harvested in order to conduct *in vitro* luciferase assays. These data nicely showed the correct function of luciferase reporter gene expression. In order to quantify these data, the measured luciferase activity was normalized to the protein content of the respective ES cell sample. However, one has to keep in mind that the number of Flp and Cre recombined ES cells upon electroporation or Ad-Cre infection differs and the gained data cannot directly be compared. Nevertheless they validate the functionality of the construct. Summing up these data, the correct function of all genetic elements involved in the *R26 Dual Reporter* construct

within the genomic context of the *Rosa26* locus in gene targeted ES cells could be demonstrated.

2.6 Generation of *R26 Dual Reporter* mouse chimeras by morula aggregation

For the generation of the new mouse line, selected positive ES cell clones were aggregated with a morula stage embryo in order to produce chimeric mice. The traditional way of generating GEMM is the blastocyst injection technique. Several targeted ES cells are selected and injected into a blastocyst which is later on implanted into a pseudo-pregnant foster mother to give birth to the chimeric offsprings (Bradley et al., 1984; Gossler et al., 1986). Alternatively a chimeric mouse can be produced by aggregating targeted ES cells with a morula-stage embryo and further implanting the aggregate into a pseudo-pregnant foster mother (Wood et al., 1993; Eakin and Hadjantonakis, 2006). Comparing both technologies for the chimera production, the morula aggregation requires drastically less amount of equipment, expertise and hands-on time (Wood et al, 1993). On the other hand, using the blastocyst injection method allows for an individual screening and selection of single ES cells. Thus a selection depending on the morphology of the cell in order to choose the ones with the highest likelihood in efficiently colonizing the germline of the resulting chimeras is possible (Nagy et al., 1993; Eakin and Hadjantonakis, 2006). The frequency of produced chimeras and, most important, germline chimeras (chimeras showing germline transmission) is reported to be equivalent using both technologies (Wood et al., 1993). Since no higher-passaged or in any other sense problematic ES cells were used for the gene targeting experiment, there is no need for a morphology-dependent selection of single ES cells in our study. Consequently the material and time saving morula aggregation technique was chosen for production of the chimeric *R26 Dual Reporter* mice (Nagy et al., 1993; Eakin and Hadjantonakis, 2006).

2.7 Characterization of the *R26 Dual Reporter* mouse – germline transmission

After the chimeric mice develop fur, it is possible to estimate the degree of chimerism since the ES cells as well as the aggregated morula are derived from mouse strains containing different fur colors. The targeted ES cells are derived from 129/S6 background and thus the more brown fur the chimeric mouse will show, the higher is the likelihood that the ES cells contributed to the generation of the germline rather than the morula-derived cell population (morula derived from CD1-background showing albino fur). After selecting the mouse with highest chimerism, it was bred with a mouse containing C57Bl6/J genetic background. The offsprings of this breeding were finally analyzed on the DNA level in order to check for the successful germline transmission of the *R26 Dual Reporter* targeted ES cells. In addition, a PCR screening strategy was developed in order to be able to distinguish between a heterozygous and a homozygous state of the *R26 Dual Reporter* allele. This will be crucial for the further breeding of this mouse line into the pancreatic cancer mouse model in terms of a routine genotyping PCR. As expected, these results demonstrated a heterozygous state of the *R26 Dual Reporter* allele in all mice showing germline transmission. Summing up the

data, the successful generation of the *R26 Dual Reporter* mouse line could be finally proofed by confirming successful germline transmission.

2.8 Distinction from other published reporter mouse models

There are already several different reporter mouse models available for *in vivo* as well as *ex vivo* imaging approaches. Numerous reporter mouse lines for fluorescence imaging have recently been reviewed by Abe and Fujimori (Abe and Fujimori, 2013). One model of particular interest is the *R26*$^{mT\text{-}mG}$ mouse model generated by Muzumdar et al, 2007. In the absence of a recombination event, the mouse expresses mem-td-Tomato ubiquitously under the control of the *CAG* promoter. Upon Cre mediated recombination, the floxed *mem-td-Tomato* gene is deleted and mem-EGFP is expressed. Similar to the *R26 Dual Reporter* mouse model, there is the ability of molecular switching between both reporters allowing a visualization of non-recombined as well as Cre recombined cell populations. However, this mouse model already expresses a reporter gene ubiquitously in all tissues in the non-recombined state. The advantage of the *R26 Dual Reporter* mouse generated in the present study is that reporter gene expression is silenced in the absence of recombination events. Thus, Flp recombined cells can be visualized as well as Cre recombined cells. In addition, the number of Flp recombined cells switching reporter gene expression due to Cre-mediated recombination can be exactly quantified. It is e.g. possible to calculate the efficiency of Cre recombination using the tamoxifen inducible *FSF-R26*^{CreERT2} system. Beside this, different compartments of organs can be visualized depending on the promoters used to drive Flp and Cre expression. This is not possible using the double fluorescence *R26*$^{mT\text{-}mG}$ reporter mouse model, since only one recombination event can be visualized. In addition, no BLI reporters for a sensitive *in vivo* imaging approach are available. The use of the membrane tag of td-Tomato is a great benefit of both models in order to visualize cellular morphology and membrane structures in more detail within the examined tissues *ex vivo* (Muzumdar et al, 2007).

In a recent publication a mouse model similar to the *R26*$^{mT\text{-}mG}$ mouse has been established (Hartwich et al., 2012). In this pink mouse the *mCherry* fluorescence reporter is ubiquitously expressed driven by the *CAG* promoter. Cre recombination leads to switching towards EGFP expression likewise to the *R26*$^{mT\text{-}mG}$ mouse model.

Another publication reports the generation of a transgenic reporter mouse model as a conditional bicistronic Cre reporter mouse line (Ishikawa et al., 2011). Here EGFP is expressed under the control of the *CAG* promoter. Cre recombination deletes the floxed *EGFP* and a bicistronic transcriptional unit containing β-galactosidase and firefly luciferase connected via an *IRES* site is expressed. Similar to the *R26*$^{mT\text{-}mG}$ mouse model, a fluorescence reporter is expressed in all non-recombined cells. Again there is no possibility to image two recombination events. Nevertheless the bicistronic second reporter expression triggered by Cre recombination allows for non-invasive real time *in vivo* BLI.

Beside reporter mouse models based on the Cre-loxP system capable of imaging only one recombination event, there are also models published for imaging of two independent recombination events. In one interesting study a reporter mouse line for Cre and Flp dependent lineage analysis has been established (Yamamoto et al., 2009). This *Rosa26* knock in is also driven by the *CAG* promoter. A floxed stop cassette silences reporter gene expression. Upon Cre recombination a FRT site-flanked, nuclear localized *β-galactosidase* reporter is expressed. Following Flp recombination, the reporter expression switches to EGFP. If Flp is expressed first, no reporter protein will be visible. Upon Cre recombination EGFP will be expressed. Using both recombinases will also lead to EGFP expression. Very similar to the *R26 Dual Reporter* mouse, the reporter gene expression is silenced in the absence of a recombinase and it is possible to image two different recombination events in a spatiotemporally inducible manner. However, since the reporter cassettes consist of only single reporter genes, the difference to the *R26 Dual Reporter* mouse model is the absence of BLI reporters for non-invasive real time *in vivo* imaging applications as well as the possibility to image Flp induced recombination.

Another recent publication demonstrates the generation of a multifunctional fluorescence reporter mouse model similar to Yamamoto et al., 2009. In this model, a *Rosa26* knock in driven by the *CAG* promoter expresses the bright teal fluorescent protein mTFP1 in a Flp as well as Cre dependent manner. Within this model, a loxP site flanked stop cassette followed by an FRT site flanked stop cassette are placed upstream of the fluorescence reporter gene. Consequently this mouse model is able to image cell populations in which both recombinases were active (Imayoshi et al., 2012).

Summing up all these different publications, there is to my knowledge no other reporter mouse model available which is able to resemble the generated *R26 Dual Reporter* mouse line demonstrated within this thesis. Here a reporter mouse model was established that is able to image two different recombination events. First of all the possibility of a spatiotemporally inducible imaging system enables a more accurate and versatile monitoring of complex and highly dynamic biological processes like cancer. Moreover the use of bicistronic reporter cassettes expressing a fluorescence and a bioluminescence reporter gene enables *ex vivo* imaging as well as non-invasive real time *in vivo* imaging of recombined cells. Consequently the generated mouse line represents a novel and versatile imaging tool with broad applicability.

3. Outlook

Mouse models of cancer are extremely useful tools in understanding and elucidating the nature of this disease. For developing new drugs and therapeutic regimens within a preclinical setting, especially non-invasive real time imaging technologies are beneficial. For this reason a novel *in vivo* reporter mouse model to image proliferation has been established in our lab. This *LSL-Pcna*$^{ATG\text{-}fLuc/+}$ mouse model will be useful to test a wide spectrum of different anti-cancer drugs or drug combinations for pancreatic cancer therapy. Based on *in vitro* screening data, potent drug candidates showing the highest overall response in different

cancer cell lines tested, can be validated within the natural environment using the *LSL-Pcna*$^{ATG\text{-}fLuc/+}$ *in vivo* imaging platform. Most important for preclinical drug development studies, the *LSL-Pcna*$^{ATG\text{-}fLuc/+}$ mouse model is a versatile and easy to handle system which enables visualization of drug effects on cell proliferation. Since inhibition of cell division is the main goal in order to stop tumor progression and metastasis formation, this platform seems to be ideal for testing novel anti-cancer chemotherapeutic as well as radiation treatment regimens. In addition, the long-time efficiency of novel therapeutic regimens can easily be investigated and hence also the tolerance as well as potential side effects of drugs are detectable. Moreover, besides real time monitoring of cancer growth *in vivo*, it is also possible to analyze therapeutic drug effects on different progression stages of murine PDAC. Thus the possibility of cancer prevention as well as intervention studies arises, screening mice with early stages of this disease compared to animals showing highly invasive and metastatic disease. In conclusion, the *LSL-Pcna*$^{ATG\text{-}fLuc/+}$ mouse model represents a cheap, fast, easy to handle and highly sensitive preclinical drug validation platform for evaluation of novel anti-cancer drugs.

In order to generate a new mouse model of PDAC which is able to recapitulate the nature of human PDAC initiation and development more closely, the dual recombination system (Cre-loxP and Flp-FRT) has been exploited. After establishment of the new PDAC mouse model in our lab, the corresponding *R26 Dual Reporter* mouse line was generated in the present thesis. With this new mouse model it is possible to visualize two distinct recombination events with different luciferase reporter proteins. Consequently, also this model can be used as a preclinical drug evaluation platform in the future to image the effects of therapeutic strategies on growth of the tumor cells. In contrast to the *LSL-Pcna*$^{ATG\text{-}fLuc/+}$ model, the *R26 Dual Reporter* will image all Cre and Flp recombined cells, respectively, not only the proliferating ones. Thus the complete tumor mass will be visualized.

Besides serving as an *in vivo* drug validation platform, the application possibilities of the *R26 Dual Reporter* mouse model are extremely broad. The use of different reporter genes enables imaging of Flp and Cre dependent recombination events within one mouse. Therefore, switching of Flp recombined cells to Cre recombination can be visualized *in vivo*, since both luciferases can be imaged using distinct substrates. Since both reporter cassettes of the *R26 Dual Reporter* mouse consist of a luciferase and a fluorescent protein, *ex vivo* imaging of tissue sections of an organ can be used to exactly quantify non-recombined, Flp as well as Cre recombined cells by fluorescence imaging. This absolute quantification is extremely useful, since it allows determination of the recombination efficiency of the Flp and the Cre recombinase, including tamoxifen-inducible systems like CreER^{T2}. By counting the different cell cohorts before and after the temporal Cre induction with tamoxifen, the percentage of Flp recombined cells which will switch reporter gene expression due to Cre recombination can be calculated. Besides imaging this temporal recombination induction also a spatial differentiated monitoring becomes feasible. Spatial separated compartments (e.g. epithelium and stroma) can be visualized by *ex vivo* fluorescence imaging of tissue sections from an organ. Consequently non-recombined (no color), Flp (green) and Cre (red)

recombined cells are distinguishable due to non-overlapping emission spectra. By visualizing spatial separated compartments of an organ, lineage tracing studies can easily be performed and also tumor-stroma interactions can be further elucidated.

In conclusion, the successfully generated conditional *R26 Dual Reporter* mouse model has a broad range of application possibilities. Use of fluorescent and bioluminescent reporter genes enables spatiotemporally inducible *in vivo* and *ex vivo* imaging, resulting in distinction between non-recombined, Flp and also Cre-recombined cell populations.

Beside using this novel reporter mouse model for cancer research and imaging of therapeutic strategies, its scope of application seems to be unlimited since it can serve and benefit in many fields of research making use of the dual recombination system.

E. Summary

Pancreatic ductal adenocarcinoma (PDAC) is one of the deadliest kinds of cancer. After many years of intensive research there is still almost no cure for this devastating disease and apart from modestly prolonged survival and palliative treatment, most of the patients die within months upon diagnosis. In order to develop new drugs preclinically, *in vivo* imaging represents an extremely useful tool. It is a relatively cheap, fast and non-invasive method enabling highly sensitive real time monitoring of biological processes within their natural context. In our lab a conditional, Cre-loxP based reporter mouse model has been established that expresses firefly luciferase (fLuc) under the control of the endogenous *proliferating cell nuclear antigen* (*Pcna*) promoter. Within this thesis it could be demonstrated that this *LSL (*loxP-STOP-loxP*)-Pcna*$^{ATG\text{-}fLuc/+}$ mouse model is a powerful tool for real time monitoring of PDAC proliferation *in vivo* as well as *ex vivo*. Furthermore, it could be shown that *Pcna* promoter activity is directly correlated with the proliferation state of a cell *in vivo*. Since anti-cancer drugs should inhibit division of malignant cells, this model is suitable for monitoring therapeutic studies. It could be shown that the *LSL-Pcna*$^{ATG\text{-}fLuc/+}$ mouse model can be used as a fast and easy to handle drug validation platform. Novel chemotherapeutics which have been previously evaluated *in vitro* can rapidly be validated *in vivo*. This represents a crucial point of the drug development process. Consequently, drug delivery, biological half-life, long-time efficiency and tolerance as well as the important role of the tumor microenvironment (tumor-stroma interactions) and the immune system can be investigated using the endogenous *LSL-Pcna*$^{ATG\text{-}fLuc/+}$ mouse model.

Since the standard Cre-loxP based PDAC mouse model is not able to fully recapitulate the sequential, step-wise progression of genetic alterations observed in the human disease, a new mouse model based on a dual recombination system (Cre-loxP and Flp-FRT) has been established in our lab. For this new model of human PDAC a novel reporter mouse line could successfully be generated within the present study. This *R26* knock in mouse line carries two conditional reporter gene expression cassettes which are driven by the *CAG* promoter and silenced by an FSF (FRT-STOP-FRT) cassette. Upon Flp mediated recombination, the FSF cassette will be deleted and enhanced green fluorescent protein (EGFP) and firefly luciferase (fLuc) will be expressed. After Cre mediated recombination, the floxed first reporter cassette with or without the FSF cassette will be deleted and reporter expression switches to membrane-tandem-dimer-Tomato (mem-td-Tomato) and humanized renilla luciferase (hrLuc). In this thesis the functionality of all genetic elements involved in the construction of the *R26 Dual Reporter* targeting vector could be demonstrated on the protein level. After establishing the *R26 Dual Reporter* mouse line by using embryonic stem cell (ES cell) culture for the gene targeting experiment, successful germline transmission of the targeted allele could be proofed. Finally the correct integration, expression and function of the *R26 Dual Reporter* construct within the genomic context of the *Rosa26* locus of gene targeted ES cells has been extensively characterized on the DNA and protein level.

The spatiotemporally inducible reporter mouse model is able to detect Flp as well as Cre mediated recombination events *in vivo* and *ex vivo* by bioluminescence and fluorescence imaging, respectively. Non-recombined, Flp and also Cre recombined cell populations can be distinguished and quantified by *ex vivo* fluorescence imaging. Different compartments of an organ (e.g. epithelium and stroma) can be visualized facilitating lineage tracing studies. In addition, using a Flp-dependent, inducible Cre recombinase, temporal molecular switching from Flp to Cre recombination can be monitored and thus Cre recombination efficiency can be quantified by *ex vivo* fluorescence imaging. Compared to the *LSL-Pcna*$^{ATG\text{-}fLuc/+}$ mouse model, all cancer cells will be visualized within an oncogenic background. Hence initiation as well as progression of tumor growth and response to therapeutic intervention can be monitored *in vivo* in real time by non-invasive bioluminescence imaging. Besides using the *R26 Dual Reporter* mouse in the context of preclinical cancer research and therapeutic drug validation studies, it shows a broad application spectrum. Accordingly it represents a novel and indispensable tool for any researcher focusing on Flp and Cre mediated recombination technology and its visualization in mice.

F. Zusammenfassung

Das duktale Adenokarzinom des Pankreas stellt eine der tödlichsten Krebserkrankungen dar. Nach langjähriger Forschung gibt es immer noch nahezu keine Heilung für diese fatale Erkrankung und abgesehen von einer geringfügigen Verlängerung der Überlebenszeit und palliativen Behandlungen sterben die meisten Patienten innerhalb weniger Monate nach der Diagnose. Um neue Medikamente mit Hilfe von murinen, präklinischen Modellen entwickeln zu können, stellt die *in vivo* Bildgebung ein sehr nützliches Werkzeug dar. Es handelt sich um eine relativ billige, schnelle und nicht invasive Methode, welche die Visualisierung von biologischen Prozessen in Echtzeit innerhalb ihres natürlichen Kontextes erlaubt. In unserem Labor wurde ein konditionales, Cre-loxP basiertes Reportermausmodell etabliert, welches die Luziferase des Leuchtkäfers (fLuc) unter der Kontrolle des endogenen *Pcna* (*proliferating cell nuclear antigen*) Promotors exprimiert. Innerhalb der vorliegenden Studie konnte gezeigt werden, dass dieses *LSL (*loxP-STOP-loxP*)-Pcna*$^{ATG\text{-}fLuc/+}$-Mausmodell ein leistungsfähiges Werkzeug für die Echtzeit-Bildgebug der Proliferation des Pankreaskarzinoms *in vivo* und *ex vivo* darstellt. Desweiteren konnte gezeigt warden, dass die *Pcna* Promotor-Aktivität direkt mit dem Proliferationsstatus einer Zelle *in vivo* korelliert. Da Krebsmedikamente die Teilung von malignen Zellen inhibieren sollten, ist dieses Modell ideal geeignet um therapeutische Studien zu monitoren. Hierzu konnte demonstriert werden, dass das *LSL-Pcna*$^{ATG\text{-}fLuc/+}$-Mausmodell als schnelles und einfach zu handhabendes Evaluierungssystem genutzt werden kann. Neue Chemotherapeutika, die im Rahmen von *in vitro* basierten Untersuchungen evaluiert wurden, können nun im Zuge dieser Bildgebungsplatform rasch *in vivo* validiert werden. Das stellt einen sehr wichtigen Punkt in der Entwicklung von Medikamenten dar. Folglich kann die biologische Halbwertszeit, die Langzeiteffizienz und Toleranz genauso wie die wichtige Rolle des Tumormikromileaus (Tumor-Stroma Interaktionen) und des Immunsystems im Zuge des endogenen *LSL-Pcna*$^{ATG\text{-}fLuc/+}$-Mausmodells optimal untersucht werden.

Da das Standard Cre-loxP basierte, murine Pankreaskarzinom-Modell nicht in der Lage ist, die sequenzielle, stufenweise Progression genetischer Veränderungen vollständig abzubilden, wurde ein neues Mausmodell in unserem Labor generiert. Dieses Modell basiert auf einem dualen Rekombinationssystem (Cre-loxP und Flp-FRT) und kann die humane Situation dieses Tumors besser widerspiegeln. Für dieses neue Modell des humanen Pankreaskarzinoms wurde in der vorliegenden Arbeit erfolgreich eine neue Reportermauslinie generiert. Diese *Duale Reporter*-Maus enthält zwei konditionale Reportergenkassetten als *Rosa26 knock in*, welche durch den *CAG* Promotor gesteuert werden. Die Expression der beiden Kassetten wird durch eine FSF-Kassette (FRT-STOP-FRT) unterbunden. Nach Flp vermittelter Rekombination wird die FSF Kassette deletiert und die Expression von “enhanced green fluorescent protein” (EGFP) und der Luziferase des Leuchtkäfers (fLuc) gestartet. Im Falle einer Cre vermittelten Rekombination wird die gefloxte erste Reporterkassette mit oder ohne der FSF Kassette deletiert und die Expression wechselt zu “membrane-tandem-dimer-Tomato” (mem-td-Tomato) und der humanisierten

Form der renilla Luziferase (hrLuc). Innerhalb dieser Studie konnte die Funktionalität aller genetischen Elemente, welche zur Konstruktion des *R26 Dualen Reporter*-Zielkonstrukts verwendet wurden, auf Protein-Ebene gezeigt werden. Nach Etablierung der *R26 Dualen Reporter*-Mauslinie unter Verwendung der embryonalen Stammzellkultur (ES-Zellkultur) konnte die erfolgreiche Keimbahn-Transmission des modifizierten Allels nachgewiesen werden. Schließlich wurde die korrekte Integration, Expression und Funktionalität des *R26 Dualen Reporter*-Konstrukts im genomischen Kontext des *Rosa26*-Lokus der genetisch veränderten, embryonalen Stammzellen umfassend auf DNA- und Proteinebene charakterisiert.

Das räumlich und zeitlich induzierbare Reportermaus-Modell ist in der Lage, sowohl Flp als auch Cre vermittelte Rekombinationsereignisse *in vivo* und *ex vivo* durch Biolumineszenz- bzw. Fluoreszenz-Bildgebung nachzuweisen. Nicht rekombinierte, Flp und auch Cre rekombinierte Zell-Populationen können durch *ex vivo* Fluoreszenz-Bildgebung unterschieden und quantifiziert werden. Unterschiedliche Kompartimente eines Organs (z.B. Epithel und Stroma) können sichtbar gemacht werden, wodurch *lineage tracing* Studien erleichtert werden. Zusätzlich kann die Aktivität einer Flp abhängigen, induzierbaren Cre Rekombinase untersucht werden. Diese stellt einen temporalen, molekularen Schalter dar, welcher Flp rekombinierte Zellen zur Cre vermittelten Rekombination veranlaßt. Die Effizienz der induzierbaren Cre Rekombinase kann durch *ex vivo* Fluoreszenz-Bildgebung exakt quantifiziert werden. Im Unterschied zum *LSL-Pcna*$^{ATG\text{-}fLuc/+}$-Mausmodell können alle Krebszellen in einem onkogenen Kontext sichtbar gemacht werden. Dies ermöglicht die Echtzeit-Bildgebung der Initiation sowie der Progression des Tumorwachstums und des Ansprechens auf therapeutische Interventionen mittles nicht-invasiver *in vivo* Biolumineszenz-Bildgebung. Neben der Anwendung des *R26 Dualen Reporter*-Modells für therapeutische Medikamenten-Evaluierungsstudien im Zuge der präklinischen Krebsforschung zeigt das neue Mausmodell ein sehr breites Einsatzspektrum in vielen verschiedenen Forschungsbereichen. Somit stellt es ein neues und unentbehrliches Werkzeug für jeden Wissenschaftler dar, der sich mit der Flp und Cre vermittelten Rekombinationstechnologie und ihrer bildlichen Darstellung in Mäusen beschäftigt.

G. Index of cloning plasmids and linkers

Name of plasmid/linker	Abbreviation	Length (bp)	Source of Supply
Acc65I-loxP-Xho1 linker	n.a.	46	Eurofins MWG Operon, Ebersberg
pBlue-FsaSF-minPGK	axz-2	5544	AG Saur, Klinikum rechts der Isar, München
pcDNA3.1	n.a.	5428	AG Saur, Klinikum rechts der Isar, München
pcDNA3.1-CMV-EGFP-P2A-fLuc-stop-BGH-pA	bes-11	7816	AG Saur, Klinikum rechts der Isar, München
pCHMWS-EGFP-P2A-fLuc-T2A-HSV1-sr39tk	bea-2	13741	AG Saur, Klinikum rechts der Isar, München
pCHMWS-EGFP-T2A-fLuc	beb-2	12642	AG Saur, Klinikum rechts der Isar, München (firefly luciferase derived from pSP-luc+NF, Promega, Wisconsin, USA)
pC-S2-TAG-mem-td-Tomato-T2A-H2B-EGFP-pA	n.a.	7110	Order ID: 26772; Addgene, Massachusetts, USA
pEntr-5´ att-dual-reporter-3´ att	bfabc-6	12026	AG Saur, Klinikum rechts der Isar, München
pEntr-CAG-FSF-minPGK-MCS-pA	bcd-7	6642	AG Saur, Klinikum rechts der Isar, München
pEntr-CAG-loxP-FSFminPGK-loxP-mem-td-Tomato-T2A-hrLuc-βG-pA	bet-2	9298	AG Saur, Klinikum rechts der Isar, München
pEntr-CAG-loxP-FSF-minPGK-pA-MCS	beh-11	6676	AG Saur, Klinikum rechts der Isar, München

Name of plasmid/linker	Abbreviation	Length (bp)	Source of Supply
pEntr-CAG-saFSF-CreER^{T2}-pA	ayg-23	9363	AG Saur, Klinikum rechts der Isar, München (*CAG* promoter with SA derived from pTriEx™ neo2; Novagen, Darmstadt)
pEntr-CAG-saFSF-CreER^{T2}-pA-Cla1-religand	bcc-1	5363	AG Saur, Klinikum rechts der Isar, München
pEntr-FsaSF-minPGK-MCS-pA	bca-3	5657	AG Saur, Klinikum rechts der Isar, München
pEntr-FSF-minPGK-MCS-pA	bcb-1	5496	AG Saur, Klinikum rechts der Isar, München
pEntr-sa-FSF-MCS-pA	atg-1	6180	AG Saur, Klinikum rechts der Isar, München
pEntry-Blue	amm-8	2703	AG Saur, Klinikum rechts der Isar, München
pEntry-Blue-EGFP-P2A	bef-8	3498	AG Saur, Klinikum rechts der Isar, München
pEntry-Blue-EGFP-P2A-fLuc-stop	bei-1	5151	AG Saur, Klinikum rechts der Isar, München
pEntry-Blue-loxP linker	beo-1	2711	AG Saur, Klinikum rechts der Isar, München
pEntry-Blue-loxP-linker-mem-td-Tomato-T2A-hrLuc	beq-22	5274	AG Saur, Klinikum rechts der Isar, München
phrG-B-Ecadh-hrLuc-pA	akb-1	4373	AG Saur, Klinikum rechts der Isar, München
phrG-B-Ecadh-Xho1-EcoR1-Bgl2-2 nt-Nco1-linker-hrLuc-pA	bed-19	4339	AG Saur, Klinikum rechts der Isar, München
phrG-B-Ecadh-mem-td-Tomato-T2A-in frame-	beg-2	5957	AG Saur, Klinikum rechts der Isar, München

hrLuc-pA			
pRosa-RFA	aqt-1	11581	AG Saur, Klinikum rechts der Isar, München
pRosa-RFA-dual-reporter	bfo-1	19408	AG Saur, Klinikum rechts der Isar, München
Xho1-EcoR1-Bgl2-2 nt-Nco1-linker	Xho1-EcoR1-Bgl2-2 nt-Nco1-linker	20	Eurofins MWG Operon, Ebersberg
Xho1-Xma1-Avr2-Pml1-loxP-1 nt-BamH1-linker	n.a.	59	Eurofins MWG Operon, Ebersberg

H. Acknowledgements

At first I want to thank Prof. Dr. Roland Schmid for giving me the opportunity to work in the pancreatic cancer research within the Klinikum rechts der Isar.

Afterwards I want to thank Prof. Dr. Bernhard Küster for taking the external supervision of my PhD thesis.

For offering the interesting topic of my PhD thesis and for the supervision during the past 4 years I want to thank Prof. Dr. Dieter Saur. Especially for always having an open ear and offering help whenever help was needed. In addition, for the critical scientific input and the many pleasant discussions and familiar atmosphere created under his leadership. And finally for the huge amount of different methods and techniques which I could learn in his lab and will profit from in my future professional life.

Very special thanks go out to Barbara Seidler who supervised me during the whole cloning procedure for generating the *R26 Dual Reporter* mouse, which has been a major part of my PhD project. For the endless scientific discussions about cloning but also about all other methodological questions arising during the every day lab work, I want to thank her very much. Especially for always having an open ear and taking the time for discussion until the respective problem was solved, no matter what topic it was about. Beside this, I want to thank her for always supporting my scientific work and, most of all, giving me the courage to move on, even if it seemed impossible. Also for her pleasant and familiar way of discussions. But most of all I want to thank her for her critical, open and always honest way which helped me so much in progressing with my scientific work. Even when I lost the endurance she always found a way to encourage me and push me forward.

Further on I want to especially thank all of the animal keepers of the Klinikum rechts der Isar for caring about my mice during the past 4 years and for the excellent collaboration.

I want to thank Heide Oller from the Institute of Stem Cell Research of the Helmholtz Center in Neuherberg for the help in generating the *R26 Dual Reporter* mouse line via morula aggregation.

Very special thanks go out to all members of the AG Saur and AG Schneider for being the best colleagues I ever had. For the familiar atmosphere also during depressing times under sometimes difficult circumstances. Special thanks to Ramona Böhm for the many scientific discussions and for encouraging me so many times.

For helping, supporting and encouraging me during my first days in the lab and for always having an open ear whenever I had questions during learning a new method, I want to thank Ursula Götz.

For reading the manuscript of my PhD thesis and giving me new ideas I want to thank Sandra Diersch. Also for the many scientific discussions in the lab.

And above all, I want to thank my parents who gave me the opportunity to realize all of this and especially for always supporting me and my scientific work, independent of my mood.

I. Declaration

Eidesstattliche Erklärung

Ich versichere an Eides statt durch meine eigene Unterschrift, dass ich die vorliegende Doktorarbeit selbständig und nur unter Zuhilfenahme der angegebenen Literatur und Quellen angefertigt habe. Die Versicherung bezieht sich auch auf in der Dissertation gezeigte Abbildungen, Diagramme, Tabellen, digitale Fotoaufnahmen und dergleichen.

München, den 07.07.2014 Unterschrift: …….....

(Andreas Arbeiter)

J. References

Amersham Pharmacia Biotech Europe GmbH - GE Healthcare Life Sciences Europe GmbH. (2000) The Recombinant Protein Handbook: Protein Amplification and Simple Purification.

Abe, T. and Fujimori, T. (2013) Reporter mouse lines for fluorescence imaging. Developement, Growth & Differentiation 55(4), 390-405.

Aguirre, A.J., Bardeesy, N., Sinha, M., Lopez, L., Tuveson, D.A., Horner, J., Redston, M.S. and DePinho, R.A. (2003) Activated Kras and Ink4a/Arf deficiency cooperate to produce metastatic pancreatic ductal adenocarcinoma. Genes & Developement 17(24), 3112-3126.

Alexopoulou, A.N., Couchman, J.R. and Whiteford, J.R. (2008) The CMV early enhancer/chicken beta actin (CAG) promoter can be used to drive transgene expression during the differentiation of murine embryonic stem cells into vascular progenitors. BMC Cell Biology 9, 2.

Amundadottir, L., Kraft, P., Stolzenberg-Solomon, R.Z., Fuchs, C.S., Petersen, G.M., Arslan, A.A., Bueno-de-Mesquita, H.B., Gross, M., Helzlsouer, K., Jacobs, E.J., LaCroix, A., Zheng, W., Albanes, D., Bamlet, W., Berg, C.D., Berrino, F., Bingham, S., Buring, J.E., Bracci, P.M., Canzian, F., Clavel-Chapelon, F., Clipp, S., Cotterchio, M., de Andrade, M., Duell, E.J., Fox, J.W., Jr., Gallinger, S., Gaziano, J.M., Giovannucci, E.L., Goggins, M., Gonzalez, C.A., Hallmans, G., Hankinson, S.E., Hassan, M., Holly, E.A., Hunter, D.J., Hutchinson, A., Jackson, R., Jacobs, K.B., Jenab, M., Kaaks, R., Klein, A.P., Kooperberg, C., Kurtz, R.C., Li, D., Lynch, S.M., Mandelson, M., McWilliams, R.R., Mendelsohn, J.B., Michaud, D.S., Olson, S.H., Overvad, K., Patel, A.V., Peeters, P.H., Rajkovic, A., Riboli, E., Risch, H.A., Shu, X.O., Thomas, G., Tobias, G.S., Trichopoulos, D., Van Den Eeden, S.K., Virtamo, J., Wactawski-Wende, J., Wolpin, B.M., Yu, H., Yu, K., Zeleniuch-Jacquotte, A., Chanock, S.J., Hartge, P. and Hoover, R.N. (2009) Genome-wide association study identifies variants in the ABO locus associated with susceptibility to pancreatic cancer. Nature Genetics 41(9), 986-990.

Anton, M. and Graham, F.L. (1995) Site-specific recombination mediated by an adenovirus vector expressing the Cre recombinase protein: a molecular switch for control of gene expression. Journal of Virology 69(8), 4600-4606.

Armstrong, J.J., Larina, I.V., Dickinson, M.E., Zimmer, W.E. and Hirschi, K.K. (2010) Characterization of bacterial artificial chromosome transgenic mice expressing mCherry fluorescent protein substituted for the murine smooth muscle alpha-actin gene. Genesis 48(7), 457-463.

Baird, G.S., Zacharias, D.A. and Tsien, R.Y. (2000) Biochemistry, mutagenesis, and oligomerization of DsRed, a red fluorescent protein from coral. Proceedings of the National Academy of Science of the U S A 97(22), 11984-11989.

Barascu, A., Grabarz, A. and Lopez, B. (2013) Chapter 4: Homologous Recombination in Mammals, Springer Science + Business Media Dordrecht.

Bardeesy, N., Aguirre, A.J., Chu, G.C., Cheng, K.H., Lopez, L.V., Hezel, A.F., Feng, B., Brennan, C., Weissleder, R., Mahmood, U., Hanahan, D., Redston, M.S., Chin, L. and Depinho, R.A. (2006) Both p16(Ink4a) and the p19(Arf)-p53 pathway constrain progression of pancreatic adenocarcinoma in the mouse. Proceedings of the National Academy of Science of the U S A 103(15), 5947-5952.

Baumann, S. (2011) Downstream Signaling of Oncogenic Kras in Pancreatic Ductal Adenocarcinoma: In Vivo and Ex Vivo Imaging of Tumor Cell Proliferation as a Tool for the Identification of Therapeutic Targets. PhD thesis, Lehrstuhl für Biotechnologie der Nutztiere, Technische Universität München.

Becher, O.J. and Holland, E.C. (2006) Genetically engineered models have advantages over xenografts for preclinical studies. Cancer Research 66(7), 3355-3358, discussion 3358-3359.

Bevis, B.J. and Glick, B.S. (2002) Rapidly maturing variants of the Discosoma red fluorescent protein (DsRed). Nature Biotechnology 20(1), 83-87.

Bhaumik, S. and Gambhir, S.S. (2002) Optical imaging of Renilla luciferase reporter gene expression in living mice. Proceedings of the National Academy of Science of the U S A 99(1), 377-382.

Bhaumik, S., Lewis, X.Z. and Gambhir, S.S. (2004) Optical imaging of Renilla luciferase, synthetic Renilla luciferase, and firefly luciferase reporter gene expression in living mice. Journal of Biomedical Optics 9(3), 578-586.

Bornmann, C., Graeser, R., Esser, N., Ziroli, V., Jantscheff, P., Keck, T., Unger, C., Hopt, U.T., Adam, U., Schaechtele, C., Massing, U. and von Dobschuetz, E. (2008) A new liposomal formulation of Gemcitabine is active in an orthotopic mouse model of pancreatic cancer accessible to bioluminescence imaging. Cancer Chemotherapy and Pharmacology. 61(3), 395-405.

Brachmann, S.M., Hofmann, I., Schnell, C., Fritsch, C., Wee, S., Lane, H., Wang, S., Garcia-Echeverria, C. and Maira, S.M. (2009) Specific apoptosis induction by the dual PI3K/mTor inhibitor NVP-BEZ235 in HER2 amplified and PIK3CA mutant breast cancer cells. Proceedings of the National Academy of Science of the U S A 106(52), 22299-22304.

Bradley, A., Evans, M., Kaufman, M.H. and Robertson, E. (1984) Formation of germ-line chimaeras from embryo-derived teratocarcinoma cell lines. Nature 309(5965), 255-256.

Branchini, B.R., Southworth, T.L., Khattak, N.F., Michelini, E. and Roda, A. (2005) Red- and green-emitting firefly luciferase mutants for bioluminescent reporter applications. Analytical Biochemistry 345(1), 140-148.

Brindle, K. (2008) New approaches for imaging tumour responses to treatment. Nature Reviews. Cancer 8(2), 94-107.

Buschow, C., Charo, J., Anders, K., Loddenkemper, C., Jukica, A., Alsamah, W., Perez, C., Willimsky, G. and Blankenstein, T. (2010) In vivo imaging of an inducible oncogenic tumor antigen visualizes tumor progression and predicts CTL tolerance. Journal of Immunology 184(6), 2930-2938.

Campbell, P.J., Yachida, S., Mudie, L.J., Stephens, P.J., Pleasance, E.D., Stebbings, L.A., Morsberger, L.A., Latimer, C., McLaren, S., Lin, M.L., McBride, D.J., Varela, I., Nik-Zainal, S.A., Leroy, C., Jia, M., Menzies, A., Butler, A.P., Teague, J.W., Griffin, C.A., Burton, J., Swerdlow, H., Quail, M.A., Stratton, M.R., Iacobuzio-Donahue, C. and Futreal, P.A. (2010) The patterns and dynamics of genomic instability in metastatic pancreatic cancer. Nature 467(7319), 1109-1113.

Campbell, R.E., Tour, O., Palmer, A.E., Steinbach, P.A., Baird, G.S., Zacharias, D.A. and Tsien, R.Y. (2002) A monomeric red fluorescent protein. Proceedings of the National Academy of Science of the U S A 99(12), 7877-7882.

Chalfie, M., Tu, Y., Euskirchen, G., Ward, W.W. and Prasher, D.C. (1994) Green fluorescent protein as a marker for gene expression. Science 263(5148), 802-805.

Chan, H.Y., V, S., Xing, X., Kraus, P., Yap, S.P., Ng, P., Lim, S.L. and Lufkin, T. (2011) Comparison of IRES and F2A-based locus-specific multicistronic expression in stable mouse lines. PLoS One 6(12), 21.

Chen, I.T., Akamatsu, M., Smith, M.L., Lung, F.D., Duba, D., Roller, P.P., Fornace, A.J., Jr. and O'Connor, P.M. (1996) Characterization of p21Cip1/Waf1 peptide domains required for cyclin E/Cdk2 and PCNA interaction. Oncogene 12(3), 595-607.

Chen, J., Jackson, P.K., Kirschner, M.W. and Dutta, A. (1995) Separate domains of p21 involved in the inhibition of Cdk kinase and PCNA. Nature 374(6520), 386-388.

Cheon, D.J. and Orsulic, S. (2011) Mouse models of cancer. Annual Review of Pathology 6, 95-119.

Cheong, W.F., Prahl, S.A. and Welch, A.J. (1990) A review of the optical properties of biological tissues. IEEE. Journal of Quantum Electronics. 26(12), 2166-2185.

Chiarini, F., Grimaldi, C., Ricci, F., Tazzari, P.L., Evangelisti, C., Ognibene, A., Battistelli, M., Falcieri, E., Melchionda, F., Pession, A., Pagliaro, P., McCubrey, J.A. and Martelli, A.M.

(2010) Activity of the novel dual phosphatidylinositol 3-kinase/mammalian target of rapamycin inhibitor NVP-BEZ235 against T-cell acute lymphoblastic leukemia. Cancer Research 70(20), 8097-8107.

Chudakov, D.M., Matz, M.V., Lukyanov, S. and Lukyanov, K.A. (2010) Fluorescent proteins and their applications in imaging living cells and tissues. Physiological Reviews 90(3), 1103-1163.

Close, D.M., Xu, T., Sayler, G.S. and Ripp, S. (2011) In vivo bioluminescent imaging (BLI): noninvasive visualization and interrogation of biological processes in living animals. Sensors 11(1), 180-206.

Conroy, T., Desseigne, F., Ychou, M., Bouche, O., Guimbaud, R., Becouarn, Y., Adenis, A., Raoul, J.L., Gourgou-Bourgade, S., de la Fouchardiere, C., Bennouna, J., Bachet, J.B., Khemissa-Akouz, F., Pere-Verge, D., Delbaldo, C., Assenat, E., Chauffert, B., Michel, P., Montoto-Grillot, C. and Ducreux, M. (2011) FOLFIRINOX versus gemcitabine for metastatic pancreatic cancer. New England Journal of Medicine 364(19), 1817-1825.

Contag, C.H., Contag, P.R., Mullins, J.I., Spilman, S.D., Stevenson, D.K. and Benaron, D.A. (1995) Photonic detection of bacterial pathogens in living hosts. Molecular Microbiology 18(4), 593-603.

Contag, C.H., Jenkins, D., Contag, P.R. and Negrin, R.S. (2000) Use of reporter genes for optical measurements of neoplastic disease in vivo. Neoplasia 2(1-2), 41-52.

Contag, C.H. and Bachmann, M.H. (2002) Advances in in vivo bioluminescence imaging of gene expression. Annual Review of Biomedical Engineering 4, 235-260.

Contag, C.H. (2006) Molecular imaging using visible light to reveal biological changes in the brain. Neuroimaging Clinics of North America 16(4), 633-654, ix.

Contag, C.H. (2007) In vivo pathology: seeing with molecular specificity and cellular resolution in the living body. Annual Review of Pathology 2, 277-305.

Corish, P. and Tyler-Smith, C. (1999) Attenuation of green fluorescent protein half-life in mammalian cells. Protein Engineering 12(12), 1035-1040.

Cormack, B.P., Valdivia, R.H. and Falkow, S. (1996) FACS-optimized mutants of the green fluorescent protein (GFP). Gene 173(1 Spec No), 33-38.

Cubitt, A.B., Heim, R., Adams, S.R., Boyd, A.E., Gross, L.A. and Tsien, R.Y. (1995) Understanding, improving and using green fluorescent proteins. Trends in Biochemical Sciences 20(11), 448-455.

Curtis, A., Calabro, K., Galarneau, J.R., Bigio, I.J. and Krucker, T. (2010) Temporal variations of skin pigmentation in C57BL/6 mice affect optical bioluminescence quantification. Molecular Imaging and Biology: MIB: The official publication of the Academy of Molecular Imaging 13(6), 1114-1123.

De Biasio, A. and Blanco, F.J. (2013) Proliferating cell nuclear antigen structure and interactions: too many partners for one dancer? Advances in Protein Chemistry and Structural Biology 91, 1-36.

de Felipe, P. and Ryan, M.D. (2004) Targeting of proteins derived from self-processing polyproteins containing multiple signal sequences. Traffic 5(8), 616-626.

de Felipe, P., Luke, G.A., Hughes, L.E., Gani, D., Halpin, C. and Ryan, M.D. (2006) E unum pluribus: multiple proteins from a self-processing polyprotein. Trends in Biotechnology 24(2), 68-75.

de Wet, J.R., Wood, K.V., Helinski, D.R. and DeLuca, M. (1985) Cloning of firefly luciferase cDNA and the expression of active luciferase in Escherichia coli. Proceedings of the National Academy of Science of the U S A 82(23), 7870-7873.

Deng, C., Thomas, K.R. and Capecchi, M.R. (1993) Location of crossovers during gene targeting with insertion and replacement vectors. Molecular and Cellular Biology 13(4), 2134-2140.

Deroose, C.M., De, A., Loening, A.M., Chow, P.L., Ray, P., Chatziioannou, A.F. and Gambhir, S.S. (2007) Multimodality imaging of tumor xenografts and metastases in mice with combined small-animal PET, small-animal CT, and bioluminescence

imaging. Journal of Nuclear Medicine: Official Publication, Society of Nuclear Medicine 48(2), 295-303.

Donnelly, M.L., Hughes, L.E., Luke, G., Mendoza, H., ten Dam, E., Gani, D. and Ryan, M.D. (2001) The 'cleavage' activities of foot-and-mouth disease virus 2A site-directed mutants and naturally occurring '2A-like' sequences. Journal of General Viroogy 82(Pt 5), 1027-1041.

Donoho, G., Jasin, M. and Berg, P. (1998) Analysis of gene targeting and intrachromosomal homologous recombination stimulated by genomic double-strand breaks in mouse embryonic stem cells. Molecular and Cellular Biology 18(7), 4070-4078.

Dothager, R.S., Flentie, K., Moss, B., Pan, M.H., Kesarwala, A. and Piwnica-Worms, D. (2009) Advances in bioluminescence imaging of live animal models. Current Opinion in Biotechnology 20(1), 45-53.

Doyle, T.C., Burns, S.M. and Contag, C.H. (2004) In vivo bioluminescence imaging for integrated studies of infection. Cellular Microbiology 6(4), 303-317.

Eakin, G.S. and Hadjantonakis, A.K. (2006) Production of chimeras by aggregation of embryonic stem cells with diploid or tetraploid mouse embryos. Nature Protocols 1(3), 1145-1153.

Edinger, M., Sweeney, T.J., Tucker, A.A., Olomu, A.B., Negrin, R.S. and Contag, C.H. (1999) Noninvasive assessment of tumor cell proliferation in animal models. Neoplasia 1(4), 303-310.

Eichhorn, P.J., Gili, M., Scaltriti, M., Serra, V., Guzman, M., Nijkamp, W., Beijersbergen, R.L., Valero, V., Seoane, J., Bernards, R. and Baselga, J. (2008) Phosphatidylinositol 3-kinase hyperactivation results in lapatinib resistance that is reversed by the mTOR/phosphatidylinositol 3-kinase inhibitor NVP-BEZ235. Cancer Research 68(22), 9221-9230.

Engelman, J.A., Chen, L., Tan, X., Crosby, K., Guimaraes, A.R., Upadhyay, R., Maira, M., McNamara, K., Perera, S.A., Song, Y., Chirieac, L.R., Kaur, R., Lightbown, A., Simendinger, J., Li, T., Padera, R.F., Garcia-Echeverria, C., Weissleder, R., Mahmood, U., Cantley, L.C. and Wong, K.K. (2008) Effective use of PI3K and MEK inhibitors to treat mutant Kras G12D and PIK3CA H1047R murine lung cancers. Nature Medicine 14(12), 1351-1356.

Eser, S., Reiff, N., Messer, M., Seidler, B., Gottschalk, K., Dobler, M., Hieber, M., Arbeiter, A., Klein, S., Kong, B., Michalski, C.W., Schlitter, A.M., Esposito, I., Kind, A.J., Rad, L., Schnieke, A.E., Baccarini, M., Alessi, D.R., Rad, R., Schmid, R.M., Schneider, G. and Saur, D. (2013) Selective requirement of PI3K/PDK1 signaling for Kras oncogene-driven pancreatic cell plasticity and cancer. Cancer Cell 23(3), 406-420.

Feil, R., Wagner, J., Metzger, D. and Chambon, P. (1997) Regulation of Cre recombinase activity by mutated estrogen receptor ligand-binding domains. Biochemical and Biophysical Research Communications. 237(3), 752-757.

Feng, G., Mellor, R.H., Bernstein, M., Keller-Peck, C., Nguyen, Q.T., Wallace, M., Nerbonne, J.M., Lichtman, J.W. and Sanes, J.R. (2000) Imaging neuronal subsets in transgenic mice expressing multiple spectral variants of GFP. Neuron 28(1), 41-51.

Fink, D., Wohrer, S., Pfeffer, M., Tombe, T., Ong, C.J. and Sorensen, P.H. (2010) Ubiquitous expression of the monomeric red fluorescent protein mCherry in transgenic mice. Genesis 48(12), 723-729.

Garcia-Echeverria, C. and Sellers, W.R. (2008) Drug discovery approaches targeting the PI3K/Akt pathway in cancer. Oncogene 27(41), 5511-5526.

Ghaneh, P., Costello, E. and Neoptolemos, J.P. (2007) Biology and management of pancreatic cancer. Gut 56(8), 1134-1152.

Gossler, A., Doetschman, T., Korn, R., Serfling, E. and Kemler, R. (1986) Transgenesis by means of blastocyst-derived embryonic stem cell lines. Proceedings of the National Academy of Science of the U S A 83(23), 9065-9069.

Gross, S. and Piwnica-Worms, D. (2005) Spying on cancer: molecular imaging in vivo with genetically encoded reporters. Cancer Cell 7(1), 5-15.

Gulbis, J.M., Kelman, Z., Hurwitz, J., O'Donnell, M. and Kuriyan, J. (1996) Structure of the C-terminal region of p21(WAF1/CIP1) complexed with human PCNA. Cell. 87(2), 297-306.

Hadjantonakis, A.K. and Nagy, A. (2000) FACS for the isolation of individual cells from transgenic mice harboring a fluorescent protein reporter. Genesis 27(3), 95-98.

Hadjantonakis, A.K., Macmaster, S. and Nagy, A. (2002) Embryonic stem cells and mice expressing different GFP variants for multiple non-invasive reporter usage within a single animal. BMC Biotechnology 2, 11.

Hartwich, H., Satheesh, S.V. and Nothwang, H.G. (2012) A pink mouse reports the switch from red to green fluorescence upon Cre-mediated recombination. BMC Research Notes 5(296), 1756-0500.

Hashizume, R., Ozawa, T., Dinca, E.B., Banerjee, A., Prados, M.D., James, C.D. and Gupta, N. (2009) A human brainstem glioma xenograft model enabled for bioluminescence imaging. Journal of Neuro-Oncology 96(2), 151-159.

Hastings, J.W. (1996) Chemistries and colors of bioluminescent reactions: a review. Gene 173(1 Spec No), 5-11.

Heim, R., Prasher, D.C. and Tsien, R.Y. (1994) Wavelength mutations and posttranslational autoxidation of green fluorescent protein. Proceedings of the National Academy of Science of the U S A 91(26), 12501-12504.

Heim, R. and Tsien, R.Y. (1996) Engineering green fluorescent protein for improved brightness, longer wavelengths and fluorescence resonance energy transfer. Current Biology: CB 6(2), 178-182.

Heyer, J., Kwong, L.N., Lowe, S.W. and Chin, L. (2010) Non-germline genetically engineered mouse models for translational cancer research. Nature Reviews. Cancer 10(7), 470-480.

Hezel, A.F., Kimmelman, A.C., Stanger, B.Z., Bardeesy, N. and Depinho, R.A. (2006) Genetics and biology of pancreatic ductal adenocarcinoma. Genes & Development 20(10), 1218-1249.

Hingorani, S.R., Petricoin, E.F., Maitra, A., Rajapakse, V., King, C., Jacobetz, M.A., Ross, S., Conrads, T.P., Veenstra, T.D., Hitt, B.A., Kawaguchi, Y., Johann, D., Liotta, L.A., Crawford, H.C., Putt, M.E., Jacks, T., Wright, C.V., Hruban, R.H., Lowy, A.M. and Tuveson, D.A. (2003) Preinvasive and invasive ductal pancreatic cancer and its early detection in the mouse. Cancer Cell 4(6), 437-450.

Hingorani, S.R., Wang, L., Multani, A.S., Combs, C., Deramaudt, T.B., Hruban, R.H., Rustgi, A.K., Chang, S. and Tuveson, D.A. (2005) Trp53R172H and KrasG12D cooperate to promote chromosomal instability and widely metastatic pancreatic ductal adenocarcinoma in mice. Cancer Cell 7(5), 469-483.

Hoffman, R.M. and Yang, M. (2006) Whole-body imaging with fluorescent proteins. Nature Protocols 1(3), 1429-1438.

Hohenstein, P., Slight, J., Ozdemir, D.D., Burn, S.F., Berry, R. and Hastie, N.D. (2008) High-efficiency Rosa26 knock-in vector construction for Cre-regulated overexpression and RNAi. Pathogenetics 1(1), 3.

Hong, H., Yang, Y. and Cai, W. (2011) Imaging gene expression in live cells and tissues. Cold Spring Harbor Protocols. 2011(4).

Hruban, R.H., Goggins, M., Parsons, J. and Kern, S.E. (2000) Progression model for pancreatic cancer. Clinical Cancer Research 6(8), 2969-2972.

Hruban, R.H., Adsay, N.V., Albores-Saavedra, J., Compton, C., Garrett, E.S., Goodman, S.N., Kern, S.E., Klimstra, D.S., Kloppel, G., Longnecker, D.S., Luttges, J. and Offerhaus, G.J. (2001) Pancreatic intraepithelial neoplasia: a new nomenclature and classification system for pancreatic duct lesions. The American Journal of Surgical Pathology 25(5), 579-586.

Hruban, R.H., Adsay, N.V., Albores-Saavedra, J., Anver, M.R., Biankin, A.V., Boivin, G.P., Furth, E.E., Furukawa, T., Klein, A., Klimstra, D.S., Kloppel, G., Lauwers, G.Y., Longnecker, D.S., Luttges, J., Maitra, A., Offerhaus, G.J., Perez-Gallego, L., Redston,

M. and Tuveson, D.A. (2006) Pathology of genetically engineered mouse models of pancreatic exocrine cancer: consensus report and recommendations. Cancer Research 66(1), 95-106.

Imayoshi, I., Hirano, K., Sakamoto, M., Miyoshi, G., Imura, T., Kitano, S., Miyachi, H. and Kageyama, R. (2012) A multifunctional teal-fluorescent Rosa26 reporter mouse line for Cre- and Flp-mediated recombination. Neuroscience Research 73(1), 85-91.

Indra, A.K., Warot, X., Brocard, J., Bornert, J.M., Xiao, J.H., Chambon, P. and Metzger, D. (1999) Temporally-controlled site-specific mutagenesis in the basal layer of the epidermis: comparison of the recombinase activity of the tamoxifen-inducible Cre-ER(T) and Cre-ER(T2) recombinases. Nucleic Acids Research 27(22), 4324-4327.

Ishikawa, T.O. and Herschman, H.R. (2011) Conditional bicistronic Cre reporter line expressing both firefly luciferase and β-galactosidase. Molecular Imaging and Biology: MIB: The official publication of the Academy of Molecular Imaging 13(2), 284-292.

Jackson, E.L., Willis, N., Mercer, K., Bronson, R.T., Crowley, D., Montoya, R., Jacks, T. and Tuveson, D.A. (2001) Analysis of lung tumor initiation and progression using conditional expression of oncogenic K-ras. Genes & Developement 15(24), 3243-3248.

Jakobs, S., Subramaniam, V., Schonle, A., Jovin, T.M. and Hell, S.W. (2000) EFGP and DsRed expressing cultures of Escherichia coli imaged by confocal, two-photon and fluorescence lifetime microscopy. FEBS Letters 479(3), 131-135.

Jang, S.K., Krausslich, H.G., Nicklin, M.J., Duke, G.M., Palmenberg, A.C. and Wimmer, E. (1988) A segment of the 5' nontranslated region of encephalomyocarditis virus RNA directs internal entry of ribosomes during in vitro translation. Journal of Virology 62(8), 2636-2643.

Jenkins, D.E., Oei, Y., Hornig, Y.S., Yu, S.F., Dusich, J., Purchio, T. and Contag, P.R. (2003) Bioluminescent imaging (BLI) to improve and refine traditional murine models of tumor growth and metastasis. Clinical & Experimental Metastasis 20(8), 733-744.

Jenkins, D.E., Hornig, Y.S., Oei, Y., Dusich, J. and Purchio, T. (2005) Bioluminescent human breast cancer cell lines that permit rapid and sensitive in vivo detection of mammary tumors and multiple metastases in immune deficient mice. Breast cancer research: BCR 7(4), R444-454.

Johnson, J.I., Decker, S., Zaharevitz, D., Rubinstein, L.V., Venditti, J.M., Schepartz, S., Kalyandrug, S., Christian, M., Arbuck, S., Hollingshead, M. and Sausville, E.A. (2001) Relationships between drug activity in NCI preclinical in vitro and in vivo models and early clinical trials. British Journal Of Cancer 84(10), 1424-1431.

Jones, S., Zhang, X., Parsons, D.W., Lin, J.C., Leary, R.J., Angenendt, P., Mankoo, P., Carter, H., Kamiyama, H., Jimeno, A., Hong, S.M., Fu, B., Lin, M.T., Calhoun, E.S., Kamiyama, M., Walter, K., Nikolskaya, T., Nikolsky, Y., Hartigan, J., Smith, D.R., Hidalgo, M., Leach, S.D., Klein, A.P., Jaffee, E.M., Goggins, M., Maitra, A., Iacobuzio-Donahue, C., Eshleman, J.R., Kern, S.E., Hruban, R.H., Karchin, R., Papadopoulos, N., Parmigiani, G., Vogelstein, B., Velculescu, V.E. and Kinzler, K.W. (2008) Core signaling pathways in human pancreatic cancers revealed by global genomic analyses. Science 321(5897), 1801-1806.

Kalnins, A., Otto, K., Ruther, U. and Muller-Hill, B. (1983) Sequence of the lacZ gene of Escherichia coli. The EMBO Journal 2(4), 593-597.

Kawaguchi, Y., Cooper, B., Gannon, M., Ray, M., MacDonald, R.J. and Wright, C.V. (2002) The role of the transcriptional regulator Ptf1a in converting intestinal to pancreatic progenitors. Nature Genetics 32(1), 128-134.

Kelman, Z. and O'Donnell, M. (1995) DNA polymerase III holoenzyme: structure and function of a chromosomal replicating machine. Annual Review of Biochemistry 64, 171-200.

Kelsen, D.P., Portenoy, R., Thaler, H., Tao, Y. and Brennan, M. (1997) Pain as a predictor of outcome in patients with operable pancreatic carcinoma. Surgery 122(1), 53-59.

Khan, A.P., Contessa, J.N., Nyati, M.K., Ross, B.D. and Rehemtulla, A. (2011) Molecular imaging of epidermal growth factor receptor kinase activity. Analytical Biochemistry 417(1), 57-64.

Kim, J.B., Urban, K., Cochran, E., Lee, S., Ang, A., Rice, B., Bata, A., Campbell, K., Coffee, R., Gorodinsky, A., Lu, Z., Zhou, H., Kishimoto, T.K. and Lassota, P. (2010) Non-invasive detection of a small number of bioluminescent cancer cells in vivo. PLoS One 5(2), 0009364.

Klein, A.P., Brune, K.A., Petersen, G.M., Goggins, M., Tersmette, A.C., Offerhaus, G.J., Griffin, C., Cameron, J.L., Yeo, C.J., Kern, S. and Hruban, R.H. (2004) Prospective risk of pancreatic cancer in familial pancreatic cancer kindreds. Cancer Research 64(7), 2634-2638.

Knibiehler, M., Goubin, F., Escalas, N., Jonsson, Z.O., Mazarguil, H., Hubscher, U. and Ducommun, B. (1996) Interaction studies between the p21Cip1/Waf1 cyclin-dependent kinase inhibitor and proliferating cell nuclear antigen (PCNA) by surface plasmon resonance. FEBS Letters 391(1-2), 66-70.

Kocher, B. and Piwnica-Worms, D. (2013) Illuminating cancer systems with genetically engineered mouse models and coupled luciferase reporters in vivo. Cancer Discovery 3(6), 616-629.

Komar, G., Kauhanen, S., Liukko, K., Seppanen, M., Kajander, S., Ovaska, J., Nuutila, P. and Minn, H. (2009) Decreased blood flow with increased metabolic activity: a novel sign of pancreatic tumor aggressiveness. Clinical Cancer Research 15(17), 5511-5517.

Konstantinidou, G., Bey, E.A., Rabellino, A., Schuster, K., Maira, M.S., Gazdar, A.F., Amici, A., Boothman, D.A. and Scaglioni, P.P. (2009) Dual phosphoinositide 3-kinase/mammalian target of rapamycin blockade is an effective radiosensitizing strategy for the treatment of non-small cell lung cancer harboring K-RAS mutations. Cancer Research 69(19), 7644-7652.

Krishna, T.S., Kong, X.P., Gary, S., Burgers, P.M. and Kuriyan, J. (1994) Crystal structure of the eukaryotic DNA polymerase processivity factor PCNA. Cell 79(7), 1233-1243.

Kurki, P., Vanderlaan, M., Dolbeare, F., Gray, J. and Tan, E.M. (1986) Expression of proliferating cell nuclear antigen (PCNA)/cyclin during the cell cycle. Experimental Cell Research 166(1), 209-219.

Larina, I.V., Shen, W., Kelly, O.G., Hadjantonakis, A.K., Baron, M.H. and Dickinson, M.E. (2009) A membrane associated mCherry fluorescent reporter line for studying vascular remodeling and cardiac function during murine embryonic development. Anatomical Record (Hoboken, N.J. :2007) 292(3), 333-341.

Lee, C.J., Spalding, A.C., Ben-Josef, E., Wang, L. and Simeone, D.M. (2010) In vivo bioluminescent imaging of irradiated orthotopic pancreatic cancer xenografts in nonobese diabetic-severe combined immunodeficient mice: a novel method for targeting and assaying efficacy of ionizing radiation. Translational Oncology 3(3), 153-159.

Lee, C.L., Moding, E.J., Huang, X., Li, Y., Woodlief, L.Z., Rodrigues, R.C., Ma, Y. and Kirsch, D.G. (2012) Generation of primary tumors with Flp recombinase in FRT-flanked p53 mice. Disease Models & Mechanisms 5(3), 397-402.

LePage, D.F. and Conlon, R.A. (2006) Animal models for disease: knockout, knock-in, and conditional mutant mice. Methods in Molecular Medicine 129, 41-67.

Li, B., Torossian, A., Li, W., Schleicher, S., Niu, K., Giacalone, N.J., Kim, S.J., Chen, H., Gonzalez, A., Moretti, L. and Lu, B. (2011) A novel bioluminescence orthotopic mouse model for advanced lung cancer. Radiation Research 176(4), 486-493.

Lipshutz, G.S., Gruber, C.A., Cao, Y., Hardy, J., Contag, C.H. and Gaensler, K.M. (2001) In utero delivery of adeno-associated viral vectors: intraperitoneal gene transfer produces long-term expression. Molecular Therapy: The Journal of the American Society of Gene Therapy. 3(3), 284-292.

Liu, T.J., Koul, D., LaFortune, T., Tiao, N., Shen, R.J., Maira, S.M., Garcia-Echevrria, C. and Yung, W.K. (2009) NVP-BEZ235, a novel dual phosphatidylinositol 3-kinase/mammalian target of rapamycin inhibitor, elicits multifaceted antitumor activities in human gliomas. Molecular Cancer Therapeutics 8(8), 2204-2210.

Long, J.Z., Lackan, C.S. and Hadjantonakis, A.K. (2005) Genetic and spectrally distinct in vivo imaging: embryonic stem cells and mice with widespread expression of a monomeric red fluorescent protein. BMC Biotechnology 5, 20.

Lorenz, W.W., McCann, R.O., Longiaru, M. and Cormier, M.J. (1991) Isolation and expression of a cDNA encoding Renilla reniformis luciferase. Proceedings of the National Academy of Science of the U S A 88(10), 4438-4442.

Luo, Y., Hurwitz, J. and Massague, J. (1995) Cell-cycle inhibition by independent CDK and PCNA binding domains in p21Cip1. Nature 375(6527), 159-161.

Lyons, S.K., Meuwissen, R., Krimpenfort, P. and Berns, A. (2003) The generation of a conditional reporter that enables bioluminescence imaging of Cre/loxP-dependent tumorigenesis in mice. Cancer Research 63(21), 7042-7046.

Maga, G. and Hubscher, U. (2003) Proliferating cell nuclear antigen (PCNA): a dancer with many partners. Journal of Cell Science 116(Pt 15), 3051-3060.

Maira, S.M., Stauffer, F., Brueggen, J., Furet, P., Schnell, C., Fritsch, C., Brachmann, S., Chene, P., De Pover, A., Schoemaker, K., Fabbro, D., Gabriel, D., Simonen, M., Murphy, L., Finan, P., Sellers, W. and Garcia-Echeverria, C. (2008) Identification and characterization of NVP-BEZ235, a new orally available dual phosphatidylinositol 3-kinase/mammalian target of rapamycin inhibitor with potent in vivo antitumor activity. Molecular Cancer Therapeutics 7(7), 1851-1863.

Massoud, T.F. and Gambhir, S.S. (2003) Molecular imaging in living subjects: seeing fundamental biological processes in a new light. Genes & Development 17(5), 545-580.

Matz, M.V., Fradkov, A.F., Labas, Y.A., Savitsky, A.P., Zaraisky, A.G., Markelov, M.L. and Lukyanov, S.A. (1999) Fluorescent proteins from nonbioluminescent Anthozoa species. Nature Biotechnology 17(10), 969-973.

McCarrick, J.W., 3rd, Parnes, J.R., Seong, R.H., Solter, D. and Knowles, B.B. (1993) Positive-negative selection gene targeting with the diphtheria toxin A-chain gene in mouse embryonic stem cells. Transgenic Research 2(4), 183-190.

Mezzanotte, L., Fazzina, R., Michelini, E., Tonelli, R., Pession, A., Branchini, B. and Roda, A. (2010) In vivo bioluminescence imaging of murine xenograft cancer models with a red-shifted thermostable luciferase. Molecular Imaging and Biology: MIB: The official publication of the Academy of Molecular Imaging 12(4), 406-414.

Miretti, S., Roato, I., Taulli, R., Ponzetto, C., Cilli, M., Olivero, M., Di Renzo, M.F., Godio, L., Albini, A., Buracco, P. and Ferracini, R. (2008) A mouse model of pulmonary metastasis from spontaneous osteosarcoma monitored in vivo by Luciferase imaging. PLoS One 3(3), e1828.

Miyazaki, J., Takaki, S., Araki, K., Tashiro, F., Tominaga, A., Takatsu, K. and Yamamura, K. (1989) Expression vector system based on the chicken beta-actin promoter directs efficient production of interleukin-5. Gene 79(2), 269-277.

Moskowitz, N.K., Borao, F.J., Dardashti, O., Cohen, H.D. and Germino, F.J. (1996) The amino terminus of Cdk2 binds p21. Oncology Research 8(9), 343-352.

Mukherjee, B., Tomimatsu, N., Amancherla, K., Camacho, C.V., Pichamoorthy, N. and Burma, S. (2012) The dual PI3K/mTOR inhibitor NVP-BEZ235 is a potent inhibitor of ATM- and DNA-PKCs-mediated DNA damage responses. Neoplasia 14(1), 34-43.

Muniraj, T., Jamidar, P.A. and Aslanian, H.R. (2013) Pancreatic cancer: a comprehensive review and update. Disease-A-Month: DM. 59(11), 368-402.

Muzumdar, M.D., Tasic, B., Miyamichi, K., Li, L. and Luo, L. (2007) A global double-fluorescent Cre reporter mouse. Genesis 45(9), 593-605.

Nagy, A., Rossant, J., Nagy, R., Abramow-Newerly, W. and Roder, J.C. (1993) Derivation of completely cell culture-derived mice from early-passage embryonic stem cells. Proceedings of the National Academy of Science of the U S A 90(18), 8424-8428.

Negrin, R.S., Edinger, M., Verneris, M., Cao, Y.A., Bachmann, M. and Contag Ch, H. (2002) Visualization of tumor growth and response to NK-T cell based immunotherapy using bioluminescence. Annals of Hematology 81 Suppl 2, S44-45.

Nguyen, V.T., Morange, M. and Bensaude, O. (1988) Firefly luciferase luminescence assays using scintillation counters for quantitation in transfected mammalian cells. Analytical Biochemistry 171(2), 404-408.

Niwa, H., Yamamura, K. and Miyazaki, J. (1991) Efficient selection for high-expression transfectants with a novel eukaryotic vector. Gene 108(2), 193-199.

Ojajarvi, I.A., Partanen, T.J., Ahlbom, A., Boffetta, P., Hakulinen, T., Jourenkova, N., Kauppinen, T.P., Kogevinas, M., Porta, M., Vainio, H.U., Weiderpass, E. and Wesseling, C.H. (2000) Occupational exposures and pancreatic cancer: a meta-analysis. Occupational and Environmental Medicine 57(5), 316-324.

Okabe, M., Ikawa, M., Kominami, K., Nakanishi, T. and Nishimune, Y. (1997) 'Green mice' as a source of ubiquitous green cells. FEBS Letters 407(3), 313-319.

Olive, K.P. and Tuveson, D.A. (2006) The use of targeted mouse models for preclinical testing of novel cancer therapeutics. Clinical Cancer Research 12(18), 5277-5287.

Olive, K.P., Jacobetz, M.A., Davidson, C.J., Gopinathan, A., McIntyre, D., Honess, D., Madhu, B., Goldgraben, M.A., Caldwell, M.E., Allard, D., Frese, K.K., Denicola, G., Feig, C., Combs, C., Winter, S.P., Ireland-Zecchini, H., Reichelt, S., Howat, W.J., Chang, A., Dhara, M., Wang, L., Ruckert, F., Grutzmann, R., Pilarsky, C., Izeradjene, K., Hingorani, S.R., Huang, P., Davies, S.E., Plunkett, W., Egorin, M., Hruban, R.H., Whitebread, N., McGovern, K., Adams, J., Iacobuzio-Donahue, C., Griffiths, J. and Tuveson, D.A. (2009) Inhibition of Hedgehog signaling enhances delivery of chemotherapy in a mouse model of pancreatic cancer. Science 324(5933), 1457-1461.

Ormo, M., Cubitt, A.B., Kallio, K., Gross, L.A., Tsien, R.Y. and Remington, S.J. (1996) Crystal structure of the Aequorea victoria green fluorescent protein. Science 273(5280), 1392-1395.

Paez, J.G., Janne, P.A., Lee, J.C., Tracy, S., Greulich, H., Gabriel, S., Herman, P., Kaye, F.J., Lindeman, N., Boggon, T.J., Naoki, K., Sasaki, H., Fujii, Y., Eck, M.J., Sellers, W.R., Johnson, B.E. and Meyerson, M. (2004) EGFR mutations in lung cancer: correlation with clinical response to gefitinib therapy. Science 304(5676), 1497-1500.

Pelaez-Luna, M., Takahashi, N., Fletcher, J.G. and Chari, S.T. (2007) Resectability of presymptomatic pancreatic cancer and its relationship to onset of diabetes: a retrospective review of CT scans and fasting glucose values prior to diagnosis. The American Journal of Gastroenterology 102(10), 2157-2163.

Pichorner, A., Sack, U., Kobelt, D., Kelch, I., Arlt, F., Smith, J., Walther, W., Schlag, P.M. and Stein, U. (2012) In vivo imaging of colorectal cancer growth and metastasis by targeting MACC1 with shRNA in xenografted mice. Clinical & Experimental Metastasis 29(6), 573-583.

Poche, R.A., Larina, I.V., Scott, M.L., Saik, J.E., West, J.L. and Dickinson, M.E. (2009) The Flk1-myr::mCherry mouse as a useful reporter to characterize multiple aspects of ocular blood vessel development and disease. Developmental Dynamics. An official publication of the American Association of Anatomists 238(9), 2318-2326.

Prasher, D.C., Eckenrode, V.K., Ward, W.W., Prendergast, F.G. and Cormier, M.J. (1992) Primary structure of the Aequorea victoria green-fluorescent protein. Gene 111(2), 229-233.

Raimondi, S., Maisonneuve, P. and Lowenfels, A.B. (2009) Epidemiology of pancreatic cancer: an overview. Nature Reviews. Gastroenterology & Hepatology 6(12), 699-708.

Rehemtulla, A., Stegman, L.D., Cardozo, S.J., Gupta, S., Hall, D.E., Contag, C.H. and Ross, B.D. (2000) Rapid and quantitative assessment of cancer treatment response using in vivo bioluminescence imaging. Neoplasia 2(6), 491-495.

Reid, B.G. and Flynn, G.C. (1997) Chromophore formation in green fluorescent protein. Biochemistry 36(22), 6786-6791.

Rice, B.W., Cable, M.D. and Nelson, M.B. (2001) In vivo imaging of light-emitting probes. Journal of Biomedical Optics 6(4), 432-440.

Roberts, P.J., Usary, J.E., Darr, D.B., Dillon, P.M., Pfefferle, A.D., Whittle, M.C., Duncan, J.S., Johnson, S.M., Combest, A.J., Jin, J., Zamboni, W.C., Johnson, G.L., Perou, C.M.

and Sharpless, N.E. (2012) Combined PI3K/mTOR and MEK inhibition provides broad antitumor activity in faithful murine cancer models. Clinical Cancer Research 18(19), 5290-5303.

Robertson, B.H., Grubman, M.J., Weddell, G.N., Moore, D.M., Welsh, J.D., Fischer, T., Dowbenko, D.J., Yansura, D.G., Small, B. and Kleid, D.G. (1985) Nucleotide and amino acid sequence coding for polypeptides of foot-and-mouth disease virus type A12. Journal of Virology 54(3), 651-660.

Rozenblum, E., Schutte, M., Goggins, M., Hahn, S.A., Panzer, S., Zahurak, M., Goodman, S.N., Sohn, T.A., Hruban, R.H., Yeo, C.J. and Kern, S.E. (1997) Tumor-suppressive pathways in pancreatic carcinoma. Cancer Research 57(9), 1731-1734.

Ryan, M.D. and Drew, J. (1994) Foot-and-mouth disease virus 2A oligopeptide mediated cleavage of an artificial polyprotein. The EMBO Journal 13(4), 928-933.

Sadikot, R.T. and Blackwell, T.S. (2005) Bioluminescence imaging. Proceedings of the American Thoracic Society 2(6), 537-540, 511-532.

Safran, M., Kim, W.Y., Kung, A.L., Horner, J.W., DePinho, R.A. and Kaelin, W.G., Jr. (2003) Mouse reporter strain for noninvasive bioluminescent imaging of cells that have undergone Cre-mediated recombination. Molecular Imaging 2(4), 297-302.

Sato, A., Klaunberg, B. and Tolwani, R. (2004) In vivo bioluminescence imaging. Comparative Medicine 54(6), 631-634.

Saur, D., Seidler, B., Schneider, G., Algul, H., Beck, R., Senekowitsch-Schmidtke, R., Schwaiger, M. and Schmid, R.M. (2005) CXCR4 expression increases liver and lung metastasis in a mouse model of pancreatic cancer. Gastroenterology 129(4), 1237-1250.

Sausville, E.A. and Burger, A.M. (2006) Contributions of human tumor xenografts to anticancer drug development. Cancer Research 66(7), 3351-3354, discussion 3354.

Schnell, C.R., Stauffer, F., Allegrini, P.R., O'Reilly, T., McSheehy, P.M., Dartois, C., Stumm, M., Cozens, R., Littlewood-Evans, A., Garcia-Echeverria, C. and Maira, S.M. (2008) Effects of the dual phosphatidylinositol 3-kinase/mammalian target of rapamycin inhibitor NVP-BEZ235 on the tumor vasculature: implications for clinical imaging. Cancer Research 68(16), 6598-6607.

Schurtenberger, P., Egelhaaf, S.U., Hindges, R., Maga, G., Jonsson, Z.O., May, R.P., Glatter, O. and Hubscher, U. (1998) The solution structure of functionally active human proliferating cell nuclear antigen determined by small-angle neutron scattering. Journal of Molecular Biology 275(1), 123-132.

Schutte, M., Hruban, R.H., Geradts, J., Maynard, R., Hilgers, W., Rabindran, S.K., Moskaluk, C.A., Hahn, S.A., Schwarte-Waldhoff, I., Schmiegel, W., Baylin, S.B., Kern, S.E. and Herman, J.G. (1997) Abrogation of the Rb/p16 tumor-suppressive pathway in virtually all pancreatic carcinomas. Cancer Research 57(15), 3126-3130.

Seidler, B., Schmidt, A., Mayr, U., Nakhai, H., Schmid, R.M., Schneider, G. and Saur, D. (2008) A Cre-loxP-based mouse model for conditional somatic gene expression and knockdown in vivo by using avian retroviral vectors. Proceedings of the National Academy of Science of the U S A 105(29), 10137-10142.

Serra, V., Markman, B., Scaltriti, M., Eichhorn, P.J., Valero, V., Guzman, M., Botero, M.L., Llonch, E., Atzori, F., Di Cosimo, S., Maira, M., Garcia-Echeverria, C., Parra, J.L., Arribas, J. and Baselga, J. (2008) NVP-BEZ235, a dual PI3K/mTOR inhibitor, prevents PI3K signaling and inhibits the growth of cancer cells with activating PI3K mutations. Cancer Research 68(19), 8022-8030.

Shah, K., Bureau, E., Kim, D.E., Yang, K., Tang, Y., Weissleder, R. and Breakefield, X.O. (2005) Glioma therapy and real-time imaging of neural precursor cell migration and tumor regression. Annals of Neurology 57(1), 34-41.

Shaner, N.C., Campbell, R.E., Steinbach, P.A., Giepmans, B.N., Palmer, A.E. and Tsien, R.Y. (2004) Improved monomeric red, orange and yellow fluorescent proteins derived from Discosoma sp. red fluorescent protein. Nature Biotechnology 22(12), 1567-1572.

Shaner, N.C., Steinbach, P.A. and Tsien, R.Y. (2005) A guide to choosing fluorescent proteins. Nature Methods 2(12), 905-909.

Sharpless, N.E. and Depinho, R.A. (2006) The mighty mouse: genetically engineered mouse models in cancer drug development. Nature Reviews. Drug Discovery 5(9), 741-754.

Shimomura, O., Johnson, F.H. and Saiga, Y. (1962) Extraction, purification and properties of aequorin, a bioluminescent protein from the luminous hydromedusan, Aequorea. Journal of Cellular and Comparative Physiology 59, 223-239.

Soriano, P. (1999) Generalized lacZ expression with the ROSA26 Cre reporter strain. Nature Genetics 21(1), 70-71.

Sotiriou, C. and Piccart, M.J. (2007) Taking gene-expression profiling to the clinic: when will molecular signatures become relevant to patient care? Nature Reviews. Cancer 7(7), 545-553.

Spibey, C.A., Jackson, P. and Herick, K. (2001) A unique charge-coupled device/xenon arc lamp based imaging system for the accurate detection and quantitation of multicolour fluorescence. Electrophoresis 22(5), 829-836.

Srinivas, S., Watanabe, T., Lin, C.S., William, C.M., Tanabe, Y., Jessell, T.M. and Costantini, F. (2001) Cre reporter strains produced by targeted insertion of EYFP and ECFP into the ROSA26 locus. BMC Developmental Biology 1, 4.

Srivastava, S., Zou, Z., Pirollo, K., Blattner, W. and Chang, E.H. (1990) Germ-line transmission of a mutated p53 gene in a cancer-prone family with Li-Fraumeni syndrome. Nature 348(6303), 747-749.

Sunmonu, N.A., Chen, L. and Li, J.Y. (2009) Misexpression of Gbx2 throughout the mesencephalon by a conditional gain-of-function transgene leads to deletion of the midbrain and cerebellum in mice. Genesis 47(10), 667-673.

Sweeney, T.J., Mailander, V., Tucker, A.A., Olomu, A.B., Zhang, W., Cao, Y., Negrin, R.S. and Contag, C.H. (1999) Visualizing the kinetics of tumor-cell clearance in living animals. Proceedings of the National Academy of Science of the U S A 96(21), 12044-12049.

Szymczak, A.L., Workman, C.J., Wang, Y., Vignali, K.M., Dilioglou, S., Vanin, E.F. and Vignali, D.A. (2004) Correction of multi-gene deficiency in vivo using a single 'self-cleaving' 2A peptide-based retroviral vector. Nature Biotechnology 22(5), 589-594.

Thastrup, O., Tullin, S., Poulsen, L.K. and BjÃ¸rn, S.P. (2001) Fluorescent proteins., Google Patents.

Thompson, J.F., Hayes, L.S. and Lloyd, D.B. (1991) Modulation of firefly luciferase stability and impact on studies of gene regulation. Gene 103(2), 171-177.

Trichas, G., Begbie, J. and Srinivas, S. (2008) Use of the viral 2A peptide for bicistronic expression in transgenic mice. BMC Biology 6, 40.

Troy, T., Jekic-McMullen, D., Sambucetti, L. and Rice, B. (2004) Quantitative comparison of the sensitivity of detection of fluorescent and bioluminescent reporters in animal models. Molecular Imaging 3(1), 9-23.

Tsien, R.Y. (1998) The green fluorescent protein. Annual Review of Biochemistry 67, 509-544.

Tuchin, V. (2007) Tissue Optics: Light Scattering Methods and Instruments for Medical Diagnosis., • SPIE Digital Library. Society of Photo-Optical Instrumentation Engineers

Uhrbom, L., Nerio, E. and Holland, E.C. (2004) Dissecting tumor maintenance requirements using bioluminescence imaging of cell proliferation in a mouse glioma model. Nature Medicine 10(11), 1257-1260.

van Heek, N.T., Meeker, A.K., Kern, S.E., Yeo, C.J., Lillemoe, K.D., Cameron, J.L., Offerhaus, G.J., Hicks, J.L., Wilentz, R.E., Goggins, M.G., De Marzo, A.M., Hruban, R.H. and Maitra, A. (2002) Telomere shortening is nearly universal in pancreatic intraepithelial neoplasia. The American Journal of Pathology 161(5), 1541-1547.

Venisnik, K.M., Olafsen, T., Loening, A.M., Iyer, M., Gambhir, S.S. and Wu, A.M. (2006) Bifunctional antibody-Renilla luciferase fusion protein for in vivo optical detection of tumors. Protein Engineering, Design & Selection: PEDS 19(10), 453-460.

Verkhusha, V.V., Otsuna, H., Awasaki, T., Oda, H., Tsukita, S. and Ito, K. (2001) An enhanced mutant of red fluorescent protein DsRed for double labeling and developmental timer of neural fiber bundle formation. Journal of Biological Chemistry 276(32), 29621-29624.

Verkhusha, V.V. and Lukyanov, K.A. (2004) The molecular properties and applications of Anthozoa fluorescent proteins and chromoproteins. Nature Biotechnology 22(3), 289-296.

Vincent, A., Herman, J., Schulick, R., Hruban, R.H. and Goggins, M. (2011) Pancreatic cancer. The Lancet 378(9791), 607-620.

Vintersten, K., Monetti, C., Gertsenstein, M., Zhang, P., Laszlo, L., Biechele, S. and Nagy, A. (2004) Mouse in red: red fluorescent protein expression in mouse ES cells, embryos, and adult animals. Genesis 40(4), 241-246.

von Burstin, J., Eser, S., Seidler, B., Meining, A., Bajbouj, M., Mages, J., Lang, R., Kind, A.J., Schnieke, A.E., Schmid, R.M., Schneider, G. and Saur, D. (2008) Highly sensitive detection of early-stage pancreatic cancer by multimodal near-infrared molecular imaging in living mice. International Journal of Cancer 123(9), 2138-2147.

Von Hoff, D.D., Ramanathan, R.K., Borad, M.J., Laheru, D.A., Smith, L.S., Wood, T.E., Korn, R.L., Desai, N., Trieu, V., Iglesias, J.L., Zhang, H., Soon-Shiong, P., Shi, T., Rajeshkumar, N.V., Maitra, A. and Hidalgo, M. (2011) Gemcitabine plus nab-paclitaxel is an active regimen in patients with advanced pancreatic cancer: a phase I/II trial. Journal of Clinical Oncology 29(34), 4548-4554.

Von Hoff, D.D., Ervin, T., Arena, F.P., Chiorean, E.G., Infante, J., Moore, M., Seay, T., Tjulandin, S.A., Ma, W.W., Saleh, M.N., Harris, M., Reni, M., Dowden, S., Laheru, D., Bahary, N., Ramanathan, R.K., Tabernero, J., Hidalgo, M., Goldstein, D., Van Cutsem, E., Wei, X., Iglesias, J. and Renschler, M.F. (2013) Increased survival in pancreatic cancer with nab-paclitaxel plus gemcitabine. New England Journal of Medicine 369(18), 1691-1703.

Vooijs, M., Jonkers, J., Lyons, S. and Berns, A. (2002) Noninvasive imaging of spontaneous retinoblastoma pathway-dependent tumors in mice. Cancer Research 62(6), 1862-1867.

Voskoglou-Nomikos, T., Pater, J.L. and Seymour, L. (2003) Clinical predictive value of the in vitro cell line, human xenograft, and mouse allograft preclinical cancer models. Clinical Cancer Research 9(11), 4227-4239.

Weissleder, R. (2002) Scaling down imaging: molecular mapping of cancer in mice. Nature Reviews. Cancer 2(1), 11-18.

Weissleder, R. and Ntziachristos, V. (2003) Shedding light onto live molecular targets. Nature Medicine 9(1), 123-128.

Wolpin, B.M., Chan, A.T., Hartge, P., Chanock, S.J., Kraft, P., Hunter, D.J., Giovannucci, E.L. and Fuchs, C.S. (2009) ABO blood group and the risk of pancreatic cancer. Journal of the National Cancer Institute 101(6), 424-431.

Wood, S.A., Allen, N.D., Rossant, J., Auerbach, A. and Nagy, A. (1993) Non-injection methods for the production of embryonic stem cell-embryo chimaeras. Nature 365(6441), 87-89.

Woolfenden, S., Zhu, H. and Charest, A. (2009) A Cre/LoxP conditional luciferase reporter transgenic mouse for bioluminescence monitoring of tumorigenesis. Genesis 47(10), 659-666.

Wyman, C. and Botchan, M. (1995) DNA replication. A familiar ring to DNA polymerase processivity. Current Biology: CB 5(4), 334-337.

Xiong, Y., Zhang, H. and Beach, D. (1992) D type cyclins associate with multiple protein kinases and the DNA replication and repair factor PCNA. Cell 71(3), 505-514.

Yamamoto, M., Shook, N.A., Kanisicak, O., Yamamoto, S., Wosczyna, M.N., Camp, J.R. and Goldhamer, D.J. (2009) A multifunctional reporter mouse line for Cre- and FLP-dependent lineage analysis. Genesis 47(2), 107-114.

Yang, M., Baranov, E., Moossa, A.R., Penman, S. and Hoffman, R.M. (2000) Visualizing gene expression by whole-body fluorescence imaging. Proceedings of the National Academy of Science of the U S A 97(22), 12278-12282.

Yang, T.T., Cheng, L. and Kain, S.R. (1996) Optimized codon usage and chromophore mutations provide enhanced sensitivity with the green fluorescent protein. Nucleic Acids Research 24(22), 4592-4593.

Zhao, H., Doyle, T.C., Coquoz, O., Kalish, F., Rice, B.W. and Contag, C.H. (2005) Emission spectra of bioluminescent reporters and interaction with mammalian tissue determine the sensitivity of detection in vivo. Journal of Biomedical Optics 10(4), 41210.

Zinn, K.R., Chaudhuri, T.R., Szafran, A.A., O'Quinn, D., Weaver, C., Dugger, K., Lamar, D., Kesterson, R.A., Wang, X. and Frank, S.J. (2008) Noninvasive bioluminescence imaging in small animals. ILAR Journal/National Research Council, Institute of Laboratory Animal Resources. 49(1), 103-115.

Zong, H., Espinosa, J.S., Su, H.H., Muzumdar, M.D. and Luo, L. (2005) Mosaic Analysis with Double Markers in Mice. Cell 121(3), 479-492.